ABSTRACT OF THESIS

Name of Candidate IAN C. MALCOLM

Address DEPT. OF PHYSICS, JAMES CLERK MAXWELL BUILDING, MAYFIELD ROAD.

Degree DOCTOR OF PHILOSOPHY *Date* JANUARY, 1976.

Title of Thesis STUDIES INTO ANGULAR MOMENTUM DEPENDENT COLLISION PROCESSES

The feasibility is investigated, of determining the relative amplitudes and phase for the transfer of different orbital angular momentum components, in the coherent electron-impact excitation of the sodium and potassium ^2P resonance levels, for incident energies in the region of 5.0 eV.

An apparatus is designed and developed which is shown to be capable of accomplishing this, by the measurement of the polarization of the subsequently emitted photon, in delayed coincidence with the corresponding inelastically-scattered electron. A value for the polarization is not, however, obtained.

Use other side if necessary.

PGS/ABST/74/5000

STUDIES INTO ANGULAR MOMENTUM DEPENDENT COLLISION PROCESSES

Thesis

Submitted by

IAN C. MALCOLM

For the degree of

DOCTOR OF PHILOSOPHY

University of Edinburgh

January, 1976.

ACKNOWLEDGEMENTS

I wish to express my gratitude to Professor N. Feather, F.R.S., for giving me the opportunity to carry out this research, and also to my supervisor, Professor P.S. Farago, for his invaluable guidance throughout its course.

I am indebted to Mr. T.E. Guthrie for his advice and help in the early stages of the work, especially with the design and construction of the electron-energy analyzer.

The computer program, used to carry out the non-linear least squares fit, the numerical integration of the resulting function to obtain the genuine coincidence rate, and the calculation of its variance, is the work of Mr. N. Robertson. For this, and his general help during the latter stages of the work, I am most grateful.

I should also like to thank Dr. R. Newell for his advice on electron-gun design; Dr. D.M. Campbell for his help and advice during the early part of the work on atomic-beam polarization measurement; and Dr. A.G.A. Rae for advice on the preparation of alkali discharge lamps.

Many useful ideas have arisen from discussions with Dr. J.S. Wykes, Dr. J. Slevin, Mrs. W. Sillitto, and Dr. D. Brandford, to whom I am most thankful.

Finally, I should like to express my thanks to the technical staff of the Physics Department, University of Edinburgh, for their help; and also to Mrs. R. Chester for her excellent work in the typing of this thesis.

SUMMARY

The feasibility is investigated, of determining the relative amplitudes and phase for the transfer of different orbital angular momentum components, in the coherent electron-impact excitation of the sodium and potassium ^2P resonance levels, for incident energies in the region of 5.0 eV.

An apparatus is designed and developed which is shown to be capable of accomplishing this, by the measurement of the polarization of the subsequently emitted photon, in delayed coincidence with the corresponding inelastically-scattered electron. A value for the polarization is not, however, obtained.

C O N T E N T S

C O N T E N T S (Contd.)

CHAPTER 1

INTRODUCTION

Information about atomic scattering processes is necessary for the understanding of many physical phenomena occurring, for instance, in the atmosphere and in laboratory plasmas. The derivation of numerical results from basic scattering theory requires, even for elementary processes, the application of simplifying approximations to make the problem mathematically tractable. It is necessary to compare the results of such calculations with measurements to test the validity of the approximation and to provide insight into the physics underlying it. The comparatively simple processes involving electron-atom scattering have been used as "proving-grounds" for the many approximation techniques.

The simplest approximation from the point of view of calculation is due to Born (1926) but it is only valid at sufficiently high energy of the incident electron, and below about 100 eV it becomes increasingly inaccurate. As many of the processes of interest involve electron energies of only a few eV, it was necessary to develop other approximations which would be more accurate at these low energies. The most notable of such is the close-coupling approximation (Massey & Mohr, 1932). It is desirable to attempt to derive the most detailed information possible from measurements in order to secure the most stringent test of the approximations.

In the study of atomic excitation by electron impact, methods falling into one of four different categories have traditionally been employed. These are measurements of

(i) scattered electron intensity, (ii) intensity of the recoil atoms, (iii) intensity of the emitted light and (iv) the polarization of the emitted light. These methods enable measurements of total and differential inelastic cross-sections to be made. For example, measurements of the differential excitation cross-section for the 4P states of K have been carried out by Slevin, Visconti and Rubin (1972) using method (ii). The angular range 10^{o} - 90^{o} of electron scattering was studied at incident energies 3.0, 4.4 and 5.2 eV. Their results compare favourably with the two-state close-coupling calculations (including exchange) of Karule and Peterkop (1965). Measurements employing method (iii) are typified by the work of Hafner (1973) on the 3P states of Na for the energy range from threshold to 4.0 eV. Agreement with the four-state close-coupling calculations (including exchange) of Moores & Norcross (1972) is again satisfactory.

In all the above mentioned types of measurements, a certain amount of information is lost due to averaging over processes involving different amounts of angular momentum transferred between electron and atom. For example, from the theory, one can calculate the cross-section for excitation of each magnetic sublevel, but due to the degeneracy it is not possible to distinguish between processes in which different sublevels have been excited, by observation of the scattered particles alone. The experimentally measured quantity is therefore an average over the cross-sections for excitation of the different substates (i.e. for the transfer of different amounts of angular momentum component).

Experiments in category (iv) have been carried out by, for example, Hafner and Kleinpoppen (1967) and Enemark and Gallagher (1972) in their measurements of the polarization of the Na D

lines. The latter made a comparison with theoretical results and showed that there is better agreement with the calculations of Moores and Norcross than with those of Karule and Peterkop. Both sets of authors obtained satisfactory agreement with the theoretically expected value of threshold polarization (see below). The intensity of the different polarization components of the emitted light, in these experiments, depends on the total cross-sections for the excitation of the different sublevels and it is thus possible to obtain information about these quantities (Kleinpoppen, 1969). But unless the scattered electron is also detected, the differential cross-sections for the various sublevels are still elusive.

Another alternative, therefore, is to measure simultaneously a property of the emitted light and the scattered electron which gave rise to it. Such an experiment has been carried out by King, Adams and Read (1972), who studied the $3^1P - 2^1S$ and $4^1S - 2^1P$ transitions in He at an incident energy of 80 eV. Electrons inelastically scattered in the forward direction were detected in coincidence with the detection of the subsequently emitted photons of particular polarizations. The light was detected at an angle of 90° to the electron beam. For a sufficiently small cone of acceptance for electrons, these particles have no component of orbital angular momentum (m_L) along the incident electron beam direction. If this direction is used as a quantization axis then the orbital angular momentum projection (M_L) of the atom cannot change and the condition $\Delta M_L = 0$ applies. If the orbital angular momentum of the atom is increased in the interaction then this condition implies, for these events, a non-uniform distribution among M_L values for the excited atoms. This is reflected in

a polarization of the emitted radiation. Because of the $\Delta M_L = 0$ condition this kind of experiment reproduces the same polarization values which would be obtained in a non-coincidence experiment where the energy of the incident electrons approach the threshold for excitation. The measurement of such a polarization is important, as the theoretical polarization values at threshold do not depend on the scattering amplitudes, and hence no approximation is used in their estimation (Percival and Seaton, 1958). The coincidence experiment has the advantage that it gives the "at threshold" result rather than the "close to threshold" one which is the best that can be done using conventional methods.

Carrying the above technique a stage further Eminyan, McAdam, Slevin and Kleinpoppen (1973, 1974) measured the electron-photon angular correlation functions associated with the 2^1P and 3^1P states of He using incident energies in the range 40 - 200 eV. For electron scattering angles (θ) in the range 16° - 40° they measured the variation in coincidence rate, as the photon detection angle (Ⓗ) was varied between 30° and 130° in the same plane as, but in the opposite sense to the electron scattering. They were then able to carry out a least-squares fit of the theoretical form of the angular correlation function to their data and thus extract values of the parameters λ and $|\chi|$ (see Chapter 2) relating to the amplitudes for the transfer of zero ($\Delta M_L = 0$) or one ($\Delta M_L = \pm 1$) unit of orbital angular momentum component, to the atom. λ is the ratio of the differential cross-section for excitation of the $M_L = 0$ sub-level to the total differential cross-section, for excitation of the P state under consideration. χ is the phase difference

between the $M_L = 0$ excitation amplitude and the $M_L = \pm 1$ amplitudes. Eminyan et al. compared their results with calculations using the First Born Approximation (FBA); using the Distorted Wave (DW) Method of Madison and Shelton (1973); and using the Many Body Green's Function (MBGF) method of Csanak, Taylor and Tripathy (1973). It was shown that the FBA gives implicitly $\chi \equiv 0$, but there is good agreement with the measured angular correlation function and for λ especially at small θ. The DW method gives better agreement for λ and $|\chi|$, but it is not quite so good for the angular correlation function at large θ. The MBGF method does not give good agreement.

Arriola, Teubner, Ugbabe and Weigold (1975) have done similar work on the $J = 1$ states of Argon ($^3P_1$ and $^1P_1$) for $\theta = 8.5^\circ$, using incident energies of 80 and 113 eV. They have compared their results with FBA calculations. Again, good agreement was obtained for both λ and the angular correlation function at both energies.

McConkey, Tan, Farago and Teubner (1975) have studied the 2'P state of He. They measured the electron-photon correlation function for azimuth differences in the range -20° - $+300^\circ$ keeping θ and Φ fixed at 42° and 90° respectively. Values for λ were obtained directly by measuring the value of the function at azimuth differences of 0° and 180° (see Chapter 2) These results are in agreement with those of Eminyan et al.

The abundant isotopes of He and Ar have zero nuclear spin and so the effects of hyperfine structure in the above investigations are absent. Also, in the case of He there is no fine structure effect, due to the absence of intercombination transitions. Argon is a special case because it

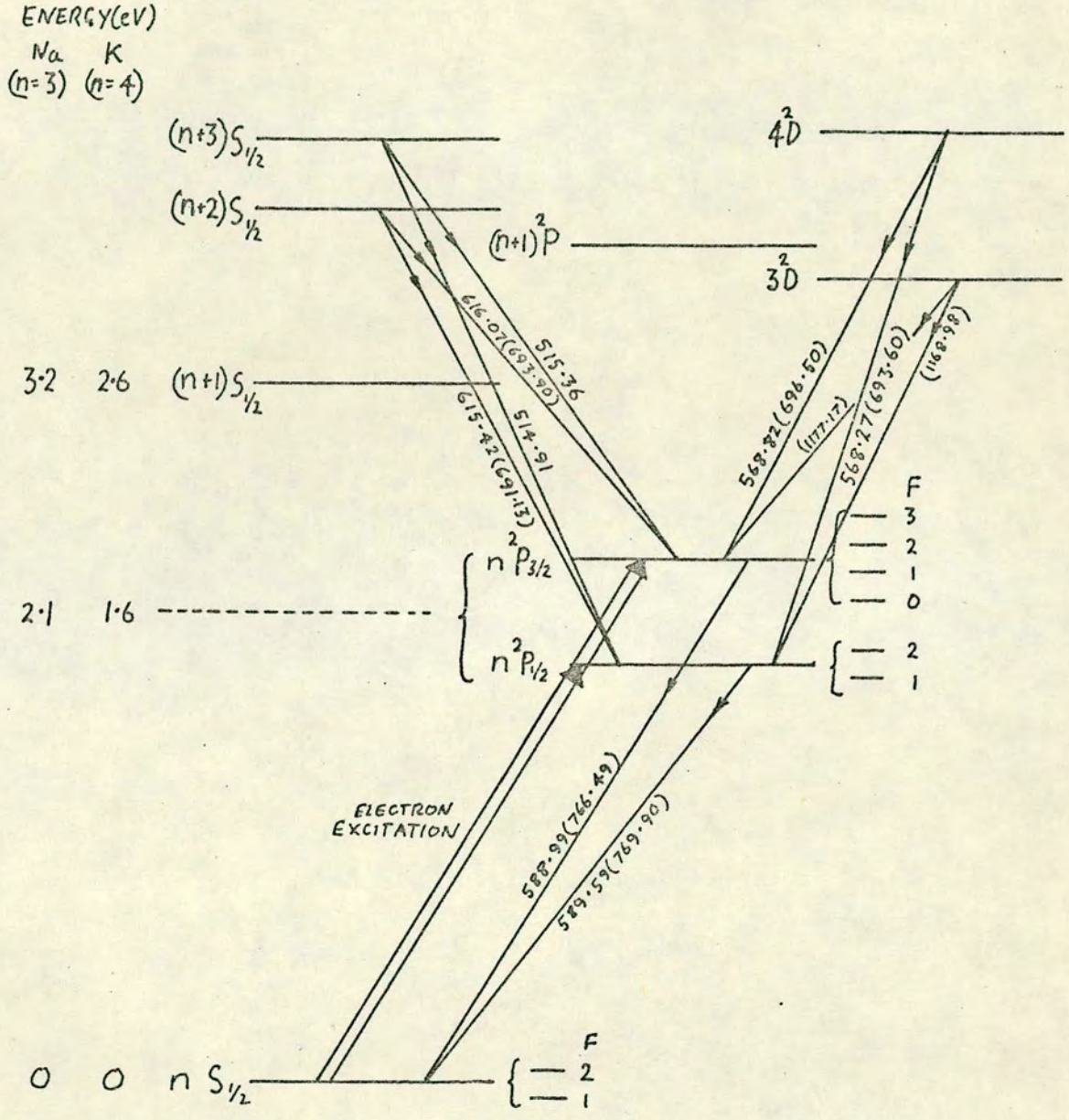

FIG. 1·1
TERM DIAGRAM FOR Na AND K

does not have perfect Russell-Saunders coupling and hence inter-combination transitions are allowed. It was necessary for Arriola et al. to take this into account and estimate the relative excitation probabilities of the singlet and triplet levels. Also, four parameters (λ_1, χ_1 and λ_3, χ_3; referring to singlet and triplet levels respectively) rather than two, are now involved and Arriola et al. make the assumptions $\lambda_1 = \lambda_3$ and $\chi_1 = \chi_3$, to facilitate the extraction of these parameters from the data.

To study the effects arising from the existence of hyper-fine structure it is necessary to use a material having a finite value of I. The abundant isotopes of the alkalis Na and K, all have $I = 3/2$, besides possessing a doublet structure in the first-excited state due to the fine-structure inter-action. They also have high excitation cross-sections for these states, and are conveniently produced as targets in the form of atomic beams. Moreover, due to the comparatively simple electronic structure, an amount of theoretical work has been carried out on scattering processes in which they are in-volved.

Wykes (1972a, b) has carried out theoretical investigations of the electron-photon coincidence rates for photons of different polarizations, for processes in which the resonance levels of Na and K are excited by electron impact in the incident energy range from threshold to 5.0 eV (see Fig. 1.1). The dependence of the [illegible] polarization on λ and χ was calculated (see Chapter 2). Also, the variation with electron-scattering and photon-emission angles was plotted. It is proposed in the pre-sent work to investigate the possibility of checking Wykes'

result empirically and of obtaining values of λ and $|\chi|$.

It was decided to work with Na initially as it is easier to deal with for two reasons: firstly, the excitation threshold for the Na resonance levels (2.1 eV) is greater than that for K (1.6 eV). The more energetic photons emitted in the decay of these levels are detected with greater efficiency. Secondly, the lifetime of the Na levels is 16 nsecs. (Schmieder, Lurio, Happer and Khadjari, 1970) which is significantly shorter than that of the corresponding levels of K (28 nsecs; Cunningham and Link, 1966). This implies better time resolution in the "Na" experiment and hence a shorter counting time for the same statistical accuracy (see section 3.2).

Subsequent work by Wykes (1973) has shown that if an experiment similar to the above is carried out using a polarized target, then provided that the degree of this polarization is known, it is possible, using an unpolarized beam of electrons and suitable photon detection angles, to determine the relative magnitudes and phases of the full set of six amplitudes (including those of spin-exchange) describing the excitation. This is in contrast to other experiments which have been proposed (Kleinpoppen, 1971) where it is necessary also to use a polarized electron beam and detect the polarization of the scattered electrons. It is also proposed, therefore, to plan the present experiment such that it may at a later date be used in investigations involving polarized targets.

The above facts determine the electron energy of 5.0 eV which will be used initially in the present experiment. This is the highest energy at which the calculations have been carried out and there are increasing difficulties due to space-charge

effects as one goes down in energy. Also the possibility of using the apparatus with a polarized target to study spin processes would imply the necessity to work in an energy region where the expected cross-section for spin-exchange is relatively high. The lower the energy, the higher is this cross-section and calculations by Moores and Norcross (1972) suggest that in the energy region around 5.0 eV the ratio of spin-exchange to total differential cross-section lies in the range 0.3 to 0.5.

Another method of determining angular momentum transfer amplitudes is being developed by Hertel and Stoll (1974). They produce target aroms in an excited hyperfine substate using a polarized dye-laser beam tuned to exact resonance. Incident electrons which are superelastically scattered are detected and it is shown that the resultant intensity depends on the amplitude for the excitation of the particular substate. It is also shown how the method can be interpreted as a time-reversed coincidence experiment.

CHAPTER 2

THEORETICAL BACKGROUND TO ELECTRON-PHOTON COINCIDENCE STUDIES

Percival and Seaton (1958) gave the first successful theory of the polarization of electron-impact radiation. Their results are those which would be obtained in an experiment where the scattered electron is not detected, the electron scattering directions being "averaged" over. Wykes (1972a,b) and Macek and Jaecks (1971) gave more general results retaining the dependence on electron scattering angle. Wykes' results were particularized to the case of the excitation of the alkali P states. His theory will be summarized below. In what follows primed quantities will refer to the initial states, unprimed ones to the intermediate (excited) states, and double-primed ones to final states.

Impulse excitation is assumed, the time of the collision being much shorter than the precession periods of $\underline{S}$ and $\underline{L}$ about $\underline{J}$ etc. For this reason, and because they are ultimately summed over, the initial states of the atom can be specified by the set of quantum numbers Γ' which is written for $\{M_S', M_L', S', L'\}$. Let Γ and Γ'' represent the sets of quantum numbers $\{J, F\ M_F\}$ and $\{J'', F'', M_F''\}$ respectively, defining the appropriate states of the atom.

Immediately after the excitation the atomic wavefunction will be:-

$$\psi(^2P_J) \equiv \sum_{M_S M_L M_J F M_F} f(m_S' M_S'\ m_S M_S M_L, \kappa, \theta, \phi) C^{F\ M_F}_{J\ \frac{3}{2}\ M_J M_I'}\ C^{J\ M_J}_{\frac{1}{2}\ 1\ M_S M_L}\ |\tfrac{3}{2}F, M_F\rangle$$

where f is the amplitude for the excitation from the given component of the $^2S_{\frac{1}{2}}$ ground state to that of the ^2P_J excited state with the emission of an electron of momentum κ into unit

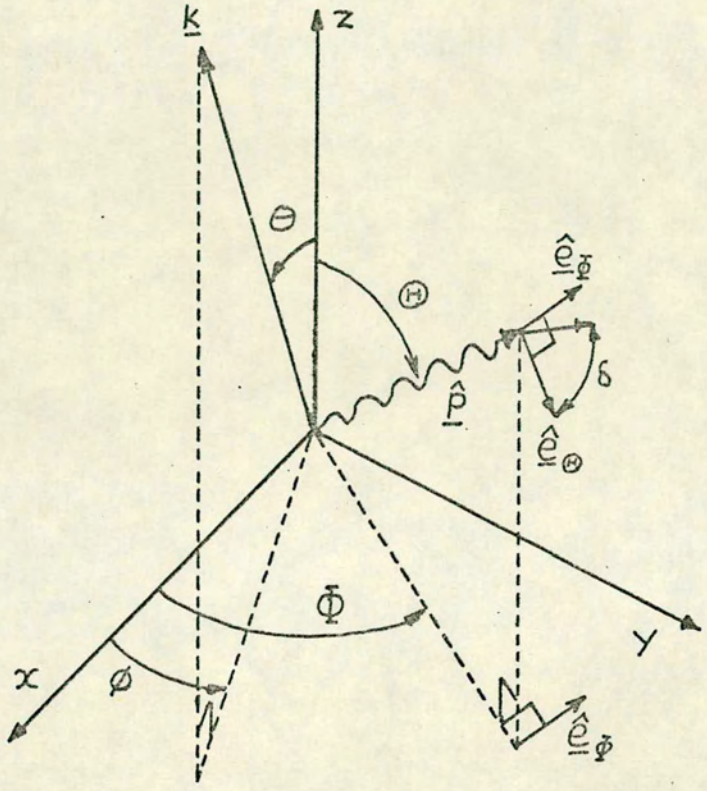

FIG. 2·1.
DEFINITION OF COORDINATES

solid angle about polar angles θ and ϕ (see Fig. 2.1). The m'_S and m_S are the appropriate spin projection quantum numbers of the continuum electron and the M_S and M'_S those of the bound electron. The C's are Clebsch Gordan coefficients. The assumption is made here that there is no overlap of the two P states so that they contribute incoherently to the resulting radiation.

These states evolve in time according to:-

$$\psi_J(t) = \sum_{\Gamma''} |\Gamma''\rangle\langle\Gamma''|U(t)|\psi(^2P_J)\rangle$$

where $U(t)$ is the evolution operator involving the interaction between the atomic electrons and the radiation field. The wavefunction has been expanded in terms of the set of eigenstates $\{|\Gamma''\rangle\}$.

The intensity of the resulting radiation emitted, at any time after the excitation, in a direction $\hat{\underline{P}}$ with direction of polarization $\hat{\underline{e}}$ is given by:-

$$W(\underline{\kappa};\hat{\underline{P}},\hat{\underline{e}}) \alpha \sum_{J\Gamma'\Gamma''m'_S m_S} |\langle\Gamma''|\psi_J(\infty)\rangle|^2.$$

It is here assumed that the doublet is not resolved, hence the sum over J.

Assuming that the impulse approximation holds, and using the above three relations:-

$$W(\underline{\kappa};\hat{\underline{P}},\hat{\underline{e}}) \alpha \sum_{\substack{J\Gamma'\Gamma'' \\ m'_S m_S}} \Big| \sum_{\Gamma M_S M_L M_J} \langle\Gamma''|\hat{e}\cdot\underline{P}|\Gamma\rangle f(m'_S\, M'_S\, m_S M_S M_L;\, \kappa,\theta,\phi) \times C^{F\ M_F}_{J\frac{3}{2}M_J M'_I}\, C^{J\ M_J}_{\frac{1}{2}1 M_S M_L} \cdot F(E)\Big|^2$$

where $\underline{P}$ is the electric dipole moment operator of the atom with respect to a plane perpendicular to $\hat{\underline{P}}$ and $F(E)$ is a measure

of the width of the individual excited hyperfine states. It occurs in the expansion of the above expression only as $F(E)F^*(E')$ which is equal to $[1 + i\varepsilon(E, E')]^{-1}$ where $\varepsilon(E,E')$ is given by :-

$$\varepsilon(E,E') = \left[E(J,F) - E(JF')\right] / h\gamma \ .$$

Here, $E(JF)$ is the energy of the hyperfine state $|JF\rangle$ and $h\gamma$ is the level width. $F(E)F^*(E')$ is thus a measure of the degree of overlap of the hyperfine states $|JF\rangle$ and $|JF'\rangle$.

The term $\hat{\underline{e}}.\underline{P}$ can be transformed using the fact that $\hat{\underline{e}}.\underline{P} = \hat{\underline{e}}.(\hat{\underline{e}}_{\Theta}\ \hat{\underline{e}}_{\Theta} + \hat{\underline{e}}_{\Phi}\ \hat{\underline{e}}_{\Phi}).\underline{p}$ (where Θ and Φ are the polar angles of photon emission and $\underline{p}$ is the electric dipole moment operator of the atom) and writing $\underline{p}$ in terms of its spherical components:- $p_0 (=p_z)$, and $p_{\pm 1} (\mp(p_x \pm ip_y)/\sqrt{2})$. Also, the resulting matrix elements can be simplified by transforming them ultimately to a representation $\{ILS\ M_I M_L M_S\}$ and writing the result in terms of the reduced matrix elements $\langle L''||\, p\,||\, L\rangle$ which is thus independent of the particular transition under consideration. A third step is concerned with the amplitudes f, and the fact that in the experiments envisaged the spins of the incident and scattered electrons are not observed. The expression for the intensity therefore has to be summed over initial and final spin states. Because of the orthogonality of the different spin functions of the scattered electrons, there are no interference terms involving different spins in the expansion of the modulus in the expression for W. Thus the spin-averaging results only in the amplitudes being replaced by averages. This leaves three different amplitudes corresponding to the three possible processes; $\Delta M_L = 0$, $\Delta M_L = \pm 1$. Finally it is shown that the

dependence of the amplitudes on M_L and ϕ is embodied in the term $\frac{M_L}{|M_L|} e^{-i M_L \phi}$ due to the reflection symmetry of the electron scattering, so that the amplitudes for the processes $\Delta M_L = \pm 1$ can be written $\pm e^{\mp i\phi} f(1,\kappa,\Theta)$. Thus the ϕ dependence can be factored out and there are only two different amplitudes to consider. These will be written $f(0,\kappa,\theta)$ and $f(1,\kappa,\theta)$ referring to the processes $\Delta M_L = 0$ and $\Delta M_L = \pm 1$ respectively. If the quantization axis is taken to lie along the direction of the incident electron beam then the final form of the expression for W is:-

$$W(\underline{\kappa};\underline{\hat{P}},\underline{\hat{e}}) \propto \sum_{JI'I''} (2J''+1) \Big| \sum_{\substack{FM_F \\ MM_J^{'}L}} \Big\{ -A_{-1}\underline{\hat{e}}\cdot(\underline{\hat{e}}_\Theta \cos\Theta + i\underline{\hat{e}}_{\bar{\Phi}}) e^{i(\bar{\Phi}-\phi)}/\sqrt{2} - A_0 \underline{\hat{e}}\cdot\underline{\hat{e}}_\Theta \sin\Theta$$

$$- A_{+1}\underline{\hat{e}}\cdot(\underline{\hat{e}}_\Theta \cos\Theta - i\underline{\hat{e}}_{\bar{\Phi}}) e^{i(\bar{\Phi}-\phi)}/\sqrt{2} \Big\} f(|M_L|,\kappa,\Theta) C^{FM_F}_{J\frac{1}{2}M_J M_I} C^{JM_J}_{\frac{1}{2}1MM_L''} F(E) \Big|^2 \qquad (2\cdot1)$$

where:-

$$A_q = (-1)^{-2J-F} [(2J+1)(2F+1)]^{\frac{1}{2}} W(JF,\tfrac{1}{2}F'';\tfrac{3}{2}1) W(1J,0\tfrac{1}{2};\tfrac{1}{2}1) C^{F''M_F''}_{F1M_F q}$$

Here, the W's are Racah coefficients.

When the above expression is expanded, it is of the form:-

$$W(\underline{\kappa};\underline{\hat{P}},\underline{\hat{e}}) \propto a(\Theta,\bar{\Phi}-\phi,\underline{\hat{e}}) |f(0,\kappa,\theta)|^2 + b(\Theta,\bar{\Phi}-\phi,\underline{\hat{e}}) |f(1,k,\theta)|^2$$

$$+ c(\Theta,\bar{\Phi}-\phi,\underline{\hat{e}}) |f(0,\kappa,\theta)| |f(1,\kappa,\theta)| \cos\chi$$

The correlation function measured by Eminyan et al. (1973, 1974) is of exactly the same form as this. But the expressions for the coefficients a, b and c are simpler due to the absence of fine and hyperfine structures. They are also averages over photon polarization states which are not observed. Eminyan et al. define a parameter λ as:-

$$\lambda(\kappa,\theta) = |f(0,\kappa,\theta)|^2 \; / \; 2|f(1,\kappa,\theta)|^2 + |f(0,\kappa,\theta)|^2 \quad .$$

λ is thus the ratio of the differential cross-section for excitation of the $M_L = 0$ substates (σ_o) to the total differential cross-section (σ). In terms of these parameters the quantity measured is given by

$$W'(\underline{\kappa},\hat{\underline{P}}) = F\sigma_o \left[a + b(1-\lambda)/2\lambda + c\sqrt{(1-\lambda)} \cos\chi/\sqrt{2\lambda}\right] \quad (2.2)$$

F is a factor depending on the absolute value of the electron beam intensity, the atomic-target density, beam overlap volume, and detector efficiencies. Providing F remains constant, a minimum of three measurements of W', each at a different angle Θ, is sufficient to determine the quantities λ, $|\chi|$, and $(F\,\sigma_o)$. However, Eminyan et al. chose to measure at a greater number of angles and to select λ and $|\chi|$ by means of a least squares fit of equation (2.2) to their data. No attempt was made to estimate σ_o presumably due to the difficulties involved in determining F. To check the constancy of F, a quantity proportional to it (namely the "singles" counting rate in the electron channel) was monitored.

The effect of drift in causing variations in F can be overcome by letting a predetermined value of total counts accumulated in the "singles" channel, determine the counting

period; by periodically scanning the detector through the range of positions at which measurements are required, counting at each position for the same period; or by use of a minimum of three photon detection channels (of known relative efficiency), counting simultaneously at different positions. A drawback of the scanning method is the possibility of systematic errors due to variations in solid angles and local fields, as the detector is traversed. In the case of the multi-detector method, severe problems would be encountered if it were necessary to apply corrections for time-dependent drifts in the detector efficiencies.

An equivalent method to that of Eminyan et al. is to measure the coincidence rates $W(\underline{\kappa};\hat{\underline{P}},\hat{\underline{e}})$, defined in equation (2.1), for two orthogonal polarization states, $\hat{\underline{e}}_{\Theta}$ and $\hat{\underline{e}}_{\Phi}$. This gives the polarization $\Pi(\kappa,\theta,\Theta,\Phi-\phi)$ defined by:-

$$\Pi(\kappa,\theta,\Theta,\Phi-\phi) = \frac{W(\underline{\kappa};\hat{\underline{P}},\hat{\underline{e}}_{\Theta}) - W(\underline{\kappa};\hat{\underline{P}},\hat{\underline{e}}_{\Phi})}{W(\underline{\kappa};\hat{\underline{P}},\hat{\underline{e}}_{\Theta}) + W(\underline{\kappa};\hat{\underline{P}},\hat{\underline{e}}_{\Phi})}$$

The effect of drift in beam intensities etc., is eliminated due to the simultaneous measurement (the factor F cancels in the above expression) and provided the relative efficiencies of the two photon detection channels are known (see Appendix I) then the correct value of Π can be obtained. Wykes (1972) showed that for alkalis with $I = {}^{3}/_{2}$, Π is given by:-

$$\Pi(\kappa,\theta,\Theta,\Phi-\phi) =$$

$$\frac{3\xi\{\sin^2\Theta|f(0,\kappa,\theta)|^2-[\sin^2\Theta-(1+\cos^2\Theta)\cos2(\Phi-\phi)]|f(1,\kappa,\theta)|^2+\sqrt{2}\,R\sin2\Theta\cos(\Phi-\phi)}{\{1+\xi(1-3\cos^2\Theta)\}|f(0,\kappa,\theta)|^2+\{2-\xi(1-3\cos^2\Theta)-3\xi\sin^2\Theta\cos2(\Phi-\phi)\}|f(1,\kappa,\theta)|^2+3\xi/\sqrt{2}\,R\sin2\Theta\cos(\Phi-\phi)}$$

where $\xi = \{54 + 20[1+\varepsilon^2(3,2)]^{-1} + 21[1+\varepsilon^2(3,1)]^{-1} + 30[1+\varepsilon^2(2,1)]^{-1} + 25[1+\varepsilon^2(2,0)]^{-1}\}/1200$

and $\mathcal{R}$ = real part of $f(0,\kappa,\theta)f^*(1,\kappa,\theta)$

It has been assumed that the external magnetic field is sufficiently small that the magnetic substates of a particular hyperfine level can be considered degenerate so that $F(E)$ is independent of M_F.

Wykes (1972) has evaluated ξ for the abundant isotopes of Na and K, from experimental spectroscopic data and obtained :

$$\xi(^{23}\mathrm{Na}) = .0492; \quad \xi(^{39}\mathrm{K}) = .0595; \quad \xi(^{41}\mathrm{K}) = .0889.$$

Putting $\Theta = 90^\circ$ and $f(1,\kappa,\theta) = 0$ to represent forward electron scattering or threshold excitation, gives

$$\Pi = 3\xi/(1+\xi) .$$

This parallels the situation studied by King et al. (1972) referred to in Chapter 1. The effects of hyperfine splitting and level widths are contained in the parameter ξ.

For $\Theta = 45^\circ$ and $(\Phi-\phi) = 180^\circ$ the interference term (that containing $\mathcal{R}$) is a maximum and the polarization is given by:-

$$\Pi(\kappa,\theta,45^\circ,180^\circ) = \frac{3\xi\{(|f(0,\kappa,\theta)|^2 + 2|f(1,\kappa,\theta)|^2) - \sqrt{8}|f(0,\kappa,\theta)||f(1,\kappa,\theta)|\cos\chi\}}{(2-\xi)(|f(0,\kappa,\theta)|^2 + 2|f(1,\kappa,\theta)|^2) - 3\sqrt{8}|f(0,\kappa,\theta)||f(1,\kappa,\theta)|\cos\chi}$$

(2.3a)

Defining r as the ratio $|f(1,\kappa,\theta)|/|f(0,\kappa,\theta)|$ the above expression becomes:-

$$\Pi(\kappa,\theta,\ 45^{o},180^{o}) \quad = \quad \frac{3\xi\{(1+2r^{2})-\sqrt{8}r\cos\chi\}}{(2-\xi)(1+2r^{2})\ -\ 3\sqrt{8}r\cos\chi} \qquad (2.3b)$$

r and λ are related by $r^{2} = (1-\lambda)/2\lambda$.

Equations (2.3a and b) describe the situation in which the photon is emitted in the plane of electron scattering. For certain other geometries the interference term vanishes making it possible to determine r or λ directly. For instance if photons are detected which are emitted in a plane perpendicular to that of electron scattering $((\Phi-\phi) = 90^{o})$ then the polarization is given by:-

$$\Pi(\kappa,\theta,\ 45^{o},\ 90^{o}) \quad = \quad \frac{3\xi\{|f(0,\kappa,\theta)|^{2}\ -\ 4|f(1,\kappa,\theta)|^{2}\}}{(2-\xi)|f(0,\kappa,\theta)|^{2}\ +\ 4(1+\xi)|f(1,\kappa,\theta)|^{2}} \qquad (2.4a)$$

or, in terms of r :-

$$\Pi(\kappa,\theta,\ 45^{o},90^{o}) \quad = \quad \frac{3\xi(1-4r^{2})}{(2-\xi)\ +\ 4(1+\xi)r^{2}} \qquad (2.4b)$$

Thus, having measured r or λ, it is then possible to determine $|\chi|$ by then carrying out a measurement of the type described in equations (2.3a, b).

In the present work it was decided, for various mechanical reasons to adopt the coplanar geometry in the first instance to test the feasibility of carrying out the above type of measurement.

Wykes (1972), using the T matrices of Karule and Peterkop's 8 partial wave, two-state, close-coupling calculations (1965),

has calculated $\Pi(\kappa,\theta, 45^{\circ},180^{\circ})$ and $\Pi(\kappa,\theta, 45^{\circ},90^{\circ})$ for θ in the range $0 - 180^{\circ}$. This has been carried out for Na and K for the energy ranges 2.5 - 5.0 eV and 1.8 - 5.0 eV respectively. More recently, these T matrices have been calculated for electron-sodium scattering using a four-state close-coupling approximation with up to 28 partial waves (Moores and Norcross, 1972).

A variation on the above method involving the measurement of Π, is one depending on the measurement of a polarization $\Pi(\delta)$ defined in terms of intensities $W(\delta)$ and $W(\delta + 90^{\circ})$ as follows:-

$$\Pi(\delta) = (W(\delta) - W(\delta+ 90^{\circ})/(W(\delta) + W(\delta+90^{\circ})) \quad .$$

$W(\delta)$ is the intensity of a polarization component making an angle δ with a fixed direction (see Fig. 2.1).

An expression for $\Pi(\delta)$ can be obtained from the theory of Wykes (1972a, b) or from that of Macek and Jaecks (1971). The following result is obtained for the convenient geometry $\textcircled{H} = \Phi-\phi = 90^{\circ}$:-

$$\Pi(\kappa,\theta,90^{\circ},90^{\circ};\delta) =$$

$$\frac{3\xi}{1+\xi}\left\{\frac{|f(0,\kappa,\theta)|^2-2|f(1,\kappa,\theta)|^2}{|f(0,\kappa,\theta)|^2+2|f(1,\kappa,\theta)|^2}\cos 2\delta + \frac{2\sqrt{2}\,|f(0,\kappa,\theta)||f(1,\kappa,\theta)|\cos\chi}{|f(0,\kappa,\theta)|^2+2|f(0,\kappa,\theta)|^2}\sin 2\delta\right\}$$

or, in terms of λ:-

$$\Pi(\kappa,\theta,90^{\circ},90^{\circ};\delta) = \frac{3\xi}{1+\xi}\{(2\lambda-1)\cos 2\delta + 2\sqrt{\lambda(1-\lambda)}\cos\chi\sin 2\delta\}$$

λ could be obtained directly by measuring $\Pi(\kappa,\theta, 90^{\circ},90^{\circ},0)$. This could be done using a single photon detector and counting with a polarization analyzer in each of the two positions $\delta = 0^{\circ}$ and $\delta = 90^{\circ}$ (or 180° and 270°) for the same fixed periods and repeatedly cycling through this process to eliminate the effects of drifts. Having obtained a value for λ, $|\chi|$ could then be obtained by measuring $\Pi(\kappa,\theta, 90^{\circ}, 90^{\circ}; 45^{\circ})$. This involves the same process as before but the measurement positions would be $\delta = 45^{\circ}$ and $\delta = 135^{\circ}$ (or 225° and 315°). It is obvious that the two measurements could be conducted "simultaneously", the analyzer being cycled repeatedly through the eight angular positions.

It should be noted that because only one detector is used here, then for the same statistical uncertainty, a measuring time is required which is twice as long as that necessary in the previous method where it is proposed to use two detectors. On the other hand the use of one photon detector makes the determination of relative detector efficiencies unnecessary. It is proposed to investigate the possibility of carrying out a measurement of λ and $|\chi|$ in this fashion after the feasibility of the present method has been established.

CHAPTER 3

THE COINCIDENCE TECHNIQUE

3.1 Introduction

The coincidence technique was originally developed for application in the field of nuclear physics (Wapstra, 1965; Bell, 1965). It appears to have been first used in the study of atomic phenomena by Heron, McWhirter, and Rhoderick (1954) who obtained the lifetime of the $3^3P - 2^3S$ transition in He by measuring the coincidence rate versus delay between incident electron beam pulses and emitted photons of the appropriate frequency, selected by an interference filter. Population of the 3^3P State by cascading from higher states with unknown lifetimes led to uncertainty in the interpretation of the result in terms of the 3^3P lifetime.

Kaul (1966) overcame this difficulty in the case of the $6^3P_1 - 6^1S_0$ transition in Hg, by exciting the 6D states by electron impact at 30 eV, and detecting the photon emitted in the $6D - 6^3P_1$ transition. The spectrum of time delays between these photons and those emitted in the $6^3P_1 - 6^1S_0$ transition was obtained by operating the "start" gate of a time-to-amplitude converter (TAC) with the pulses due to the first photon, and using the second photon pulse as the "stop" signal. The output pulses of the TAC have amplitudes proportional to the time delay between the "start" and "stop" signals. These output pulses were analyzed and stored in a multichannel analyzer (MCA).

Imhof and Read (1970, 1971) originated the electron-photon coincidence technique with its use in their measurement of the lifetimes of the 3^3D, 4^3S and 4^1S states of He. An electron

having excited the state of interest, passed through an appropriately-tuned energy analyzer and was detected in a channel electron multiplier (CEM). The time of detection minus the electron flight time marked the time of excitation of the state of interest. The photon emitted in the decay of this state was selected with an interference filter and was then detected in a photomultiplier. The spectrum of delays between the detector pulses due to these electron and photon events, were recorded using the method of Kaul. This spectrum contained the lifetime curve.

Cascade effects were eliminated as the state in question was selected by applying a double constraint:- electron energy and photon wavelength. Electron energies in the incident beam were 30, 50 or 240 eV depending on the state being studied. Energy resolution was 0.23% overall. Time resolution was 10.5 nsecs using the leading edge method (see section 3.4).

A similar technique to the above was used by King, Adams and Read (1972) in their study of the threshold polarization in He, described in Chapter 1.

King and Adams (1974) and King, Adams and Cvejanovic (1975) again used the same method to measure the lifetime of states of Hg.

Pochat, Rozuel and Peresse (1973) were able to measure the differential cross-sections for excitation of the states 4^1S, 4^1D, 5^1S and 5^1D of He using the electron-photon coincidence technique. These states could not be resolved purely by electron spectroscopy.

The work of Eminyan et al. (1973, 1974) has already been mentioned in Chapter 1. The scattered electron and U.V. photon were each detected in a CEM. Energy resolution was ·25 eV at 80 eV incident energy. Overall time resolution using constant

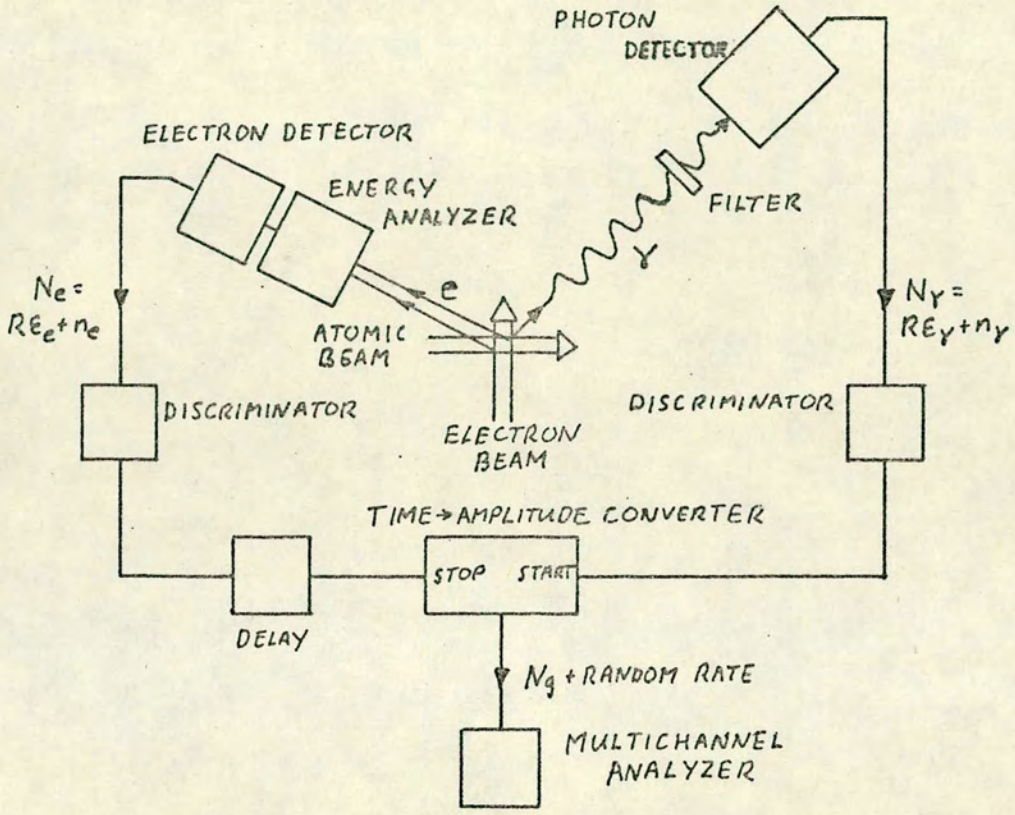

FIG. 3·1
SCHEMATIC ELECTRON-PHOTON COINCIDENCE EXPERIMENT

fraction timing discrimination was 6.4 nsecs. (see section 3.4).

Experiments conducted by Arriola et al. (1975) and McConkey et al. (1975) using the method of electron-photon correlations have also been described in Chapter 1. Again, the use is to be noted of a CEM as a detector of the u.v. photons in both these experiments. The time resolution in the latter case is quoted as 10 nsecs.

3.2 Theory of the Delayed Coincidence Technique as Applied to Electron-Photon Correlations

Consider the typical electron-photon coincidence experiment shown in Fig. 3.1. Let R be the source strength (i.e. the number of excitations per second of the level under study). Let ε_γ and ε_e be the overall counting efficiencies of the photon and electron channels respectively, and let $n_c(t)dt$ be the total coincidence rate due to a small portion, dt, of the range of the TAC, occurring a time t after the arrival of a "start" pulse. T is the net delay between the arrival of a "start" pulse and that of the corresponding "stop" pulse, for the case where an electron and a photon are simultaneously emitted from the interaction region. This delay includes that due to:- the electron flight time between interaction region and detector; electron transit times in the detectors, and excess cable length introduced into the "stop" channel.

The correlation which naturally exists between a photon emitted in the decay of a state and the scattered electron resulting from the excitation of this particular state, gives rise to the genuine coincidence rate N_g. That part of N_g which is due to a small portion dt of the converter range, is given by:-

$$n_g(t)dt = R\varepsilon_e\varepsilon_\gamma f(t - T)dt$$

where $f(t)$ is the overall resolution function. It is the convolution of the instrumental time resolution function $g(t)$ (due to time fluctuations in analyzer, detectors and electronics), and the function $h(t)$ which represents the time-dependence of the photon-emission process. $g(t)$ is assumed to have a gaussian form, while for the cases to be considered $h(t)$ is of exponential form. It will be assumed that $f(t)$ is normalized such that:-

$$\int_{-\infty}^{+\infty} f(t)dt = 1 \quad .$$

Even for uncorrelated events in the "start" and "stop" channels there is a finite probability that a "stop" signal will occur within a time interval dt, a time t after a "start" signal. This will give rise to a random coincidence rate, $n_r dt$. The above probability is $R\varepsilon_e dt$. Thus the rate of random coincidences is $R^2\varepsilon_\gamma\varepsilon_e dt$ or $N_\gamma N_e dt$, where N_γ and N_e are the "singles" counting rates in the photon and electron channels. In general, however, these channels will contain other events also, which are not derived from the process under study. For instance the electron-energy analyzer will not be perfect and the electron detector will register the arrival of electrons which have either undergone only elastic scattering,or have derived from the excitation of states other than the one of interest. Spurious events will also be recorded in the photon channel due to: photocathode dark current (if a photomultiplier is used); photons from some other transition which are admitted due to the finite resolution of the interference filter; and also "stray" photons from sources such as

the electron gun filament and ionization gauges. These spurious events will be included together in the rates n_γ and n_e. The total singles rates will therefore be given by:-

$$\begin{aligned} N_\gamma &= R\varepsilon_\gamma + n_\gamma \\ N_e &= R\varepsilon_e + n_e \end{aligned} .$$

The random coincidence rate is thus given by:-

$$n_r dt = N_\gamma N_e dt .$$

The quantity of interest is the total genuine coincidence rate N_g given by:-

$$N_g \equiv \int_{-\infty}^{+\infty} n_g(t)dt \equiv R\varepsilon_\gamma\varepsilon_e \int_{-\infty}^{+\infty} f(t-T)dt \equiv R\varepsilon_\gamma\varepsilon_e \tag{3.1}$$

This is not directly measurable due to the presence in the time spectrum of the term $n_r dt$. A quantity which can be obtained directly is the total coincidence rate N_c defined by:-

$$N_c \equiv \int_{T-\tau/2}^{T+\tau/2} n_c(t)dt = \int_{T-\tau/2}^{T+\tau/2} (n_g(t)+n_r)dt = \int_{T-\tau/2}^{T+\tau/2} n_g(t)dt + n_r\tau .$$

This integration is carried out over a finite portion (τ) of the time spectrum which includes the contribution from $f(t - T)$. The total random coincidence rate (N_r) can be obtained directly by carrying out the integration over a portion of the spectrum of width $m\tau$ where $f(t - T)$ is negligible. N_r is defined by:-

$$N_r \equiv \frac{1}{m}\int_{t'-m\tau/2}^{t'+m\tau/2} n_r dt = n_r\tau = N_\gamma N_e \tau, \quad m > 1. \tag{3.2}$$

The difference between N_c and N_r is given by:-

$$N_c - N_r = R\varepsilon_\gamma\varepsilon_e \int_{T-\tau/2}^{T+\tau/2} f(t-T)dt = R\varepsilon_\gamma\varepsilon_e \int_{-\tau/2}^{+\tau/2} f(t)dt .$$

The form of $f(t)$ implies that τ can be made sufficiently large to ensure that $\int_{-\tau/2}^{+\tau/2} f(t)dt$ is close to unity. In this case N_g is given by:-

$$N_g = N_c - N_r.$$

Obviously τ should be as small as possible to ensure the above condition otherwise the statistical uncertainty in N_r will dominate that of N_g. This choice of τ defines the time resolution.

The measurements of the "singles" rates N_γ and N_e obviously present no difficulties and in some instances it will be also possible to measure n_γ and n_e (or they may be negligibly small). In these cases $R\varepsilon_\gamma$ and $R\varepsilon_e$ can be determined and hence also R, ε_γ, and ε_e using N_g (Dunworth, 1940).

It should be noted that if n_γ and n_e contain contributions from the same transition then there will be a contribution to the coincidence rate which will be indistinguishable from the genuine one. This may also be the case even if n_γ contains no contributions from impact radiation. For instance if n_e contains contributions from the excitation of a state higher in energy than the one of interest, the latter may be populated by cascading and hence N_γ will contain events due to correlated photons.

If measurements are carried out for a time t, the number of genuine coincidences will be:-

$$N_g t = N_c t - N_r t .$$

The variance in this quantity will be given by:-

$$\sigma^2(N_g t) = \sigma^2(N_c t) + \sigma^2(N_r t) .$$

Because, in general, $N_r t$ can be obtained by averaging over a time $m\tau$ $(m > 1)$, its variance is given by

$$\sigma^2(N_r t) = N_r t/m .$$

Thus:-

$$\sigma^2(N_g t) = N_c t + N_r t/m = N_g t + (1 + \tfrac{1}{m})N_r t .$$

The relative standard deviation (ρ) is defined by:-

$$\rho^2 \equiv \left(\frac{\sigma(N_g t)}{N_g t}\right)^2 = \frac{1 + (1 + \frac{1}{m})N_r/N_g}{N_g t} .$$

So that for a given value of ρ the necessary counting time will be:-

$$t = \frac{1 + (1 + \frac{1}{m})N_r/N_g}{N_g \rho^2} \qquad (3.3)$$

or, in terms of R, ε_γ, ε_e, n_γ, n_e and τ:-

$$t = \frac{1 + (1 + \frac{1}{m})R\tau(\varepsilon_\gamma + n_\gamma/R)(\varepsilon_e + n_e/R)/\varepsilon_\gamma\varepsilon_e}{R\varepsilon_\gamma\varepsilon_e \rho^2} . \qquad (3.4)$$

Given a typical set of values for the parameters occurring in this expression it would be then possible to decide which parameters to change in order to achieve the most efficient reduction

of t.

The quantities R, ε_r, and ε_e are related to other physical quantities as follows:-

$$R = \frac{iN_A Q}{eA} \tag{3.5}$$

where i is the electron current passing through the interaction volume of cross-sectional area A; N_A is the number of atoms in the interaction volume; Q is the total cross-section for excitation of the state of interest; and e is the electronic charge.

$$\varepsilon_i = \frac{\eta_i}{Q} \int \sigma_i d\Omega_i \tag{3.6}$$

where η_i is the efficiency of the detector in the appropriate channel, (including the transmission of the energy, or wave-length analyzer), σ_i is the differential cross-section for the process concerned, and the integration is carried out over the solid angle subtended by the appropriate detectors at the interaction-region.

3.3 Estimate of Count Rates and Counting Time

i, A It will be shown in Chapter 4 that at 5.0 eV the maximum current allowed by the effects of space-charge, that can be put into a 1 mm diameter spot with a maximum convergence angle of 2.0° is 5.2×10^{-7} amps. This will be the value assumed for i, while A will be taken as 8×10^{-7} m^{-2}.

N_A Experience and calculation (see section 4.6) suggest that an Na atomic beam density of approximately 5×10^{15} atoms m^{-3} should be possible. Assuming that a 1.0 mm diameter electron beam intersects at right angles a 2.0 mm diameter atomic beam, and taking the interaction volume to be a cylinder of cross-sectional area 8×10^{-7} m^2 and length 2×10^{-3} m gives $N_A = 8.0 \times 10^6$ atoms.

Q Measurements by Zapesochnyi and Shimon (1965) and by Enemark and Gallagher (1972) both give values for Q of 2.0×10^{-19} m^2 for excitation of the Na resonance levels by electron impact at 5.0 eV.

η_γ The photon detection efficiency is made up of: (a) The transmission of the interference filter, typically 0.7. (b) The transmission (including the effects of absorption and reflection losses) of all the other optical components (e.g. Wollaston prism, lenses, mirrors, windows), estimated to be 0.6. (c) The quantum efficiency of the photomultiplier photocathode. The most sensitive photocathode, in the wavelength region of interest, available,was the extended S20 having a quantum efficiency at 590 nm of .095. (d) The collection efficiency of the photocathode (K) - first dynode (D1) electrode structure. If it is assumed that the tube is run with the optimum K-D1 voltage then the collection efficiency will typically be 0.9. (e) Discriminator level settings. As will be discussed later, with the timing electronics adopted there is no virtue in having these levels set very high. They are in fact set as low as is possible without triggering an electronically generated noise. Under these conditions the loss in counts will be small and will be neglected here. (f) A factor 0.5

should be included to take account of the effect of the polarization analyzer (a Wollaston prism), assuming the degree of polarization of the incident light to be small. One thus obtains a net photon detection efficiency $\eta_\gamma = \cdot 017$.

η_e The electron detection efficiency has contributions from: (a) The transmission of the energy analyzer. It is difficult to give an a priori estimate of this quantity. However measurements made of incident and transmitted currents, during testing of the completed analyser (see section 4.5) suggest a value of approximately 0.25. This would be contributed to by the 80% transparent micromesh used to shield the analyser field from the high potential applied to the CEM. (b) The efficiency of the electron detector. Because of its small size, and the saturation property of its gain, the use of a channel electron multiplier (CEM) will be assumed. There is a wide variation amongst the different measurements of CEM efficiency. Bosqued and Reme (1967) measured the efficiency of a Bendix 4010 and gave values of 0.4 at 100 eV incident energy, rising to 0.9 at 400 eV. Sharber, Winningham and Sheldon (1968) measured the efficiency of a CEM, the exact type being unspecified excepting the fact that it had a spiral structure and a funnelled mouth. They obtain efficiencies in the range 0.5 to 0.7 (maximum) in the energy range 80 - 600 eV. Borodini (1971) measured the relative efficiencies of a Bendix 4028 resorting to calculation at a single energy to put these in absolute terms. Values obtained were 0.4 at 10 eV rising to 0.9 at 100 eV and peaking near to 1.0 in the range 150 - 250 eV. It was also shown that the efficiency was fairly insensitive to supply voltage. It is proposed in the present work to accelerate the electrons through a potential difference of 90 V

before allowing them to impinge on the CEM mouth. It is also proposed to use a Mullard CEM type B312BL/01 due to its small size and its comparatively large, conveniently-shaped rectangular mouth. It is unlikely that a value smaller than that obtained by Bosquet and Reme will be encountered and an efficiency of 0.4 will therefore be assumed. (c) Discriminator level settings. Because of the approximately poissonian form (due to the saturation of the gain) of the CEM pulse height distribution, the discriminator setting has little effect on counting efficiency even up to relatively high values. As a CEM is used it "ages" and its gain falls, the pulse height distribution becomes more asymmetric with the peak at lower amplitudes and eventually it takes on an exponential form. Under these conditions the discrimination level has an increasingly greater effect on efficiency. For the purpose of these estimates it will be assumed that the CEM is "new" and the effect of the discriminator level will be neglected. The above considerations give $\eta_e = 0.10$.

σ_γ There is little information on this quantity. It will be assumed that photon emission is uniform so that $\sigma_\gamma = Q/4\pi$.

σ_e This cross-section becomes greater at smaller angles of scattering. Initially it will be desirable to conduct measurements at the smallest possible angle. This is determined by the requirement that the analyzer does not intercept the line of the incident electron beam. The angle will be assumed to be 10°. Moores and Norcross (1972) give $\sigma_e = 1.8 \times 10^{-19}$ m^2 for Na at 10° and 4.0 eV.

$\int d\Omega_\gamma$ A design for an optical system having a rectangular entrance aperture of 2.0 × 7.0 mm. at a distance of 27 mm from the interaction centre, gives (taking into account the finite size of the interaction volume) a maximum horizontal entrance angle at 3.5° and a maximum vertical angle of 8.5°. This gives reasonably good angular resolution in the plane in which θ varies (the horizontal plane) and a solid angle subtended by the aperture at the interaction centre, of 1.9×10^{-2} steradians.

$\int d\Omega_e$ A design for an electron energy analyzer having an effective entrance aperture of dimension 1.0 × 1.0 mm, a distance of 40 mm from the interaction centre gives a maximum entrance angle in both vertical and horizontal directions of 1.5°. The solid angle subtended at the interaction centre is 6.2×10^{-4} steradians.

τ The time resolution is determined by contributions from four sources: (a) Transit-time fluctuations in the detectors of the order of 1.5 nsecs. (b) The timing electronics. It is shown in the next section that the chosen electronic system has a resolution (FWHM) of approximately 14 nsecs. (c) Transit time variations in the energy analyzer. Due to the finite angular range of acceptance angles of the analyser and the finite energy resolution, a variation of approximately 3 nsecs among the various possible trajectories is expected (see section 4.5). (d) The lifetime of the state under study will contribute to the variation in delay times between the arrival of a photon in a detector and the arrival of the corresponding electron. The lifetime of the 3P states of Na is 16 nsecs. If it is assumed for the purpose of calculation that these quantities combine as if they referred to the widths

(FWHM) of normal distributions, a resultant width of 22 nsecs is obtained. However this would be slightly optimistic especially in view of the nature of the lifetime curve. A value of twice this amount will therefore be taken, i.e. $\tau = 44$ nsecs.

Using these quantities R, ε_γ and ε_e may be calculated, making the assumption in the case of ε_e that σ_e can be taken to be constant over the detector solid angle. The results for Na, using an incident energy of approximately 5.0 eV and a scattering angle of around 10°, are (using (3.5) and (3.6))

$$R = 6.50 \times 10^6 \text{ excitations/sec.}$$
$$\varepsilon_\gamma = 2.57 \times 10^{-5}$$
$$\varepsilon_e = 5.58 \times 10^{-5} \ .$$

The genuine coincidence rate is now given by (3.1) as $N_g = 33$/hour, the photon signal rate by $R\varepsilon_\gamma = 160$/sec, and the electron signal rate by $R\varepsilon_e = 360$/sec. This difference in counting rates in fact determines (assuming n_e and n_γ are in roughly the same proportion) that the photon channel should drive the "start" input of the TAC so that dead-time is minimized.

Before the random coincidence rate can be calculated estimates have to be made of n_γ and n_e ..

n_γ There will be two main contributions to this quantity:

(a) Photomultiplier dark current. The lowest limit to the dark current is achieved on cooling to below -40°C. The manufacturers' specifications for the relevant tube give for the dark current under these conditions, a value of 10/sec.

(b) Stray light from the electron gun filament. This cannot

be estimated a priori. It will be assumed to be of the same order as the dark current so that the total value of n_γ is 20/sec.

n_e Again it is difficult to estimate this quantity. Even for what in principle would be an analyzer with extremely good resolution, the measured resolution would be inferior due to space charge effects and, more importantly, the high reflection coefficient for electrons of metallic surfaces at the low energies envisaged (Marmet and Kerwin, 1960; McGowan, 1967). It will be assumed that n_e is of the same order as the signal rate. i.e. n_e = 500/sec.

The random rate can now be calculated from (3.2) and is given by:-

$$N_r = 25/\text{hour}.$$

Before the counting time can be calculated from (3.3) or (3.4) it is necessary to decide on a value of ρ. The quantity to be measured is the polarization Π, given in terms of the two mean genuine coincidence rates (N_{g1}, N_{g2}) due to photons of mutually orthogonal polarization states (see Appendix Ia). If t is the counting time, and A the channel asymmetry:-

$$\Pi = (N_{g1}t - N_{g2}t)/(N_{g1}t + N_{g2}t) - A .$$

It is shown in Appendix IIa that, provided Π is small, the standard deviation in Π is given by

$$\sigma^2(\Pi) = \frac{1}{2}\frac{\sigma^2(N_g t)}{(N_g t)^2} = \frac{\rho^2}{2} .$$

In the energy and angular range considered, the calculations of Wykes (1972) indicate a variation of the polarization

in the range 0 - .08. So that if $\sigma(\Pi)$ is required to be .014 then a value for ρ of .02 is necessary. Equation (3.3) now gives, assuming that the term $^1/m$ can be neglected:-

$$t = 133 \text{ hours } (5\tfrac{1}{2}\text{days}).$$

Due to the uncertainty as to the value of the above parameters this result can only be regarded as a rough guide. Although the value of N_g obtained is expected to be correct to within a factor 2, no such limit can be placed on the estimate of N_r as this depends critically on n_e and n_r the values of which, so far, can only be guessed at.

The above order of counting time is not unreasonable in an experiment of this nature. Fluctuations in electron and atomic beam intensities over this time will be unimportant due to the fact that the parameter of interest (the polarization) depends only on the ratio of two intensities which are measured simultaneously. The only trouble may come from drift of the photomultiplier gains and efficiencies, invalidating any prior calibration of the relative channel efficiency. This would really entail the monitoring of thisquantity throughout the duration of the run by, for example, rotating the Wollaston prism periodically through 180° so that each channel samples both polarization states for equal times. In this way any variation with time of the relative channel efficiency can be compensated whilst making optimum use of available counting time. (See Appendix Ib.) It only remains to measure and correct for the relative transmissions of the two states of polarization through the Wollaston. For the time being, this will not be done. The relative channel efficiencies will be measured once

and for all and reliance will be placed on the stability of the photomultiplier voltage supplies. The validity of this approach can be judged by checking the repeatability of the polarization measurements. If necessary, the rotating-Wollaston method will be developed for use in subsequent experiments.

It should be noted that the above estimate of counting time differs substantially from that (19 hrs.) made by Wykes (1972b) for the same situation. This is because of over-estimates by Wykes of: (i) The size of the interaction volume. Wykes assumed $A = 2.5 \times 10^{-5} m^2$. This would give poor angular resolution. (ii) The electron collection solid angle. This was assumed to be 3×10^{-2} Str. It would be difficult to design an energy analyser with such a collection angle which would have a suitably small energy resolution. (iii) The electron detection efficiency which was assumed to be 100%.

The random coincidence rate was underestimated by Wykes because of neglect of photomultiplier dark current, stray light, and contributions to the electron count rate from elastic scattering off residual gas molecules, due to a non-ideal energy analyser.

3.4 Electronic Systems for the Coincidence Measurement

Introduction

In the application of the coincidence technique to problems in atomic physics a difficulty is involved which is not encountered in the study of nuclear phenomena. This is due to the great difference in energy between the particles, rays, or photons associated with the two fields of investigation. A photomultiplier is inevitably used in the detection process

in both fields with the difference that in the nuclear domain a scintillator is first used to convert the comparatively large energy of the particle into a burst of many "visible" photons which, in turn, result in a release of a burst of many photo-electrons from the photocathode, resulting in a large anode pulse. This is to be compared to the situation in the atomic domain where each incident photon gives rise to either a single photoelectron or none at all. Hence, the two consequences of this are, firstly, that in the latter case the counting efficiency is limited by the quantum efficiency of the photocathode, while in the former case there is no limit and conversion from photon-burst to anode pulse takes place with 100% efficiency. Secondly, anode pulses in the latter case, corresponding to an incident photon, result from the emission of a single electron from the photocathode as do pulses resulting from thermally emitted electrons (dark current). Both processes give rise to a similar exponential-type anode pulse height spectrum (PHS) and cannot therefore be distinguished from one another by pulse height discrimination. This is in contrast to the former case where the large anode pulses give rise to an easily identifiable feature on the PHS. The events of interest are readily selected by using "window" discrimination and so background due to dark current etc., is much reduced. In the case of the structureless "atomic" type of PHS, on the other hand, the whole distribution of pulse heights has to be accepted to maximize counting efficiency but this is at the expense of including an enormous amount of background events. This also implies a larger dynamic range of pulses which makes good resolution difficult to achieve in timing experiments.

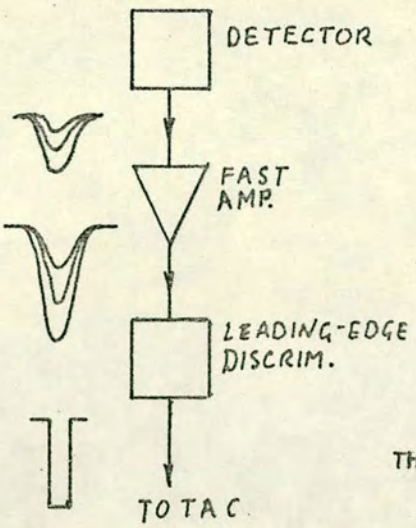

FIG. 3·2 a
LEADING-EDGE TIMING SYSTEM

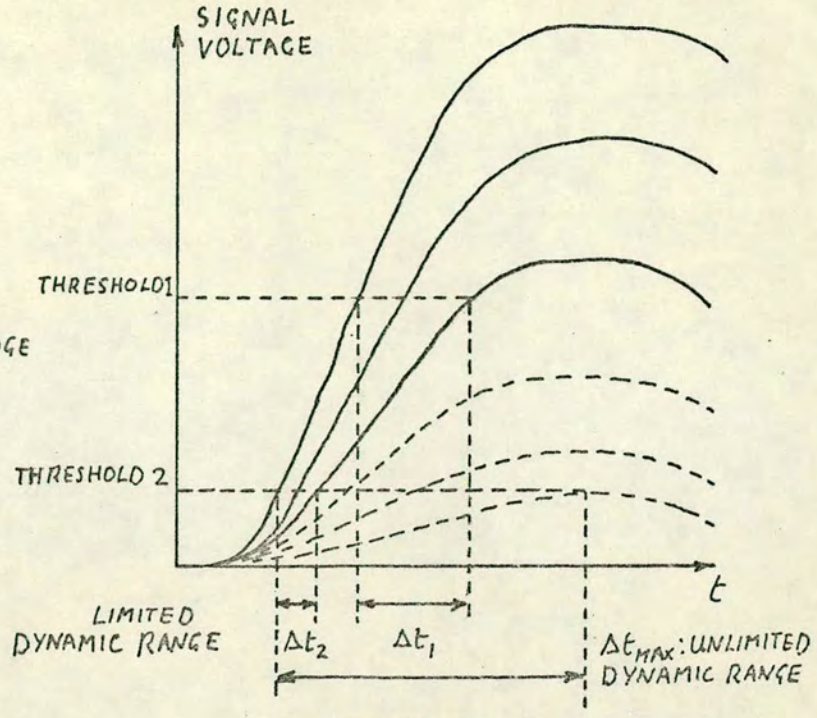

FIG. 3·2 b
"WALK"

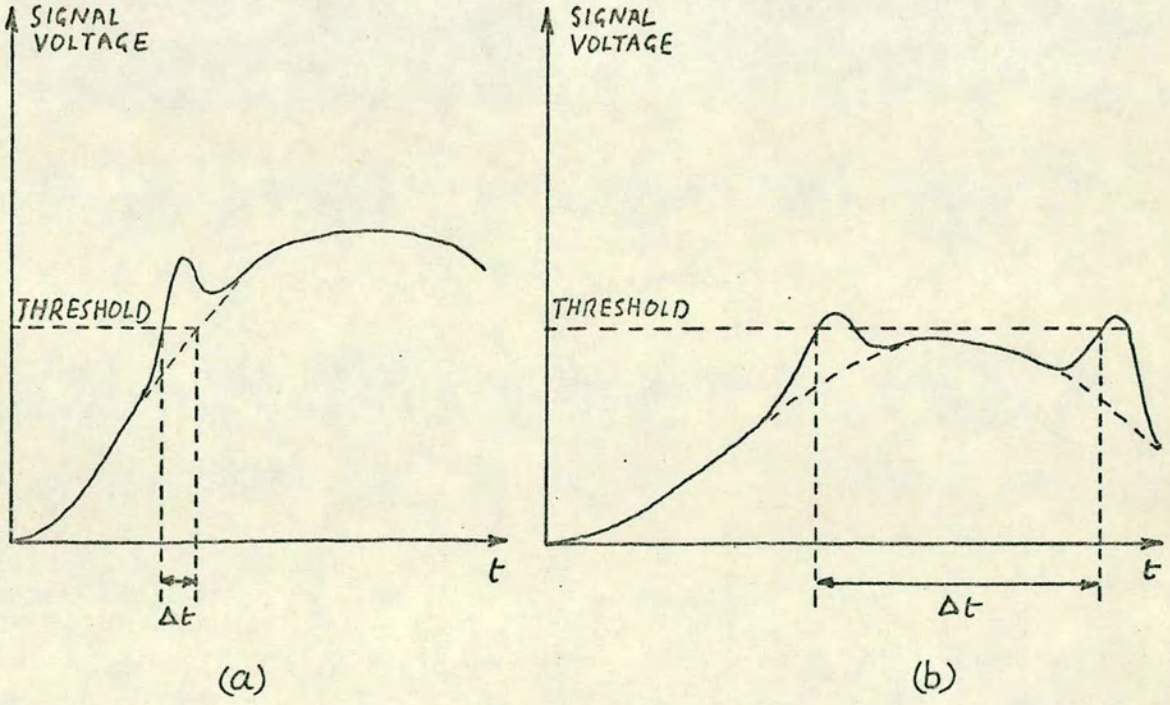

FIG. 3·3
"JITTER"

As was pointed out in the previous section, the more accurately the time of emission of a particle can be determined (i.e. the better the time resolution) then the shorter the counting time for the same statistical uncertainty. How this timing is done is therefore a most important consideration in the design of the system. Two timing systems were immediately available, one using leading-edge timing and the other employing the zero-crossover method. It was necessary to form a comparison between the two systems, bearing in mind the nature of the detectors to be used, so that a decision could be made as to which should finally be adopted.

The Leading-Edge Timing Method In this method the detector pulses, after amplification if necessary, are passed to a leading-edge discriminator which produces a fast, standard output pulse at the instant which the input pulse exceeds a preset threshold, or bias, voltage level (see Figs. 3.2a, b). It can be seen from Fig. 3.2b showing input pulse waveforms, that the instant of triggering is dependent on the amplitude of the particular detector pulse. This effect is called a "walk". The amount of "walk" is obviously proportional to the risetime of the detector pulses, which should therefore be as short as possible. The "walk" is also proportional to the dynamic range of the pulse amplitudes and hence is dependent on the threshold level. In the case where the events of interest give rise to a pronounced peak in the detector PHS the amount of "walk" is correspondingly limited because of the narrow pulse amplitude range. The "walk" is monatonically reduced towards zero as the threshold level is reduced to zero. In practice the minimum possible setting of this level is

determined by the necessity to avoid triggering on electronically-generated noise pulses. The case just described would correspond to the situation where a scintillator is used with a photomultiplier or that where a CEM is used to detect single electrons. The latter has the property that above a certain supply voltage, the gain "saturates" due to space-charge effects and the PHS of the output pulses takes on a poissonian form.

For the case of a photomultiplier detecting single photons the situation is not so simple because of the exponential nature of the PHS. Due to the wide dynamic range of the detector pulses, reduction of the threshold level increases "walk", while raising the level reduces it disproportionately at the expense of counting efficiency.

In any case there is a further cause of deterioration in time resolution. This is the superposition of noise pulses on the detector pulses. This effect is called "jitter". There are two distinctly different ways in which it can occur. If a noise pulse occurs on the leading edge of a detector pulse which otherwise would cross the threshold at a particular instant, then the effect of this noise pulse, if of sufficient amplitude, is to trigger the discriminator at some earlier time (see Fig. 3.3a). The magnitude of this effect is of the same order as the rise time of the detector pulse. The other way in which a "jitter" can occur is if the noise pulse is superposed on a detector pulse which otherwise would not cross the threshold level. If the noise pulses are of sufficient amplitude, then the discriminator is triggered at instants depending on the position of the noise pulse relative to the detector pulse. "Jitter" is now of the order of the pulse width (see Fig. 3.3b).

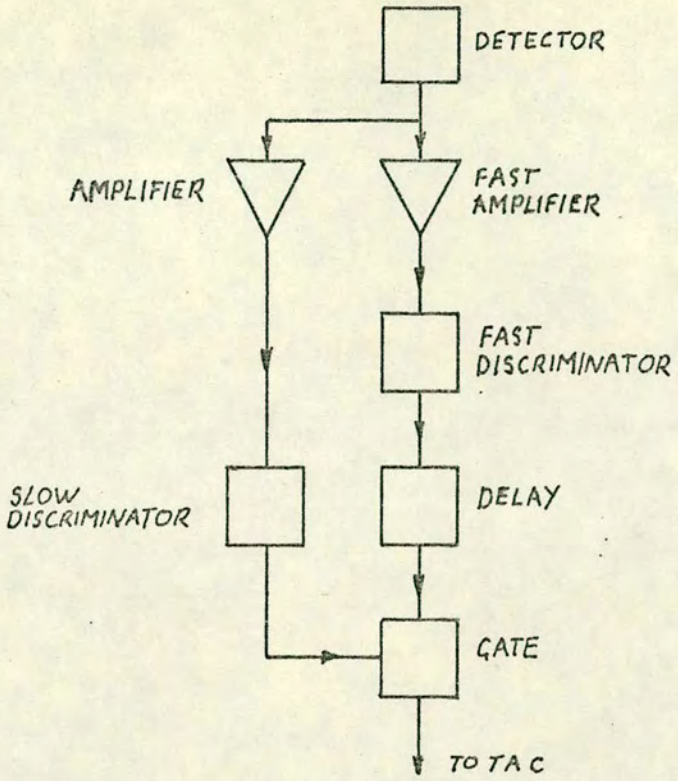

FIG. 3·4
FAST/SLOW "LEADING-EDGE" SYSTEM

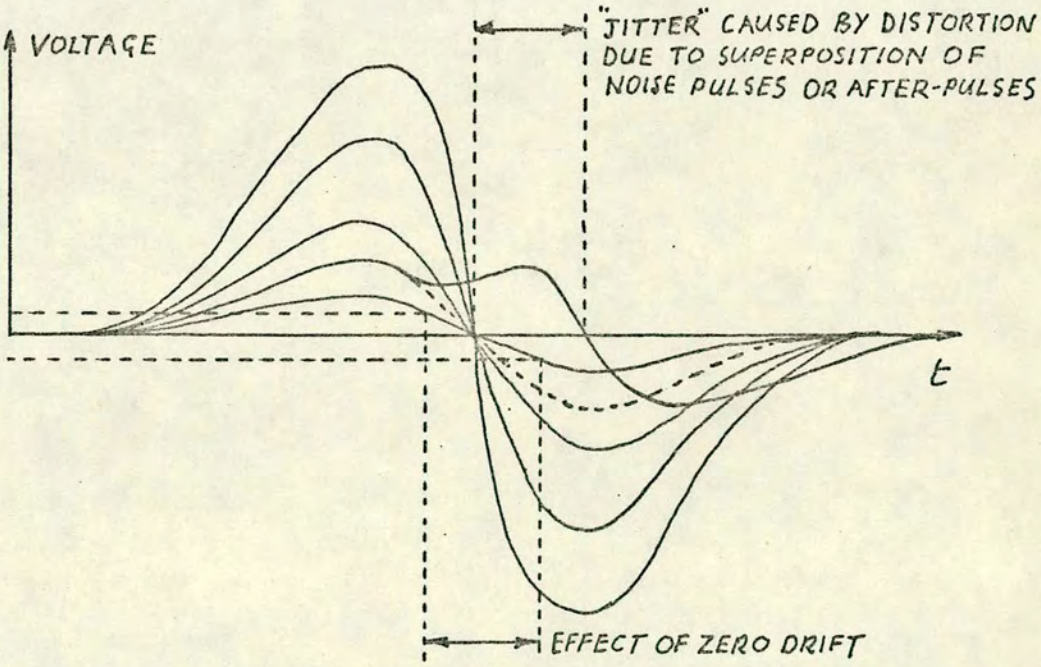

FIG. 3·5
"WALK"-FREE ZERO-CROSSING POINT

This type of "jitter" is therefore more serious than the first.

It can be seen from Figs. 3.2b and 3.3b that "walk" in the case of photomultiplier pulses, and the latter type of "jitter", can both be reduced by limiting the dynamic range of the detector pulses ultimately accepted, using a discriminator to operate a gate. A second discriminator is then used with a threshold set as low as possible, to produce the time information. The former discriminator is referred to as a "slow" discriminator, while the latter is of necessity fast. A practical arrangement is shown in Fig. 3.4. It is found satisfactory to operate the slow discriminator level just above the noise level and to set the fast level as low as possible - within the noise if necessary. The overall counting efficiency is determined by the higher level, but the noise is usually of sufficiently low amplitude that there is little loss in efficiency involved in setting the level just above the noise. The lowest possible setting of the fast discriminator threshold is found in practice to be limited by the onset of oscillation which tends to be triggered off by noise pulses. In any event the amount of "walk" and "jitter" using this system should be limited by the rise time of the detector pulses.

The Zero-Crossover Method If the detector pulse is doubly-differentiated to produce a zero-crossing point on the waveform, then providing pulse shapes are similar, the instant of zero-crossing is independent of pulse amplitude. A discriminator set to trigger when the waveform passes through zero should thus have no "walk". (See Fig. 3.5). This is the basis of the system developed by Orman (1963). In practice, however, the utility of this method is limited by four factors; electronic

stability, electronic noise, photomultiplier after-pulsing, and variation in detector pulse shape or risetime (see Fig. 3.5).

The first three factors have greater effect for small-amplitude pulses and are thus more serious in the present investigation where exponential-type PHS are encountered. They produce either premature or delayed triggering depending on the direction of drift of the zero-sensing circuits, or depending on the position of the superposed pulses relative to the detector-pulse waveform. The effects can be lessened by eliminating detector pulses having amplitudes below a preset level. This can be done, as before, using a separate leading-edge discriminator controlling a gate on the output of the zero-crossing discriminator. The higher the threshold of this controlling discriminator, the smaller the above effects but the counting efficiency is also reduced. A noise pulse at any point on the detector waveform is able to trigger the zero-discriminator if it has sufficient amplitude. The upper limit to the magnitude of these effects is then determined by the duration of the waveform (see Fig. 3.5). Short time constants should therefore be employed even though this may tend to increase the effect of noise pulses.

Variations in detector pulse shape or risetime will obviously produce corresponding variations in the position of the crossover. These variations stem from two causes; the statistical nature of the secondary emission process at the photomultiplier dynodes and of the electron trajectories between dynodes; and the distortion caused in large amplitude pulses which overload the electronics (Whittaker, 1966). The effect of the latter can be reduced using a second leading-edge

discriminator to eliminate the larger-amplitude pulses. This reduces counting efficiency further.

A variation of the above system has been devised (Gedcke and McDonald, 1967) which also eliminates "walk." For pulses of fixed shape but varying amplitude, a discriminator triggers at the instant at which the waveform attains a fixed fraction of its peak amplitude. In the case of pulses with varying rise-times, although the discriminator no longer triggers at a fixed fraction of peak amplitude, it can be shown that it does trigger at an instant independent of risetime (Chase, 1968).

Comparison of the Two Systems

Concerning the zero-crossover system, it has been mentioned that short time constants are preferable. Unfortunately in the system available the circuitry was constructed such that rise and fall times were long (of the order of 500 nsecs.). It would seem therefore that the leading-edge method would produce better results than this particular system. This was borne out in tests using the two systems to examine the time spectrum of delays between the pairs of annihilation γ rays produced by the positron emission of ^{22}Na. Nuclear Enterprises NE102A plastic scintillators, optically coupled to E.M.I. 9656L photo-multipliers were used to detect the γ rays. These were necessarily different multipliers from the ones to be used in the electron-photon coincidence experiment (E.M.I. 9659B) due to the different wavelengths of light involved in the two cases. However it was expected that their performance would be indicative of that of the 9659B's, as the specified rise time of the anode pulses is 10 nsecs. in both cases.

Because of the high directional correlation of the positron annihilation process, the detectors were placed diametrically opposite one another on either side of the source to maximize

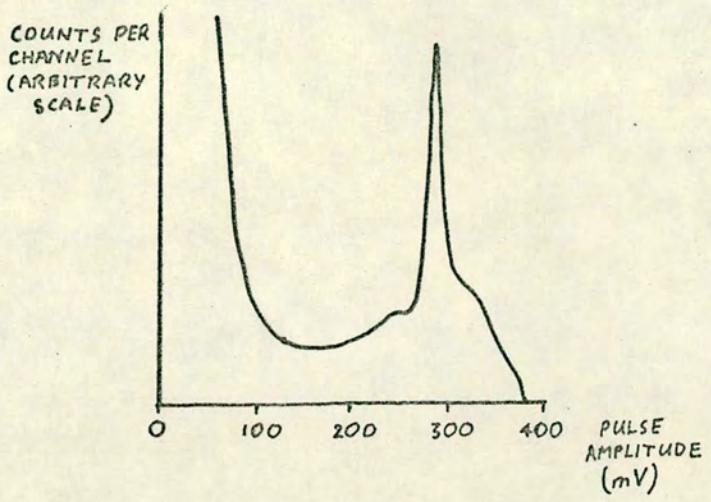

FIG. 3·6
"SCINTILLATOR" PULSE-HEIGHT SPECTRUM

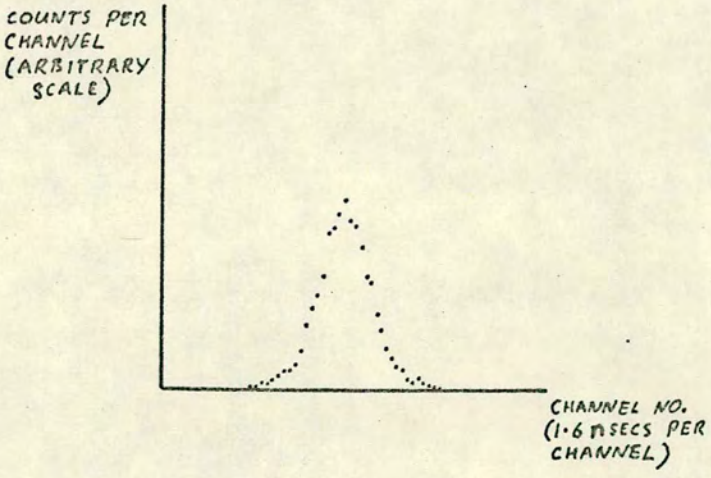

FIG. 3·7
^{22}Na "PROMPT" SPECTRUM
USING "LEADING EDGE" TIMING SYSTEM

the genuine/background ratio for the coincidence rate. The leading-edge system tested consisted simply of an Ortec 260 time pick-off unit (containing a fast amplifier followed by a tunnel-diode discriminator) feeding an Ortec 403A time pick-off control unit (containing further amplification and bias supplies). No slow gating circuit was used. This would be of little advantage in this case due to the nature of the PHS (see Fig. 3.6). The discriminator level was set to its minimum value.

The zero-crossing system tested consisted of an NE5289SC preamplifier feeding an NE 4658 pulse-shaping amplifier which produced a double-differentiated pulse. This in turn fed an NE4616 timing discriminator used in the crossover-pick off mode.

The two outputs of each system were fed to the "start" and "stop" inputs of an NE 4645 TAC set to a range of 500 nsecs. The "stop" input was fed via a 64 nsec. delay. The spectrum of output pulse heights was obtained using a Laben 400 multi-channel analyzer (MCA).

Voltage supplies to the multipliers were sufficient to give large pulses without overloading the preamps. Approximately 900 V was applied to the multipliers. The discriminator level of the NE4616 was adjusted so as to give similar counting rates to those obtained with the leading-edge system. This ensured that the counting efficiencies of the two systems were the same, enabling a fair comparison to be made of their time resolutions.

Time spectra in both cases were of gaussian form. The FWHM of the "leading-edge" spectrum was 16 nsecs, which is of the order expected purely on the basis of detector rise time. That of the "zero-crossover" spectrum was 40 nsecs. A typical "leading edge" result is shown in Fig. 3.7.

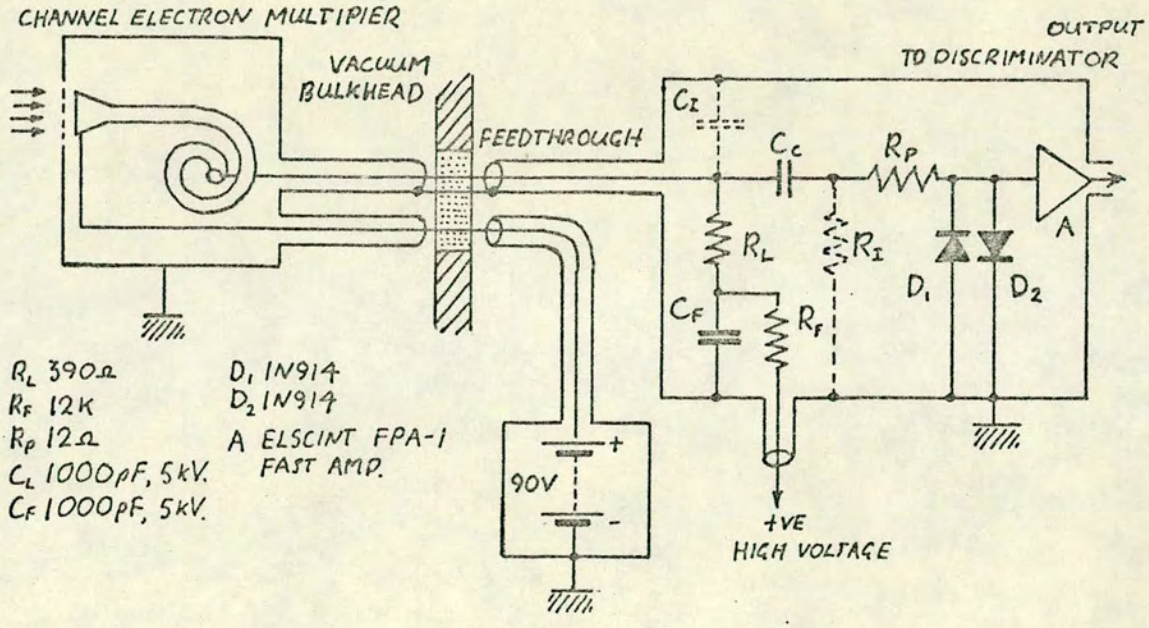

FIG. 3·8
C.E.M. INTERFACING CIRCUIT

Because of the difference in PHS and because of the contribution to the detector-pulse rise time from the scintillator decay (time constant 2.4 nsecs.) no quantitative extrapolation can be made to the situation encountered in the electron-photon coincidence experiment. However the above result does strengthen the belief that the leading-edge system should be adopted.

3.5 Detectors and Inferfacing

As it has been decided to use the leading-edge timing method it is important to preserve the rise time of the detector pulses, to obtain optimum time resolution. The interfacing of the detectors with the corresponding timing circuits and voltage supplies will thus be important in this respect. The detectors and interfacing in the electron and photon channels will be described below.

Electron Channel A channel electron multiplier (CEM) is used to detect the electrons for the reasons given in Section 3.3. For vacuum reasons all electrical components are located outside the vacuum chamber and the signal lead from the CEM is kept as short as possible (25 cms.) to avoid degradation of the signal pulse due to mismatching. The arrangement of the CEM and its associated interfacing is shown in Fig. 3.8. C_i represents the parallel combination of amplifier-input and cable capacitances, which will be assumed to be negligible so that the pulse rise time will depend solely on the properties of the CEM. The specified rise time of the CEM pulse is 5 nsecs. C_c is a high-voltage coupling capacitor (which should be large so that the detector current produces maximum voltage across the amplifier

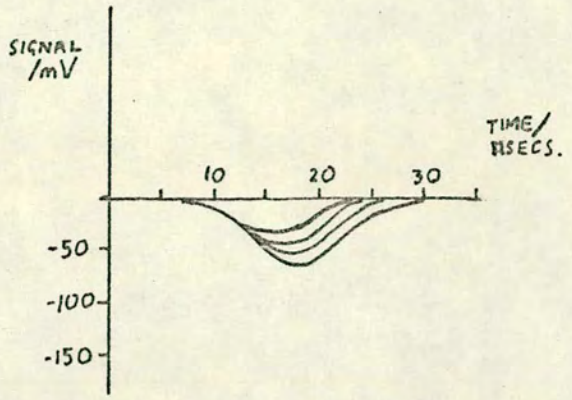

FIG. 3·9
CHANNEL ELECTRON-MULTIPLIER SIGNAL PULSES (EHT: 3·3 kV)

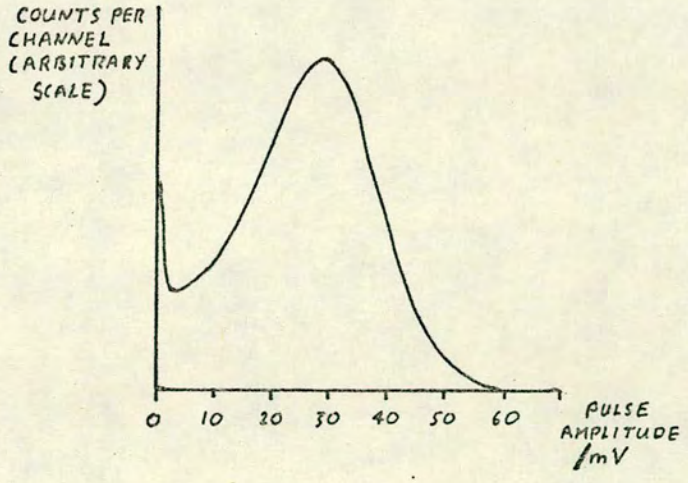

FIG. 3·10
CHANNEL ELECTRON-MULTIPLIER
PULSE HEIGHT SPECTRUM
(EHT: 3·3 kV)

input resistance $R_i(50\Omega)$. C_F is a high-voltage decoupling capacitor and forms with R_F a low-pass filter to reduce the effect of voltage transients which may be present on the high voltage supply line. Ideally therefore C_F and R_F should be large. R_L is the load resistor. The usual constraints on the value of this component, imposed by the necessity to preserve information contained in the "area" of the pulse, are not relevant in the present application. R_F and R_L should be small compared to the resistance of the detector ($10^9\ \Omega$ in this case) to avoid excessive drop in the supply voltage. The recovery of the circuit is determined by the time constants $(R_L + R_i)(C_F + C_c)$, $(R_L + R_F + R_i)C_c$ or R_FC_F whichever is the largest. This value should be much smaller than the inverse of the maximum expected pulse repetition rate (10^{-4} secs.), while the smallest of these time constants should be much greater than the pulse risetime (5×10^{-9} secs.) to avoid loss of pulse voltage and excessive overshoot. Capacitors of 1000 pF., rated at 5.0 kV and manufactured by Suflex Ltd., were readily obtainable, so that if the choices $C_F = C_c = 10^{-9}F$ and $R_F = 12K\Omega$ are made, the longest time constant will be $(R_L + R_F + R_i)C_c$ ($= 10^{-5}$sec) provided $R_L \ll 12\ K\Omega$. The shortest time constant will now be $(R_L + R_i)(C_F + C_c)$ or $2(R_L + 50) \times 10^{-9}$ which is required to be much greater than 5×10^{-9}. A choice for R_L of 390Ω easily satisfies the above three conditions. Fig. 3.9 shows the signal voltage pulses across the 50Ω input resistance of the fast amplifier. Rise and fall times are 8 nsecs and the maximum amplitude is 60 mV with 3.3kV applied to the CEM. The amplifier is necessary because the discriminator used has a fixed threshold of 150 mV. A variable attenuator is used

between amplifier and discriminator to give, effectively, a variable threshold. The output impedance of the amplifier is 50Ω and all subsequent circuitry and coaxial cables are matched to this value. Fig. 3.10 shows the PHS of the signal pulses, displaying the poissonian form due to space-charge saturation.

It was found that the input transistor of the amplifier was periodically destroyed. The cause was difficult to establish but it was presumed to be due to large transients stemming from high voltage discharges across insulators within the vacuum chamber. The two fast diodes D1 and D2 were added to clip the transients. This attempt failed, probably due to the smallness of the transient rise time compared to the switching time of the diode (1.6 nsecs). The small resistance R_p was added in the hope that, in combination with the input capacitance of the amplifier and that of the diodes, it would slow down the transients sufficiently to give the diodes time to switch. This proved successful and, as was hoped, the signal pulse was unaffected.

Photon Channel The quantum efficiency of photocathodes falls off in the wavelength region of the Na D lines (589.0, 589.6 nm). The extended S20 photocathode has the highest quantum efficiency in this region (9.5%). The only photomultiplier available at the design stage with this photocathode, and with sufficient gain was the E.M.I. 9659B. This tube has only eleven stages but for single-photon detection a tube with more stages and hence higher gain would be preferable. The anode-pulse rise time of the 9659B is specified as 10 nsecs. This sets the upper limit to the time resolution using leading-edge timing.

A tube giving faster anode pulses would also be preferred therefore. Because the overall time resolution is ultimately limited by the lifetime of the Na ^2P states (16 nsecs) and because little would be gained by making the electronic contribution to the resolution much less than this, it was decided that the 9659B would be acceptable. (Provided of course that one was not interested in resolving the lifetime curve itself.) Recently more suitable tubes have become available, having the same photocathode efficiency, but having fourteen stages and pulse risetimes of 2 to 3 nsecs. These are the E.M.I. 9816B, the Mullard 56TVP, and the RCA 7265. It is hoped eventually to try one of these types.

For single-photon detection it is necessary to obtain the maximum possible K-D1 collection efficiency. This depends on the K-D1 voltage. The optimum K-D1 voltage for maximum collection efficiency is given by the manufacturers as 150V. This choice of K-D1 potential is not incompatible with fast anode-pulse rise time as this quantity depends on the spread in transit times of electrons within a bunch and hence, in single photon detection, is only dependent on inter-dynode voltages. (Gatti and Svelto, 1966.)

The aforementioned transit time spread is inversely proportional to the inter-dynode voltage (Poultney, 1972). Hence this should be as large as possible, consistent with the prevention of breakdown, to achieve minimum possible rise time. This also gives maximum possible gain which is an important factor in single-photon detection. The maximum inter-dynode voltage specified for the 9659B is 190V. However it was decided to err on the side of caution and 170V was chosen. This gives an overall

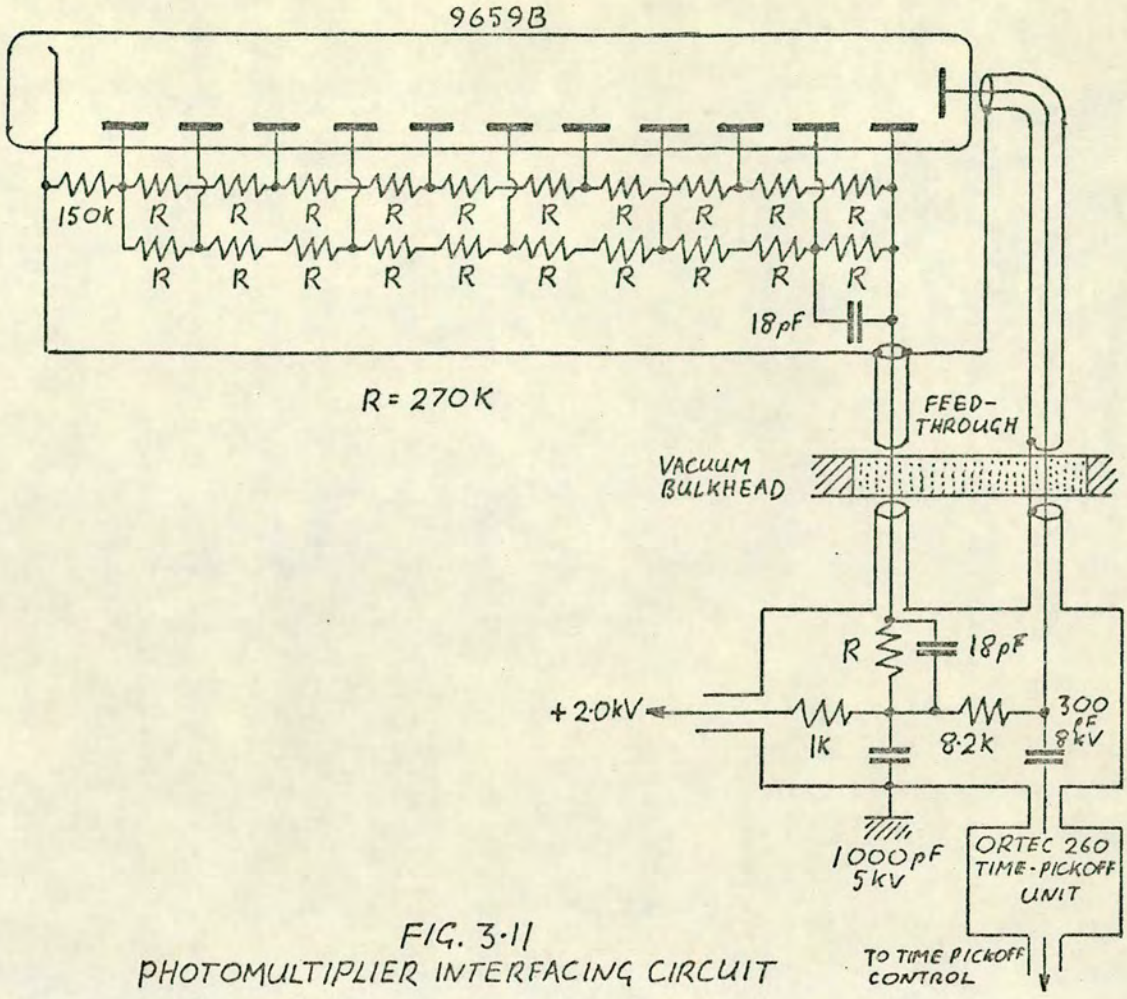

FIG. 3·11
PHOTOMULTIPLIER INTERFACING CIRCUIT

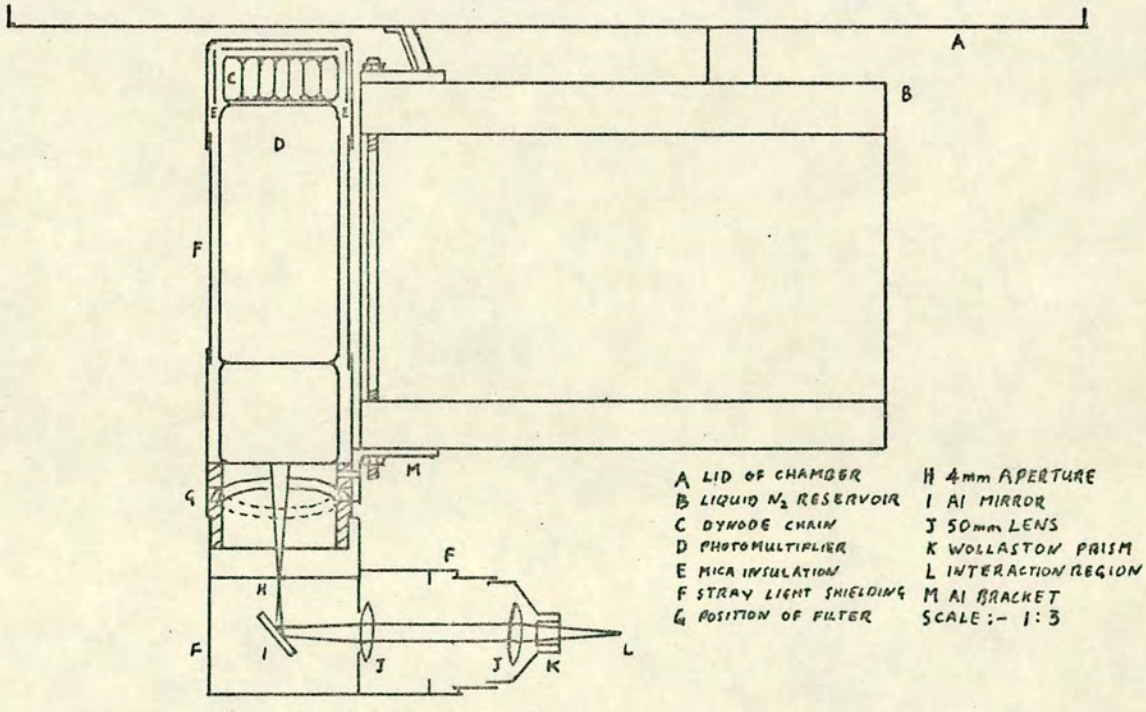

FIG. 3·12
ARRANGEMENT OF PHOTOMULTIPLIERS AND OPTICAL SYSTEM

tube voltage of approximately 2.0 kV.

With this voltage distribution the gain of the photomultiplier is of the order of 5×10^7. The charge induced on the anode due to a single incident photon is therefore 8×10^{-12}C, and for a maximum envisaged count rate of 1kHz, the mean anode current is 10^{-2} μA. However the current averaged over the duration of the pulse ($\simeq 2 \times 10^{-8}$ secs.) is 0.4 mA. It would be undesirable to have a dynode current much larger than this because of possible power-dissipation problems. (For convenience the dynode chains are mounted on the photomultiplier bases inside the vacuum chamber.) As a compromise a dynode current of 0.5 mA (in each chain) is chosen, fixing R (see Fig. 3.11) at 270kΩ. Excessive voltage drops may now occur over the last two stages. The most serious effect of this in the present application would be a deterioration in pulse rise time. To prevent such voltage changes the last two stages are decoupled by capacitors C whose value is chosen as 18 pF by requiring that the voltage across them changes by only 0.5v. when 8×10^{-12}C of charge is removed. The maximum pulse rate is now limited by the time taken to recharge these capacitors through the dynode chain, the time constant being 5×10^{-5} secs. The expected repetition rate of less than 1kHz should lie well within this limit. The double dynode chain facilitates the arrangement of resistors around the photomultiplier base.

Originally it was intended to use a 150V zener diode to set the K-D1 voltage but it was subsequently found that the zener voltage and stabilization of the device were affected by the reduced temperature (less than - 40°C) at which it was necessary to operate the tubes in order to reduce dark current.

At present this voltage is determined by a 150 kΩ resistor. All resistors used in the dynode chain are of the high stability carbon film type (½ watt), whose temperature coefficients are so small that there is little measurable change in their resistance even at liquid-nitrogen temperature.

It should be noted that as well as pulse rise time, there is another factor which will affect time resolution. This is the variation or "jitter" in the transit times of successive photoelectrons due to their different possible trajectories. These differences arise from variations in position and velocity of the photoelectron as it is emitted from the photocathode. The effect is inversely proportional to the K-D1 voltage (Poultney, 1972) and can be reduced therefore by increasing the K-D1 voltage from its optimum value of 150V. But this will be at the expense of efficiency which is already on the verge of being insufficient. The order of this transit-time jitter is 1.5 nsecs (manufacturer's data) and so any improvement is likely to be fractions of 1 nsec. Compared to the contribution to the resolution from the rise-time (10 nsecs) and the lifetime (16 nsecs) this is insignificant therefore 150V is retained between the cathode and first dynode.

The interfacing circuit (see Fig. 3.11) for the photomultipliers is similar to that used for the CEM except for the extra connection to the dynode chain and some empirical changes in component values necessitated by the slightly different timing electronics employed.

It is preferred to have the multipliers inside the vacuum chamber to avoid some of the complications involved

in cooling them (e.g. window-misting). This location is also more compatible with the arrangement of the rest of the optical system. To achieve maximum reduction in the dark current of the S-20 photocathodes it is necessary to cool them to at least -40°C. Making a slightly indirect connection to a liquid nitrogen trap via an aluminium bracket (see Fig. 3.12) it was found that, with the tubes running (each tube's dynode chain dissipated 2 watts) and the chamber evacuated, the temperature of the envelope adjacent to the photocathode became -70°C. The reduction in dark current achieved by this means is enormous. At room temperature, dark current is some tens of kilohertz, while below -40°C it is approximately 45 Hz.

Fears that the quantum efficiency of the photocathode may be reduced at the low temperatures were alleviated by the work of Young (1963) who found that in the case of the S-20 type, no significant reduction took place even at liquid-nitrogen temperature.

Signal pulses at the inputs to the timing circuits are similar in shape to those obtained from the CEM except that the rise and fall times have the expectedly longer values of 12 nsecs. The maximum pulse amplitude observed on an oscilloscope is 0.5V. The coaxial signal-leads from the multipliers are as short as possible to reduce the effect of mismatching.

Information about the rise time of the detector pulses enables an estimate to be made of the electronic contribution to the time resolution. Assuming that the finite rise times give rise to gaussian spectra with FWHM of the order of the respective rise times t_e and t_γ for the electron and photon detectors, the resultant electronic resolution function is

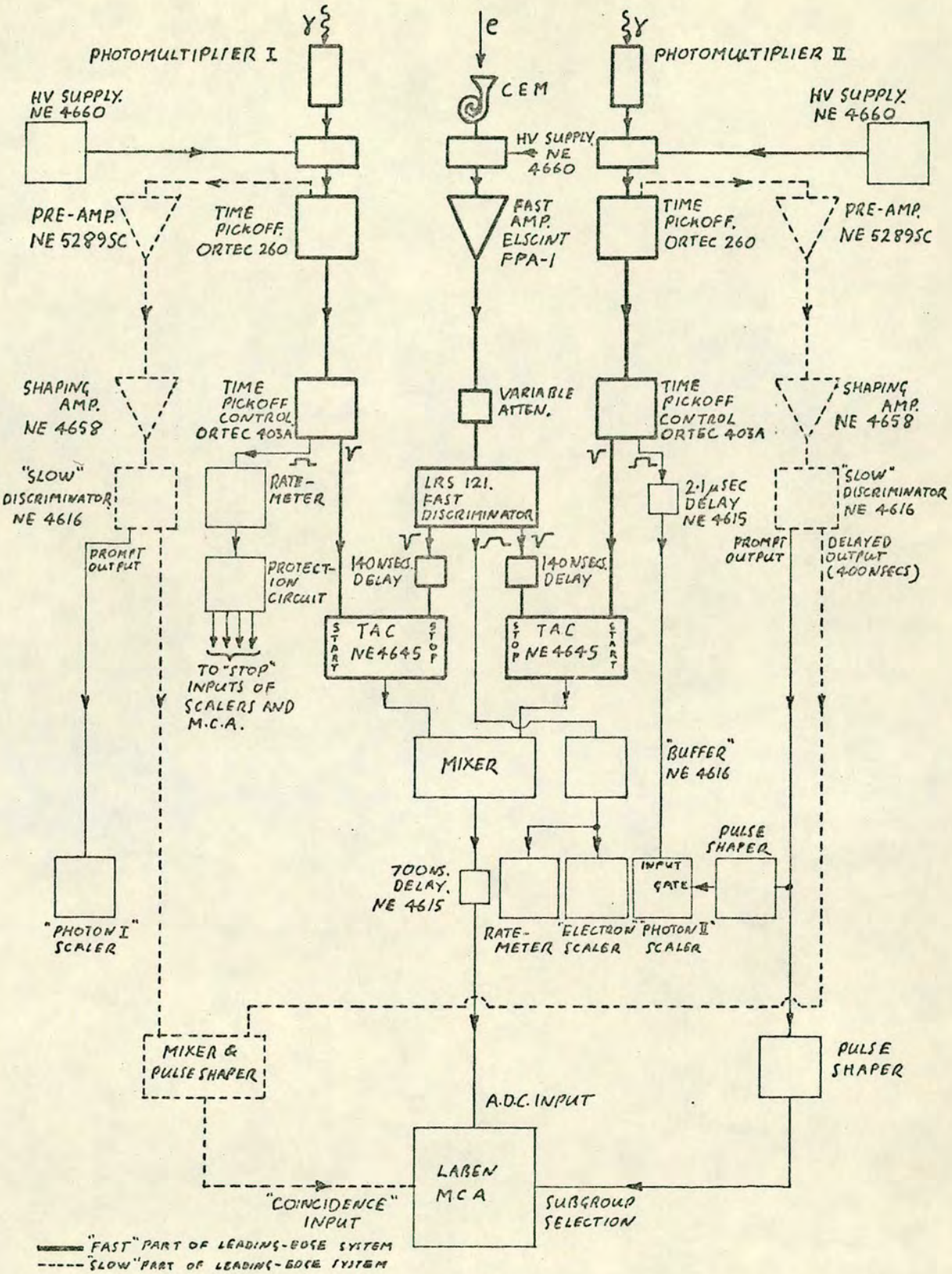

FIG. 3·13
COMPLETE COINCIDENCE ELECTRONICS

again gaussian with an FWHM given by

$$\tau_e^2 = t_e^2 + t_\gamma^2 \quad .$$

Using the above values for t_e and t_γ it is found that τ_e = 14 nsecs. This is greater than the overall time resolution of the experiments of Eminyan et al. (1973, 1974) and McConkey et al. (1975) and can be attributed in some degree to the necessity, in the present work, of using a photomultiplier, rather than a CEM, as a photon detector.

3.6 The Complete Electronic System

A block-diagram of the system is shown in Fig. 3.13. The leading edge system used with the photomultipliers consists of a head unit, the Ortec 260 time pick-off (TPO), which is placed close to the detector output feed-through. The TPO is connected via a 50Ω coaxial cable to the 50Ω input of the Ortec 403A time pick-off control, (TPOC), providing a fast (4 nsec rise and fall time, 30nsecs width) negative pulse (amplitude 1.0v) into the "start" input of an NE4645 TAC. The above composes the "fast" part of the photomultiplier timing system.

The TPO's are also provided with a "slow" positive output. In channel I, this is used to drive a ratemeter which, besides giving an immediate visual indication of the state of operation of the "fast" circuit, also provides an analogue signal which is monitored by a protection device. This device prevents the accumulation of data if the photon count rate varies outside a preset range. An excess of random coincidences would otherwise result if, for example, the atomic-beam oven became

empty, or if the photomultiplier cooling-system failed. The details of this protection device are given in Appendix IIIa.

The "slow" output of TPOC II is fed to the input of a scaler to obtain "singles" counts. Not all of these contribute to the coincidence rate because of the gating of the MCA by the "slow" discriminator circuits (see below). The scaler is therefore gated "on" by the same pulses which gate the MCA in order to give true "singles" counts. A 2.1μsec (NE4615) delay is inserted in the input to the scaler to allow the gating pulses time to "catch up". This scaler gives a visual indication of the operation of the "fast" and "slow" circuits in channel II. The "singles" scaler in channel I is fed directly from the "slow" discriminator output.

An output from each of the TPO's provides pulses for the "slow" discriminator circuits which are composed of NE5289SC preamplifiers followed by NE4658 shaping amplifiers, which provide correctly shaped pulses to trigger the "slow" discriminators (NE4616). The delayed outputs of the discriminators are fed to a non-summing mixer (see Appendix IIIb). This provides an inverted pulse of shape suitable for gating the "coincidence" input of a Laben 400 MCA. The prompt output from "slow" discriminator I is fed directly to the input of the "singles" scaler as described above, while that of discriminator II is used to gate the corresponding "singles" scaler via a suitable pulse shaping network (see Appendix IIIc).

In the electron channel, pulses from the CEM are amplified (×30) in an Elscint FPA-1 fast amplifier placed as close as possible to the CEM output feed-through. The output pulses were then passed via a 50Ω coaxial cable to a 50Ω variable

attenuator and hence to the 50Ω input of an LRS 121 fast discriminator. This device is provided with two fast negative outputs each of which feed 15 metres of 50Ω coaxial cable followed by a Chronetics variable delay set to its maximum of 63.5 nsecs. The outputs of the delay are fed via 50Ω cable to the 50Ω "stop" inputs of the two TAC's. The total delay on each input is approximately 140 nsecs. There is some degradation in pulse quality in traversing the delay. At the outputs of the 121 the pulse has a rise and fall time of 2.5 nsecs, a width of 20 nsecs, and an amplitude of 0.8V, while at the inputs to the TAC's the rise and fall times are 4 nsecs and the amplitude is 0.7V. This is still sufficient to trigger the 0.5V thresholds of the TAC's.

The "slow" positive output of the "121" is used to provide pulses for the electron "singles" scaler. The output itself is insufficient to drive a scaler directly and so an NE4616 is used to provide 5V pulses for the purpose.

The TAC outputs are fed to a non-summing mixer (Nuclear Enterprises Ltd.) which provides the input pulses for the MCA via a 0.7 μsec delay (NE4615).

In the two photomultiplier channels, the timing system is thus basically like that described in section 3.4 and shown in Fig. 3.4. In the electron channel, on the other hand, it is sufficient to use only a fast discriminator because of the more favourable PHS of the detector (see Fig. 3.10).

As two different time spectra (one for each photon polarization state) are to be recorded simultaneously, it is necessary to provide means of selection between the two subgroups of the MCA's 400 channels. In the "Laben", the sub-

group is determined by the presence or absence of a pulse at rear BNC socket 5, during the time the signal pulse is present at the input. The prompt output of "slow" discriminator II, as well as providing a scaler gating pulse, is also used therefore to drive the subgroup selection socket via suitable pulse shaping and inversion (Nuclear Enterprises Ltd.). An input pulse to the MCA is analyzed in subgroup II (Channels 200-399) if a subgroup selection pulse is simultaneously present (and if a "coincidence" pulse is also present). Thus coincidences due to detector II are stored in subgroup II, while those due to detector I are stored by default in subgroup I. It is the function of the 0.7 μsec delay and the "built in" variable delay of the "slow" discriminators, to ensure that the input pulse, the "coincidence" pulse and the subgroup selection pulse, all arrive simultaneously at the MCA.

The dead time of the coincidence circuit is determined mainly by the TAC range setting which is 500 nsecs, and the TAC output pulse width. This was chosen to be 2.0 μsecs which is compatible with the MCA input. Input pulses to the TAC will not be accepted until the conversion process has ended (taking between 0 and 500 nsecs.) and until the output pulse has returned to zero (taking a further 2.0 μsecs.). Thus the total dead time per "start" pulse could be as short as 500 nsecs (if

CONTRI-BUTION / CHANNEL	FLIGHT TIME (CALCULATED 2·9eV)	ANALYZER TRANSIT TIME (CALCULATED 2·9eV)	DETECTOR TRANSIT TIME (SPEC.)	TOTAL	EXTRA CABLE LENGTH	TOTAL
ELECTRON	40	62	20	122	140	262
PHOTON	—	—	55	55	—	55
				67		207
				NET DELAY BEFORE CABLE		NET DELAY AFTER CABLE

TABLE 3·1
CONTRIBUTIONS TO NET DELAY IN ELECTRON CHANNEL (nSECS.)

no "stop" pulse arrives during that time) or as long as 2.5 μsecs (if a "stop" pulse arrives near the end of the conversion ramp). With a mean photon rate of 200/sec only .05% are within 2.5 μsecs of one another and thus there will be negligible dead-time loss. Dead time however does have the important function of "protecting" the system against spurious events caused by after pulsing or "ringing" on the detector pulses. The system is thus "protected" for at least 500 nsecs after a genuine signal pulse. This is substantially larger than the expected time delay between the arrival of a photon signal at the TAC and the arrival of a correlated electron signal (207 nsecs, see table 3.1) and so as far as correlated after-pulsing etc. in the photon channel is concerned it would be impossible for it to cause the correlation to be shifted in time, provided that there are no similar effects in the electron channel. This is certainly so in the case of "ringing". There is in fact negligible "ringing" on either channel. As for afterpulsing, this is an effect peculiar to photomultipliers and has not been observed in spiral CEM's of the type used. (The spiral structure being designed to prevent ionic feedback which would produce effects similar to those of afterpulses). It is concluded then, that the dead time inherent in the TAC's is sufficiently large to prevent spurious events due to afterpulsing etc., while being sufficiently small to make dead time correction unnecessary.

Typical settings of controls are given in Appendix IV(a).

A general test of the electronic system, particularly of the overall linearity of the TAC's and MCA, is conducted using

PARAMETER		TOTAL	RATE
COUNTING TIME (SECS.)		3.456×10^5	—
"ELECTRON" COUNTS		1.133×10^9	3.279 kHz.
"PHOTON" COUNTS		5.504×10^7	160 Hz.
RANDOM COUNTS (INTEGRATED OVER 140 CHANNELS : 215–354)		8.7001×10^4	621/CHANNEL
TIME/CHANNEL (nSECS.)	CALCULATED FROM ABOVE DATA	3.43	
	MEASURED USING "CHRONETICS" VARIABLE DELAY	$3.2 \pm .3$ (AVERAGED OVER CHANNELS 235-245. NEGLECTS ANY SYSTEMATIC ERROR IN CALIBRATION OF DELAY.)	

TABLE 3.2
PARAMETERS OBTAINED FROM "RANDOMS" TEST
(SUBGROUP II)

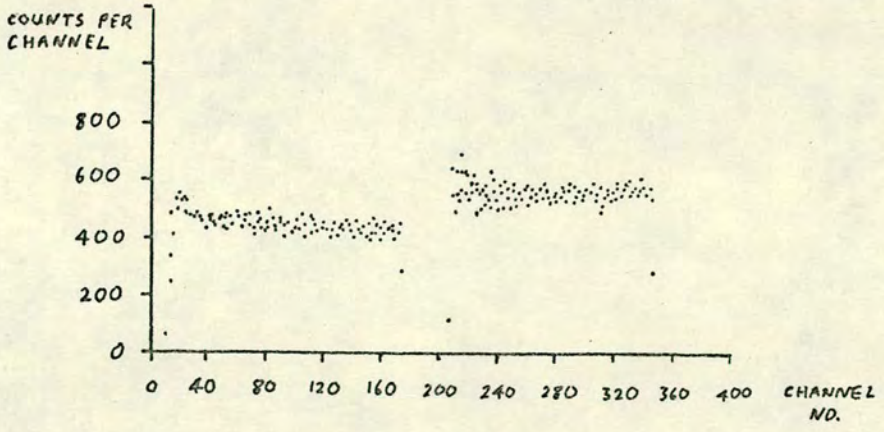

FIG. 3.14
"RANDOMS" TIME-SPECTRA

the dark currents of two E.M.I. 9656L photomultipliers to provide random input signals to the two photon channels. High voltages and discriminator levels are adjusted to give singles rates of about 200 Hz (similar to those obtained in an actual run) but otherwise the control settings are just as they would be during a run. The electron channel is fed with pulses from a pulse generator at about 3kHz. The results of one such test are given in Fig. 3.14 and Table 3.2. The mean time represented by each channel is calculated from the "singles" rates using relation (3.2) and agrees with measurements made by feeding pulses from the same generator simultaneously into the electron channel and a photon channel, the Chronetics variable delay being used to shift the time peak thus obtained, by known amounts.

Neglecting the grossly non-linear first twenty channels in each subgroup, 55% and 75% of the channels have contents lying within one standard deviation of the mean, in subgroups I and II respectively.

A final test is that of the subgroup selection circuits. Dark-current pulses are fed into each photon channel in turn. It is noted that in each case no coincidences are observed in the unused channel.

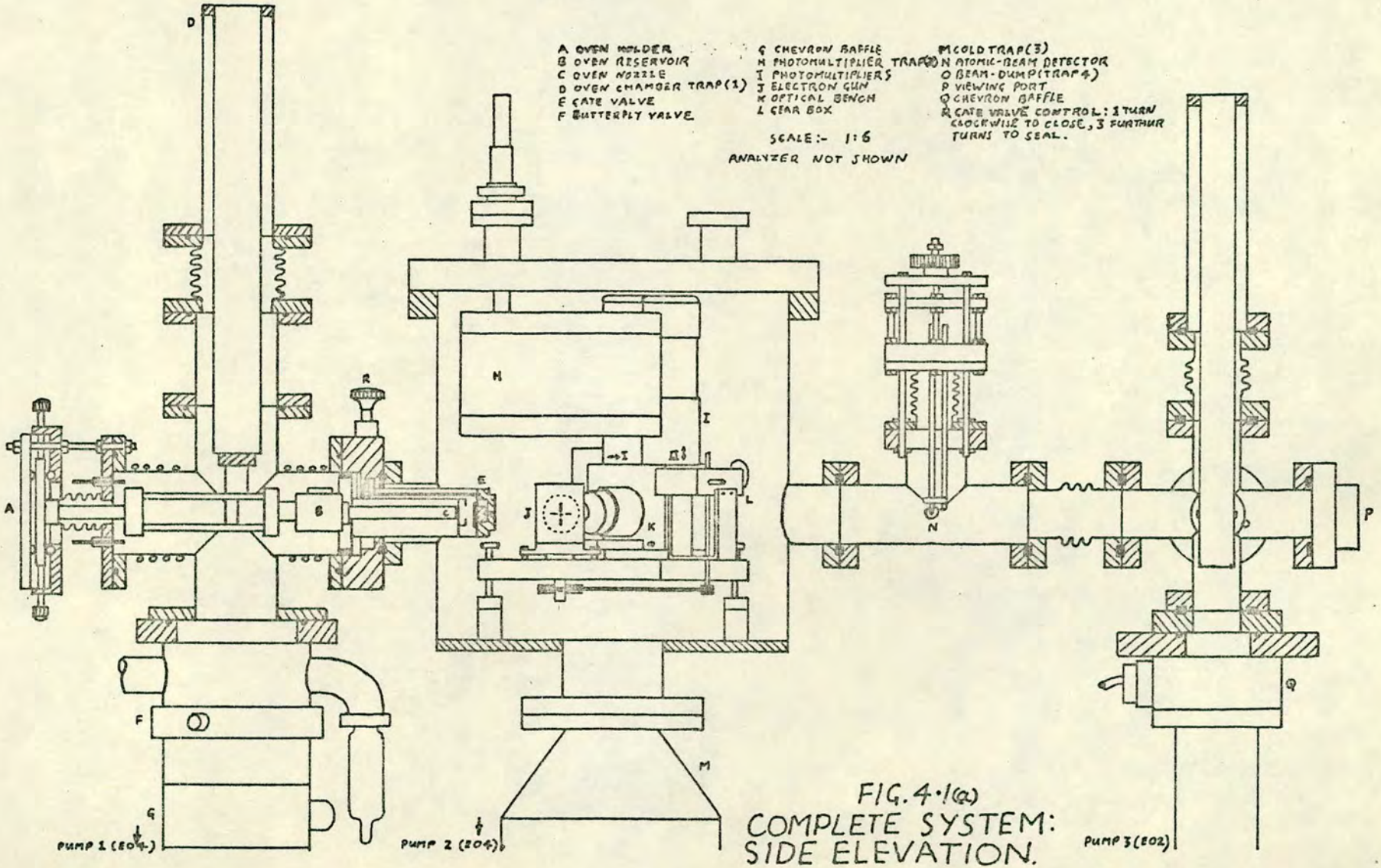

FIG. 4·1(a)
COMPLETE SYSTEM:
SIDE ELEVATION.

A "COLD" ARM
B OVEN RESERVOIR
C OVEN NOZZLE
D SUPPORTING TABLE
E GATE VALVE
F ANALYZER

G FARADAY CUP
H OPTICAL SYSTEM
I GEAR BOX
J ELECTRON GUN
K DEFLECTORS
FEEDTHROUGHS & COMPTS. MOUNTED ON LID NOT SHOWN

SCALE :- 1:6

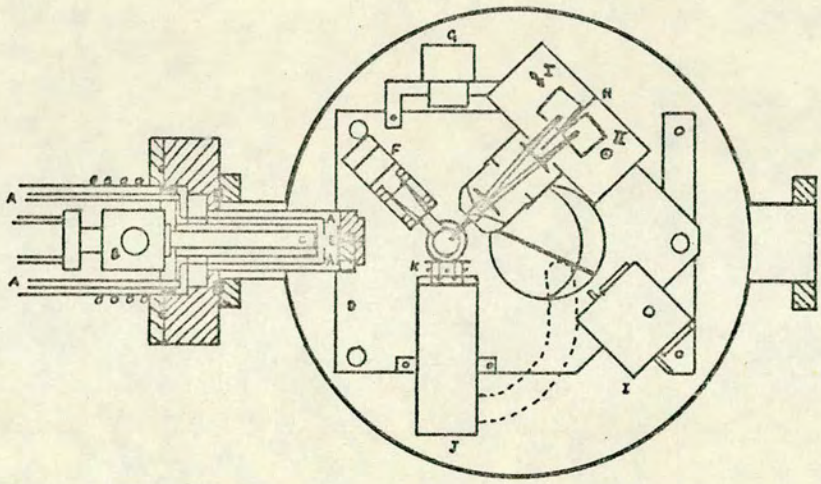

FIG. 4·16)
PLAN OF SCATTERING CHAMBER

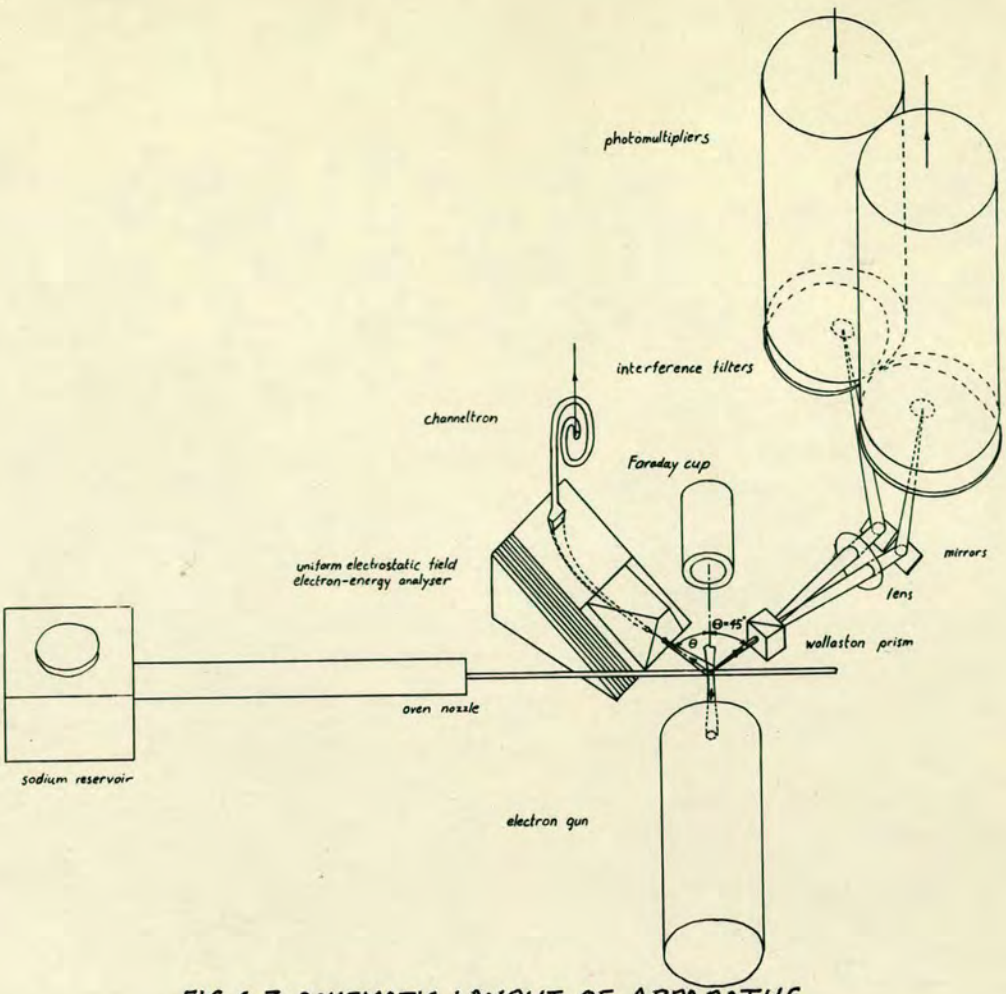

FIG. 4·3 SCHEMATIC LAYOUT OF APPARATUS

FIG. 4·2 VIEW OF APPARATUS SHOWING SCATTERING CHAMBER (CENTRE) & OVEN CHAMBER (LEFT)

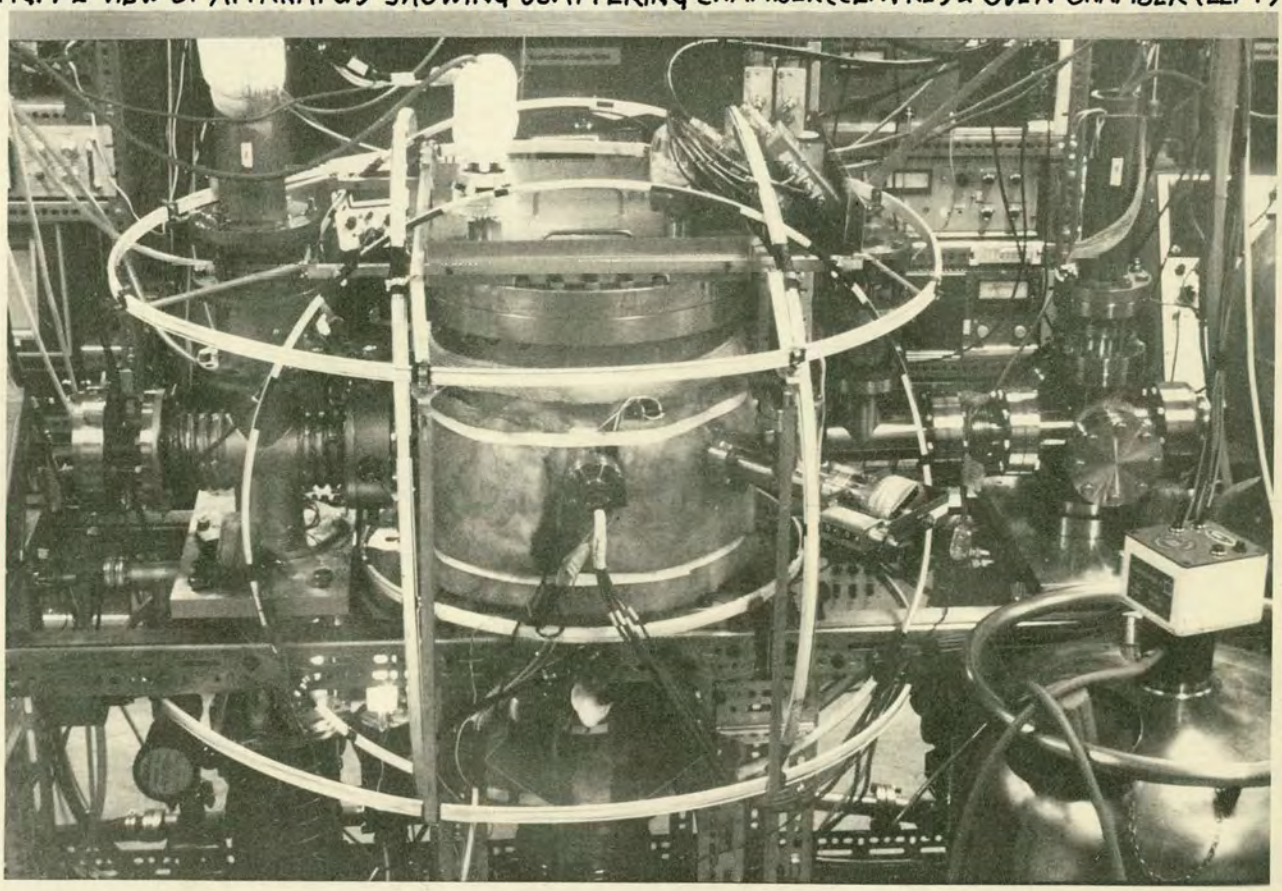

CHAPTER 4

THE APPARATUS

The various components of the apparatus (i.e. the atomic-beam, optical and electron-optical systems, etc.) and their required properties have been alluded to in the previous chapters. The general arrangement is shown in Figs. 4.1(a), (b), 4.2 and 4.3. Details of these systems will be described in the present chapter.

4.1 The Vacuum System (see Figs. 4.1(a), (b) and 4.2).

It is desirable to have as good a vacuum as possible for three reasons. Firstly, the background count rate in the electron channel arises mainly from elastic scattering from residual gas. The atomic-beam density in the target region is of the order of 10^{15} atoms m^{-3}. A background gas density of this amount corresponds to a pressure of 3×10^{-8} torr. Secondly, the cathode used in the electron gun (see section 4.4) is of the reactivatable type but is very easily "poisoned" by the presence of impurities. To maintain maximum emission it is necessary to eliminate contaminants such as oxygen, water vapour, and hydrocarbons, and it is necessary to maintain a total pressure of less than 10^{-7} torr. for successful operation of the cathode. Thirdly, the operation of the rest of the electron-optic system is sensitive to the condition of the electrode surfaces at the low electron energies used. The build up of any insulating layer (e.g. oil, oxides) on these surfaces, which will inevitably become charged, will lead to

distortions in the field and give rise to erratic operation of the electron-optical system. These constraints transcend the usual one of requiring that the intensities of the incident beams are negligibly reduced by scattering from background gas.

To reduce outgassing and render the system bakeable the vacuum chamber is fabricated from non-magnetic stainless steel (EN58B). Copper-gasket seals ("conflats") are used on all small diameter flanges (e.g. feedthroughs) and a gold or indium wire seal is used for the scattering-chamber lid. The scattering chamber and oven chamber are pumped by Edwards E04 oil-diffusion pumps and the detector chamber by an E02 diffusion pump. The pumping fluid is Santovac 5. All pumps are equipped with water-cooled chevron baffles and liquid nitrogen-cooled traps, to reduce backstreaming of oil vapour into the system and improve the ultimate vacuum. The liquid nitrogen trap on the E02 also servesas a beam dump. Another liquid nitrogen trap mounted beneath the lid of the scattering chamber, is used to cool the photomultipliers as well as to provide extra pumping speed. Automatic replenishment of the liquid nitrogen traps is accomplished by means of a device described in Appendix III(d). Alumina traps are fitted to all "backing" and "roughing" ports to reduce the ingress into the system of oil vapour from the rotary pumps. An Edwards ED330 rotary pump is used to "rough out" the scattering chamber and to "back" the corresponding E04 and E02 diffusion pumps. A separate rotary pump (ED50) is used for the oven chamber to facilitate reloading of the oven while the scattering chamber remains under vacuum.

Only materials with low vapour pressures and outgassing rates are used in the fabrication of components inside the

vacuum chamber. This optimizes the effect of baking and ensures that the highest ultimate vacuum is obtainable. Non-magnetic stainless steel (EN58B or J) nuts, bolts, shafts and gears are used. Electron-optical components are manufactured from gold-plated, oxygen-free copper; and bearings from bronze. Other structures (e.g. supporting table, brackets etc.) are made from dural. Before installation, the stainless-steel components are checked for residual magnetization with a magnetometer. Components giving rise to a field greater than 3×10^{-7}T at the interaction region are discarded. Insulating components are either in ceramic or mica and sleeving for conducting wires is glass-fibre. In a few cases it is more convenient to use PTFE and nylon in small amounts. This, and the fact that a channel electron multiplier (CEM) is present in the system, limits the baking temperature to 120°C.

A system bakeout is commenced with the liquid-nitrogen traps empty and when the system pressure has fallen to approximately 10^{-6} torr. (after 3-4 hours pumping). The temperature is slowly raised to 120°C during the day and left at this temperature overnight. The system is then allowed to cool and the traps are filled. After a further 12 hours the pressure in the scattering chamber has fallen to 10^{-8} torr. It is of course necessary to remove the optical bench, (holding, for example, the Wollaston prism), the interference filters and the photomultipliers prior to baking. The photomultipliers and filters are especially sensitive to temperature and will suffer permanent damage if it exceeds 50°C. It is found that provided the system is let up to an atmosphere of dry nitrogen,

in order to replace the optical components, the effect of the bakeout is not lost and on the next pump-down the original pressure is still obtained.

The diffusion pumps are automatically switched off by a protection circuit if the pump cooling-water supply fails, if the system pressure rises above a preset level (5×10^{-4} torr.) or if the mains supply to the rotary pumps is interrupted. This protection device is also arranged to switch off, under these conditions, the detector high voltage supplies, the electron gun heater, the atomic beam oven heater, the liquid-nitrogen replenishers, and atomic-beam detector filament.

4.2 The Helmholtz Coils (see Fig. 4.2)

The theory of Wykes (1972) outlined in Chapter 2 assumes that the level structure is that appropriate to zero external magnetic field. Therefore three mutually perpendicular pairs of Helmholtz coils are used to compensate the earth's field and reduce it to zero at the interaction region; non-magnetic materials are used for the construction of the apparatus to avoid any irregularities in this otherwise zero field; and, for the same reason, only electrostatic fields are used in the electron-optical system. The size of the Helmholtz coils is determined by the required uniformity in the resultant magnetic field, that is, the maximum tolerable fluctuation from zero over a specified volume. This in turn depends upon the above "atomic structure" constraint and also on the constraint that the operation of the electrostatic electron-optic system is not degraded by the presence of a finite magnetic field.

In the case of the former constraint the most critical assumption of Wykes is that all the magnetic sublevels of a particular hyperfine state are completely degenerate. Any splitting of these sublevels should therefore be very small compared to the level width if this assumption is to be justified. Another way of expressing this condition is that the precession period of the atomic dipole in the external field should be very long compared to the natural lifetime of the excited state. A precession period in a field B Tesla is of the order $\mu_o h/\mu_\beta B$ where $\mu_o = 4\pi \times 10^{-7}$ henry m^{-1} (permeability of free space) and $\mu_\beta = 1.165 \times 10^{-29}$ weber m (Bohr magneton). The period becomes therefore $7.1 \times 10^{-11}/B$ secs. It is required therefore that

$$7.1 \times 10^{-11}/B \gg 1.6 \times 10^{-8}$$

or

$$B \ll 4.5 \times 10^{-3} T .$$

This should be fulfilled over the interaction volume which is of the order of 2×10^{-3}m in extent, and B should be of the order of 10^{-5}T over this region.

The latter constraint, involving a consideration of the distortions in electron trajectories caused by the presence of an external field, is more stringent as will now be shown. An electron of energy U ev travelling a distance ℓ in a magnetic field of magnitude B and direction perpendicular to that of the initial velocity of the electron, suffers a defection d given approximately by:-

$$d \approx \ell^2 B \sqrt{\frac{e}{m}\frac{1}{2U}}$$

Taking U to be 2 eV and ℓ to be 0.12 m, and requiring that $d < 10^{-3}$ m (a typical slit width) gives:-

$$B < 3.3 \times 10^{-7} \text{ T.}$$

This should be fulfilled over the whole length of the trajectory, i.e. 0.12m.

The design of the Helmholtz coils is thus determined by the requirement that the field should be homogeneous to within 3×10^{-7}T over a distance of 0.12m. The Helmholtz condition: coil separation = coil radius $\equiv a$, results in maximum homogeneity given by (Reitz and Milford, 1962):-

$$\frac{B(a/2) - B(z)}{B(a/2)} = \frac{144}{125} \left(\frac{z - a/2}{a}\right)^4$$

where B is the axial component of the field, and z is the distance from the plane of one coil to a point along the common axis. The worst case is for the pair of coils compensating the earth's vertical component. So, putting $B(a/2) = 4 \times 10^{-5}$T, $B(a/2) - B(z) = 3 \times 10^{-7}$T and $z - a/2 = 0.12$m the following condition is obtained for a:-

$$a > 0.42\text{m.}$$

For a given a and B the number of ampere terms (ni) in each coil is given by

$$ni = \frac{1.398aB}{\mu_o} .$$

In the case of the pair with vertical axis it is convenient to choose $a = 0.49$m which gives $ni \approx 21$. Each coil consists of 25 terms of 20 S.W.G. enamelled copper wire and i is therefore approximately 0.87A. The constraints on the other two pairs of coils are less critical and, again for convenience, are chosen to have $a = .39$m. One pair has slightly smaller

diameter to enable the pairs to interlock. Because of the relative ease of winding the smaller coils and the necessity of minimizing the load on the power supply, 60 turns of 20 S.W.G. wire are wound on each coil of these two pairs. For the pair whose axis lies approximately N-S:
$B(^a/2) \approx 1.5 \times 10^{-5}$T and i $\approx$ 0.11A. The third pair will obviously require much less current. Smoothed, current-regulated power supplies are used to power the coils.

The currents in the coils are accurately set using a Hewlett-Packard magnetometer. The probe is placed at the interaction region and set up successively along the axis of each Helmholtz pair. At each position the current in the corresponding pair is adjusted to give zero net field. To compensate for errors due to misalignment of the probe with respect to the axes or misalignment of the Helmholtz pairs with respect to one another, the above process is repeated until all the components are zero to within 3×10^{-7}T. The resulting settings are given in Appendix IV(b). The whole setting up process is carried out with all components of the apparatus present in their exact final positions, and the coil currents are not adjusted further.

4.3 The Optical System

General Arrangement

The size of the scattering chamber determines the arrangement of components of the optical system (see Fig. 4.3). The light from the interaction region is passed first to a Wollaston prism where it is analyzed into two plane, orthogonally polarized components. The polarization state of the light is thus

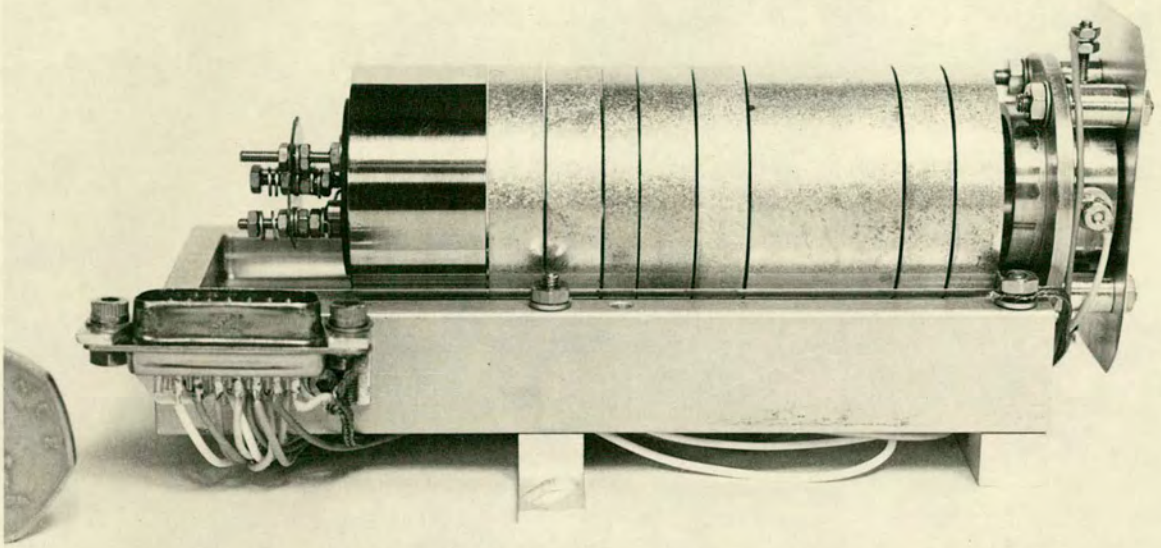

FIG.4·8:- ELECTRON GUN (COVER REMOVED)

FIG.4·4:- OPTICAL BENCH (COVER REMOVED)

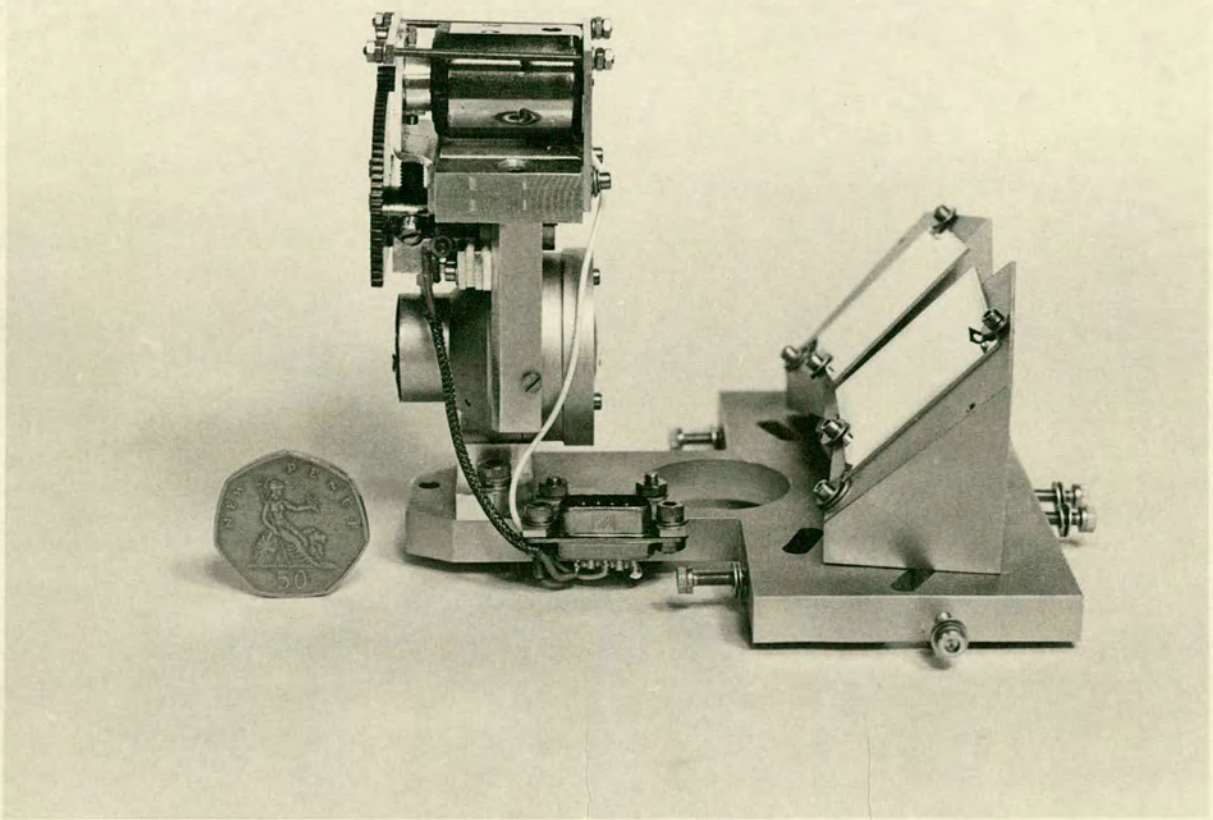

determined before it is possible for it to be degraded or changed due to refraction or reflection. A calcite prism is used because, for a given refracting angle the angular separation of the exit beams is larger than for a quartz prism. The prism is of type CW09 manufactured by Rank Precision Ltd. The full aperture is 10mm × 10mm and the beam separation is 16° at 500 nm. In the scanning plane of the electron detector (the horizontal plane) the maximum angle of incidence is required to be $\pm 3.5^{\circ}$ so that the expected structure in the polarization versus θ curve is resolvable. If the Wollaston prism is 27mm from the interaction region then this implies an entrance-aperture width of 2mm. In the perpendicular plane a larger angular resolution is tolerable, and is to be preferred in order to maximize light collection efficiency. An aperture height of 7 mm is therefore chosen. Two borosilicate crown lenses focus both emergent light beams, each onto a 4 mm diameter aperture in a screen enclosing the window of the corresponding photomultiplier (see Fig. 3.12). An aluminium mirror is used to deflect each beam onto the appropriate aperture. The system of entrance aperture, prism, lenses, mirrors and exit apertures are mounted on an optical bench (see Fig. 4.4; in this figure the exit apertures are not shown) and aligned with respect to each other before installation. The optical bench is attached to the supporting table, within the scattering chamber, by three adjusting screws which enable the bench to be aligned with respect to the interaction region. After this initial alignment the optical bench can be removed and replaced, the only readjustment necessary being that of orientation about a fixed point in the

horizontal plane. This is easily carried out using a light-emitting diode (LED), correctly positioned to simulate the interaction volume, and diffusing screens placed over the exit apertures to locate the images.

The interaction region is defined with respect to the supporting table by the intersection of an imaginary line and plane; the line being the (vertical) axis of rotation of the analyzer, the bearing of which is set into the table surface. The plane is parallel to that of the table surface and is at the same height above this surface as the centre of the analyzer entrance-aperture. A conical-ended screw can be fitted into the end of the axle carrying the analyzer so that they are coaxial. The height of the tip of the cone above the table surface is adjusted to be precisely equal to height above this surface of the analyzer entrance-aperture. This is done using a surface gauge. The cone tip is now used in all subsequent alignment procedures, to define the centre of the interaction region, excepting the case of optical-bench alignment. In this case, a similar screw, carrying at its end an LED, is fitted into the axle. The height of the centre of the LED is adjusted, in a like manner, to be equal to that of the analyzer entrance-aperture.

The whole of the optical system is enclosed in an aluminium box to eliminate stray light. The photomultipliers are contained in aluminium tubes attached to the "lid" liquid-nitrogen trap (see section 3.5). The ends of these tubes contain filters and locate into recesses (in the top of the box enclosing the optical system) when the lid of the scattering chamber is in position. The photomultipliers have therefore

to be very carefully aligned with respect to the trap, and extreme care must be exercised when lowering the lid (which has a mass of 50 Kg). The location of the components can be observed, during this operation, through a viewing port in the side of the scattering chamber. Internal aluminium screens in the optical system divide it into two completely separate halves beyond the lenses so as to eliminate the possibility of "crosstalk". All the screening is coated with aquadag to reduce reflection. Although soot is used elsewhere (scattering-chamber walls, table surface etc.) for this purpose it was thought unwise to use it in this application because of the possibility of its getting on to the optical surfaces.

Filters To prevent systematic errors due to the detection of photons from the decay of states other than those of interest, it is necessary to limit the range of wavelengths detected, by using band-pass interference filters. For Na the lines closest to those under study stem from the transitions $4^2D - 3^2P$ (569nm) and $5S - 3^2P$ (615 nm) (see Fig. 1.1). Similarly, in the case of K the only troublesome transitions would be $4^2D - 4^2P$ (697 nm) and $3^2D - 4^2P$ (1168 nm). Suitable filters of 47 nm bandwidth and 70% peak transmission were obtainable from Grubb Parsons Ltd. Although filters of this bandwidth would seem only on the borderline of being sufficient, it should be borne in mind that the intensities of the undesirable lines should be much lower than those of the resonance transition because at all energies, the excitation functions for levels of the S and D series are a factor

15 or more smaller than those of the P series (Zapesochnyi and Shimon, 1965; Zapesochnyi, Shimon and Sosnikov, 1965).

Filters of narrower bandwidth would have three disadvantages:- They have, in general, lower peak transmission; they are more sensitive to incorrect orientation with respect to the direction of the incident beam, and it would be necessary to use a parallel light beam otherwise the surface rays of a conical bundle would be incorrectly filtered. An added disadvantage of such filters in the present arrangement is that the filters are cooled as they are in contact with the photomultipliers. Their temperature is lowered to approximately -70°C which leads to a shift in the wavelength of peak transmission of approximately 2 nm. In the case of the present filters this would not lead to a serious reduction in transmission. Another effect of cooling on some filters originally obtained was that the interference layer became crazed, resulting from the relative expansion of the substrate and bonding compound. Fortunately Grubb Parsons Ltd. were able to supply filters employing a special compound which eliminated this effect of cooling.

A possible advantage of narrower bandwidth filters would be the reduction of background light from the electron-gun filament. Stemming, as it does, from a black body at approximately 1000°C, it is present in ever increasing amounts at wavelengths above those of interest. In spite of the fact that the photocathode response is falling off sharply in this region it is still detected in significant amounts as was shown by operating the system with and without filters. Without filters present, the light from the electron-gun

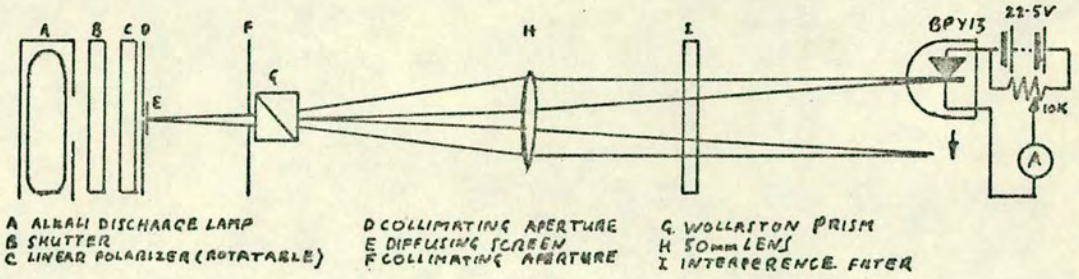

FIG. 4·5
TESTING OF THE OPTICAL COMPONENTS

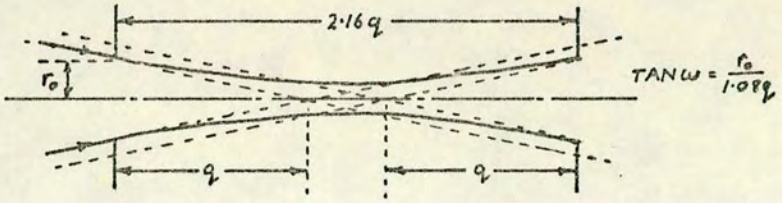

FIG. 4·6
EFFECT OF SPACE CHARGE ON FOCUS
OF ELECTRON BEAM

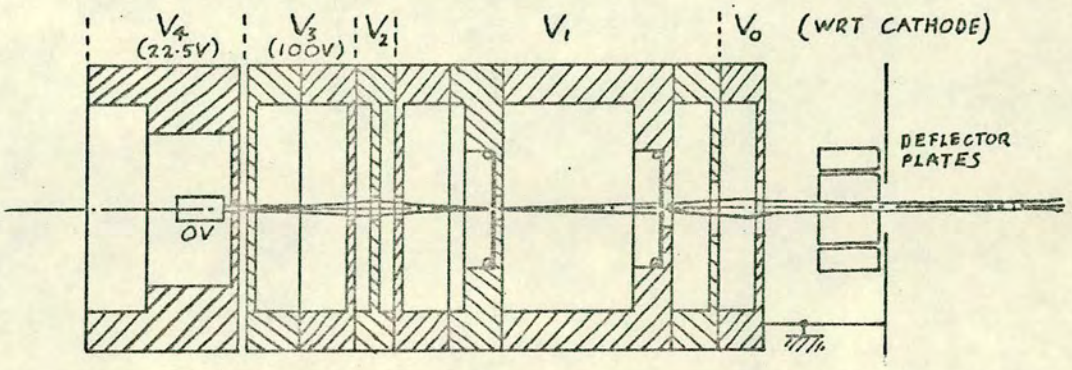

FIG. 4·7
THE ELECTRON GUN (SCALE 1:1)

filament contributed approximately 480 Hz to the overall count rate while with the 47 nm filters this was reduced to approximately 20 Hz. This was not significantly reduced when a 7 nm filter was substituted, indicating that this contribution to background was due mainly to light "leaks" in the shielding. The 47 nm filters were therefore used.

Determination of the Asymmetry of the Photon Channels. As was stated in section 3.3 it is necessary to determine the relative efficiencies in the two photon channels in order that corrections, if necessary, can be made to the measured polarization (see Appendix I). A measurement of the channel efficiencies implies the use of appropriately polarized light in each channel. It is also necessary to know, however, what fraction of light is transmitted by one channel which has the necessary polarization to be transmitted with maximum efficiency by the other. This test is carried out using the arrangement shown in Fig. 4.5.

An HN32 polaroid (Polarizers UK Ltd.) is used to select the direction of polarization of the light from an Na discharge lamp. A system of collimating apertures defines the solid angle of acceptance of the Wollaston to be the same as that to be used in the main experiment. The light intensity transmitted by the Wollaston into each of the two channels, is monitored by letting the light impinge on a back-biased BPY13 photodiode. A lens focuses the light in each beam onto the photodiode and an interference filter is used to cut down stray light and to eliminate the background due to the intense infra-red component produced by the lamp (to which the photo-

PHOTODIODE CURRENT × 10⁷/A (CORRECTED FOR BACKGROUND AND SOURCE POLARIZATION)		WOLLASTON CHANNEL	
		↕ (2)	↔ (1)
POLAROID ORIENTATION (H H32)	↕	4·74	0·01
	↔	0·01	4·57

TABLE 4·1
RELATIVE TRANSMISSION OF WOLLASTON CHANNELS
FOR DIFFERENT INCIDENT POLARIZATIONS (Na LIGHT)

CATHODE – EARTH POTENTIAL V_0	POSN. OF FOCUS	2·0	2·5	3·0	3·5	4·0	4·5	5·0	5·5	6·0	6·5
V_1	INTERACTION REGION (IR) $V_1 = 9V_0$	18·0	22·5	27·0	31·5	36·0	40·5	45·0	49·5	54·0	58·5
	ANALYZER (A) $V_1 = 5V_0$	10·0	12·5	15·0	17·5	20·0	22·5	25·0	27·5	30·0	32·5
$\frac{V_3}{V_1} \equiv \frac{100}{V_1}$	IR	5·56	4·44	3·70	3·18	2·78	2·47	2·21	2·02	1·85	1·71
	A	10·0	8·0	6·67	5·72	5·0	4·44	4·0	3·64	3·33	3·08
$\frac{V_2}{V_1}$	IR	8·0	8·5	8·5	8·5	8·0	8·0	8·0	7·5	7·0	7·0
	A	8·0	8·5	8·5	8·5	8·5	8·5	8·5	8·5	8·5	8·5
V_2	IR	155	191	230	268	278	324	360	371	378	410
	A	80	106	127	149	170	191	212	234	255	276

NB. TAKING INTO ACCOUNT THE EFFECTS OF CONTACT POTENTIALS ETC. THE FIRST LINE WOULD CORRESPOND MORE CLOSELY TO THE FINAL BEAM ENERGY IN eV

TABLE 4·2
LENS VOLTAGES

diode is very sensitive). The current through the BPY13 is measured using a Keithley 602 electrometer. Using a calibrated neutral density filter, the current is found to be accurately linear with light intensity at the wavelength of interest.

The polaroid is rotated until maximum intensity is transmitted through one Wollaston channel. The detector is now traversed to the position of the other beam and its intensity is measured. The process is repeated after rotating the polaroid through 90^{o}. These measurements are repeated using a K light source, HN7 polaroid, and appropriate filter. Typical results are shown in Table 4.1. Background contributions have been subtracted. The magnitude of these was measured after closing a shutter in front of the light-source. The quality of the Wollaston as a polarization analyzer can be judged from these results. At worst (assuming a perfect polaroid) the Wollaston is seen to transmit only 0.2% of the "wrong" component. The results in Table 4.1 have been corrected for the small polarization of the source. (By removing the Wollaston and rotating the polaroid between the two above positions a ratio of the component intensities of 1.22 : 1 is obtained.) The Wollaston will thus be assumed perfect as far as the present work is concerned. (It should be noted also that the same upper limit can be placed on the quality of the respective polaroids for the wavelengths concerned.)

In order to obtain an accurate calibration of the channel asymmetry for the whole optical system (including photomultipliers) it is necessary to carry this out with the system in the same environment that would prevail during a run (i.e. the same

temperature, magnetic field distribution etc.) This entails having a source of known polarization inside the vacuum chamber and located at the centre of the interaction region. It was decided to use the actual light from the transition under study and to obtain from this a beam of known polarization by interposing a polaroid followed by a wave plate. These two components are embodied in each of two polarizers manufactured by Polarizers U.K. Ltd. The HNCP24 contains what is nominally a $\lambda/4$ plate at Na resonance wavelength, while the HNCP7 is the equivalent for K resonance wavelengths. The exact ellipticity (including orientation) is initially measured using a similar arrangement to that shown in Fig. 4.5 but with the "circular polarizer" (HNCP24 or HNCP7) replacing the linear polarizer (HN32 or HN7) and this replacing the Wollaston prism. The linear polarizer is rotated and the intensities and directions at the maxima and minima are obtained. The results are as follows:-

Source	Polarizer	Intensity Ratio
Na	HNCP24	1.31 ± .01
K	HNCP7	1.36 ± .01

In obtaining these results it has been assumed that the linear polarizers are ideal. This is justified by the results of the previous investigation.

The HNCP24 is arranged such that when it is intercepting the incident beam, the minor axis of the ellipse is parallel to the plane defined by the output beams of the Wollaston.

Originally the NHCP24 could be brought in and out of the incident beam, while the system was under vacuum, using a small D.C. motor (see Fig. 4.4), but the magnetic field produced by

this interfered with the operation of the electron optics to such an extent that it became necessary to remove it. This mechanism was replaced by a copper arm, pivoted at its centre and carrying the HNCP24 and a counter-weight at its extremities. The counter-weight causes the arm to swing out of the beam under gravity, but is prevented from doing so by a 0.1 mm diameter tungsten wire. When the whole system is running the "singles" count rates in the two photon channels are compared, with and without the atomic beam target present. This provides the measurement of the channel asymmetry with the help of the above measurement of intensity ratios. The results of the channel asymmetry measurements will be presented in Chapter 5.

When the calibration has been performed, the HNCP24 is removed by passing 5.5A (3.5V) through the tungsten wire, melting it, and allowing the arm to swing the polarizer out of the beam. A run can now be started for the measurement of Π.

The polarizer is constructed from insulating materials and as it is positioned only 20mm from the interaction region it is liable to become charged with deleterious effects to the electron beam. To reduce possible distortions in the field to a minimum, the polarizer is surrounded by an earthed 20 cps micromesh fabricated from gold-plated copper (EMI Ltd.). The measurement described above, of the maximum/minimum intensity ratio of the HNCP24, was carried out with and without the presence of this mesh and was found to be the same in both cases.

4.4 The Electron Gun

Introduction The required properties of the electron beam have already been mentioned in Chapter 1 and in section 3.3 i.e. an energy in the range 2 - 5 eV, a maximum convergence angle of 2° and a spot diameter of approximately 1.0 mm.

The gun is designed according to the principles set out by Simpson and Kuyatt (1963a). The dispersive effects of space charge in the otherwise field-free region of the focus (Thompson and Headrick, 1940; Pierce, 1954) limits the current to:-

$$I_{max} = 38.5\ U^{3/2} \tan^2\omega\ \mu A \qquad (4.1)$$

where U is the energy (eV) and ω is the maximum angle of convergence. (See Fig. 4.6.) For $U = 5.0$ eV and $\omega = 2^{\circ}$ $I_{max} = 5.2 \times 10^{-7}$A. The minimum diameter of the beam is (neglecting thermal effects) $2r_o/2.35$. This determines the image-distance of the final lens to be 30.5 mm. It is shown that the position of the minimum beam diameter is at a distance of $1.08 \times 30.5 = 33$ mm. The minimum current density (J_c) at the cathode necessary to provide the resulting density at the "focus" is determined by the relation (Langmuir, 1937; Pierce, 1939):-

$$J_{max} \leq J_c\left[1 + \frac{11600U}{T}\right]\sin^2\omega \qquad (4.2)$$

where T is the cathode temperature ($^{\circ}$K). For a worst case of $U = 2.0$ eV and for $T = 1273^{\circ}$K: $J_c \geq 30\mu A\ mm^{-2}$. To overcome space charge limitations at the cathode, an anode-cathode potential (V_3) is required, determined by (Langmuir, 1913):-

$$J_c \leq \frac{2.34V_3^{3/2}}{d^2}\ \mu A\ mm^{-2} \qquad (4.3)$$

where d is the anode-cathode distance (mm). For d = 3.0 mm this gives $V_3 \geq 24V$. Thus a multipotential gun is required (Simpson and Kuyatt, 1963b) consisting of an extraction stage followed by a deceleration stage. This deceleration is provided in two stages at potentials V_1 and V_2 with respect to the cathode. (See Fig. 4.7.) The first lens (V_2), designed according to calculations carried out by Read (1970), possesses constant image and object distances as the final beam energy is varied (i.e. variation of V_1 and V_o:- the cathode-earth potential). A range of operation can also be chosen so that the magnification is relatively constant.

Immediately following this lens, while it is still at relatively high energy, the beam is collimated by two 0.5mm diameter molybdenum apertures to produce the desired ultimate angle of convergence. These apertures also serve the purpose of limiting the diameter of the beam to be significantly smaller than that of the final lens apertures. This avoids possible erratic operation due to the charging of deposits around the periphery of these apertures.

The final deceleration is carried out by a two-aperture lens (V_o, V_1) designed according to data given by Spangenberg and Field (1943). The potentials V_1 and .V2 for various values of V_o (determining the final beam energy), taken from the data of Read, and Spangenberg and Field, are listed in Table 4.2. This is helpful in the setting-up of the gun. These values should only be regarded as guides as the effects of contact potentials, thermal velocities, and finite aperture-thicknesses are not taken into account.

The extraction stage is based on a design of Soa (1959). The anode (extractor) potential (V_3) is fixed at 100 V easily satisfying condition (4.3). The grid ("Wehnelt") potential (V_4) is chosen empirically to maximize the beam current (i.e. so that the crossover is imaged by the subsequent lenses.)

Construction and Alignment of the Gun

The cathode is fitted to the inside of the "Wehnelt" cylinder by mounting it on a ceramic plug. It is a dispenser cathode, type M (Phillips Metalonics) which is reactivatable and is capable of giving a high emission density (0.06A mm^{-2} at 1000°C) more than sufficient for the present purpose. To aid the reactivation of the cathode, e.g., after the optical system has been installed; mica-insulated, stainless steel heating coils are contained in longitudinal slots cut into the surface of the "Wehnelt" cylinder. This enables the cathode and the electrodes immediately surrounding it, to be baked independently of the rest of the system. The coils are wound from 0.5 mm diameter wire. Stainless steel is chosen because of its relatively high resistivity and its low percentage of Ni compared to other materials of similar resisticity (i.e. nichrome). The cathode is easily poisoned by the presence of nickel and the use of this element must therefore be limited in the region of the cathode. The baking of the cathode evolves gases which must be quickly pumped away. This is assisted by the presence of 6.0 mm diameter radial holes through the surface of the "Wehnelt". The resistance of the "Wehnelt" heater is 10Ω when cold.

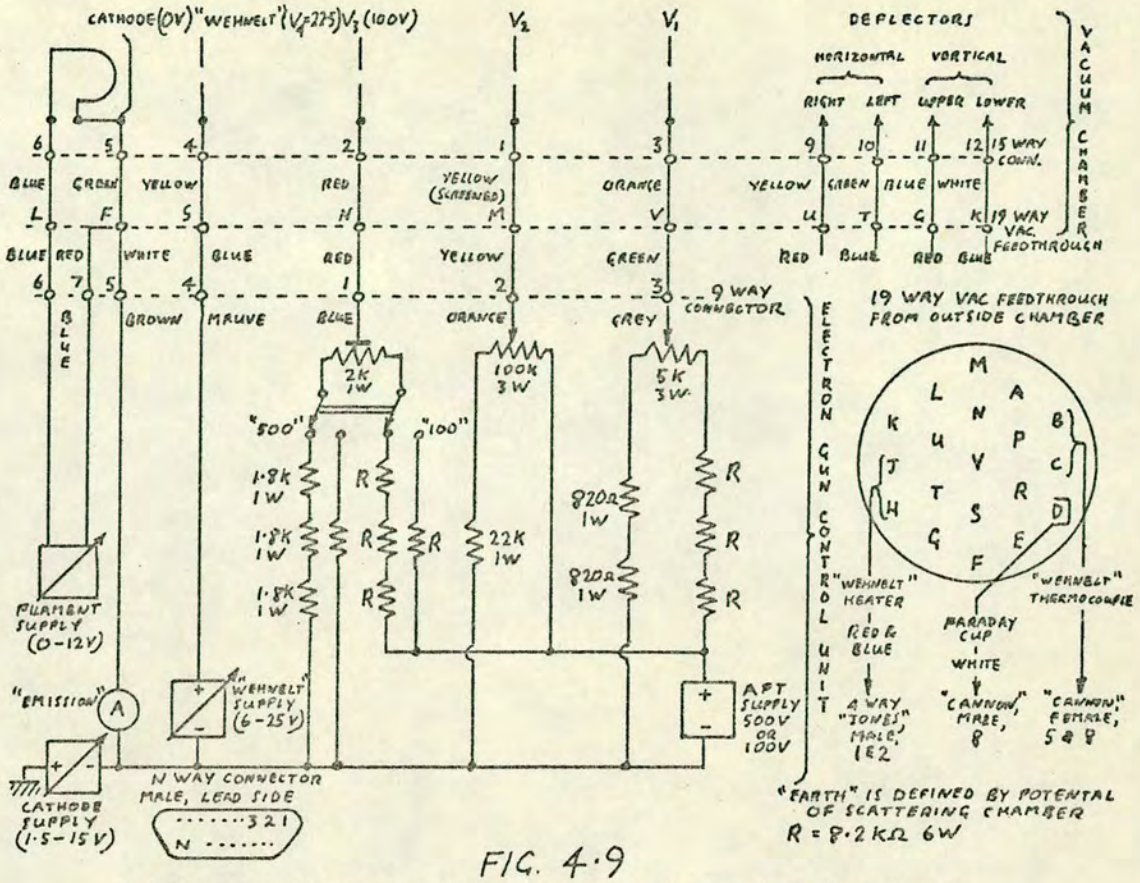

FIG. 4·9

ARRANGEMENT OF ELECTRON GUN POWER SUPPLIES

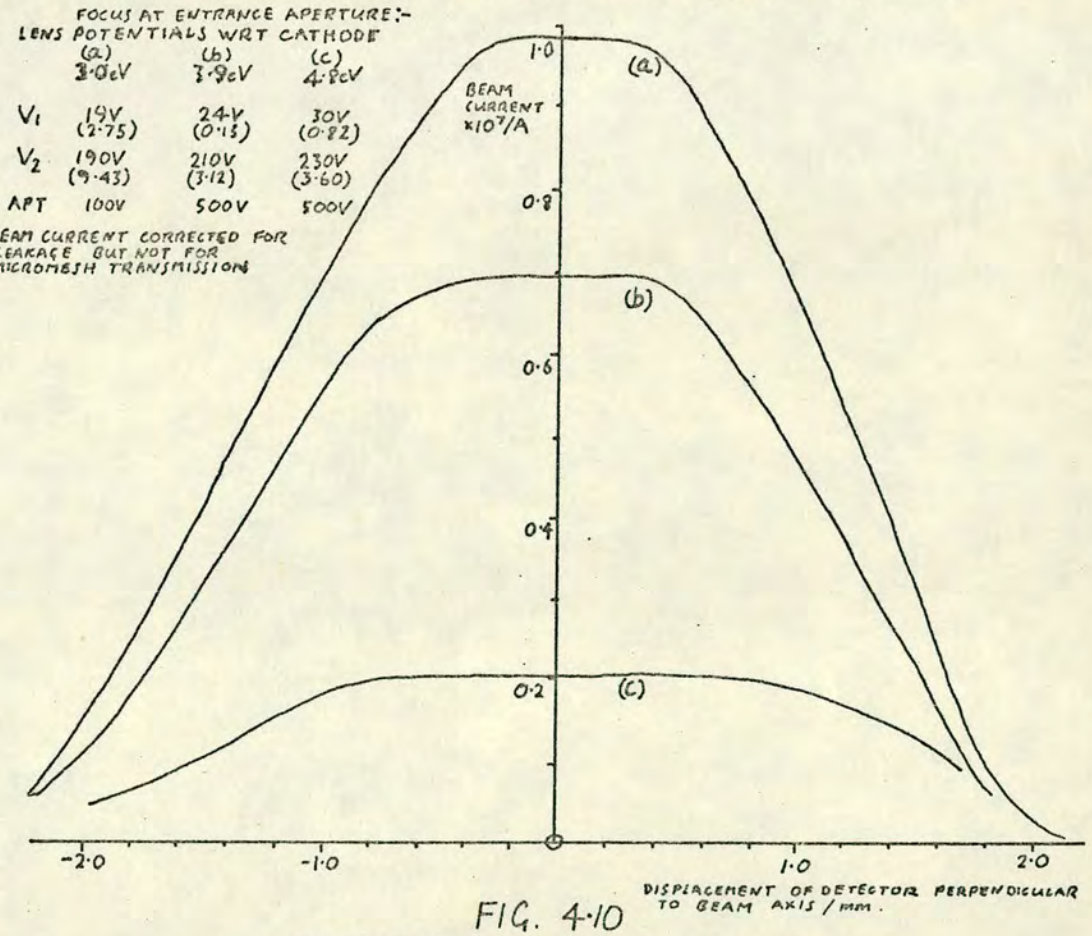

FIG. 4·10

ELECTRON BEAM PROFILES AT ANALYZER ENTRANCE APERTURE.

The outer peripheries of the lens elements are formed into cylindrical shells (see Fig. 4.7) to enclose the gun structure and provide electrostatic shielding. These cylinders are of 27 mm internal diameter and their influence on the operation of the gun is negligible (Read, 1969). The elements are turned from oxygen-free copper, degreased, cleaned in dilute nitric acid, and gold-plated. They are mounted on a pair of quartz rods maintained parallel in a milled recess of a dural base. The apertures of the lenses are thus in precise alignment. Figure 4.8 shows the complete electron gun save for the "Wehnelt" heater. As the "Wehnelt" cylinder surrounds the cathode, its temperature rises appreciably and it is therefore fabricated from stainless steel (EN58B), rather than copper, to reduce outgassing. This is also mounted on the above quartz rods. The complete electron gun is enclosed in a box fabricated from 0.25 mm copper sheet, the inside of which is coated in aquadag. The purpose of this is to cut down the amount of stray light due to the cathode heater. Small apertures, one at each end of the box, serve to transmit the electron beam, and allow power leads into the gun. To improve the pumping of the interior of the box, while still preventing the emission of stray light, a 20 mm diameter, 200 mm long copper pipe leads from here into the mouth of the E04.

The power leads to the various lens elements have fibre-glass insulation which is screened from the view of the interaction region by earthed copper sheets, as are the terminals of the vacuum feedthrough to which they are attached. A schematic diagram of the arrangement of the various power supplies is shown in Fig. 4.9. The smoothing

and voltage-regulation of the supplies for the cathode and Wehnelt voltages are:- < 1mV RMS and < 0.2% respectively. An APT 500V power supply is used for the other lenses. The corresponding parameters for this unit are:- < 1mV RMS and < 0.02% respectively.

The electron gun is attached to the main supporting table in the scattering chamber by three screws locating in slots on the electron-gun base. These screws allow complete orientation and position adjustments to be made in both the horizontal and vertical planes. The alignment-cone is fitted and the gun is aligned with respect to this and the analyzer entrance aperture, by removing the cathode and sighting these down the axis of the gun, through its apertures. The position of the analyzer is noted as this defines the forward-scattering direction ($\theta = 0^{\circ}$).

To circumvent any effects of alignment error once the system is under vacuum, and to provide fine adjustment of alignment, two orthogonal pairs of electrostatic defector-plates are fitted following the final lens of the gun.

Testing of the Gun

At the cathode activation temperature of 1100°C the gun is operating well inside the space-charge limited region. The cathode is thus unnecessarily bright - increasing the background in the photon channels and reducing cathode life. After activation, the cathode heater current is reduced, therefore, until it is just above that value where there is a noticeable drop in beam current (900-1000°C , 11V, 0.8A). The beam is now operating just at the space-charge limit.

The emission in this condition is 6.5 mA.

The required energy is set by the cathode-earth potential difference; The analyzer, in the "beam current" mode, (see section 4.5) is set at $\theta = 0^{\circ}$; the deflectors are set at zero; and V_1 is set according to Table 4.2 for focusing on the analyzer. Using Table 4.2 as a guide, V_2 and V_4 are varied to obtain optimum beam current. V_1 is readjusted to further optimize the current. This process is repeated until no more improvement is obtained. The deflectors are now adjusted to give maximum beam current. The above procedure may need to be repeated but the process soon "converges". The optimum "Wehnelt" potential is found to be +22.5V wrt the cathode. As expected, this is independent of energy.

Peak currents obtained through the 1 mm^2 entrance aperture of the analyzer at 3.0, 3.9 and 4.8 eV, when corrected for the transparency of the micromesh preceding the collector (see section 4.3) are :- 1.23, 0.86 and 0.26×10^{-7}A respectively; which are to be compared to 1.35, 0.99 and 0.67×10^{-7}A calculated from equation (4.1) assuming $\omega = 0.55^{\circ}$.

Bearing in mind the small uncertainties in ω and the micromesh transparency (assumed to be 80%) the situation is seen to be described well by equation (4.1) even though it does not take thermal effects into account.

The beam profile is investigated by measuring the collector current as a function of θ (angular setting of the analyser with respect to the direction of the electron beam). Results are shown in Fig. 4.10 for energies of 3.0, 3.9 and 4.8 eV. The approximately trapezoidal shapes of the

distributions imply that the beams are well localized and that the actual profiles are approximately rectangular, of widths (taking into account the width of the analyser entrance aperture) 1.5, 2.0 and 2.5 mm respectively. Values of the various lens potentials are shown in Fig. 4.10 for comparison with Table 4.2.

Energy Calibration Purely on the basis of cathode potential, the beam energy will be uncertain because of the uncertainty in the cathode-lens contact potential and the effects of thermal energies. An energy calibration is therefore carried out by employing the retarding potential difference (RPD) method, and making use of a copper Faraday cup (50 mm deep, 25mm internal diameter, 12 mm diameter aperture) fixed at $\theta = 0^{\circ}$ which is normally used to collect the unscattered electron beam.

The inside of the cup is coated with soot to reduce loss of electrons by reflection (Marmet and Kerwin, 1960; McGowan, 1967). The soot is obtained from a gas flame, the gas having been passed through benzene. The cup is normally held at + 22.5v with respect to earth and an earthed 20 cps gold-plated copper micromesh (EMI Ltd.) encloses it to prevent the escape of secondary electrons. This served the dual purpose of shielding the rest of the beam from the voltages placed on the cup. The surface of the cup thus resembles as closely as possible those adjacent to the interaction region (i.e. soot-coated copper). This helps to minimize the effects of contact potentials.

An energy calibration is performed by arbitrarily setting the cathode-earth voltage at 6.57V and focussing the electron

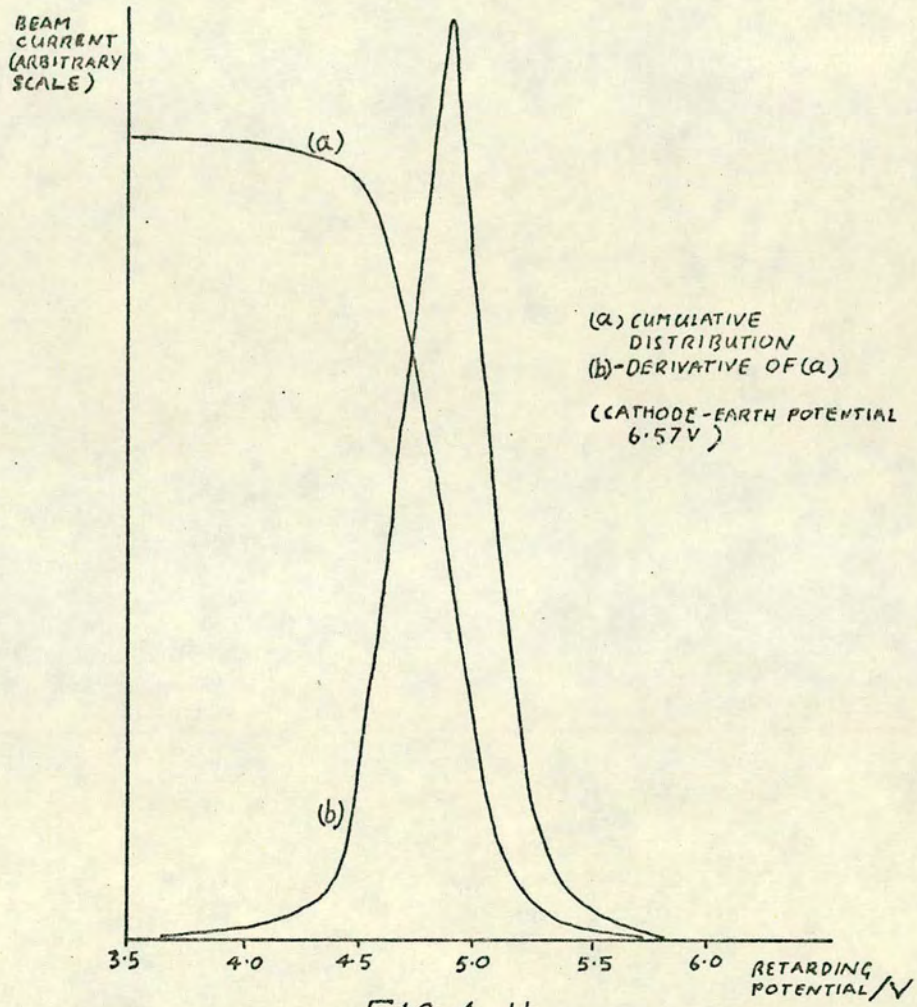

FIG. 4·11
RPD DETERMINATION OF ELECTRON ENERGY DISTRIBUTION

beam on the Faraday cup. The current to the cup is measured, using a Keithly 602 electrometer, as a function of retarding potential applied to the cup. The output of the electrometer is applied to the "y" input of an x-y recorder, and the Faraday-cup supply is connected to the "x" input. Voltages are defined in terms of the EMF of Weston cells. A DVM, used as a secondary standard is calibrated against these. All measurements are made with this DVM.

The result of this calibration is shown in Fig. 4.11. The position of the peak is at 4.9V ± .1. The cathode-lens contact potential and the effects of thermal energies, therefore give rise to the correction factor 1.7V ± .1, and the relationship between the cathode-earth voltage, V_o, and the beam energy, U, is:-

$$V_o = U + 1.7.$$

Subsequent measurements with the analyzer suggest that any systematic error in this factor due to contact potentials between Faraday cup and interaction region must be less than 0.1 eV.

The FWHM of the curve in Fig. 4.11 is 0.31 eV. The FWHM of the distribution, due to thermal velocity spreads is 2.54 kT (Klemperer, 1965) which is 0.27 eV at 1000°C. The discrepancy could be caused by the finite angular range (ω) of electrons incident on the grid of the Faraday cup. The retarding potential affects only the longitudinal momentum component (Simpson, 1961). This effect contributes an amount $U_o \sin^2\omega$ to the width, and would therefore imply a value for ω of 5° whereas, if the beam is correctly focussed ω should be approximately 2°. In this case the contribution

to the width would be only 0.006 eV. Heddle (1967) has shown that the effects of space charge give rise to a potential distribution, transverse to the beam axis, of magnitude

$$\Delta U_{SC} = 1.5 \times 10^{-2} \, I \, U^{-\frac{1}{2}} \text{ eV} \qquad (4.5)$$

for a beam current of $I\,\mu A$ at an energy of U eV. In the present case ($I \approx 2 \times 10^{-7} A$) U_{SC} is only of the order of 0.002 eV and cannot, therefore, give rise to the above discrepancy. It would therefore seem more likely to be due to incorrect focussing of the electron beam.

4.5 The Electron-Energy Analyzer

Resolution Requirements

Without energy analysis of the scattered electrons, false events would be recorded due to the population of the resonance levels by cascading from higher excited states. As can be seen from Fig. 1.1 the levels lying closest to the levels of interest (n^2P) are the $(n+1)S$ levels which are separated by 1.0 eV from the n^2P levels. The analyzer must be capable of resolving these levels. The spread in energy of the incident beam due to thermal effects is 0.3 eV FWHM. For maximum counting efficiency the resolution of the analyzer should be greater than this. This efficiency is only slightly reduced by choosing an analyzer base width resolution of 0.3 eV at 5.0 eV. The efficiency will be more noticeably reduced at lower beam energies of course. With this choice, the n^2P and $(n+1)S$ levels should be easily resolvable. It does not seem necessary under these conditions to provide

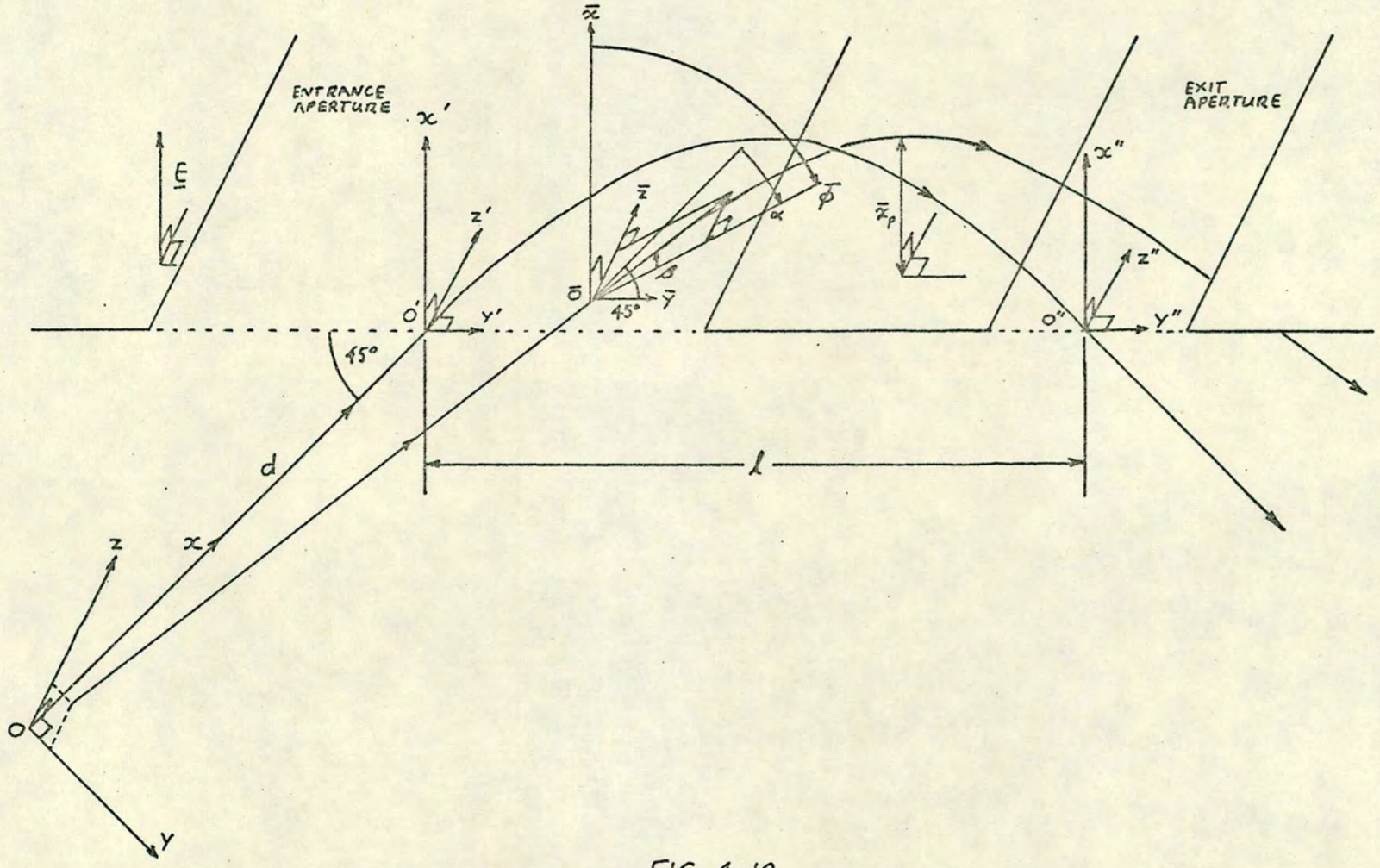

FIG. 4·12
GEOMETRY OF ELECTRON TRAJECTORIES IN ANALYZER

energy selection for the incident beam.

The most easily constructed electrostatic analyzer capable of giving the required resolution is of the uniform-field type (Harrower, 1955).

Design of the Analyzer Let a coordinate system $\bar{o}\ \bar{x}\ \bar{y}\ \bar{z}$ be defined whose origin $\bar{O}$ lies in the plane of the entrance aperture at the point of entry of an electron (see Fig. 4.12) The $\bar{x}$ axis is perpendicular to the plane of the aperture, parallel to the electric field; the $\bar{y}$ axis is in the plane of the aperture and is in the direction of the exit aperture; and the $\bar{z}$ axis is perpendicular to both these directions. If $\bar{\theta}$ is the polar angle of the electron trajectory at $\bar{O}$ then the angle β is defined by: $\beta = 90 - \bar{\theta}$. Similarly, if $\bar{\phi}$ is the azimuthal angle then α is defined by: $\alpha = \bar{\phi} - 45$. If U is the energy (eV) of the electron, its velocity $\underline{\bar{v}}$ at $\bar{O}$ is given by:-

$$\underline{\bar{v}} = \sqrt{\frac{2eU}{m}}\,(\cos\beta\cos\bar{\phi}\ ,\ \cos\beta\sin\bar{\phi},\ \sin\beta)\ . \qquad (4.6)$$

If E is the electric field (parallel to $\bar{x}$) within the analyzer, then the transit time t_A of the electron from $\bar{O}$ to the plane of the exit aperture is given by:-

$$\bar{v}_x = \frac{eEt_A}{2m}$$

$$\therefore \quad t_A = \frac{2}{E}\sqrt{\frac{2Um}{e}}\ \cos\beta\cos\bar{\phi}\ . \qquad (4.7)$$

The point of exit is given by:-

$$\underline{\bar{r}} = (0,\ \bar{v}_y t_A,\ \bar{v}_z t_A)$$
$$= \frac{2U}{E}(0,\ \cos^2\beta\sin 2\bar{\phi},\ \sin 2\beta\cos\bar{\phi})\ .$$

If α and β are small then to lowest order in α and β :-

$$\underline{\bar{r}} \approx \frac{2U}{E}(0,\ 1-2\alpha^2-\beta^2,\ \sqrt{2}\beta).$$

Let the particular trajectory from the centre (O) of the interaction region to the centre of the entrance aperture (O') with $\alpha = \beta = 0$, leave the analyzer at point O". Let new coordinate systems O'x'y'z' and O"x"y"z" be defined with corresponding axes parallel to those in $\bar{O}\ \bar{x}\ \bar{y}\ \bar{z}$. Let the distance O' O" = ℓ. Let the point of entry with respect to O'x'y'z' be (0,y'z'). Then the point of exit with respect to O" is given by:-

$$y'' = y'+\bar{y}-\ell \approx y' - \frac{4U}{E}\alpha^2 - \frac{2U}{E}\beta^2 + \frac{2U}{E} - \ell .$$

$$z'' = z' + \bar{z} \approx z' + \frac{2\sqrt{2}U}{E}\beta .$$

Let U_o be defined by $\ell = \frac{2U_o}{E}$ and ΔU_o by $U = U_o + \Delta U_o$. Then:-

$$y'' \approx y' - 2\ell\alpha^2 - \ell\beta^2 + \frac{e\Delta U_o}{U_o} \qquad (4.8)$$

$$z'' \approx z' + \sqrt{2}\,\ell\beta + \sqrt{2}\,\ell\frac{\Delta U_o}{U_o}\beta . \qquad (4.9)$$

Let a coordinate system Oxyz be defined, where Ox lies along OO'; Oy is perpendicular to Ox and lies in the plane defined by O, O', and O"; and Oz is perpendicular to both Ox and Oy. Let d be the distance OO'. Then for an electron leaving the interaction region at the point (x,y,z) in a direction with polar angle 90-β and azimuthal angle α (with respect to Oxyz), the point of entry (O, y', z') is given by:-

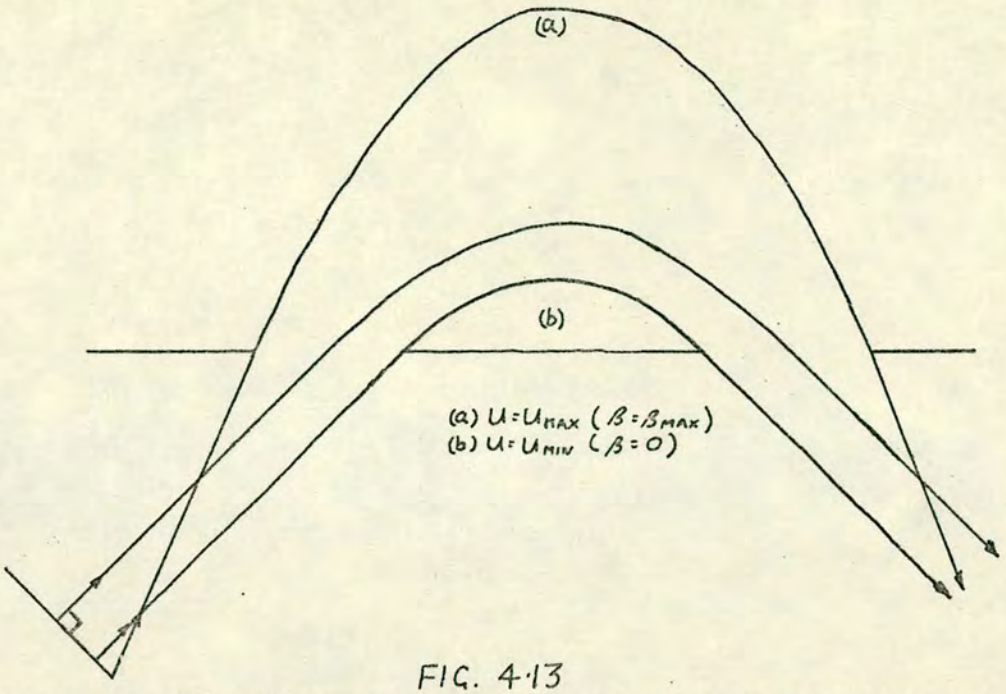

FIG. 4·13
TRAJECTORIES OF ELECTRONS TRANSMITTED WITH MAXIMUM AND MINIMUM POSSIBLE INITIAL ENERGY.

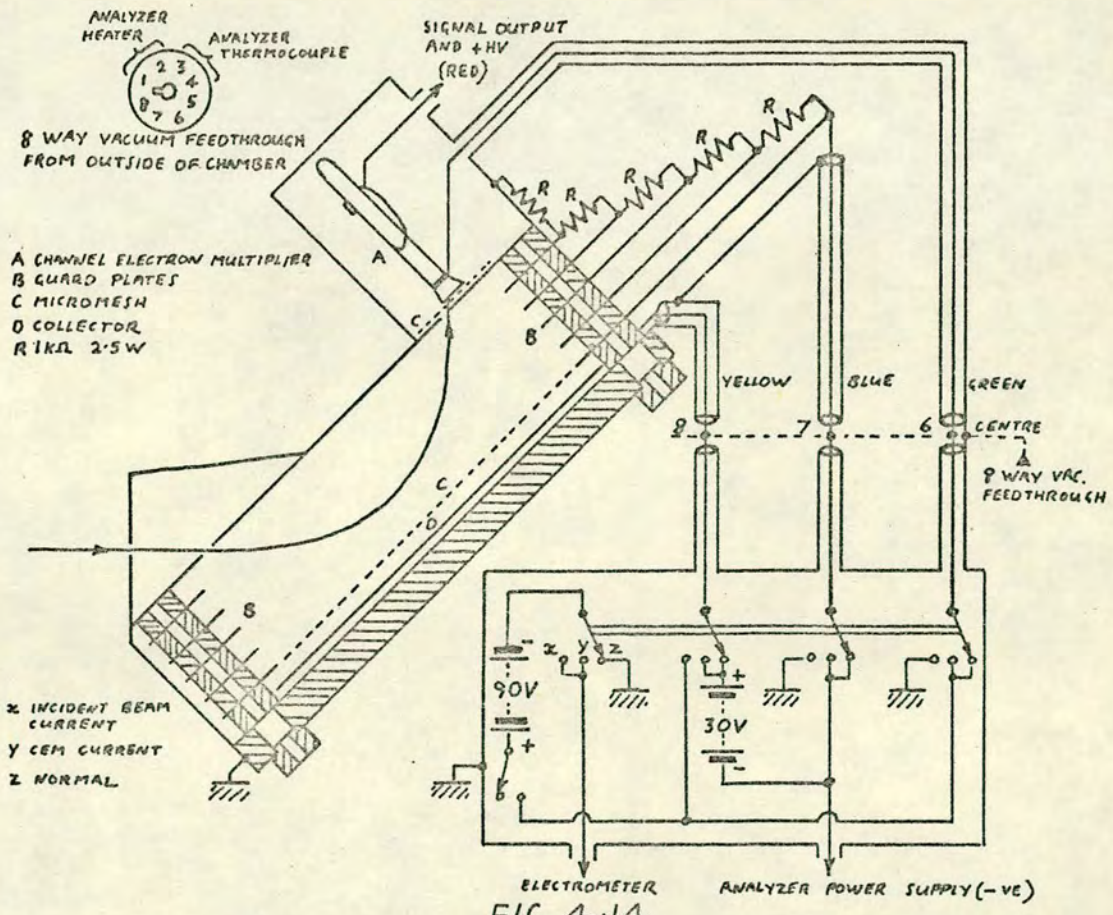

FIG. 4·14
ELECTRON ENERGY ANALYZER (SCALE:- 1:1) AND ASSOCIATED CIRCUITRY

$$y' = y\sqrt{2} - \frac{(y+d-x)\sqrt{2}}{1 - \cot\alpha}$$

$$z' = z + \frac{(y+d-x)\tan\beta}{\cos\alpha - \sin\alpha} \quad .$$

To lowest order in small quantities these become

$$y' = y\sqrt{2} + (y+d-x)\sqrt{2}\,\alpha \qquad (4.10)$$

$$z' \approx z + d\beta + (y-x)\beta + d\alpha\beta + (y-x)\alpha\beta$$

Combining these with (4.8) and (4.9) one obtains for the exit point (0, y", z") (to first order in small quantities)

$$y'' = y\sqrt{2} + d\sqrt{2} + \frac{\ell\Delta U_o}{U_o} \qquad (4.11)$$

$$z'' = z + (d+\sqrt{2}\ell)\beta \; . \qquad (4.12)$$

If the entrance aperture is made 1.4 mm (y' direction) by 1.0 mm (z' direction), then it presents an effective area of 1.0 mm^2 to the interaction region. If the maximum value of α and β is required to be 1.5^o and the interaction region is assumed to present an area 1.0 mm × 1.0 mm to the analyzer, then the required angular resolution is obtained by taking d to be 40 mm (see section 3.3). The dimensions of the exit aperture will depend on the required energy resolution and are related to it with reference to Fig. 4.13. Electrons of the highest energy that will be transmitted by the analyzer will follow trajectory (a), the electrons exiting at (y''_{Max}, z''_{Max}). The necessary initial conditions are:- $\frac{\Delta U_o}{U_o} = 0.03$; $y = y_{Max} = 0.5$ mm, $z = z_{Min} = -0.5$mm; $\alpha = \alpha_{Min} = -0.026$ rad.; and $\beta = \beta_{Max} = +0.026$ rad. The exit point is thus given for this trajectory by (4.11) and (4.12) as:-

$$y''_{Max} = -0.76 + 0.03\ell$$
$$z''_{Max} = 0.54 + 0.04\ell \ .$$

Electrons of the lowest transmitted energy will follow trajectory (b). The initial conditions will be $\frac{\Delta U}{U_o} = -0.03$; $y = y_{Max} = 0.5$ mm; $z = z'' = 0$; $\alpha = 0$; and $\beta = 0$. The exit point is again obtained from (4.11) and is given by:-

$$y''_{Min} = 0.50 - 0.03\ell$$

The dimensions g and h of the exit aperture are given by:-

$$g = y''_{Max} - y''_{Min} = -1.26 + 0.06\ell$$
$$h = 2z''_{Max} = 1.08 + 0.08\ell \ .$$

If g is chosen to be 1.4 mm (as the entrance aperture) then $\ell = 44$ mm and $h = 4.6$ mm. These dimensions suggest the use of a Mullard CEM type B312BL/01 to detect the emerging electrons. This type has a rectangular mouth of dimensions 8.0 × 2.5 mm.

A parameter of some importance is the penetration depth $\bar{x}_p$ of electrons into the analyzer (see Fig. 4.12). This is given by:-

$$\bar{x}_p = \frac{m\bar{v}_x^2}{2eE} \ .$$

Using $\bar{v}_x$ from equation (4.6) and writing the result to first order in small quantities:-

$$\bar{x}_p = \frac{U}{2E}(1 - 2\alpha + \frac{\Delta U}{U}) \ .$$

This is the penetration depth for an analyzer field E and electrons of energy $U+\Delta U$. If the analyzer is tuned to accept

electrons of energy close to the particular value U_o then $E = 2U_o/\ell$ and the penetration depth of these electrons is:-

$$\bar{x}_p(U_o + \Delta U_o) = \frac{\ell}{4}(1 - 2\alpha + \frac{\Delta U_o}{U_o}) \quad . \qquad (4.13)$$

With the analyzer so tuned, the penetration of an electron with energy close to some arbitrary value U will be:-

$$\bar{x}_p(U + \Delta U) = \frac{\ell}{4}\frac{U}{U_o}(1 - 2\alpha + \frac{\Delta U}{U}) \quad . \qquad (4.14)$$

Of interest is the minimum difference between the quantities $\bar{x}_p(U_o + \Delta U_o)$ and $\bar{x}_p(U + \Delta U)$ for the cases of interest. U_o will correspond to the energy of inelastically scattered electrons while U will be the energy of the electrons incident on the target. Electrons of this energy will enter the analyzer as unscattered or elastically scattered electrons. The largest value of $\bar{x}_p(U_o + \Delta U_o)$ would occur for the smallest energy of scattered electrons likely to be encountered. Putting therefore $U_o = 1.0$ eV, $\alpha = -0.026$ and $\Delta U_o = + 0.015$ eV (ΔU_o is now the spread in incident energy due to thermal effects) in (4.13) gives:-

$$\bar{x}_p(U_o + \Delta U_o)_{Max} = 11.7 \text{ mm.} \qquad (4.15)$$

The smallest value of $\bar{x}_p(U + \Delta U)$ would occur for the smallest values of U/U_o and the largest value of U. For the cases to be considered this would occur for electrons of energy 5.0 eV incident on K. U_o would be then 3.4 eV. Using these values, $\alpha = + 0.026$, and $\Delta U = - 0.015$ eV in (4.14) gives:-

$$\bar{x}_p(U + \Delta U)_{Min} = 15.3 \text{ mm.} \qquad (4.16)$$

To avoid build up of space charge inside the analyzer which might result from reflection of the more penetrating (and unwanted) "elastic" electrons, it is desired to design the analyzer such that these electrons are absorbed (Marmet and Kerwin, 1960). This is ensured by making the rear of the analyzer from 80% transparent, 200 cp's, gold-plated, copper micromesh (EMI Ltd.). (See Fig. 4.14). A few millimetres behind this, is situated a soot-coated (see section 4.4) collector maintained at + 30V with respect to the mesh. The distance of the mesh from the front of the analyzer is so chosen that unwanted electrons pass through it, while the trajectories of the "inelastic" electrons remain unaffected. The unwanted electrons strike the collector. Reflection is reduced by the coating and secondary electrons are prevented from re-entering the analyzer by the retarding field. The fineness of the mesh, whilst allowing the passage of electrons out of the analyzer, prevents penetration of the collector field into the analyzer interior. The collector serves a dual purpose: The whole analyzer including the CEM can be set at earth potential (excluding, of course, the collector). An electrometer can be put in series with the collector to enable it to be used as an electron-beam monitor. The analyzer is now in the "beam-current" mode, referred to in section 4.4 (see also Fig. 4.14). Apart from the normal "analyzing and pulse counting mode", a third mode of operation is possible - the "CEM current" mode. Here the analyzing function is unaffected but the CEM is connected as a Faraday cup. In this mode, the operation of the analyzer can be easily checked by setting it to $\theta = 0^{o}$ and monitoring the current arriving at the CEM as a function of analyzer field. (See Fig. 4.14).

On the basis of results (4.15) and (4.16) an ideal choice would be 15 mm for the depth of the analyzer. But unfortunately there were difficulties in obtaining suitable insulators for spacing the guard plates. Eventually ceramic insulators were obtained from Steatite Ltd. (type 52745) but use of these resulted in a depth of 17 mm.

It is necessary to check the values, at this stage, of two other important parameters:- the transit time (t) of an electron from leaving the interaction region to arriving at the CEM; and the spread in transit times. The former enables one to estimate at what point on the time spectrum the genuine coincident events are likely to appear. The latter affects the time resolution of the system and hence the counting time.

The transit time of the trajectory within the analyzer is given by equation (4.7) which, to lowest order in small quantities can be written:-

$$t_A = \sqrt{\frac{m}{eU_o}} \cdot \ell\left(1 - \alpha - \frac{\beta^2}{2} + \frac{\Delta U_o}{2U_o}\right).$$

The flight time t_F for the trajectory between interaction region and analyzer entrance aperture is given by:-

$$t_F = \frac{d/\sqrt{2} - y/\sqrt{2} + y'}{\bar{v}_y} .$$

Using (4.10) for y' and expressing the result to lowest order, one obtains:-

$$t_F = \sqrt{\frac{m}{eU_o}} \cdot \frac{d}{\sqrt{2}} \left(1 + {}^{y}/_{d} + \alpha + \frac{\beta^2}{2} - \frac{\Delta U_o}{2U_o}\right) .$$

The total transit time t is given by :-

$$t = t_A + t_F$$

$$= \sqrt{\frac{m}{eU_o}}\left(\ell + {}^{d}/_{\sqrt{2}} + {}^{y}/_{\sqrt{2}} - (\ell - {}^{d}/_{\sqrt{2}})\alpha - \tfrac{1}{2}(\ell - {}^{d}/_{\sqrt{2}})\beta^2 + \tfrac{1}{2}(\ell - {}^{d}/_{\sqrt{2}})\frac{\Delta U_o}{U_o}\right) \qquad (4.17)$$

As $(\ell - {}^{d}/_{\sqrt{2}})$ is +ve, the maximum value of this quantity (t_{Max}) will occur for the conditions $y = y_{Max}(= 0.5$ mm); $\alpha = \alpha_{Min}(= -0.026$ rad.); $\beta = 0$, $\frac{\Delta U_o}{U_o} = \frac{\Delta U_{o\ Max}}{U_o}$ $(= +0.03)$ (trajectory (a) of Fig. 4.13). The minimum possible value (t_{Min}) will occur for the conditions: $y = y_{Min}(= -0.5$mm); $\alpha = \alpha_{Max}(+0.026$ rad.); $\beta = \beta_{Max}(= +0.026$ rad.); and $\frac{\Delta U_o}{U_o} = \frac{\Delta U_{o\ Min}}{U_o}$ $(= -0.03)$. This is really a lower bound on the minimum as, under these conditions, the transmission of energies $U_o + \Delta U_{o\ Min}$ may be impossible.

The maximum possible spread t in transit time is given from (4.17) as:-

$$\Delta t = t_{Max} - t_{Min}$$

$$= \sqrt{\frac{m}{eU_o}} \cdot (\ell - \frac{d}{\sqrt{2}})({}^{\Delta y}/_{\sqrt{2}} + \Delta\alpha + \beta^2 {}^{Max}/_{2} + \Delta U_o/U_o) \qquad (4.18)$$

where $\Delta y = y_{Max} - y_{Min}$ and $\Delta\alpha = \alpha_{Max} - \alpha_{Min}$.

The nominal value (t_o) of the transit time is given by putting $y = \alpha = \beta = \Delta U_o = 0$ in (4.17):-

$$t_o = \sqrt{\frac{m}{eU_o}}\,(\ell + {}^{d}/_{\sqrt{2}}) \quad . \qquad (4.19)$$

Putting the above numerical values in (4.18) and (4.19) the transit time and its spread are:-

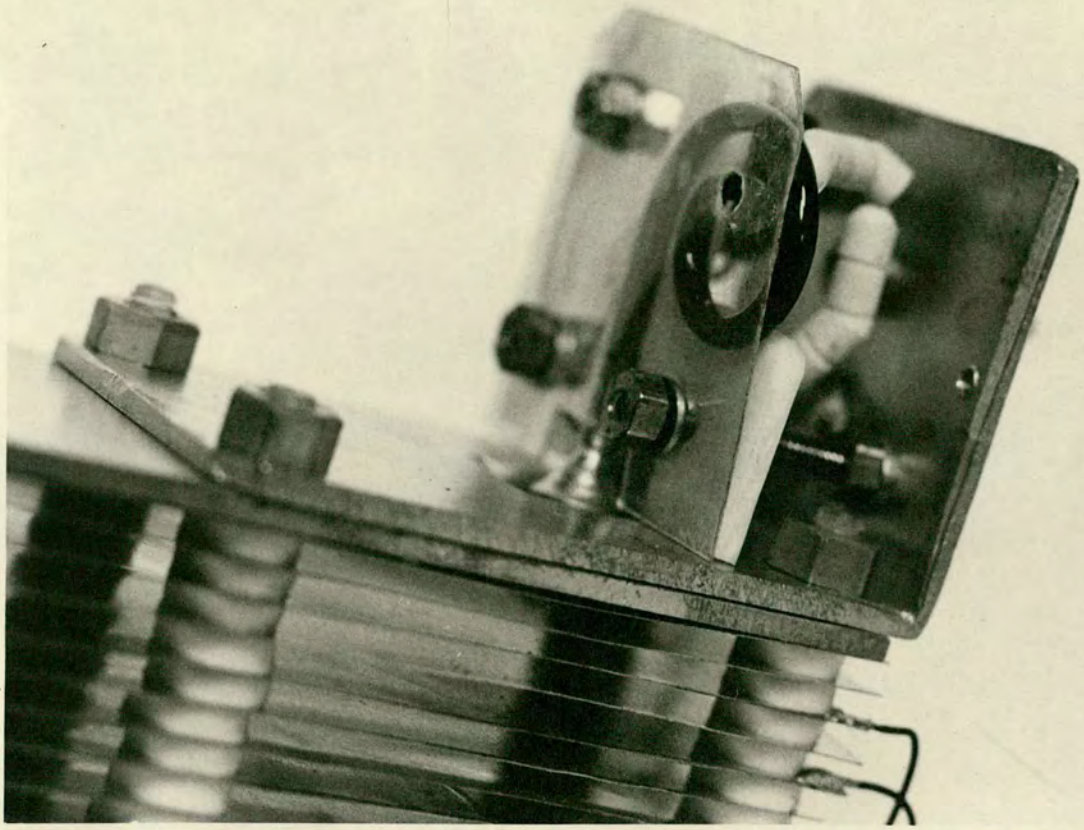

FIG. 4·16 :- LOCATION AND MOUNTING OF THE CEM (COVER REMOVED)

FIG. 4·15 :- ELECTRON ENERGY ANALYZER (SIDE PLATES REMOVED)

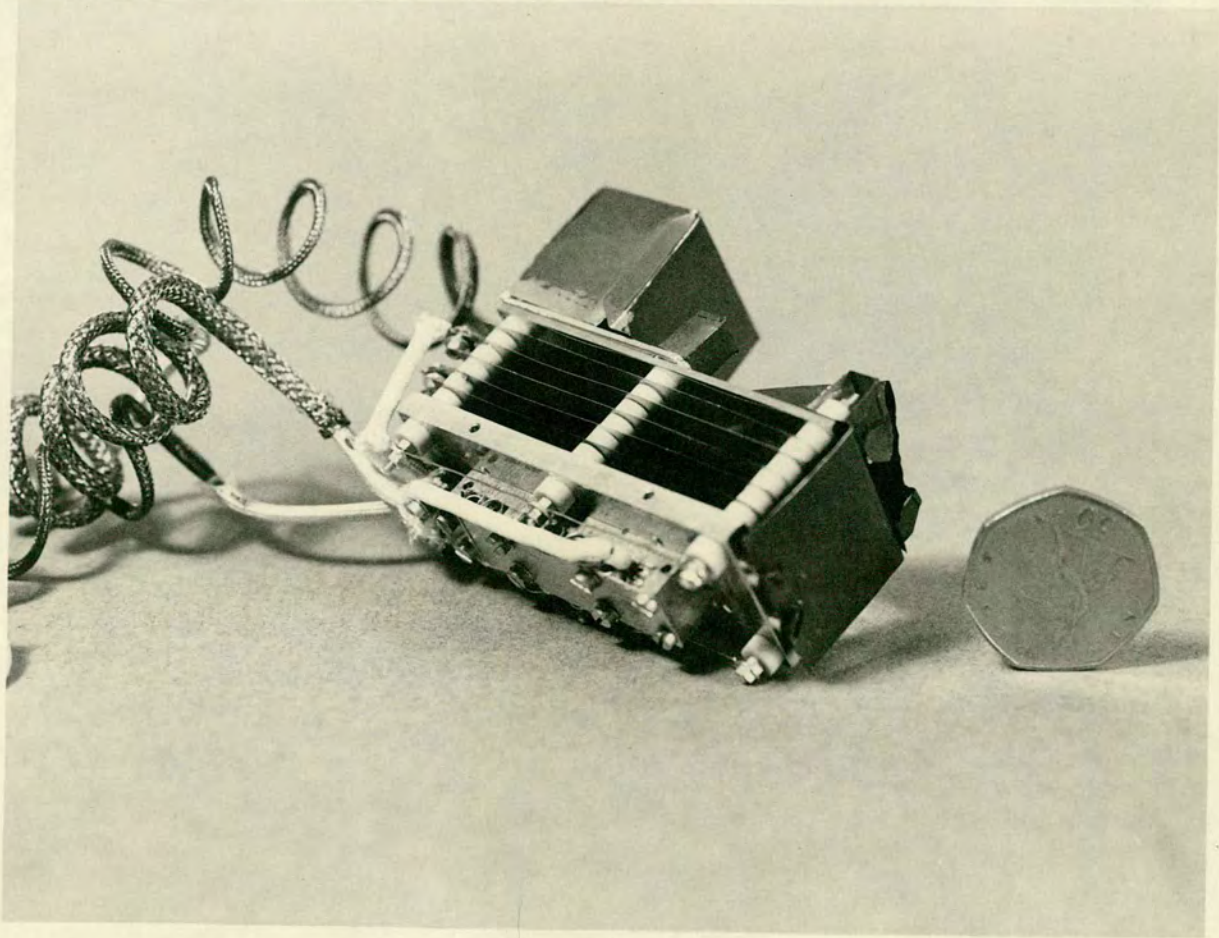

$$t_o = 172.4/\sqrt{U_o} \text{ nsecs.}$$

$$\Delta t = 5.66/\sqrt{U_o} \text{ nsecs.}$$

where U_o is the energy (eV) to which the analyzer is tuned. The largest spread likely to be encountered in these investigations is for $U_o = 1.0$ eV when $\Delta t = 5.7$ nsecs. This will not contribute seriously to the resolving time of the system as this is ultimately limited by the atomic lifetime which is larger, being of the order of 16 nsecs.

To provide the field E within the analyzer a voltage V is applied between the front plate of the analyzer and the rear mesh. Using the value of 17 mm for the depth of the analyzer, and the tuning condition $E = 2U_o/\ell$ (where $\ell = 44$mm), the following relationship is obtained for V and U_o:-

$$V = CU_o \qquad C = \frac{2d}{\ell} = 0.773 \pm 0.015. \quad (4.20)$$

This assumes 0.25 mm uncertainty in the above dimensions.

The power supply for the analyzer is described in Appendix III(e). It includes the possibility of manual adjustment of the analyzer field as well as automatic and repetitive sweeping.

Construction of the Analyzer (see Figs. 4.14, 4.15 and 4.16)

The region of electric field between the front plate (carrying the entrance and exit apertures) and mesh, is maintained uniform by four parallel guard plates spaced at 3.5 mm intervals by ceramic bushes. Spigots on the bushes prevent the plates being shorted together by contact with any of the six 10BA brass rods which hold the assembly to a dural base-plate.

The correct potential distribution is maintained by connecting each guard plate to the appropriate point on a divider network consisting of five 1kΩ, 2.5 W, vitreous-enamel resisters, connected in series. The chain is connected across the analyzer supply and draws approximately 0.5 mA. This current produces, in the vicinity of the electron trajectory, a magnetic field which is entirely negligible.

The front plate, guard plates, and rear plate (carrying the mesh) are constructed from 0.125 mm copper sheet which is gold plated and coated with soot, to reduce electron reflection (see section 4.4). Care is necessary to prevent soot being deposited on insulators.

The CEM is mounted immediately following the exit aperture (see Fig. 4.16). It is held in place between two mica sheets. A 200 cps micromesh is placed across the exit aperture to prevent penetration into the analyser of the strong fields associated with the CEM. (A 90V accelerating potential is applied between the front plate and the mouth of the CEM; and up to 4.0 kV is applied across the CEM itself.)

The complete analyzer and CEM are enclosed in an earthed copper box. This prevents stray electrons from entering the analyzer and detector; and also shields the interaction region from the effects of the electric fields associated with these.

A copper spout mounted around the entrance aperture holds a 1.5 mm diameter collimating aperture at a distance of 10 mm. Its purpose is to limit the range of entrance angles, particularly those of electrons scattered from residual gas molecules, which, coming from a relatively large region,

would otherwise degrade the resolution from the calculated value.

To enable the analyzer to be independently baked, a copper-block containing slots in which are embedded mica-insulated heating coils, is attached to the dural base plate. The coils are formed by winding 0.5 mm diameter stainless-steel wire on a 3.0 mm diameter former. Their total resistance when cold is 10Ω and a mild baking temperature of 100°C can be achieved by supplying 0.8A. Unfortunately, the analyzer cannot be baked during a run because this current produces disastrously large magnetic fields in the region of the electron trajectory.

Electrical connections to the analyzer and CEM are made using PTFE-insulated wire screened from external sources of pickup by earthed copper braid. This also serves to screen the interaction region from possible charges on the insulation. For the same reason, insulators used in the construction of the analyzer are screened from view of the electrons by earthed copper boxes. The exposed connections to the vacuum feedthrough are also screened by earthed copper sheets to prevent possible distortions of the field at the interaction region due to the high potentials on some of these contacts.

The analyzer is attached to a brass axle which rotates in a bronze bearing set into the main supporting table. Motion from a rotary vacuum feedthrough on the side of the scattering chamber, is transferred to this axle via a universal coupling (to allow movement of the whole supporting table for alignment purposes.), a 20:1 worm and wheel assembly, and a

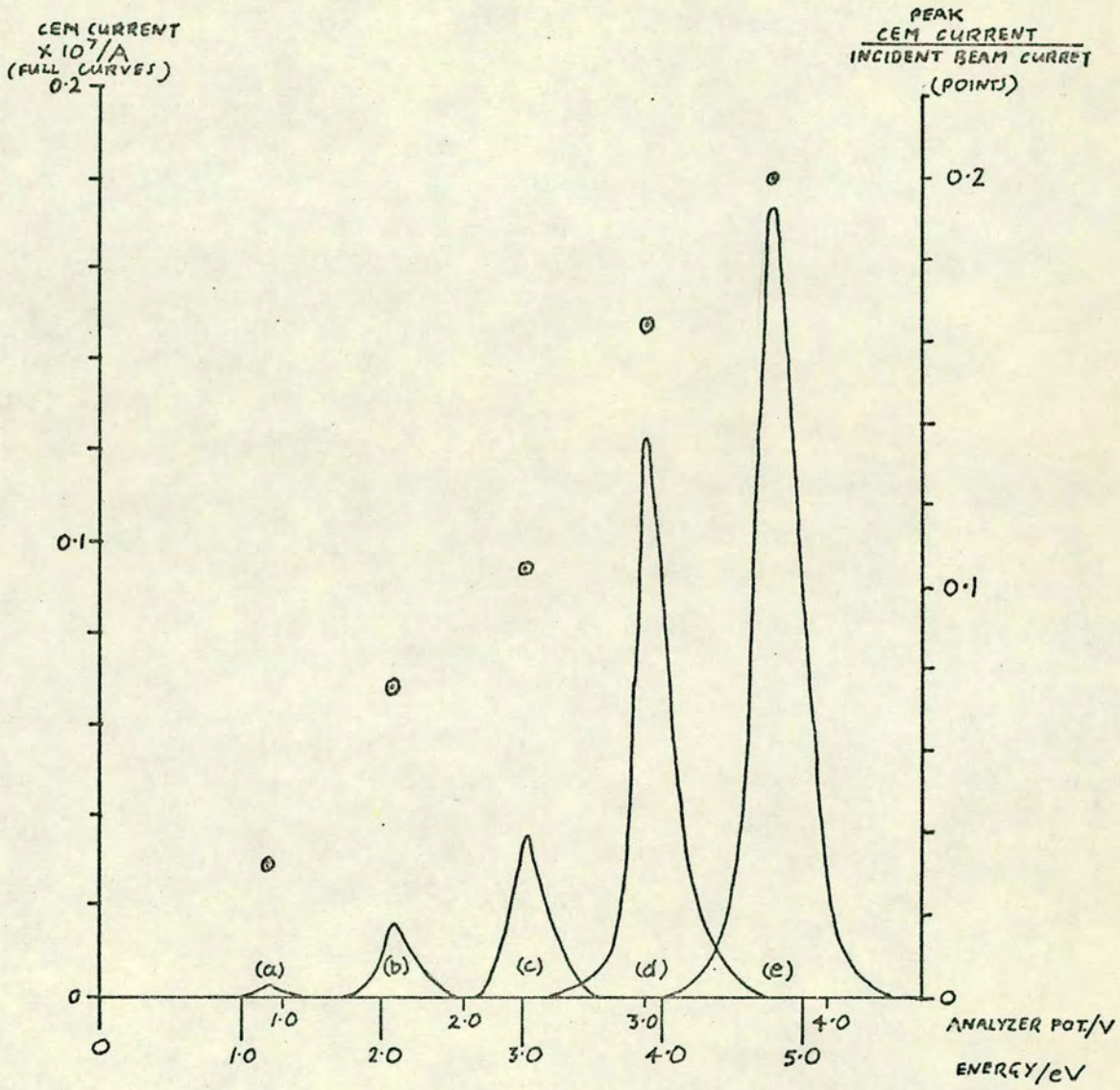

FIG. 4·17
NET ENERGY DISTRIBUTIONS ($\theta = 0$) FOR INCIDENT PEAK ENERGIES OF 1·2 (a), 2·1 (b), 3·0 (c), 3·9 (d) AND 4·8 (e) eV.

4:1 stainless steel, non-slip drive chain. Positive, non-slip attachment of gears and chainwheels etc. to shafts is ensured by drilling radial holes in the shafts in which are located the ends of the attaching grub-screws.

Testing of the Analyzer. The electron beam is focused on the analyzer as described in section 4.4. (The analyzer being set at $\Theta = 0^{\circ}$). With the analyzer in the "beam current" mode, the incident beam current is measured. The analyzer is then put into the "CEM current" mode and the CEM current is measured as a function of V (see equation (4.20)), using a Keithly 602 electrometer and X-Y recorder. This is carried out for various values of incident electron energy (or cathode voltage V_o, see equation (4.4)). The results of these measurements are shown in Fig. 4.17. The width of each peak represents the total energy spread due to thermal effects in the incident beam, and to finite analyzer resolution. Also shown in Fig. 4.17 are points representing the normalized peak CEM currents (peak CEM current/collection current) for each energy, so that a comparison can be made of the relative transmission of the analyzer for various energies. It can be seen that these points lie very close to a straight line with +ve gradient, passing through the origin. This result is to be expected as the analyzer resolution is less in general than the energy spread of the incident beam. This means that the width of the peaks for the lower incident energies (where the absolute analyzer resolution is smallest) should accurately reflect the thermal spread. For energies of 3.9 eV and below, the FWHM of the peaks has the constant value of 0.29 eV which compares very

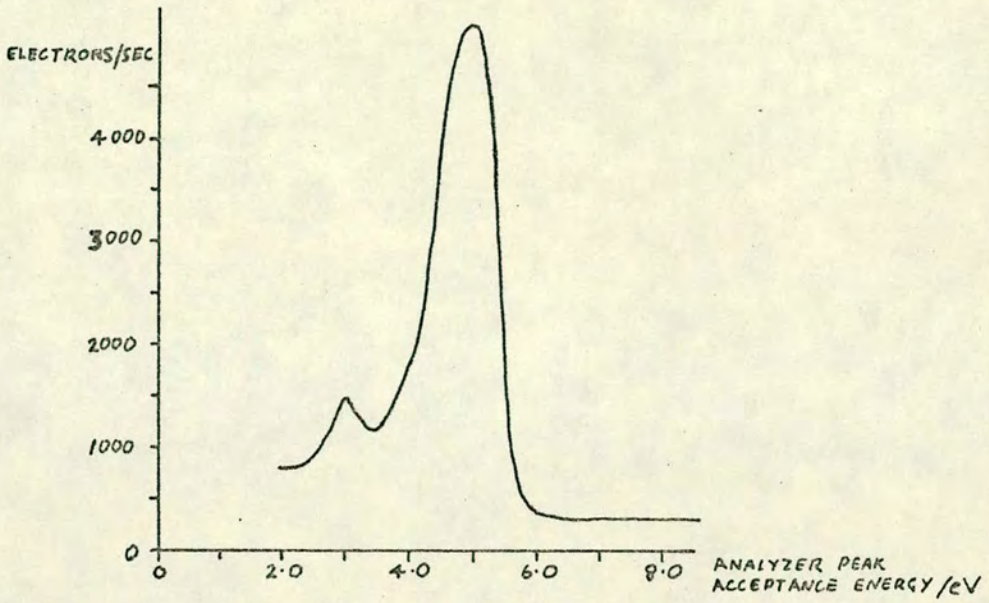

FIG. 4·18
ENERGY DISTRIBUTION OF ELECTRONS SCATTERED FROM SODIUM.
($\Theta = 9°$, $B = 0$) INCIDENT ENERGY 5·0 eV
OVEN TEMP. 340°C

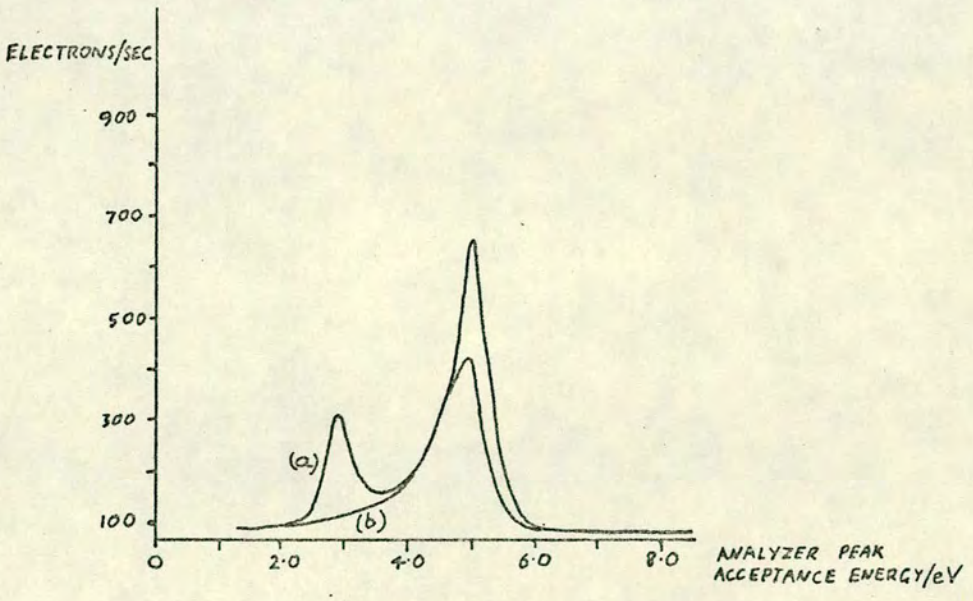

FIG. 4·19
ENERGY DISTRIBUTION OF ELECTRONS SCATTERED FROM SODIUM.
($\Theta = 18°$, B FINITE). (a) Na BEAM ON. (b) Na BEAM OFF.
INCIDENT ENERGY 5·0 eV
OVEN TEMP. 390°C

favourably with that calculated in section 4.4 on the basis of a cathode temperature of 1000°C (0.27 eV).

Even at 4.8 eV where the calculated analyzer resolution should be approximately the same as the thermal spread, the measured FWHM is only 0.39 eV. In this respect it would seem that the analyzer performance is exceeding its specification. This is not unexpected when it is remembered that the resolution (0.3 eV) of the analyzer refers to the base width of the distribution, so that the FWHM should be somewhat less, providing the range of input angles is as specified and is not weighted towards larger angles. This should certainly be the case for the electron beam.

That this is not the case in general is suggested by the energy spectra of scattered electrons. Fig. 4.18 shows the situation for electrons incident at 5.0 eV on Na, for $\theta = 9^{\circ}$. Going to smaller scattering angles produces severe distortion of the spectrum due to the admission to the analyzer of a significant portion of the unscattered electron beam, while at large angles a reduced "inelastic" intensity is obtained due to the fall-off of differential cross-section with θ. The spectrum in Fig. 4.18 is obtained by first adjusting the electron gun for focusing on the analyzer at $\theta = 0^{\circ}$ as described in section 4.4. The analyzer is then rotated to $\theta = 9^{\circ}$ and used in the pulse-counting mode. An energy spectrum is obtained by automatically sweeping the analyzer with a sawtooth voltage waveform. (See Appendix III(e)). The quality of the spectrum is then optimized by alternate adjustment of the electron-beam deflection and focusing (by adjustment of the potentials V_1 and V_2). The best spectrum is obtained

with the gun focused on some point between the interaction region and the analyzer (see Appendix IV(c) for voltage settings), presumably because the divergent part of the beam, after the focus, will, in this situation, be less likely to be admitted to the analyzer. The large peak at higher energy is due to elastic scattering (analyzer voltage 3.81V), predominantly from residual gas; while the small peak (2.30V) is due to scattered electrons having excited the 3^2P states of Na. This can be verified by shutting off the atomic beam, in which case the "inelastic" peak disappears and the amplitude of the elastic peak is reduced (see Fig. 4.19). Further verification is provided by the results of the application of formula (4.20) under the assumption that the peak energies are 5.0 eV and 2.9 eV. This gives analyzer voltages (V) of 3.86V ± 0.08 and 2.24 ± 0.05 respectively. It might appear that the "inelastic" peak lies slightly higher than the correct energy. This is to be expected due to the distortion produced by its position on the shoulder of the "elastic" peak. The FWHM of the elastic peak in Fig. 4.18 is 1.26 eV which is much greater than that in the case of Fig. 19 where the only differences are that also the Helmholtz currents are adjusted from their usual settings (especially the "vertical" one, which is increased) to further optimize the spectrum quality. This leads to no improvement for $\theta = 9^\circ$, but significant improvement is obtained if θ is increased. This is, at first surprising. (The fall off with θ of the cross-section has been somewhat compensated for by an increase in oven temperature.) The FWHM of the elastic peak is now 0.72 eV.

The unexpectedly poor resolution obtained in Fig. 4.18 is probably due to a preponderance of electrons entering the analyzer with large angles of incidence due to reflection from metallic surfaces. At this comparatively small scattering angle ($\theta = 9^{o}$) the majority of these electrons will be ones which, having passed through the target region unscattered, strike the sides of the collimator obliquely and gain access to the analyzer by reflection. For the case where $\theta = 0^{o}$ (Fig. 4.17) there will be comparatively few oblique collisions. Similarly for the case of Fig. 4.19 some energy pre-selection will be performed by the finite magnetic field which is now predominately in the upward direction. The electron beam will now be steered to the left (towards the analyzer) but the "inelastic" electrons, after the interaction, will suffer a larger deflection. Thus the scattering angle of the "inelastic" electrons received by the analyzer will be effectively less than 18^{o} - leading to a greater than expected count rate - and also the effect of the unscattered electrons will be reduced due to the selective deflection performed by the magnetic field.

Contributions to the FWHM from space charge effects are negligible. Application of equation (4.5) due to Heddle (1967) gives a contribution of the order of 2 meV. as was shown at the end of section 4.4.

The remaining difference in resolution between the situations shown in Figs. 4.17 and 4.19 may be due to a degradation in the latter case due to field penetration from the CEM into the analyzer.

4.6 The Atomic Beam System (see Figs. 4.1(a) and (b)

Introduction An atomic-beam target is demanded by four requirements: (i) a geometrically well defined target is required, of extent no greater than is necessary to provide the required angular resolution. In this way radiation-trapping (which would lead to depolarization) is reduced to a minimum. (ii) The well defined and collimated nature of the beam eases the problems of dumping and trapping the beam. This again reduces the possibility of radiation-trapping effects due to background alkali vapour. (iii) Independent control over beam intensity and dimer-concentration can be achieved using beam sources. (iv) The desire of ultimately using a polarized target will necessitate the use of a state-selecting hexpole magnet (see section 4.7) which relies for its operation on the existence of the target material in the form of a beam.

The Beam Source This is of the effusion type (Ramsey, 1969). To obtain maximum forward beam intensity and to improve beam directionality, a multi-capillary nozzle is used. A suitable type, manufactured by the Brunswick Corporation, was obtained consisting of an array of parallel, stainless-steel capilliaries, each 0.05 mm diameter (d) and 3 mm in length (ℓ). An area 2 mm diameter is utilized which contains approximately 550 capilliaries. Provided the condition $\Lambda > \ell >> d$ (Λ is the mean free path of alkali atoms within the oven) holds then the usual cosine distribution of intensity (for an aperture) is modified such that although the same intensity per channel is obtained in the forward

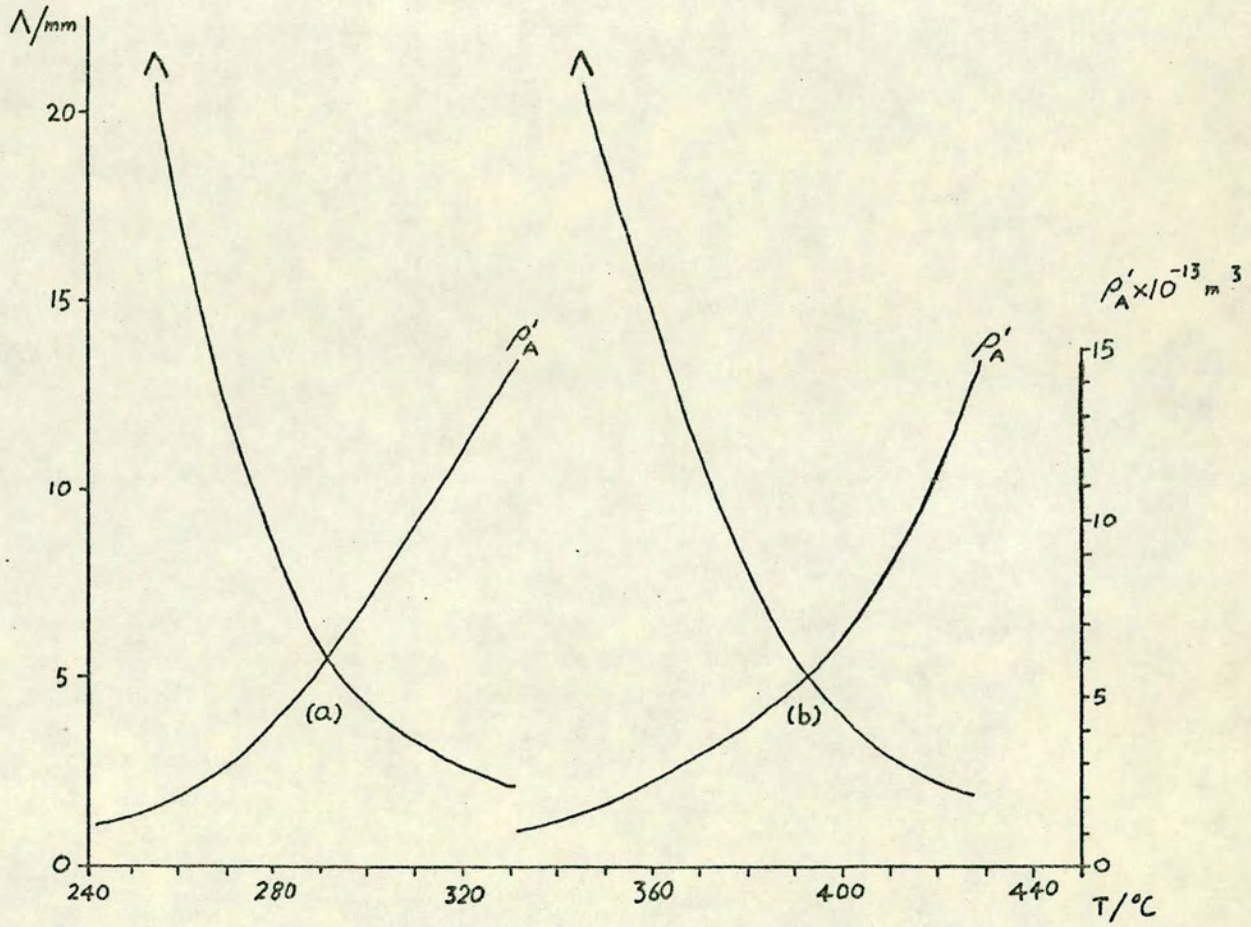

FIG. 4·20

MEAN FREE PATH (Λ) AND BEAM DENSITY IN FORWARD DIRECTION DUE TO A SINGLE CHANNEL (ρ_A'), FOR POTASSIUM (a) AND SODIUM (b)

direction as for a single aperture of the same diameter, the total material emitted by each channel due to the more forward-peaked nature of the modified distribution, is reduced by a factor $4d/3\ell$ (Clausing, 1931). The forward intensity per channel is given by (Ramsey, 1969):-

$$I = 1.118 \times 10^{26} \frac{PA_s}{\ell_o^2 \sqrt{MT}} \text{ atoms } m^{-2} sec^{-1} \quad (4.21)$$

where
- P is the source vapour pressure (torr.)
- A_s is the area of the channel cross-section (m^2)
- ℓ_o is the source-target distance (m)
- M is the molecular weight of the beam material.
- T is the source temperature (^oK)

The beam density (ρ_A') at the interaction region is I/v_{mp} where v_{mp} is the most probable velocity of the beam atoms ($157.3\sqrt{T/M}$). Thus:-

$$\rho_A' \propto \frac{P(T)}{T} \quad (4.22)$$

Because P increases with T, faster than T, ρ_A' increases with T. The variation of ρ_A' with T is shown for Na and K in Fig. 4.20 which also shows the variation of Λ with T of these substances. The values of Λ result from "order of magnitude" calculations using the vapour-pressure data compiled by Nesmeyanov (1963). It can be seen that the condition $\Lambda > \ell$ implies $T < 400^oC$, 310^oC for Na and K respectively. In practice it is found that for Na at 340^oC, little increase in beam density, with increase in T, is obtained at the expense of large amounts of material emitted with large divergence angles. This is therefore chosen as the working temperature ($\Lambda = 6\ell$) for Na.

For ℓ_o = 0.1m equations (4.21) and (4.22) now give:-

$$I = 1.1 \times 10^{16} \text{ atoms } m^{-2} \text{ sec}^{-1}$$

$$v_{mp} = 810 \text{ msec}^{-1}$$

$$\rho_A' = 1.36 \times 10^{13} \text{ atoms } m^{-3}.$$

If it is assumed that all 550 channels of the nozzle contribute equally to the density in the interaction region (ρ_A), a value of 7.5×10^{15} atoms m^{-3} is obtained. This represents an upper limit to the total beam density and would only be attained if the nozzle array consisted of focused channels.

Dimer Concentration The presence of dimer molecules (Na_2, K_2) in the interaction region may give rise to misleading results. Data tabulated by Lapp and Harris (1966) show that the dimer concentration of a saturated vapour increases with T but that for Na at 340°C the concentration is only 1.6% and for K at 300°C it is only 0.4%. The oven is constructed (see below) such that the reservoir and nozzle can be operated at different temperatures. In order to reduce the dimer concentration still further to negligible proportions, the reservoir is held at 340°C (determining the vapour pressure and hence beam intensity) while the nozzle is operated at 500°C causing reduction of dimer concentration by thermal dissociation of the emerging molecules (Long, Raith and Hughes, 1965; Enemark and Gallagher, 1972). This temperature distribution has the added advantage that the tendency of the nozzle to clog (especially on cooling) is reduced.

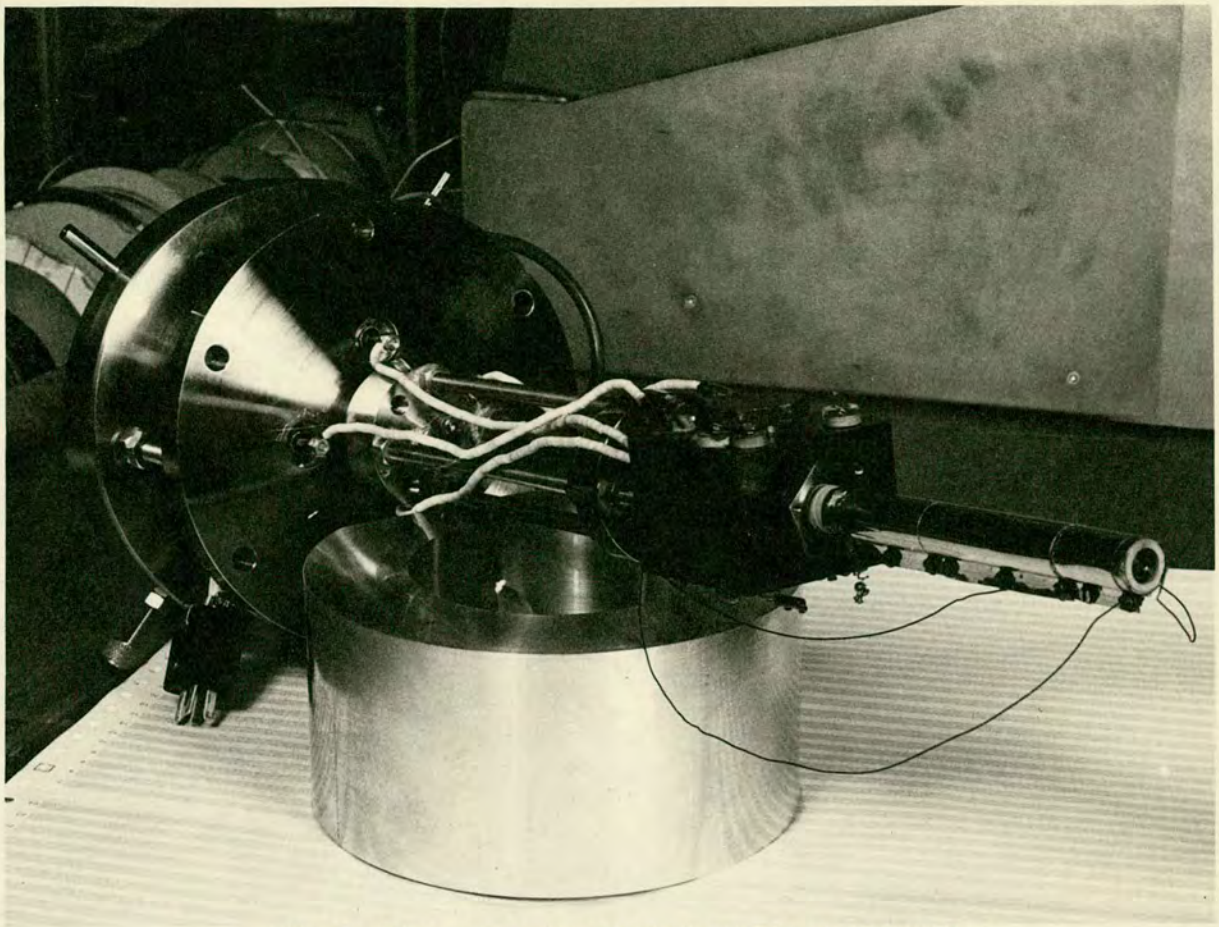

FIG. 4·21 :- ATOMIC BEAM OVEN ASSEMBLY

FIG. 4·22 :- OVEN CHAMBER : COLD-ARM AND HEAT SHIELD (APERTURE SUBSEQUENTLY ENLARGED)

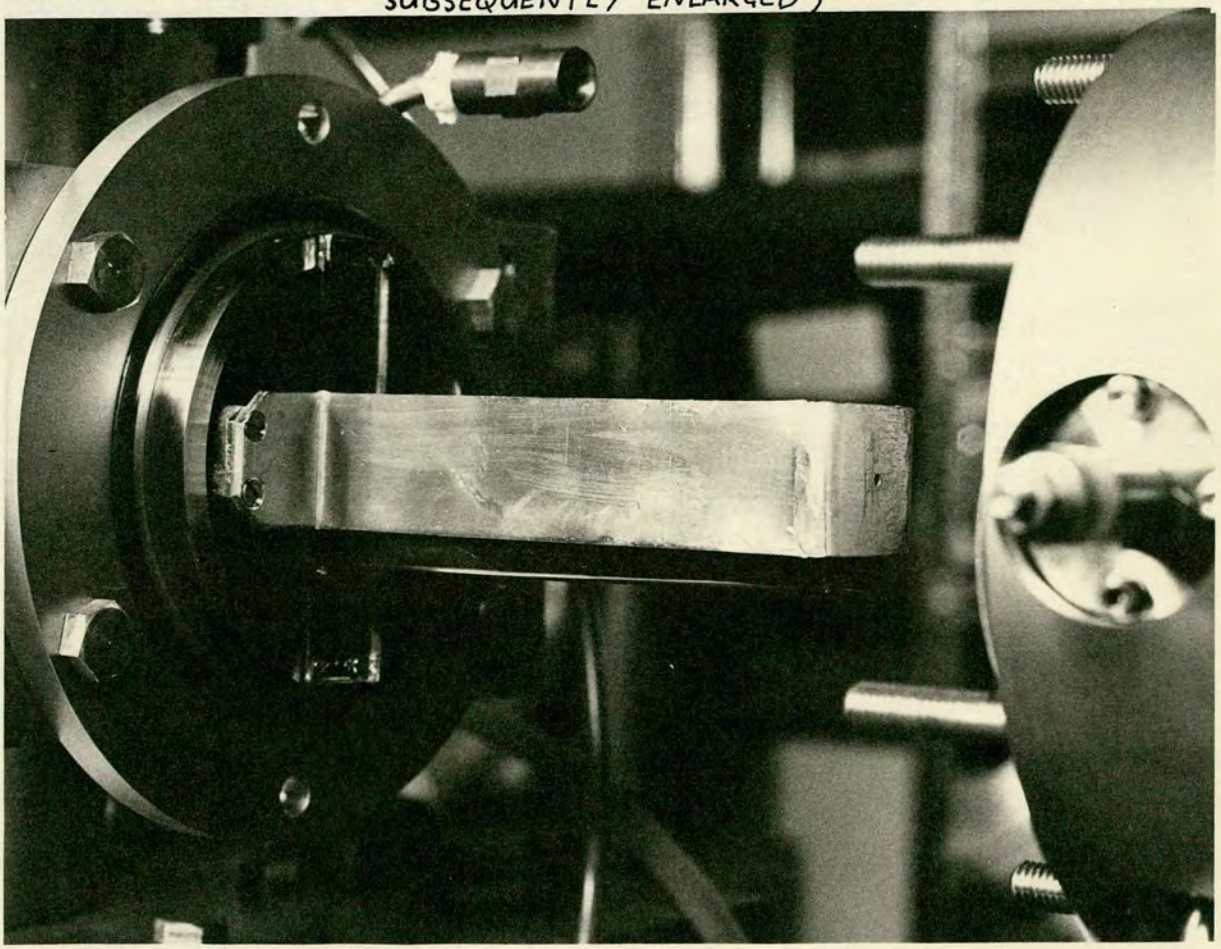

The Oven (see Fig. 4.21) The design of the oven is determined partly by the requirement that it should be possible to reload it without disturbing the scattering-chamber vacuum and thus avoid the necessity of carrying out a re-activation of the cathode. Oven reloadings will be inevitable during runs lasting over 100 hours.

Another constraint on the design of the oven is that it should be fairly massive to minimize gross fluctuations in temperature of the reservoir (due, for example, to emptying of the liquid nitrogen trap). The material of the oven should also be able to withstand attack by hot alkali.

For these reasons the oven reservoir is constructed from a block of EN58B stainless steel, 50 mm × 50 mm × 40 mm deep. A cylindrical recess (20 mm in diameter, 35 mm in depth) forms the alkali reservoir. Four parallel, 6.35 mm diameter holes in the block contain ceramic tubes which hold heating coils (total resistance 15 Ω) wound from 0.5 mm diameter, nichrome wire. The oven is mounted in a side arm off the scattering chamber communicating with it via a 3 mm diameter, 13 mm long, channel, providing differential pumping. This oven chamber is separately pumped by an Edwards E04 oil diffusion pump, with chevron baffle and butterfly valve. To minimize the source-target distance and hence obtain maximum beam density in the interaction region, an EN58B stainless-steel tube (3 mm. I.D. 5 mm O.D, 120 mm in length) is connected to the oven-body with a flange, clamping nut, and copper gasket, so that it communicates with the reservoir. At its other end it carries the multi-capilliary nozzle which is now within 0.1m of the interaction region. A re-entrant section is

provided in the side of the scattering chamber which forms the part of the oven chamber containing the extension tube. A 12.7 mm O.D. ceramic tube in whose outer surface a double helical groove has been cut, fits over the extension tube, and the nozzle is mounted on the threaded end of the tube with a copper sealing-gasket and clamping nut. A double length of 0.5 mm diameter nickrome wire is wound in the helical groove. An insulating-layer of mica covers the winding and the assembly is held together by a surrounding sheath of molybdenum. The nature of the molybdenum surface reduces heat loss by radiation and the bifilar winding eliminates magnetic fields at the interaction region. The resistance of the winding is 15Ω. Although the reservoir and nozzle heaters can be operated independently it is found that with the above choice of resistances the required temperature distribution is obtained for equal heater currents of 1.55A RMS at a total voltage of 45V RMS.

A copper cold-arm (see Fig. 4.22) connected to a liquid nitrogen trap (see Figs. 4.1(a) and (b)) and passing through the oven chamber on either side of the oven, provides a means of reducing the effects of the backstreaming of oil vapour from the E04. The arm terminates in a plate with a 6.5 mm. diameter aperture positioned in front of the nozzle. This serves to trap excess Na vapour, emitted by the nozzle. To maintain a sufficiently large temperature difference between the extension tube and cold-arm, while minimizing the boil-off rate of the liquid nitrogen reservoir, a heat shield fabricated from 0.2 mm stainless steel sheet (see Fig. 4.22) surrounds the extension tube, separating it from the cold arm. The shield is connected at one end, to the water-cooled wall of the vacuum chamber, and so is held nominally at room temperature. Again,

the high reflectance of the shield material reduces radiative heat transfer. For the same reason, the copper cold arm is silver-plated. Sodium vapour is easily trapped on surfaces at temperatures considerably higher than that of liquid nitrogen so that the extreme end of the cold arm, near the nozzle, is not required to be so cold. The boil-off rate is further reduced, therefore, by inserting mica spacers inbetween the two sections of the cold arm. In this way, while the nozzle is maintained at + 500°C, the extreme end of the cold arm attains -40°C and the liquid nitrogen boil-off rate is 1.3 litres/hour.

The oven is mounted on four 6 mm diameter stainless-steel rods 110 mm in length, to reduce heat loss by conduction. The rods are connected at their other ends to a holder (see Figs. 4.1(a) and 4.21) which can be translated in two mutually orthogonal directions transverse to the beam axis, from the outside of the vacuum chamber. The whole arrangement is mounted on the end of the vacuum chamber such that the beam axis can be tilted with respect to the axis of the apparatus. Alignment of the oven with respect to the axis of the apparatus (defined by a 3 mm diameter communicating aperture between oven and scattering chambers and a 2 mm diameter aperture in the beam-dump) is carried out by placing a small light bulb in the oven reservoir, viewing this through the two apertures and the capilliary array, and adjusting tilt and transverse position until maximum brightness is obtained.

The supporting table carrying the mutually aligned electron gun, analyzer, and optical bench, is also aligned with

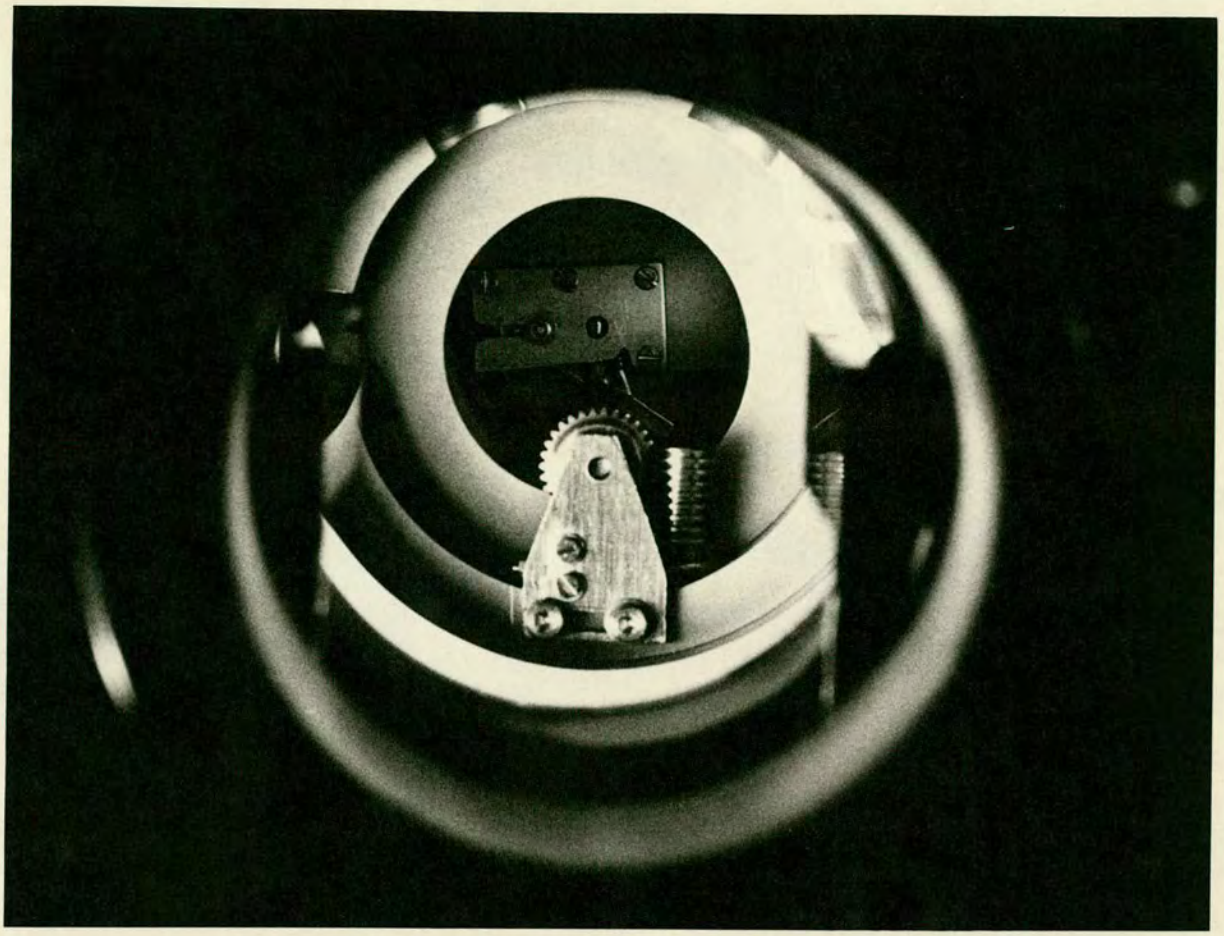

FIG. 4·23 :- OVEN CHAMBER : GATE VALVE

FIG. 4·24 :- SCATTERING CHAMBER PRIOR TO APPLICATION OF SOOT : LOCATION OF COMPONENTS (RE-ENTRANT SECTION, OPTICS EXIT APERTURES & GUN COVER, NOT SHOWN)

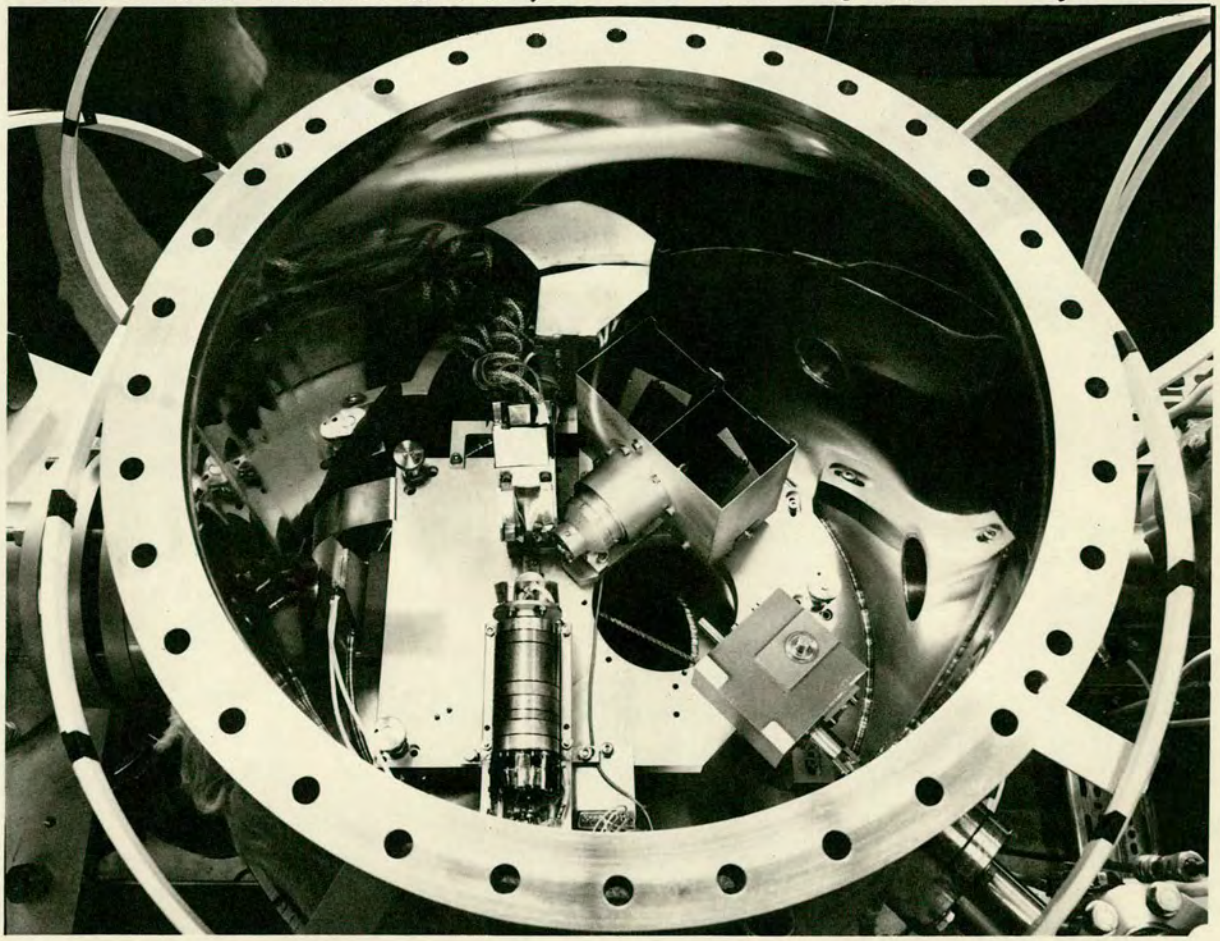

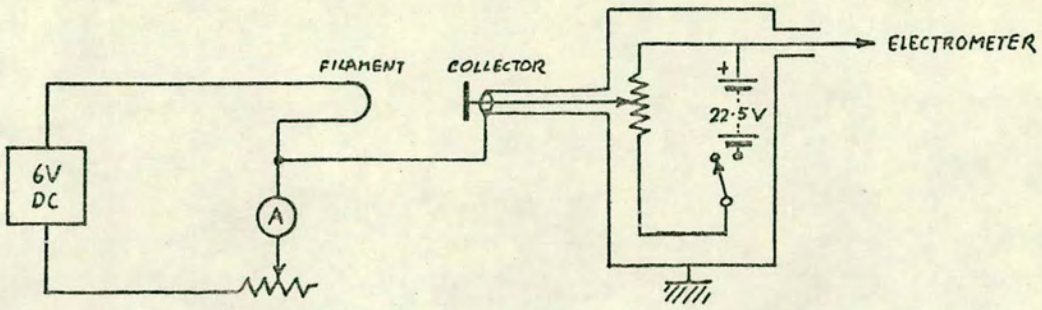

FIG. 4·25
ATOMIC BEAM DETECTOR CIRCUIT

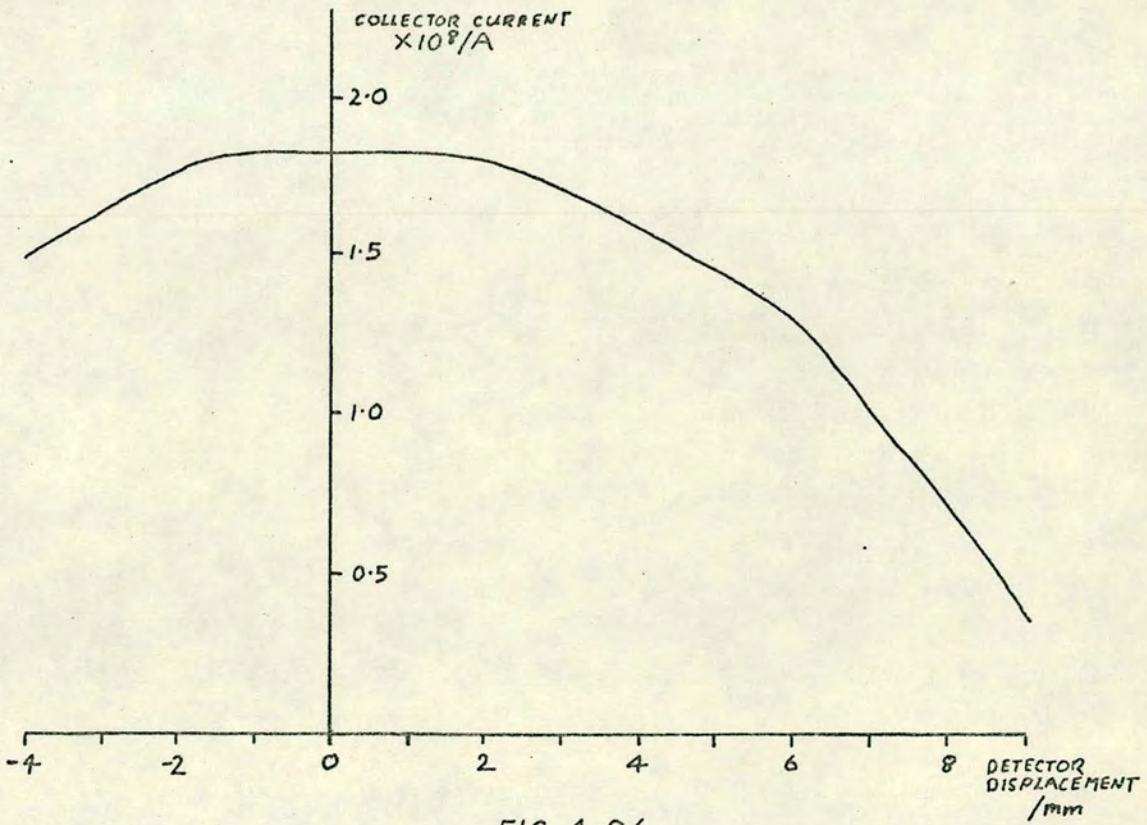

FIG. 4·26
ATOMIC BEAM PROFILE (330°C)

respect to the above apertures, using the conical-tipped screw mentioned in section 4.3 to define the interaction region. Three M8 threaded rods, whose effective length can be varied to adjust the position of the table, act as legs. They have hemispherical ends which are located kinetically in supports on the base of the scattering chamber. Once set, the table can therefore be removed and replaced without disturbing the alignment.

For the purpose of oven reloading, the communicating aperture between the oven and scattering chambers can be closed off by a gate valve, controlled remotely from a rotary feed through. A view of this looking into the re-entrant section of the oven chamber from the position of the oven, is shown in Fig. 4.23. A view of all the components located in the scattering chamber is shown in Fig. 4.24.

The Atomic Beam Detector (see Figs. 4.1(a) and 4.25) The atomic-beam detector is necessary in order to gain information as to the intensity of the beam and the beam profile. For the latter purpose the detector is made translatable by mounting it on a flange connected to the vacuum chamber by metal bellows.

The detector itself is of the Langmuir-Taylor surface ionization type and consists of a 30 mm long 0.1 mm diameter tungsten filament, coaxial with a 10 mm diameter molybdenum cylinder (the "collector") in which is etched two diametrically opposite longitudinal slots (17 mm long × 1 mm wide). The filament is heated to 1200°C (measured using an optical pyrometer) by passing 0.82A through it. Atoms of sufficiently low ionization potential relative to the work function of tungsten

are ionized with an efficiency ε on striking the hot surface. The collector is biased negatively with respect to the filament. The ions are attracted to the collector and give rise to a current in the external circuit which is measured by means of a Keithly 602 electrometer (see Fig. 4.25). The current thus contains no contribution from thermionic emission and is directly proportioned to beam intensity. A bias voltage of -9V was empirically found to be sufficient to produce a voltage-independent current indicating that the current is not space-charge limited.

Testing of the Atomic-Beam System Sodium lumps are obtained from Hopkins, Williams Ltd. The purity is 99.84% with major impurities being K (0.1%) and Ca (0.05%). To load the oven, the surface oxide is pared from a 10 mm cube ($\tilde{\sim} 10^{-3}$Kg) of the material. Freshly cut surfaces are kept covered with liquid paraffin while the other surfaces are being prepared. The lump is then quickly washed in diethyl ether to remove the paraffin and placed in the oven reservoir which is closed off by screwing in a tapered plug. The oven assembly is then inserted into the vacuum chamber with the help of a pair of guide rods and the chamber is pumped down.

When the pressure has fallen to approximately 5×10^{-7} torr (after a few hours) the oven reservoir and nozzle are heated up. This is carried out slowly to avoid sudden outgassing and consequent "spritzing" (the splashing of the alkali on melting) which could lead to blocking of the tube or nozzle. A suitable rate of heating is obtained by increasing the heater current in three $1\frac{1}{2}$ hour stages:- (i) on at 0.75A RMS at $+25^{\circ}$C

(ii) up to 1.35A RMS at + 90°C, (iii) up to 1.55A RMS at 225°C. The temperature of the reservoir approached + 340°C after a further 1½ hours. This process was carried out automatically by a controller described in Appendix III(f). The time intervals and current increments are presettable, as is the initial instant of switch-on.

A plot of detector current as a function of transverse position is shown in Fig. 4.26. There is a well defined plateau region extending to ±1.5mm, bordered by "wings". The sections between 1.5 mm and 6.0 mm from the centre, can be attributed to the presence of an aperture (2.0 mm in diameter) which it was found necessary to insert immediately in front of the gate valve to prevent the deposit of alkali on the sealing surface. That section, extending outwards from 6.0 mm, is due to the 3.0 mm diameter communicating channel between the oven and scattering chambers.

A crude estimate of the beam density at the interaction region can now be made. The detector current measured at the plateau was 1.8×10^{-8}A (leakage having been subtracted). This is due entirely to the atomic flux on the exposed length (17 mm) of 0.1 mm diameter wire. Extrapolating the wings of the beam profile and carrying out a numerical integration shows that the plateau region contributes a fraction 0.253 to the total measured current. Assuming that the ion trajectories in the detector are radial, the geometry of the collector determines that a fraction 0.87 of these ions will be collected. The atomic beam flux at the centre of the beam, on the detector filament is therefore given by:-

$$I_{det} = \frac{0.253 \times 1.8 \times 10^{-8}}{0.87\varepsilon eA} \text{ atoms } m^{-2} \text{ sec}^{-1}$$

where e is the assumed ionic charge $= 1.6 \times 10^{-19}$ C

A is the area of the filament exposed to the plateau region of the beam $= 3.5 \times 10^{-7}$ m^2

ε is the ionization efficiency for Na on W at 1200°C.

Therefore:-

$$I_{det} = \frac{0.93}{\varepsilon} \times 10^{17} \text{ atoms } m^{-2} \text{ sec}^{-1}$$

The nozzle-interaction region distance is 100 mm and the nozzle-detector distance is 486 mm so that the intensity at the interaction region will be a factor 23 greater than given above. Also, the most probable velocity of the beam atoms for a reservoir temperature of 340°C is 810 $msec^{-1}$. Therefore the beam density at the interaction region is given by

$$\rho_A = \frac{23 I_{det}}{810} = \frac{2.6}{\varepsilon} \times 10^{15} \text{ atoms } m^{-3} .$$

This is to be compared with the value of 7.5×10^{15} atoms m^{-3} obtained by direct calculation. For consistency, ε could not be smaller than 0.35.

Mayer and Rahn (1968) obtained a value for ε of 0.01. Use of this value would give a large disagreement here. Mayer and Rahn took great care to obtain a pure tungsten surface and they found that impurities drastically affected their results. It is possible that the filament used in the present work contained an amount of adsorbed oxygen. Datz and Taylor (1956) showed that for K on W, oxygenation of the filament produced a substantial increase in ionization efficiency at all

temperatures studied. The situation may be resolved by use of a Pt filament. Datz and Taylor give $\varepsilon = 0.95$ in this case so that the possible uncertainty in a measurement of ρ_A ought to be reduced. For the present one can only conclude that as far as this measurement of ρ_A is concerned, ε lies in the range $1 > \varepsilon > 0.35$, the minimum value of ρ_A is 2.6×10^{15} atoms m^{-3} and ρ_A may be anywhere in the range $7.5 \times 10^{15} > \rho_A > 2.6 \times 10^{15}$ atoms m^{-3}.

4.7 Atomic-Beam Polarization Measurement

Introduction In Chapter 1 the desirability of the measurement of the spin-dependence of the excitation amplitudes was mentioned. This involves the use of a polarized atomic beam and also a knowledge of this polarization. Although a coincidence experiment involving polarized atomic beams has not yet been attempted, some initial work has been done on the problems involved in the determination of such polarizations.

The traditional method of obtaining such knowledge is to employ a Stern-Gerlach analyzer. Good resolution in this instrument is necessary and this requires the use of a narrow entrance slit (a fraction of 1 mm) compared to the width ($\sim$ 1 mm) of the atomic beam. It follows that only a small part of the beam cross-section can be sampled at a time. In the experiments envisaged, the polarization averaged over the whole beam width is required, as the full width will be illuminated by the incident electrons. The use of a Stern-Gerlach analyzer would thus entail many successive measurements, each with the entrance slit at a different position in the beam cross-section.

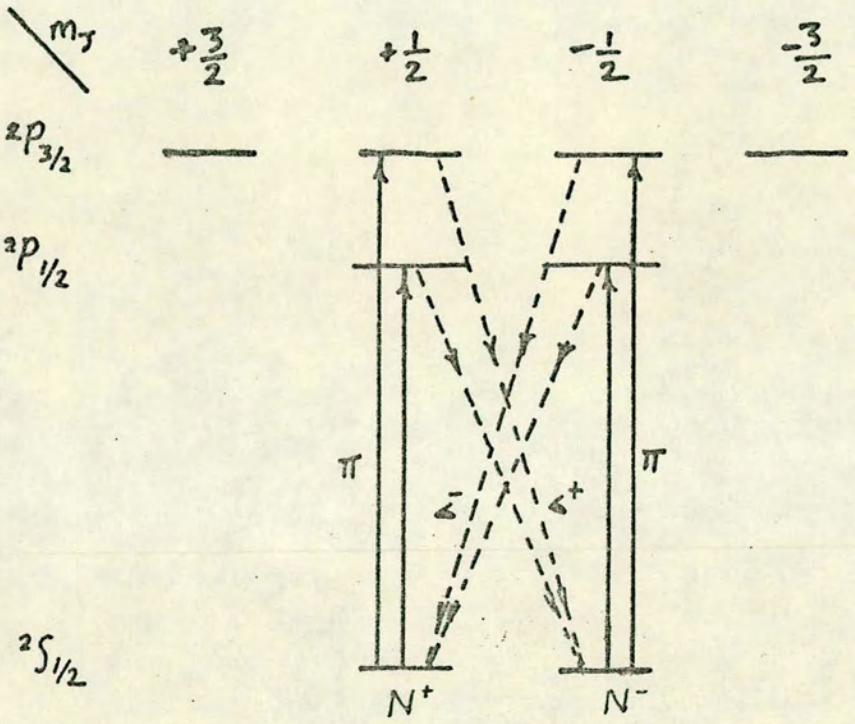

FIG. 4·27.

LEVEL DIAGRAM OF IDEALIZED ALKALI WITH I=0 SHOWING π EXCITATION AND RESULTING Δ RESONANCE FLUORESCENCE.

To overcome this disadvantage it is suggested that, for atoms with a $J = \frac{1}{2}$ ground state, use can be made of a method described by Kastler (1957). Consider an alkali atom with zero nuclear spin (Fig. 4.27). Let plane-polarized resonance light be incident on an ensemble of such atoms with the electric vector defining a quantization axis. Then Π-transitions to the ^2P excited states are induced. The populations of the $M_J = \pm\frac{1}{2}$ sub-levels of the excited states are thus proportional to the respective populations of the ground state sub-levels. If σ^+ radiation is observed in the decay of the excited states, then the σ^+ intensity will be proportional to the population (N_+) of the $M_J = +\frac{1}{2}$ sub-levels of the excited states, and hence that of the ground state $M_J = +\frac{1}{2}$ sub-level. Similarly, the intensity of σ^- radiation is proportional to the population (N_-) of the $M_J = -\frac{1}{2}$ sub-level.

The polarization of the atomic beam is defined as

$$P \equiv \frac{N_+ - N_-}{N_+ + N_-} \quad .$$

The asymmetry of the resonance light is defined as

$$\mathcal{A} \equiv \frac{I(\sigma^+) - I(\sigma^-)}{I(\sigma^+) + I(\sigma^-)}$$

where $I(\sigma^\pm)$ are the respective intensities of the $\sigma^\pm$ components of the resonance light emitted in the decay of the excited states.

By the above reasoning:-

$$P = \mathcal{A} .$$

Thus in the simple case of an alkali with zero nuclear spin, a measurement of the asymmetry will yield directly the polarization

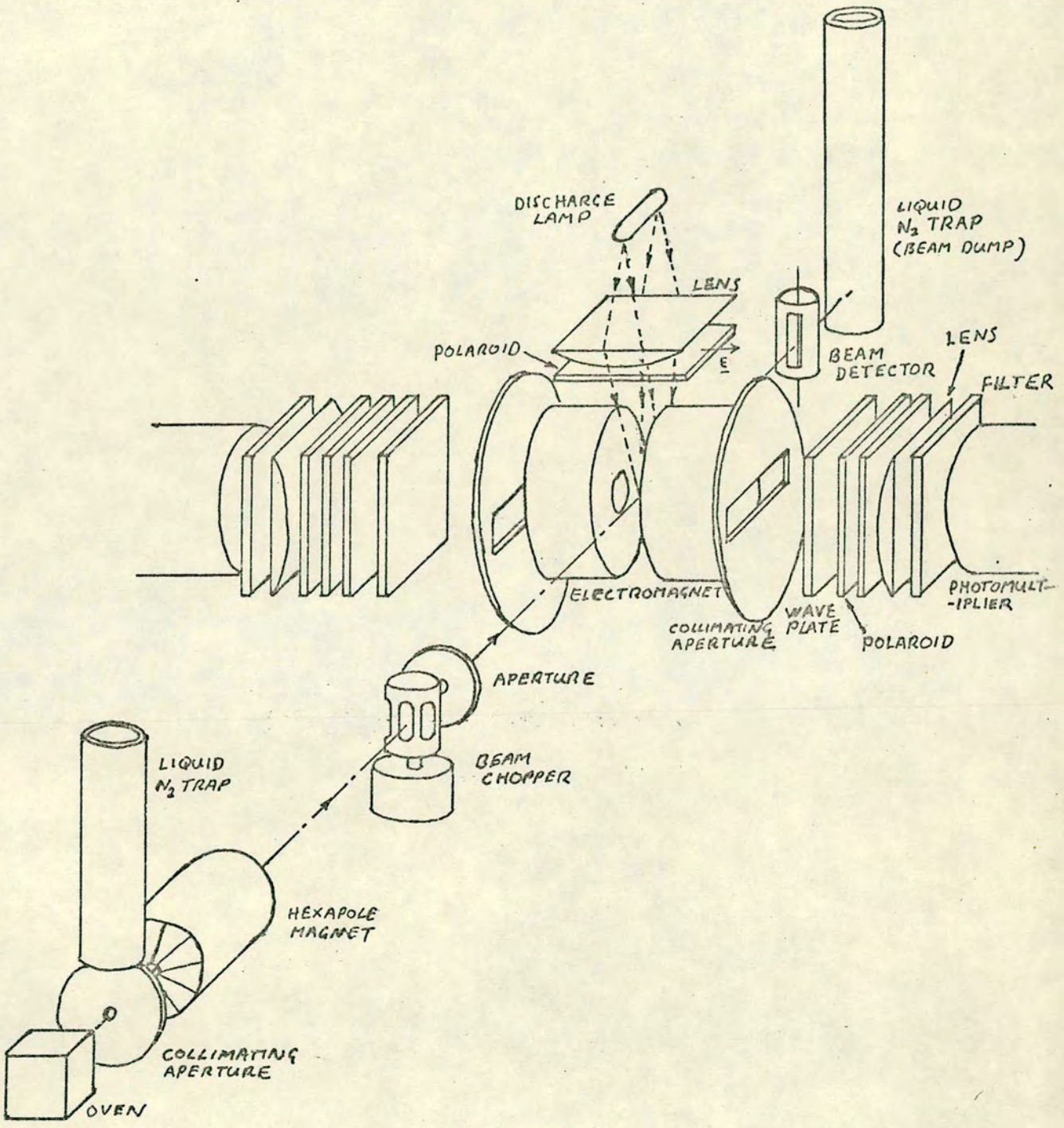

FIG. 4·28

THE APPARATUS USED IN THE MEASUREMENT OF ATOMIC BEAM POLARIZATION

of the atomic beam. This will be the "average" polarization as discussed above.

In the more usual cases, where there is a non-zero nuclear spin, the states are no longer eigenstates of J and M_J, and interpretation of P in terms of $\mathcal{A}$ is more difficult unless one can apply a sufficiently strong magnetic field in the region of the interaction to decouple the electronic and nuclear spins. In this high-field case, the relationship $P = \mathcal{A}$ still holds. In the case of certain alkalis, it is possible to apply a sufficiently strong field with relative ease. (For potassium $B > 50$ mT). In other cases, it is less convenient (for sodium $B > 200$ mT).

In the measurements on K which are to be described, it is only possible to obtain a field of 34 mT in the interaction region, but it is still possible to interpret the results in such low fields using the concept of effective magnetic moment if certain additional assumptions are made. It is then possible to compare the results with the hexapole calculations of Brash (1969), who gives P as a function of hexapole field (B_o). Thus a check can be made on the validity of this method of measurement.

It is shown in Appendix V that provided hyperfine coupling in the excited states is negligible (i.e. for reasonably high fields) then P and $\mathcal{A}$ are related by:-

$$P = \frac{\mathcal{A}}{\bar{\mu}_{eff}/\mu_\infty} \quad .$$

The Apparatus (see Fig. 4.28) A natural mixture of K is heated to a temperature in the region of 300°C in a stainless-steel oven with a single orifice 0.4 mm in diameter and 1.5 mm in length. It is not necessary to use a multichannel source here, as sufficient intensity is obtained in the interaction

region due to the focusing action of the hexapole magnet. It would be undesirable, in any case, to use such a source because its extended nature would lead to a reduction in polarization.

The resulting beam is passed through a liquid nitrogen-cooled, 3 mm diameter collimating aperture followed by the hexapole electromagnet (manufactured by Newport Instruments). This part of the system is described elsewhere (Brash, 1969). On emerging from the hexapole the beam is "chopped" at 21 Hz and finally passes through a 4 mm diameter aperture before reaching the interaction region where it is illuminated with plane-polarized light from a potassium discharge lamp. The interaction region is immersed in a uniform 34 mT magnetic field produced by a pair of solenoids, each consisting of 1200 turns of 22 SWG enamelled copper wire carrying 1.2A. The design is based on equations given by Klerk (1965). The atomic beam is detected with a Langmuir-Taylor hot wire detector with a 0.06 mm diameter tungsten filament. Each σ component of the resonance radiation from the beam is passed firstly through a "circular" polarizer type HNCP7 manufactured by Polarizers UK Ltd. It is then focused, using cylindrical perspex lenses, onto an RCA 7102 end-window photomultiplier operating at an HV of 1.25 kV. In this way, no change in polarization due to refraction is induced prior to analysis. Also the solid angle of acceptance is limited so that maximum angle of incidence on the polarizers was 10^{o}.

The system is evacuated to 2×10^{-6} torr by three Edwards E02 oil diffusion pumps.

Light Source The discharge tube consists of a 60 mm long, 10 mm diameter pyrex tube which had been thoroughly cleaned with a solution of Decon 75 and flushed with distilled water followed by acetone. The tube is evacuated to 10^{-6} torr and outgassed at 400°C. A natural mixture of K (99.97% purity) is then distilled into the tube until an almost opaque film forms on the cooler end. A buffer gas of krypton at a pressure of 1.6 torr. is now introduced. This preparation is described by Bell, Bloom and Lynch (1961), who operated their lamp under RF excitation. However, for the following reasons it was decided to use microwave excitation in the present work.

Firstly, due to skin effect, only a very thin shell of the vapour is excited at microwave frequencies. Therefore, sufficient thermal uniformity is maintained over the thickness of the shell to eradicate self-reversal (Dagnall and West, 1968). Secondly, a common difficulty with alkali lamps is the shortness of their life due to reactions of the hot alkali with materials within the pyrex. This leads, after a short time, to instability and finally to complete break down. It is found [illegible] that at microwave frequencies the mobility and hence reactivity of alkali ions within the pyrex is much reduced, so prolonging lamp life and increasing stability. Thirdly, high powers are conveniently generated, transmitted and controlled at microwave frequencies.

A frequency of 2.45 G Hz is used. This is generated by a Microtron "200" generator manufactured by EMS Ltd. A cavity produced by the same manufacturers, is used in which to excite the discharge tube.

It is found that, to excite a K discharge, a sufficient vapour pressure is obtained only if the lamp temperature is above 100°C. A grating spectrometer is used to compare the intensities of the D lines at various temperatures. Some results obtained are as follows:-

Lamp Temperature (°C)	D Line Intensity Ratio
130	1.6 : 1
140	1.3 : 1
150	1.2 : 1
160	1.0 : 1

The ratio obtained at 130°C suggests very little self-absorption at that temperature. The self-absorption obviously increases as the temperature approaches 160°C. The total intensity in the D lines increases by a factor of 5 as the temperature is raised from 130°C to 160°C, but, at the higher temperature, because of insufficient resolution it is not certain whether or not self-reversal has increased to a prohibitively high degree. As a compromise, a working temperature of 140°C is chosen.

Once the discharge has been started it is possible to maintain the correct temperature by regulating the power level of the oscillator. Unfortunately it is found that, due to the construction of the cavity, the ends of the discharge tube are substantially cooler than the main body where the discharge is taking place. The K vapour gradually condenses onto the cool ends so lowering the vapour pressure below the critical value for correct operation of the discharge. It is only possible to restart the discharge by

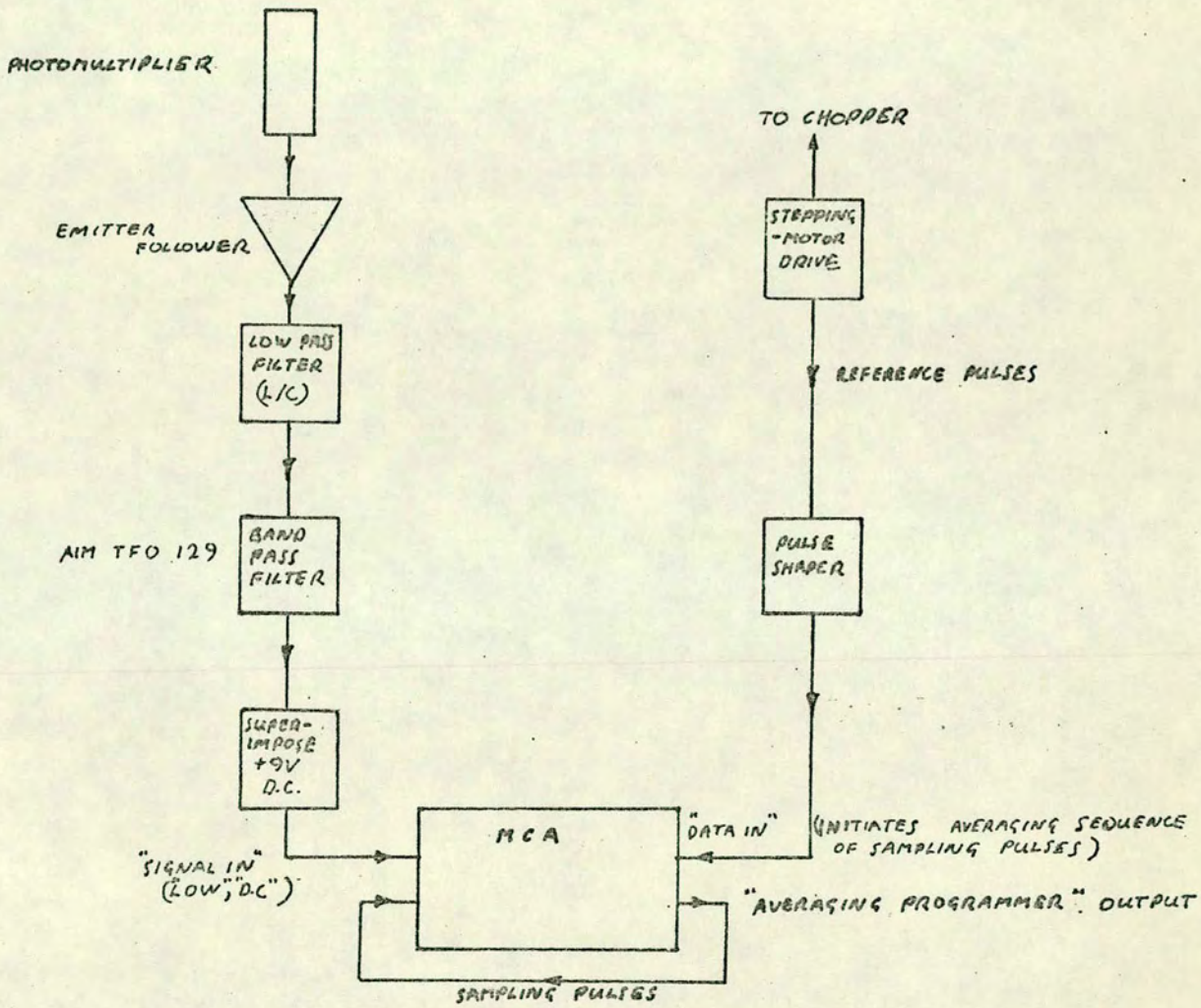

FIG. 4·29
SIGNAL-AVERAGING SYSTEM

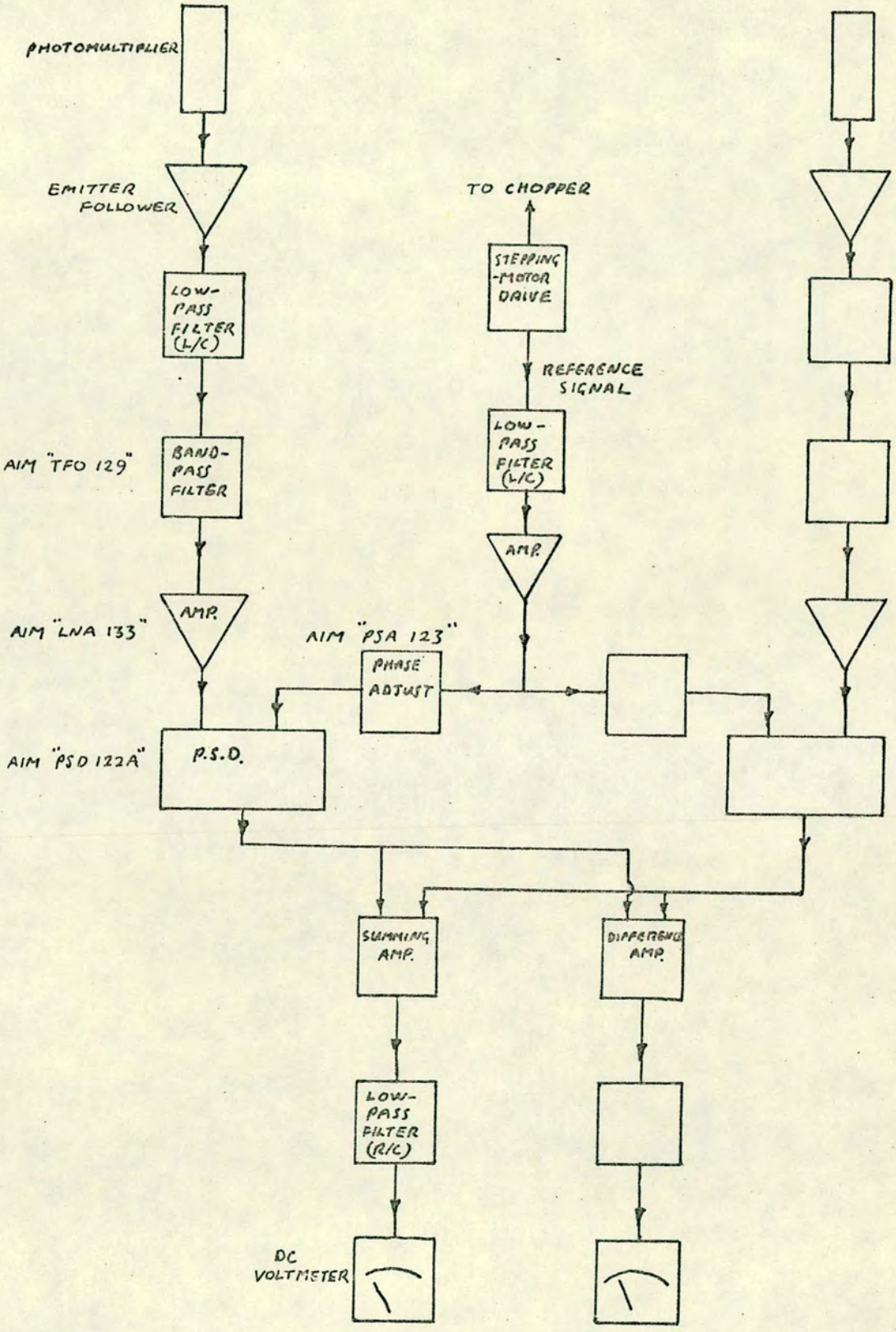

FIG. 4·30
PHASE-SENSITIVE DETECTION SYSTEM.

removing the tube and coaxing the K back to the centre with a gas flame. To overcome this inconvenience, heating coils are positioned within the hollow inner conductor of the cavity and adjacent to the ends of the discharge tube. In this way, the temperature gradient along the tube can be controlled. The temperature of the centre of the tube is monitored using a thermocouple. A stable discharge can now be obtained and it is found unnecessary to provide feedback control of the temperature.

Signal Processing Even after filtering the signals from the photomultipliers, nothing is observable at the chopping frequency of 21 Hz. This is due to the very high dark current of the high-red-response photomultipliers. Rather than eliminating this by cooling and thus introducing condensation problems, two electronic methods of signal extraction were tried; phase sensitive detection, using the AIM PSD 122A, and signal averaging using a Laben 400 MCA. Block diagrams of the two systems involved are shown in Figs. 4.29 and 4.30. The only essential difference between these two systems is that the MCA method enables longer averaging times to be used and thus it is of more use for situations giving rise to smaller signals. (For instance, when the oven is run at a lower temperature.)

A practical difference is that because two PSD 122A's were available the $\sigma^{\pm}$ signals could be obtained simultaneously, thus eliminating errors caused by drifts in the atomic beam and lamp intensities. However, it is necessary to carefully equalize the channel gains initially. The effectiveness of the equalization can be checked by reversing the decoupling field

and re-calculating the asymmetry. It should be noted that no hysteresis error is induced in the magnitude of the field during the reversal, as only non-ferrous materials are used in the construction of the electromagnet. As only one MCA is available, it is necessary with this method to take successive measurements of $\sigma^{\pm}$ signals. It is also necessary, therefore, to keep a check on the stabilities of the atomic beam and lamp by observing continuous records of beam-detector output and lamp temperature. Of course, the use of only one channel obviates the need for gain equalization. The $\sigma^{\pm}$ intensities are obtained from the single channel by alternating the direction of the decoupling field.

The ability to reverse the decoupling field direction is useful in another respect. When using the PSD system, the higher intensity signal can be produced in either channel. This aids the optimisation of the phase for maximum signal strength, which would be a very difficult procedure if the smaller signal were used. The limit of 34 mT on the magnitude of the decoupling field is set by the dissipation, which, in turn, is determined by the amount of outgassing which could be tolerated from the enamel on the windings. At this field the temperature on the inside of the windings is 70°C.

As shown in the block diagram, the sum and difference of the relative $\sigma^{\pm}$ intensities from the PSD's are provided in analogue form, being read off a pair of meters. The MCA system provided print-out and screen display of the relative $\sigma^{\pm}$ intensities.

The beam chopper consists of a rotating aluminium cylinder in which three equally-spaced, longitudinal slots had been cut

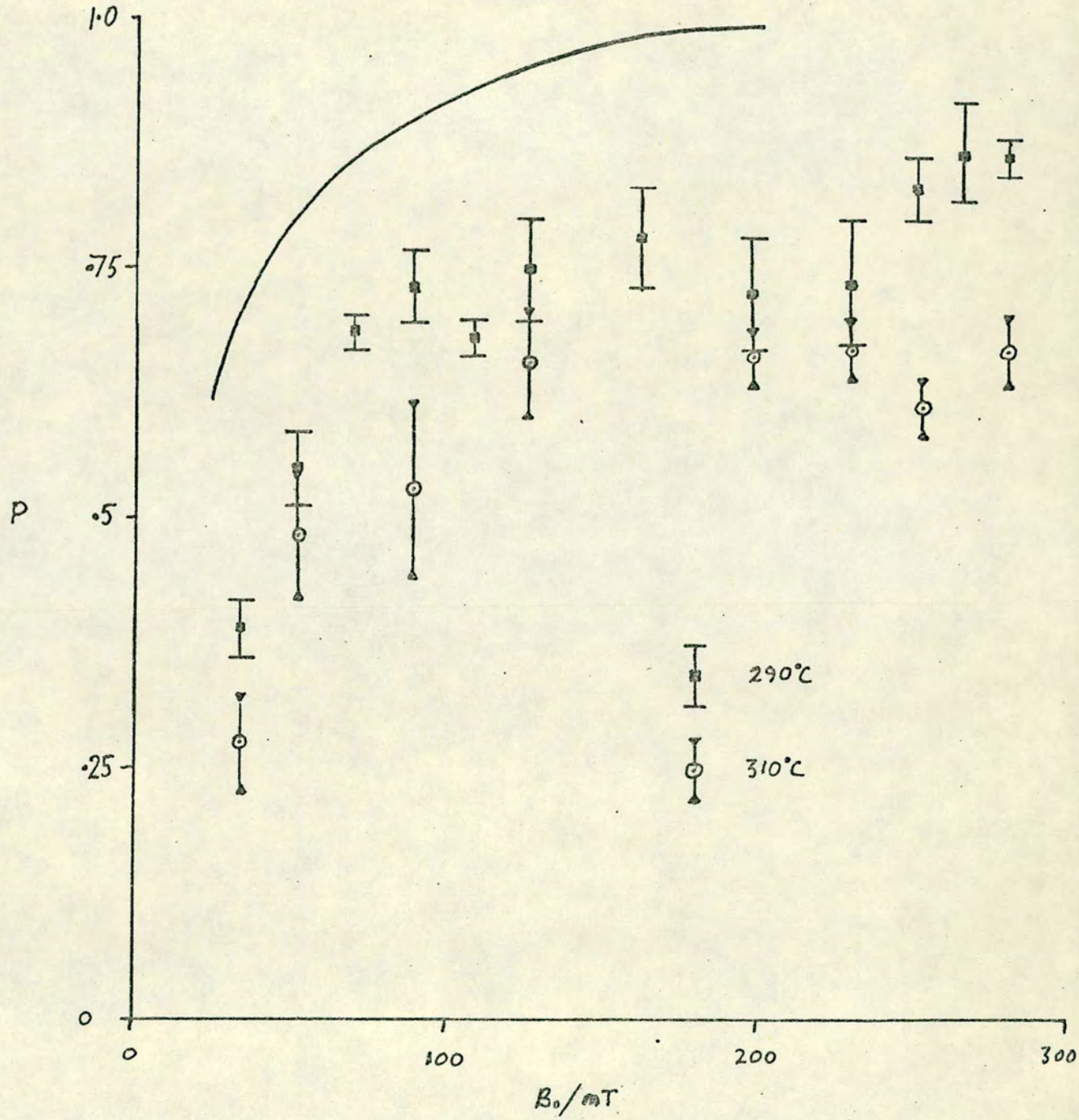

FIG. 4·31

MEASURED VALUES OF POLARIZATION (P) AS A FUNCTION OF HEXAPOLE FIELD (B_0) FOR VARIOUS OVEN TEMPERATURES. THE FULL CURVE IS THE RESULT OF THE CALCULATIONS OF BRASH (1969) FROM HEXAPOLE PARAMETERS.

passing through the axis. Thus the atomic beam is able to pass through the cylinder six times per revolution. The cylinder is attached to the spindle of a stepping motor rotating at 3.5 Hz. The tolerable level of outgassing determines the motor temperature and therefore the drive-pulse amplitude. This, in turn, determines the maximum possible rate of rotation. Pulses of 12 V peak height are used. When the PSD system is being used, it is necessary to readjust the phase whenever the stepping motor is started.

A chopper consisting of a vibrating reed driven by an electromagnet had been tried previously but this was discarded because it was found that the alternating field of the electromagnet was modulating the gain of the photomultipliers (in spite of extensive shielding), so producing spurious signals at the chopping frequency.

Results Measurements of polarization are made for various oven temperatures and various values of B_o, (the flux density at the pole tips of the hexapole magnet). Fig. 4.31 shows P as a function of B_o for oven temperatures of 290°C and 310°C. Corrections to these results necessitated by the imperfection of the HNCP7 polarizer (see section 4.3) are calculated in Appendix VI. Also shown is a theoretical curve calculated by Brash (1969) for a geometry identical to that used in the measurements, and for an oven temperature of 310°C. These calculations were based on the six-pole theory set out by Brash et al. (1969).

It is seen that an increase in oven temperature leads to a decrease in polarization. This is to be expected since the hexapole will best function as a state-selector when the

source of atoms is very small. The smallness of the source is limited by the diameter of the oven orifice. In practice, however, inter-atomic collisions at the exit of the orifice can produce an effective source which has a diameter larger than that of the orifice. The chance of an inter-atomic collision increases with source temperature, and so, therefore, does the size of the effective source. This in turn lowers the efficiency of the hexapole as a polarizer.

Both sets of experimental points lie below the calculated curve. This again is expected because of the idealizations made in the calculation. These were, firstly; the assumption of a point source, and secondly; the assumption that electronic and nuclear spins were completely decoupled at all points within the hexapole tube. The effects produced by the invalidity of the first assumption will be apparent from the previous discussion of oven temperature effects. The falseness of the second assumption leads to error also, as the magnetic flux density is zero on the axis of the hexapole and so in this region, at least, the electronic and nuclear spins are not de-coupled. So, for atoms passing through this central region, the hexapole does not select $\{J, M_J\}$ states and is therefore an imperfect polarizer as far as these states are concerned.

The results for 310^{o}C are obtained with the PSD system using a 10 sec. time constant. The error bars represent maximum fluctuation of the outputs on either side of the mean for a number of runs made at that temperature. One measurement was made with the MCA system. This was found to agree with the corresponding PSD result to within the error bars.

Because of the lower signal intensities, the results for

290°C are obtained with the MCA system using an averaging time of 2 mins.

The fluctuations noted in the outputs from the PSD system, besides being due to remnant photomultiplier noise, probably have a component caused by the pressure fluctuations described by Fite and Brackman (1958). The random nature of pumping by the diffusion process produces a frequency spectrum of fluctuations in the background pressure of the system. Corresponding fluctuations appear therefore in the atomic beam intensity and hence also in the signals. Fluctuation components with a frequency near that of the chopper will not be completely removed by phase sensitive detection or averaging, and they will add to the true signal output giving it a slowly and randomly varying amplitude as the phase of the pressure fluctuations varies randomly. As suggested by Fite and Brackman, because the volume of the system being pumped acts like a low-pass filter with time constant V/L (V is the volume of the system, L the pumping speed) to these pressure fluctuations, it would prove advantageous to lower the chopping period below V/L. The system time constant for the apparatus used is approximately 20 ms, so that a chopping frequency of approximately 100 Hz would be desirable in order that the pressure fluctuations at this and higher frequencies would be effectively averaged to zero. However, as mentioned earlier, the present chopping system precludes the use of such high frequencies. The performance of a piezoelectrically driven chopper is being investigated for possible future use.

Conclusion In view of the idealisations made in the calculations of Brash (1969) the measurements would seem to give a reasonable indication of the polarization of the atomic beam. However, two factors so far unconsidered would cause the measured polarization to differ from the actual polarization, firstly;- the possibility that atoms in the interaction region could be excited more than once would give rise to a reduction in A . The effects of these processes can be ignored on the basis of experiments performed by Rae and Wykes (1972), which give a single excitation probability of approximately 10% using a typical discharge lamp intensity. Secondly;- the condensation of small amounts of K on the HNCP7 analyzer would lead also to a reduction in A . The magnitude of this effect cannot be calculated or measured but it can only be small because otherwise the light intensities would be drastically reduced.

The "dips" in the experimental results around 100 mT and 230 mT, which are absent from the theoretical curve, are probably due to some asymmetry in the geometry of the hexapole magnet.

It is planned to repeat these measurements with "zero" decoupling field. This will enable exact corrections to be applied to give the polarization which would be obtained in a high field, the relationship between zero field and high field wavefunctions being know exactly. These corrections have been calculated by Wykes (1973). The "zero field" method will also be applicable to other alkalis, such as caesium, which would normally require inconveniently high decoupling fields, and for which the assumptions made in the interpretation of the above

measurements on potassium can no longer be made.

These zero-field measurements will be more relevant to the proposed coincidence experiments using polarized atomic beams (see Chapter 1) where, for electron-optic reasons, it is necessary to work in very low magnetic fields.

CHAPTER 5

MEASUREMENT OF COINCIDENCE RATES AND RESULTS

5.1 Sources of Systematic Error and Corrections

Determination of the Relative Efficiency of the Photon Channels

The necessity for this determination has been discussed in Chapter 2 and in section 3.3, and to enable it to be carried out, the properties of a polarizer were measured as described in section 4.3.

The system is set up as if for an actual run (see section 4.5 and Appendix IV), except that the polarizer is positioned so as to intercept the light reaching the Wollaston prism from the interaction region, and such that the polarization direction of minimum intensity is parallel to that accepted by channel I. In each photon channel, eleven pairs of 100-second "singles" counts are taken with the atomic beam alternately "on" and "off" (by opening and closing the gate valve), the effect of drifts in beam intensities thereby being eliminated. For each channel, the difference (Δ) between the count totals for the "beam on" and "beam off" conditions, is proportional to the detection efficiency (η) for that channel. One obtains:-

$$\Delta_1/\Delta_2 = 1.054 \pm .008 \ ,$$

the uncertainty being one standard deviation. To obtain the relative channel efficiency this has to be corrected for the effect of the difference in incident intensities of the two polarization components, expressed by their ratio (see section 4.3):-

$$I_2/I_1 = 1.31 \pm .01 \ .$$

The relative channel efficiency is given, therefore, by the product of the above factors:-

$$\eta_1/\eta_2 = 1.38 \pm .015 .$$

The channel asymmetry A, defined in Appendix I, is:-

$$A = + 0.160 \pm .006 .$$

When this calibration has been completed the polarizer can be removed, as described in section 4.3, without disturbing the system; and runs for the measurement of the coincidence rates may be commenced.

The Effect of Radiation Trapping. It is necessary to consider the possibility of systematic error in P due to radiation trapping. Holstein (1947) gives the probability T(r) of a photon traversing a distance r in a vapour, before absorption, as a function of the parameter $(k_o r)$. k_o is the absorption coefficient at the centre of a doppler-broadened line and is given by:-

$$k_o = \frac{\lambda_o^3 \rho}{8\pi^{3/2}} \cdot \frac{g_j}{g_o} A_{jo} \left(\frac{m}{2kT}\right)^{\frac{1}{2}}$$

where λ_o is the wavelength at the centre of the line, ρ is the number-density of the vapour, g_j and g_o are the statistical weights of the excited and ground states respectively, A_{jo} is the probability/sec. of a transition to the ground state which, in the present case, is given by $1/\tau'$, m is the mass of the target atom, k is Boltzmann's constant, T is the absolute temperature of the vapour, and r is the distance across the

interaction volume. Using values appropriate to the case under study and putting T equal to the oven temperature, one obtains

$$k_o r \approx 2 \times 10^{-3} .$$

According to Holstein's theory T(r) is approximately unity for values of $(k_o r)$ below 10^{-2} (Phelps, 1958) and so on this basis, it appears that radiation trapping would be negligible. However, the above theory does not quite describe the situation prevailing in the present work, the target here being in the form of a beam rather than a true vapour. Therefore, the possible variation of P with oven temperature will have to be investigated and an extrapolation to zero T made if necessary, although significant departure from the result of the above theory is not anticipated.

5.2 Observed Values of the Parameters Estimated in Section 3.2

Photon Channel Unfortunately, between the calibration and the start of the run, photomultiplier I began to exhibit an anomalously high apparent dark current (some tens of kHz) which may have been due to breakdown inside the tube. It was necessary to reduce the high voltage to 1.4 kV to bring the count rate down to a manageable value. This also has the effect of reducing the efficiency of the channel due to the reduction of gain and the lowering of the K-D1 collection efficiency (not to mention a degradation in time resolution). The above calibration was therefore rendered invalid. Although the tube was still sensitive to the presence of light, it would not have been possible to carry out a recalibration without letting the system up to atmospheric pressure

	OBSERVED			ESTIMATED
	INITIALLY	AFTER 53 HOURS	AVERAGED OVER RUN	
ATOMIC BEAM ON (N_γ)	156 ± 3	180 ± 3	206	180
ATOMIC BEAM OFF (n_γ)	67 ± 2	75 ± 2	88	20
SIGNAL ($N_\gamma - n_\gamma \equiv R\xi_\gamma$)	89 ± 4	105 ± 4	118	160

(UNCERTAINTIES CORRESPOND TO ONE STANDARD DEVIATION)

TABLE 5·1
COMPARISON OF ESTIMATED AND OBSERVED "SINGLES" COUNT RATES (×SECS): PHOTON CHANNEL II
(ELECTRONS INCIDENT AT 5·0 eV ON Na., OVEN TEMP. 340°C, $\theta = 9°$, $\Phi - \phi = 180°$)

	OBSERVED			ESTIMATED
	INITIALLY	AFTER 53 HOURS	AVERAGED OVER RUN	
ATOMIC BEAM ON (N_e)	1273 ± 7	1900 ± 10	1820	860
ATOMIC BEAM OFF (n_e)	927 ± 6	1576 ± 9	1485	500
SIGNAL ($N_e - n_e \equiv R\xi_e$)	346 ± 9	324 ± 13	335	360

(UNCERTAINTIES CORRESPOND TO ONE STANDARD DEVIATION)

TABLE 5·2
COMPARISON OF ESTIMATED AND OBSERVED "SINGLES" COUNT RATES (×SECS): ELECTRON CHANNEL
(CONDITIONS AS ABOVE)

in order to remove the lid so that the polarizer could be replaced. As all other systems were behaving well it was decided to go ahead with the run so that on the basis of the coincidence rates in the remaining channel, an investigation of the feasibility of this type of measurement could at least be carried out.

The observed singles rates for channel II are compared with the original estimates (column 4) in Table 5.1. Three pairs of 10-second, alternating "beam on - beam off" counts were taken. This was carried out initially (column 1) and after 53 hours of live running time (column 2). The third column shows the total photon count rate averaged over the duration of the run (69.50 hours live time) obtained from the total accumulated "singles" photon counts. The fact that the increment, with time, of the signal ($R\xi_\gamma$) and background (n_γ) rates are both in approximately the same proportion suggests that it is due to a long term drift in photomultiplier gain rather than a change in beam intensities. Under this assumption, estimates of the corresponding averages for $R\xi_\gamma$ and n_γ can be inserted in column 3.

Electron Channel. Fig. 4.18 shows the energy spectrum of scattered electrons, at 5.0 eV incident energy, taken prior to the run. Data corresponding to those in the above table are given for the electron channel in Table 5.2. Again the third column contains the total electron rate averaged over the run. But now there is no evidence that the signal rate has changed and its estimated average in column 3 is now the mean of the values in columns 1 and 2. The average value of n_e can now be estimated.

Although the signal rates ($R\xi$) lie reasonably close to

	OBSERVED (AVERAGED OVER RUN)	ESTIMATED
RANDOM COINCIDENCE RATE (N_r)	$16{\cdot}4\times10^{-3}$/SEC.	$7{\cdot}0\times10^{-3}$/SEC
GENUINE COINCIDENCE RATE ($N_g = R\xi_e\xi_\gamma$)	$(4{\cdot}06\pm{\cdot}38)\times10^{-3}$/SEC.	$9{\cdot}3\times10^{-3}$/SEC
ELECTRON SIGNAL RATE ($R\xi_e$)	335/SEC.	360/SEC
PHOTON SIGNAL RATE ($R\xi_\gamma$)	118/SEC.	160/SEC
ξ_e	$(3{\cdot}44\pm{\cdot}25)\times10^{-5}$	$5{\cdot}58\times10^{-5}$
ξ_γ	$(1{\cdot}22\pm{\cdot}09)\times10^{-5}$	$2{\cdot}57\times10^{-5}$
EXCITATION RATE (R)	$(9{\cdot}7\pm1)\times10^{6}$/SEC.	$6{\cdot}5\times10^{6}$/SEC.

(UNCERTAINTIES CORRESPOND TO ONE STANDARD DEVIATION)

TABLE 5·3

COMPARISON OF OBSERVED COINCIDENCE RATES, EFFICIENCES AND EXCITATION RATE, WITH ESTIMATES.

	FOUR PARAMETERS	FIVE PARAMETERS
RANGE (INCLUSIVE)	205-320 (CHANNELS)	205-320 (CHANNELS)
GAUSSIAN CENTROID POSITION (T)	$266{\cdot}1\pm{\cdot}3$ (CHANNEL NO.)	$266{\cdot}2\pm{\cdot}4$ (CHANNEL NO.)
GAUSSIAN FWHM (w)	12 ± 3 (nSECS.)	12 ± 3 (nSECS)
LIFETIME (τ')	FIXED AT 16·0 nSECS.	$15{\cdot}5\pm3$ (nSECS.)
BACKGROUND PER CHANNEL (A)	$275\pm1{\cdot}7$	$275\pm1{\cdot}7$
GENUINE COINCIDENCES ($N_g t$)	1022 ± 80	1021 ± 97
GENUINE COINCIDENCE RATE (N_g)	$4{\cdot}06\times10^{-3}$/SEC. (14·7/HOUR)	$4{\cdot}06\times10^{-3}$/SEC. (14·7/HOUR)
UNCERTAINTY IN N_g	7·8%	9·5%
χ^2	129·7	129·7
DEGREES OF FREEDOM	112	111
97·5% =	PROB($\chi^2<142{\cdot}5$)	PROB($\chi^2<141{\cdot}5$)

(UNCERTAINTIES CORRESPOND TO ONE STANDARD DEVIATION)

TABLE 5·4

COMPARISON OF VALUES OBTAINED FROM FOUR AND FIVE -PARAMETER LEAST SQUARES FITS.

the estimated values, the signal/background ratios are more than a factor 3 worse. It is particularly poor in the electron channel and, even initially, it is very much inferior to what was originally considered to be a pessimistic estimate. The long-term increase in n_e is likely to be due to effects of surface charging in the region of the analyzer entrance aperture, leading to an increasing deviation of part of the unscattered beam into the aperture. The observed photon channel background rate (n_γ) is somewhat higher than that (20 Hz) used in the estimate of counting time, in section 3.3. The actual contributions to the background rate are: 45-60 Hz from photomultiplier dark current and 20-30 Hz from the cathode heater.

Estimates of the excitation rate R and the efficiencies ξ_γ and ξ_e can be made as described in section 3.2, using the average values of $R\xi_\gamma$ and $R\xi_e$ from column 3 of Tables 5.1 and 5.2, and the observed mean coincidence rate $R\xi_\gamma\xi_e$ obtained from the result of the run (see next section). These values are compared in Table 5.3 with the estimates of section 3.3. The discrepancies between the present values of the efficiencies and those originally estimated could be due to errors in the cross sections, neglect of the effect of discriminator levels in the calculation of the detection efficiencies (η), and, in the case of the photon channel, overoptimistic specifications of photomultiplier quantum and collection efficiencies. The larger than expected value of R may be due to the larger effective interaction volume produced by the "wings" of the atomic beam profile, while that of N_r is obviously due to the large values of n_e and n_γ.

5.3 The Run to Determine the Coincidence Rates

Because of the malfunction of photomultiplier I, mentioned in the previous section, it was not even possible to obtain a meaningful measurement of the coincidence rate in channel I, which in turn precludes a determination of P. The purpose of the run therefore is to determine the coincidence rate in channel II and, more importantly, the accuracy with which it is possible to obtain this measurement.

The Accumulation of Data. Before the main run is commenced, an initial test run is carried out, lasting for 47 hours, during which time, interlaced time spectra are obtained by alternately tuning the analyzer on and off the "inelastic" peak, to a point on the high-energy shoulder of the "elastic" peak where the electron "singles" rate is of similar magnitude (analyzer voltage = 4.02V). A peak is obtained in the otherwise uniform time spectrum only in the case where the analyzer is "on tune". This peak occurred in the position expected on the basis of the estimated delay of 67 nsecs (20 channels) between the production of a pulse due to a promptly emitted photon and that due to the corresponding electron (see Tables 3.1 and 3.2). The extra delay introduced purposely into the electronics of the "stop" channel had previously been determined by feeding the pulses from a single detector simultaneously into the electron channel and each photon channel in turn. For channel II, events accumulated in MCA channel 245, so that the peak corresponding to genuine coincidences is expected around MCA channel 265.

Also noteworthy in the results of the above test, is the absence of any spurious coincidence peaks which, in this work,

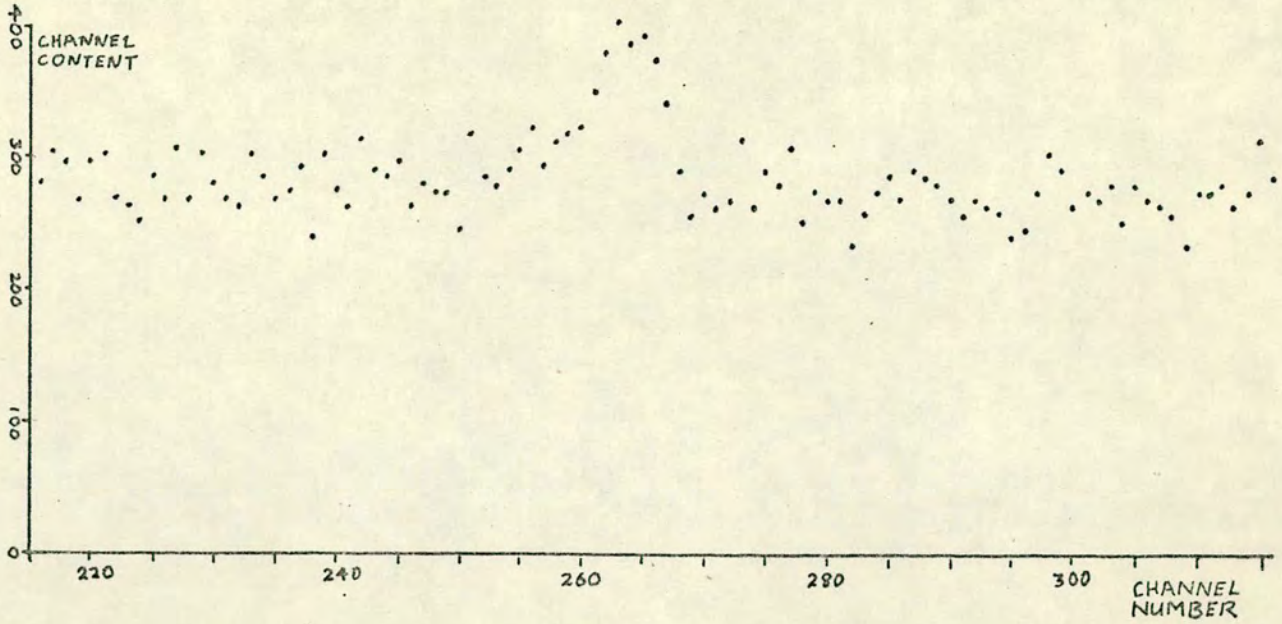

FIG.5·1
TIME SPECTRUM OBTAINED IN COINCIDENCE CHANNEL II
AFTER 69·50 HOURS LIVE RUNNING TIME (3·43 nSECS/CHANNEL)

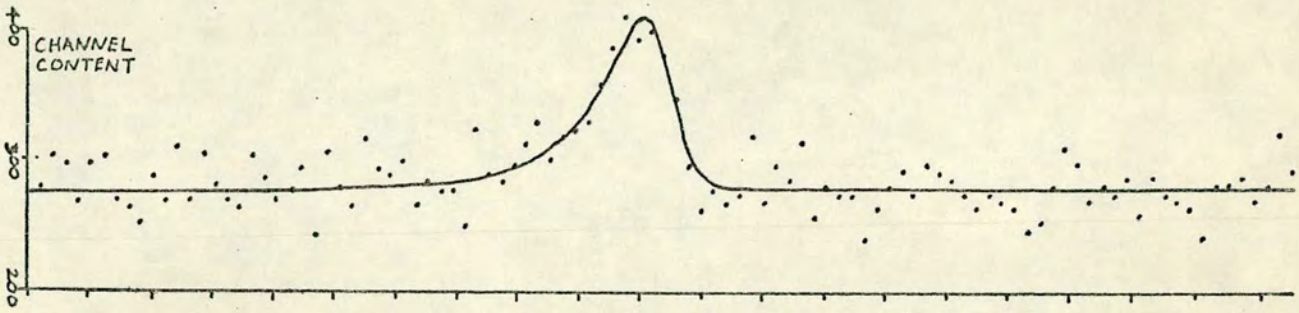

FIG. 5·2
FUNCTION RESULTING FROM 4-PARAMETER FIT
TO THE DATA OF FIG. 5·1

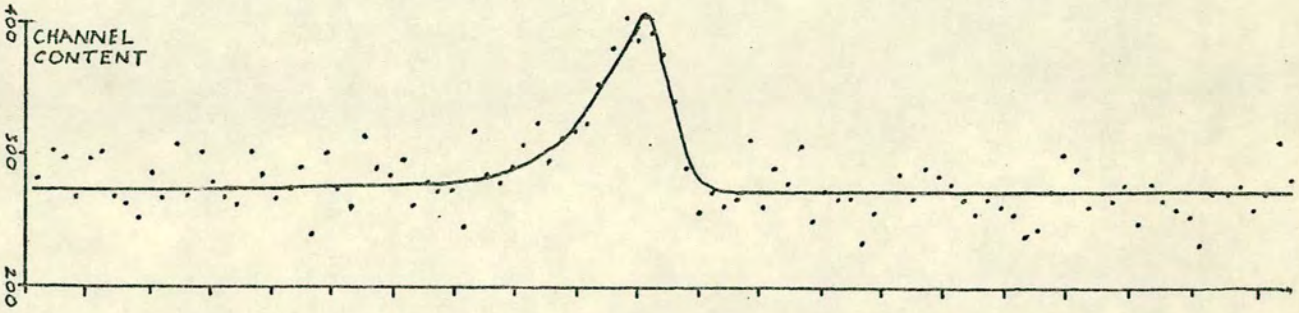

FIG.5·3
FUNCTION RESULTING FROM 5-PARAMETER FIT
TO THE DATA OF FIG. 5·1

are in danger of being produced as a result of switching transients on the mains supplies filtering through to the detection channels. Although switching operations in the lab. were avoided, if possible, during a run, some switching was inevitable - in the automatic liquid nitrogen replenishers for example. Pick-up from this source into the "fast" channels has in fact been observed, but many tests have failed to show any effect in the "slow" channels which ultimately determine the acceptance of data; and the present test justifies the reliance placed on the selectivity of these channels.

The main run lasted for 78 hours "real" time. During this time the accumulation of data was intermittently stopped to allow checks on electron and photon signal rates, data print outs, and other switching operations to be carried out. "Live" time was 69 hours 30 mins.

The time spectrum in subgroup II is shown in Fig. 5.1. The lifetime curve is seen to be just resolved. The exponential component lies towards shorter time delays because the photon pulses are used to start the time-conversion ramp, artificial delays having been inserted in the electron channel. The position of the peak is at channel 264 and the centroid of the gaussian component is given by a curve fitting procedure (see below) to lie at channel 266. The predicted position of the centroid is channel 265 (see above). But this provides verification of the detector specifications (Table 3.1) as much as proving the authenticity of the feature.

The Treatment of the Data - The Extraction of the Genuine Coincidence Rates. Straightforward numerical integrations of the data as described in section 3.2 give the following results:-.

Total background integrated over channels 209-253 and 269-313 inclusive:	24761
Mean background per channel:	275 ± 1.7
Mean background per 15-channel group ($N_r t$):	4127
Signal + background ($N_e t$; integrated over the 15 channels 254-268 inclusive):	5094
Signal ($N_g t$):	967 ± 75
Mean genuine coincidence rate (N_g):	$(3.86 \pm .30)\times10^{-3}$/sec(14/hr.)
Percentage uncertainty	7.8%

The given uncertainties are statistical and correspond to one standard deviation. The range of integration of 15 channels (50 nsecs) is chosen to cover the peak in the time spectrum.

The question arises as to whether a more accurate result would be obtained if the area under the peak was to be evaluated by making use of a curve fitting procedure. Following Gale (1962) and Imhof and Read (1971), the function postulated to describe the contents of the jth channel (see also section 3.2) is given by:-

$$A + \frac{2h}{\sqrt{\pi}} B f(t_j)$$

where

$$f(t_j) = \int_{-\infty}^{+\infty} g(t_j - t')h(t')dt'$$

$$g(t) = \exp\left[-h^2(t-T)^2\right]$$

$$h(t) = \begin{cases} \exp\left[t/\tau'\right] & t \leq 0 \\ 0 & t > 0 \end{cases}$$

and t_j is the time delay to which channel j corresponds. The result of the integration gives:-

$$f(t_j) = \frac{\sqrt{\pi}}{2h} \exp\{\frac{1}{4h^2\tau'^2} + \frac{t_j - T}{\tau'}\}\{1 - \mathrm{erf}[h(t_j - T) + \frac{1}{2\tau'}]\}.$$

Erf is the normalized error function, and the parameters appearing in the above expressions are as follows: A is the total background of random coincidences per channel. B is proportional to the combined amplitudes of the gaussian and exponential components, and therefore depends on the total number of genuine coincidences ($N_g t$). T is the position of the centroid of g. h is related to the FWHM (w) of g by $h^2w^2 = 4\ln 2$, and depends therefore on the instrumental time resolution. τ' is the lifetime of the atomic state under study. w and τ' together determine the overall time resolution (τ). The values of these five parameters (A, B, T, w, and τ') can all be determined from the curve fitting. However, of all these parameters, only one (τ') has a value independent of the conditions of the experiment, depending only on the material of the target and the states studied, namely the 3^2P states of Na. The value of τ' in this case has been measured by Schmieder, Lurio, Happer and Khadjari (1970) who obtain a value of 16.0 ± .5 nsecs, using a level-crossing technique. Because the present instrumental time resolution has been estimated to be of the same order as this (14 nsecs), it is unlikely that a curve-fitting of the data will yield a value of τ' with the same accuracy as that obtained by Schmieder et al. For this reason, τ' is treated as a constant with a value 16.0 nsecs. Thus the number of unknown parameters is reduced to four.

A non-linear least squares fit of the above function to the data is carried out using the method summarized in Appendix VII. The function resulting from the fit is compared to the data in Fig. 5.2. The parameters having been chosen, a numerical integration of the function $(2h/\sqrt{\pi})Bf(t_j)$ is performed over all channels to give $N_g t$, and the variance is calculated from the relation (Brandt, 1970):-

$$\sigma^2(N_g t) = \frac{4h^2}{\pi} . B^2 \sum_{ij} c_{ij} \frac{\partial[\int f(t)dt]}{\partial x_i} . \frac{\partial[\int f(t)dt]}{\partial x_j} \qquad i,j = 1,2$$

where the x_i represent the parameters B and w, the partial derivatives with respect to A and T being identically zero; and the c_{ij} are the elements of the covariance matrix of the parameters (see Appendix VII) given by the least squares procedure. The resulting values of the parameters, the coincidence rate, and their standard deviations, are given in column 1 of Table 5.4. The value of χ^2 (see Appendix VII) is also given as an indication of goodness of fit.

It can be seen from Table 5.4 that there is no improvement in statistical accuracy (7.8%)over that given by the original method. However the results of the two methods are in agreement, and, more importantly, possible systematic error due to the rather arbitrary selection of integration range (to "cover the peak") in the earlier method, is now eliminated.

The FWHM of the gaussian component representing the instrumental time resolution (i.e. the total time spread due to transit time fluctuations in analyzer and detectors; and "jitter" in the discriminators caused by finite risetimes) is given as 12 ± 3 nsecs which is of the order expected (an estimated value of 14 nsecs was obtained in section 3.3; and a test of the

discriminators using similar detectors and a ^{22}Na source, described in section 3.4, yielded a value of 16 nsecs). The fact that the present instrumental time resolution is slightly inferior to that obtained in similar work by Eminyan et al. (1973, 1974) and McConkey et al. (1975), can be attributed to the ability in these cases, to use CEM's as photon detectors which produce faster pulses with a more favourable height distribution (see section 3.4). It should be noted that these authors appear to define "time resolution" in the same way as "instrumental time resolution" is defined in the present work.

It is of interest to allow the fifth parameter (τ') to vary to check for consistency with the previous measurements of Schmieder et al. (1970). It is expected, of course, that the value of $N_g t$ obtained from this fit will be less accurate than that obtained in the 4-parameter case. This is in fact the case as can be seen from the results displayed in column 2 of Table 5.4. The lifetime (τ') given by the fit is 15.5 ± 3 nsecs which is in agreement with the value obtained by Schmieder et al., and has the expectedly large statistical uncertainty. It is again comforting to note that the values of all the other parameters are in agreement with those obtained by the two previous methods. The function resulting from the five-parameter fit is compared to the data in Fig. 5.3.

The result of the "randoms" calibration of section 3.6, is used in the conversion of the above results from "number of channels" to "time".

5.4 Conclusion

The Necessary Counting Time and its Reduction. Apart from the malfunction of photomultiplier I, the large statistical uncertainty in $N_g t$ would preclude a meaningful estimate of Π. Ways will therefore have to be found of improving the statistical uncertainty while keeping the counting time within reasonable limits.

In section 3.2, equation (3.4), an expression for the counting time is given in terms of the quantities R, ξ_e, ξ_γ n_e, n_γ and τ. This expression can be rearranged to give the following:-

$$t = F + (G + Hn_\gamma + In_e)R^{-1} + J\, n_\gamma n_e R^{-2} \qquad (5.1)$$

where

$$F = \frac{(1 + {}^1/_m)\tau}{\xi_e \xi_\gamma \rho^2} = 3.5 \times 10^5 \text{ secs.}$$

$$G = \frac{1}{\xi_e \xi_\gamma \rho^2} = 6.0 \times 10^{12}$$

$$Hn_\gamma = F\frac{n_\gamma}{\xi_\gamma} = 2.5 \times 10^{12}$$

$$In_e = F\frac{n_e}{\xi_e} = 1.5 \times 10^{13}$$

$$Jn_e n_\gamma = F\frac{n_\gamma}{\xi_\gamma} \cdot \frac{n_e}{\xi_e} = 1.1 \times 10^{20}/\text{sec.}$$

The numerical values have been obtained from Tables 5.1, 2 and 3; and ρ, as in section 3.3, is required to be .014. As the excitation rate, R, is of the order 9.7×10^6/sec, the terms in n_e are seen to dominate the expression (5.1), being an order of

magnitude greater than the others. Most improvement in the situation would therefore be obtained by a reduction of n_e. If this could be reduced by an order of magnitude, then further impression could be made by an increase in R, although the efficiency of this will be reduced as the values of the terms in R fall below that of F.

Further reduction in t for fixed ρ will require either a decrease in τ, which is not possible because it is already limited by τ', or an increase in ξ_e or ξ_γ. This cannot be done by increasing detection-solid angles unless a deterioration in angular resolution can be tolerated. The possibilities however, do exist, of increasing the efficiency of the CEM by raising the energy of incident electrons, and of using a different orientation of the CEM (see Fig. 4.14). In the former case, care must be exercised to prevent significant penetration of the accelerating field into the analyzer as this is already suspected of leading to the poor resolution encountered (see section 4.5). It is not possible to increase ξ_e through σ_e by working at smaller scattering angles (θ), because at the present angle of 9°, some of the unscattered beam is already being accepted.

R can be increased simply by moving the atomic beam source nearer to the interaction region. The present nozzle-interaction region distance is determined by a combination of scattering-chamber geometry (implying that the atomic beam should be in the plane of scattering) and the desire to be able to detect scattering at angles up to 60°. Recent experience has shown that, with the present geometry, such measurements are out of the question anyway, due to the reduced cross section at larger

angles. A reduction of the source-target distance to at least half its present value is therefore possible, provided also that the re-entrant section of the oven chamber is extended, it being felt that the inclusion of the atomic beam source in the same chamber as the scattering apparatus will lead to problems caused by excess vapour. (e.g. radiation trapping and depolarization, loss of electron beam intensity due to cathode poisoning, and contact potential effects due to the deposition of material on electrode surfaces.)

It is difficult to increase R by attempting to increase the electron beam current, as the gun is already operating near the space-charge limit at this energy. However, an increase will be obtained at higher beam energies and ξ_e will also be increased as a result of the increase of σ_e.

An increase in atomic beam diameter will lead to an increase in R through the resulting increase in interaction volume, though this is at the expense of angular resolution.

Further possibilities for the reduction of n_e and the increase of ξ_e will be discussed in connection with the analyzer in the next subsection.

Reduction in n_γ is difficult as it involves either a further reduction in dark current or a reduction in electron-gun cathode temperature and consequent loss in beam intensity. This at present is undesirable because the corresponding reduction of t would be inefficient due to the larger value of the term in G in expression (5.1).

If n_e could be reduced to negligible proportions (say by a factor 20) then, by equation (5.1), all else remaining constant, t would be 339 hours (14 days). The terms in F,

G and H would contribute 97, 171 and 71 hours respectively, the terms in R^{-1} (G and H) between them comprising 71% of the total counting time. It would now be profitable to increase R. Halving the source-target distance will increase R by a factor 4 and the contribution from the terms in R^{-1} will now be 60 hours, giving a total counting time of 157 hours ($6\frac{1}{2}$ days).

It is possible that if the instrumental time resolution could be reduced below the present value of 12 nsecs (e.g. by using faster photomultipliers), so that the lifetime curve is better resolved, a situation may be attained where it would be sensible to fix τ' at 16 nsecs and w at zero so that only a 3-parameter fit is required. In this case the fit may provide the required statistical accuracy after a shorter counting time than is suggested by the above analysis.

The Possibility of Reducing Electron Background. From what has been said in the previous subsection it is obvious that the first priority in improving the situation must be a reduction in n_e. The results of section 4.5 suggest that the actual resolution of the analyzer is very much inferior to the design value. The apparent difference in FWHM's of the "inelastic" (0.5eV) and "elastic" (1.26eV) peaks in Fig. 4.18 support the view put forward in that section that the anomalously large width is primarily due to unscattered electrons gaining entry to the analyzer at large oblique angles due to elastic reflections from the edges of the collimating aperture. Possible methods of reducing n_e, involving changes in the structure of the analyzer, will be described below.

An improvement in the present resolution is desirable from another point of view. Besides reducing unwanted background (e.g. from "elastic" scattering), energy analysis is also necessary to discriminate against electrons which have excited the 4^2S state, otherwise a spurious contribution to the coincidence rate will occur due to cascading. (See beginning of section 4.5). This is, perhaps, not so serious, even in the present case, because of the comparatively small excitation cross section of the 4^2S state.

If the reasons given above, for the poor energy resolution, are correct then an improvement would be achieved by replacing the single collimation aperture by a succession of such apertures, each heavily sooted. More efficient dumping of the unscattered beam is also required, especially at the small scattering angles used, where the existing Faraday cup is partially obscured by the body of the analyzer.

The effect on energy resolution of possible field penetration from the CEM chamber into the analyser, has been referred to in the previous subsection. A withdrawal from the region of the exit aperture, of the CEM and accelerator will reduce any such effect, but the amount of withdrawal will be limited by solid angle requirement (to maintain ξ_e) and the size of the CEM "mouth".

Other causes of poor energy resolution could be the non-optimum depth of the analyzer (see section 4.5) and, more importantly, the nature of the rear mesh whose transmission, for electrons impinging at large angles of incidence, tends to zero due to the presence of the transverse component of the weave. These electrons rather than being absorbed, are reflected back into the analyzer. This effect can be overcome

by using only longitudinal wires (parallel to the plane of the trajectory) to define the rear potential. Such an arrangement will be difficult to fabricate with spacings sufficiently small to prevent distortion of the analyzer field.

Monochromation of the incident electron beam is still considered to be unnecessary because at present the overall energy resolution is four times greater than the thermal spread, and the only effect of a reduction in incident-beam energy spread would be a loss of beam current and consequent reduction in genuine coincidence rate.

A final possibility for improvement of the situation, is concerned with the nominal angle of incidence on the analyzer of 45°. At this angle the only pair of conjugate planes (putting $d = 0$ in equation (4.11)) are those of the entrance and exit apertures, where a first-order image is produced. If a larger angle of incidence is used then a first order image of a point outside the entrance aperture can be formed at, or outside the exit aperture. For the particular case of 60° incidence, it can be whown that a second-order image is obtained (Green and Proca, 1970). It was thought, originally, that such large angles of incidence would enhance the effect of fringing fields at the entrance aperture. But subsequently such an analyzer has been constructed (J. Gibson, 1975) to investigate back-scattering after excitation of the 6^3P_1 state of Hg at 8.0 eV incident energy, and it has been shown to operate according to specification. The adoption of this geometry in the present case will lead to an increase in efficiency without incurring a degradation in resolution.

Although it has not been possible to obtain a measurement of P and therefore Π, It has been shown that measurements of the necessary coincidence rates are possible at low incident-electron energies (5.0eV) but a sufficiently accurate determination of P requires, at least, a substantial (a factor 20) reduction in the electron background rate (n_e) to bring the necessary counting time within reasonable limits. Reasons have been given for the anomalously poor energy resolution leading to the present value of n_e, and it has been possible, therefore, to put forward suggestions regarding modifications to the analyzer, necessary to achieve improvement.

The data in Table 5.1 suggest that there will be significant time dependence in the relative efficiency of the photon channels. Correction for this will entail the use of a rotating Wollaston prism (see section 3.3 and Appendix I) or the method described at the end of Chapter 2 involving a rotating polaroid. It should be noted that in the case of the latter, the implementation of all the above improvements is essential, as the use of this method doubles the necessary counting time.

APPENDIX I

THE EFFECT OF CHANNEL ASYMMETRY ON POLARIZATION CORRELATION

(a) Time-Independent Case

Let $\eta_1(t)$ and $\eta_2(t)$ be the efficiencies of the two photon channels (which may depend on time) and let the asymmetry (A) be defined as:-

$$A(t) = (\eta_1(t) - \eta_2(t))/(\eta_1(t) + \eta_2(t)).$$

The ratio of the efficiencies can be expressed in terms of A:-

$$\eta_2(t)/\eta_1(t) = (1 - A(t))/1 + A(t)) \quad . \qquad (A1.1)$$

Let Π be the theoretical value of the polarization which it is desired to measure. It is given in terms of the mean coincidence rates W_1 and W_2 (which are written for convenience instead of $W(\underline{k};\hat{\underline{P}},\hat{\underline{e}}_{\Theta})$ and $W(\underline{k};\hat{\underline{P}},\hat{\underline{e}}_{\Phi})$):-

$$\Pi \equiv (W_1 - W_2)/(W_1 + W_2) \equiv (1 - W_2/W_1)/(1 + W_2/W_1). \qquad (A1.2)$$

The measured polarization P is defined by:-

$$P \equiv (N_{g1} - N_{g2})/(N_{g1} + N_{g2})$$

where the mean measured coincidence rates N_{g1} are given by:-

$$N_{gi} = \frac{1}{T}\int_o^T \eta_i(t)k(t)W_i dt = (W_i/T)\int_o^T \eta_i(t)k(t)dt \qquad (A1.3)$$

$k(t)$ is a time-dependent factor describing the effect of the time variation of the electron and atomic beam intensities. The same factor appears in the equations for N_{g1} and N_{g2}

if the measurements of these quantities are carried out simultaneously.

If the η_i are independent of t, the N_{gi} are given by:-

$$N_{gi} = W_i \eta_i \cdot \frac{1}{T} \int_0^T k(t)dt \quad .$$

P is now given by

$$P = (W_1\eta_1 - W_2\eta_2)/(W_1\eta_1 + W_2\eta_2) \qquad (A1.4)$$

the common factor $\frac{1}{T} \int_0^T k(t)dt$ cancelling.

Using (A1.1) and (A1.4) the ratio W_2/W_1 can be written in terms of P and A:-

$$W_2/W_1 = (1-P)(1+A)/(1+P)(1-A) \quad .$$

Substitution of this into (A1.2) gives:-

$$\Pi = (P - A)/(1 - PA) \quad .$$

If P and A are small compared to unity, then to first order in PA one can write

$$\Pi = (P - A)(1 + PA)$$

So that the effect of the channel asymmetry (if time independent) to lowest order can be regarded as a shift in Π by an amount A with a fractional error PA. In the experiment envisaged P and A are both only of the order 0·2.

(b) Time-Dependent Case

In the above case, A could be determined once and for all during some initial experiment, and would be constant thereafter. In general A is time-dependent and the measured intensities are given by (A1.3) and the expression equivalent to (A1.4) becomes:-

$$P = (W_1 q_1 - W_2 q_2)/(W_1 q_1 + W_2 q_2)$$

where $q_i = \frac{1}{T}\int_o^T \eta_i(t)k(t)dt$.

It is now necessary to separate the contributions to $\eta_i(t)$ into time-dependent and time-independent parts. It will be assumed that the transmissions u_1 and u_2 of the polarization analyser for the two orthogonal polarization plates, are time independent; and that the transmissions and efficiencies of the rest of the optical channels $v_1(t)$ and $v_2(t)$ depend on time. Then one can define q_{ij} and $\bar{v}_j$ as follows:-

$$q_{ij} \equiv (\frac{u_i}{T}) \int_o^T v_j(t)k(t)dt \equiv u_i \bar{v}_j .$$

If, as is in our case, the polarization analyzer is a Wollaston prism then, by rotating it through 180^o it is possible to measure two different polarizations:-

$$P_1 = (W_1 q_{11} - W_2 q_{22})/(W_1 q_{11} + W_2 q_{22})$$

and $$P_2 = -(W_2 q_{21} - W_1 q_{12})/(W_2 q_{21} + W_1 q_{12}) .$$

Note that these measurements must be interlaced to ensure that $\bar{v}_j$ is the same in both the above expressions.

One actually measures the four different quantities $(W_i\ u_i\ \bar{v}_j)$, $i,j = 1,2$. Let these be called a_{ij}. The following relations hold:-

$$W_1/W_2 = a_{11}\ u_2\ \bar{v}_2/a_{22}\ u_1\ \bar{v}_1, \quad W_1/W_2 = a_{12}\ u_2\ \bar{v}_1/a_{21}\ u_1\ \bar{v}_2 .$$

From these relations it follows that:-

$$\left(\frac{\bar{v}_2}{\bar{v}_1}\right)^2 \equiv \frac{a_{12}\ a_{22}}{a_{21}\ a_{11}} \equiv \beta^2 . \qquad \text{(A1.5)}$$

This defines the parameter β.

If one measures once and for all the quantity u_2/u_1 then one can define the time independent quantity α as

$$\alpha = u_2/u_1 .$$

The theoretical polarization Π given by (A1.2) can be written in terms of the four measured quantities a_{ij} taking into account the fact that W_1 and W_2 are each, in effect, measured twice:-

$$\Pi = \frac{a_{11}\alpha\beta + a_{12}\alpha - a_{22} - a_{21}\beta}{a_{11}\alpha\beta + a_{12}\alpha + a_{22} + a_{21}\beta} .$$

Finally, using the relationship (A1.5) between β and the a_{ij}:-

$$\Pi = \frac{\alpha\sqrt{a_{11}^2 a_{12} a_{22}} + \alpha\sqrt{a_{11} a_{12}^2 a_{21}} - \sqrt{a_{11} a_{21} a_{22}^2} - \sqrt{a_{12} a_{21}^2 a_{22}}}{\alpha\sqrt{a_{11}^2 a_{12} a_{22}} + \alpha\sqrt{a_{11} a_{12}^2 a_{21}} + \sqrt{a_{11} a_{21} a_{22}^2} + \sqrt{a_{12} a_{21}^2 a_{22}}}$$

(A1.6)

This is the exact expression.

Alternatively one can define in terms of the measured a_{ij}, the quantity P' as follows:-

$$P' = \frac{a_{11} + a_{12} - (a_{21} + a_{22})}{a_{11} + a_{12} + a_{21} + a_{22}} .$$

Using the above definition of the a_{ij} and cancelling the resulting common factor $(\bar{v}_1 + \bar{v}_2)$ one obtains:-

$$P' = \frac{W_1 u_1 - W_2 u_2}{W_1 u_1 + W_2 u_2} .$$

Defining A' as:-

$$A' \equiv \frac{u_1 - u_2}{u_1 + u_2} \equiv \frac{1 - \alpha}{1 + \alpha}$$

and using the results of section (a) the following expression for Π is obtained:-

$$\Pi = \frac{P' - A'}{1 + P'A'}$$

which can be written in approximate form in the usual way.

APPENDIX II

STANDARD DEVIATION OF POLARIZATION CORRELATION

(a) Case of Time-Independent Channel Asymmetry

It was shown in Appendix I that for this situation the polarization Π is given by the approximate but sufficiently accurate formula:-

$$\Pi = P - A,$$

where A is the channel asymmetry which is assumed to be known with negligible error, and P is a function of the measured quantities N_{g1} and N_{g2} defined in section 3.3 and Appendix I. Thus the standard deviation $(\sigma(\Pi))$ of Π is given approximately by:-

$$\sigma^2(\Pi) = \sigma^2(P) = \left[\frac{\partial P}{\partial(N_{g1}t)}\right]^2 \sigma^2(N_{g1}t) + \left[\frac{\partial P}{\partial(N_{g2}t)}\right]^2 \sigma^2(N_{g2}t)$$

where $P = (N_{g1}t - N_{g2}t)/(N_{g1}t + N_{g2}t)$ and t is the counting time for each quantity. The partial derivatives appearing above are thus given by:-

$$\frac{\partial P}{\partial(N_{g1}t)} = \frac{2N_{g2}t}{(N_{g1}t + N_{g2}t)^2} \qquad \frac{\partial P}{\partial(N_{g2}t)} = \frac{-2N_{g1}t}{(N_{g1}t + N_{g2}t)^2}$$

If Π and A are small (compared to unity) then P is also

small and the approximation $N_{g1}t = N_{g2}t$ can be made. To this approximation the partial derivatives are:-

$$\frac{\partial P}{\partial (N_{g1}t)} = \frac{1}{2N_g t} \qquad \frac{\partial P}{\partial (N_{g2}t)} = \frac{-1}{2N_g t}$$

where $N_g t \equiv N_{g1}t \equiv N_{g2}t$.

The following result is obtained therefore for $\sigma(\Pi)$:-

$$\sigma(\Pi) = \sigma(N_g t)/\sqrt{2}\, N_g t \ .$$

(b) Case of the Time-Dependent Channel Asymmetry

In this case $\sigma^2(\Pi)$ is given by:-

$$\sigma^2(\Pi) = \sum_{i,j=1}^{2} \left[\frac{\partial \Pi}{\partial \alpha_{ij}}\right]^2 \sigma^2(a_{ij})$$

where the a_{ij} are defined in Appendix I, and Π is given by equation (A1.6). Again, using the approximation that the a_{ij} are all equal to a, the following relations are obtained:-

$$\frac{\partial \Pi}{\partial a_{11}} = \frac{\partial \Pi}{\partial a_{12}} = \frac{\alpha}{2a(\alpha+1)} \ , \quad \frac{\partial \Pi}{\partial a_{21}} = \frac{\partial \Pi}{\partial a_{22}} = \frac{-1}{2a(\alpha+1)} \ .$$

This now gives for $\sigma(\Pi)$ the following:-

$$\sigma(\Pi) = \frac{1}{\sqrt{2}} \sqrt{\frac{\alpha^2+1}{(\alpha+1)^2}}\ \frac{\sigma(a)}{a} \ . \qquad \text{(A2.1)}$$

Putting $\alpha = 1$ and $a = N_g t/2$ to take account of the fact that for experiments of the same total counting time, four quantities (a_{ij}) are measured in the latter case, compared to only two ($N_{g1}t$ and $N_{g2}t$) in the former, gives the same result as was obtained in section (a), which is as expected.

If only one detector is used then the time-dependent part of the channel efficiency does not enter and the polarization is given in terms of the two measured quantities a_{11} and a_{21} as follows:-

$$\Pi = (a_{11}\alpha - a_{21})/(a_{11}\alpha + a_{21}) .$$

The following partial derivatives can be obtained using the usual approximation:-

$$\frac{\partial \Pi}{\partial a_{11}} = \alpha/a(\alpha+1)$$

$$\frac{\partial \Pi}{\partial a_{21}} = -1/a(\alpha+1) .$$

Using the previous rechniques $\sigma(\Pi)$ is now given by:-

$$\sigma(\Pi) = \sqrt{\frac{\alpha^2+1}{(\alpha+1)^2}} \frac{\sigma(a)}{a} . \qquad (A2.2)$$

For experiments of the same overall counting time (A2.2) compares directly with (A2.1) as a in each case results from the same period of counting. As expected, $\sigma(\Pi)$ for the case of the single detector is a factor $\sqrt{2}$ larger than that for the two-detector case.

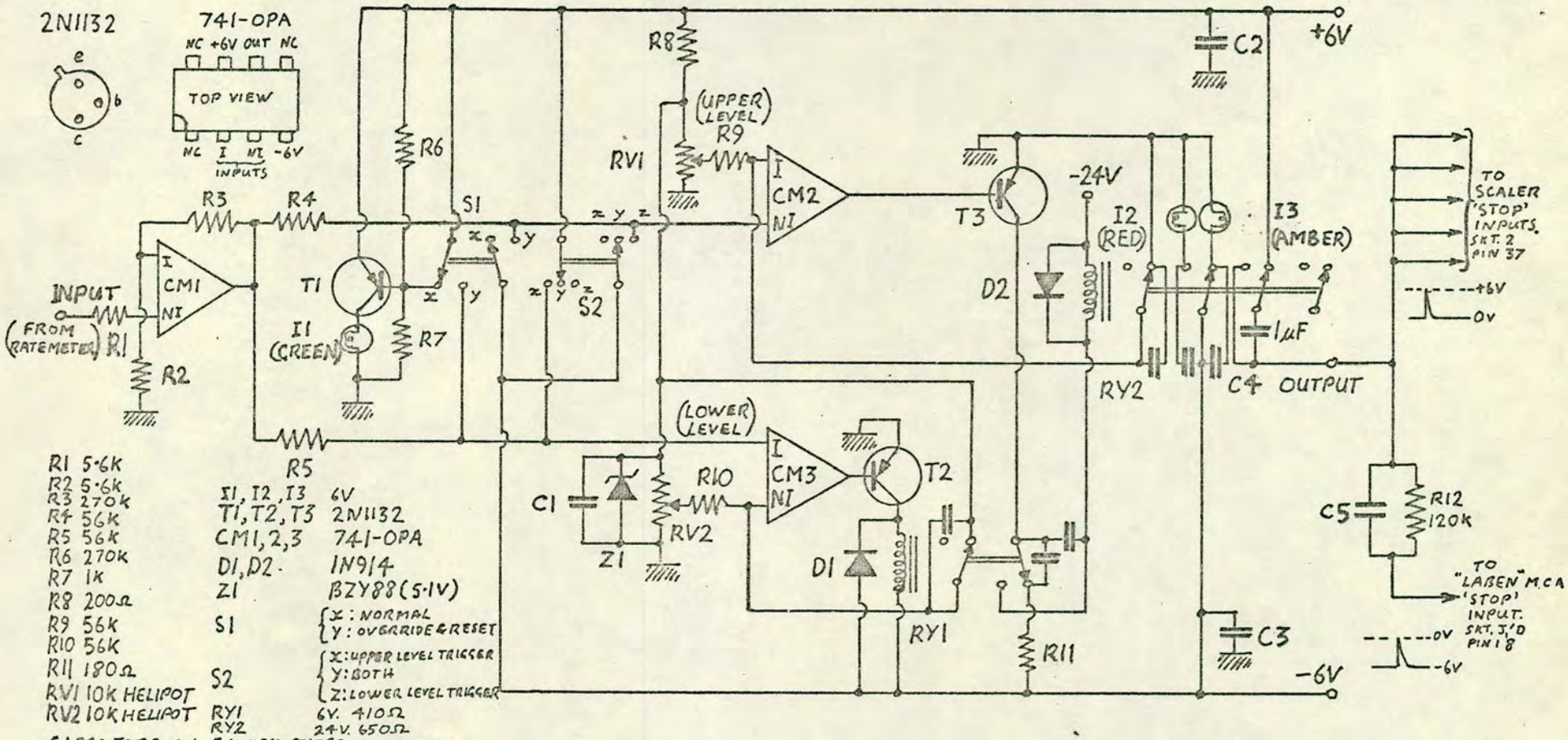

R1 5·6K		
R2 5·6K		
R3 270K	I1, I2, I3	6V
R4 56K	T1, T2, T3	2N1132
R5 56K	CM1, 2, 3	741-OPA
R6 270K	D1, D2	IN914
R7 1K	Z1	BZY88(5·1V)
R8 200Ω	S1	{x: NORMAL; y: OVERRIDE & RESET
R9 56K		
R10 56K		
R11 180Ω	S2	{x: UPPER LEVEL TRIGGER; y: BOTH; z: LOWER LEVEL TRIGGER
RV1 10K HELIPOT	RY1	6V. 410Ω
RV2 10K HELIPOT	RY2	24V. 650Ω

CAPACITORS 0·1μF UNLESS STATED OTHERWISE.
BOTH TRIGGERS SHOWN IN 'STOP' STATE

FIG. AIII·1
COUNT-RATE SENSING PROTECTION CIRCUIT

APPENDIX III

ELECTRONIC CIRCUITS

(a) Count-Rate Sensing Protection Circuit (see Fig. AIII.1)

A voltage level in the range 0 - +100 mV (depending on count rate) is applied to the non-inverting input of the operational amplifier CM1 which has a gain of 50 determined by the ratio of the feedback resistance (R3) to the input resistance (R2). The amplified output is applied to the non-inverting and inverting inputs, respectively, of the operational amplifiers CM2 and CM3, used as voltage comparators. The upper triggering level is determined by RV1 which divides the voltage across the zener reference diode Z1. When the output of CM1 exceeds that on the inverting input of CM2, its output, due to the extremely high gain, immediately switches from -6V to +6V thus switching T3 from the fully conducting to the "off" state. The coil of relay RY2 is in the collector circuit of T3 and is therefore switched off. This state is indicated by the lamp I3. Also, capacitor C4 becomes charged from the +6V supply. The resulting positive-going transient is passed via the output socket to the "stop" line and hence to the scalers and MCA. C5 is necessary to provide D.C. isolation between the different quiescent D.C. levels of the scalers (OV) and the MCA (-6V), while also passing the pulse. R12 "resets" (discharges) C5 to its quiescent state and is sufficiently large to provide some D.C. isolation.

The low-level trigger (CM3 and T2) operates in a similar fashion, the triggering level being determined by RV2. Relay RY1 is controlled by T2 and operates a switch in series with the coil of RY2. Thus, triggering of either CM2 or CM3 will

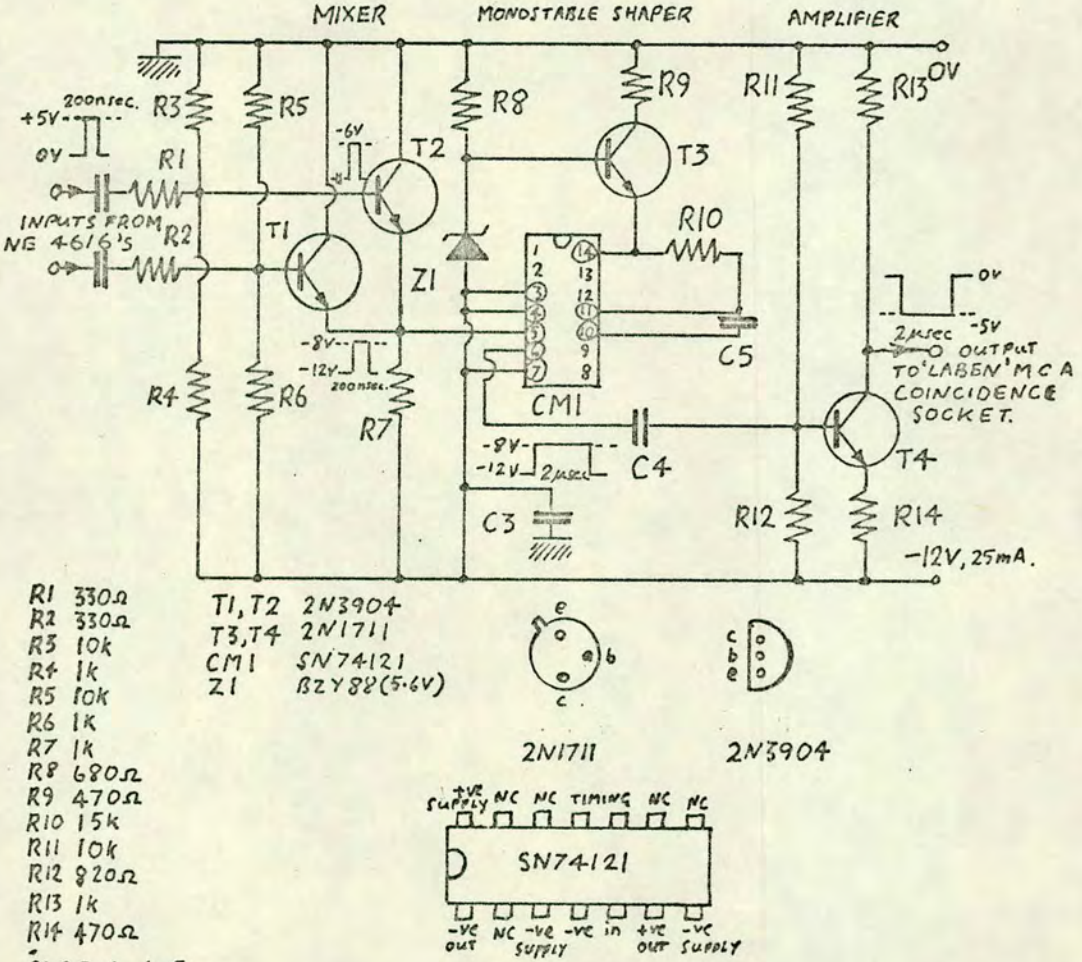

FIG. AIII·2
MIXER AND PULSE SHAPER

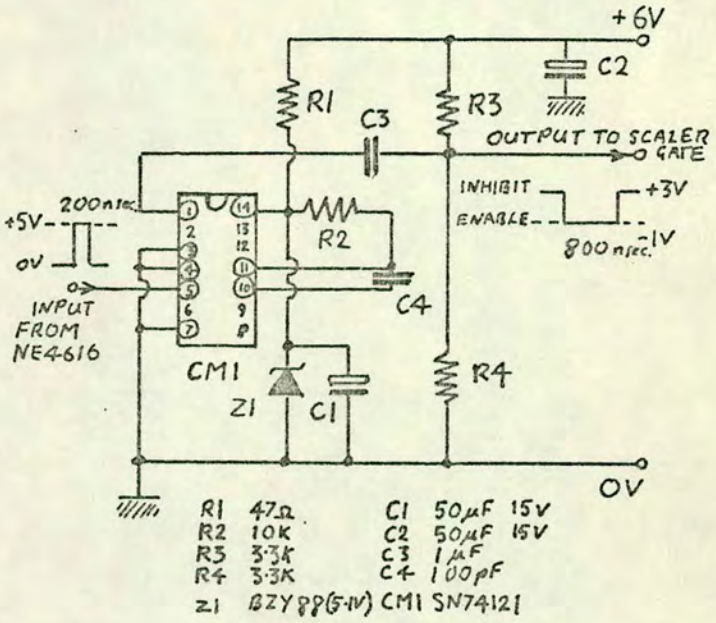

FIG. AIII·3
PULSE SHAPER AND INVERTER

initiate a "stop" signal.

Resetting, or overriding of the process can be accomplished by holding the non-inverting input of CM2 at a large negative level, and simultaneously holding that of the inverting input of CM3 at a high positive level. This is the function of switch S1. Indication of the "override" state is given by allowing T1 to conduct, hence operating lamps I1. T2, T3, RY1 and RY2 are "on" and C4 is discharged. This state is indicated by I2.

Operation with upper or lower level triggering only, can be provided by either "shorting" I of CM3 to +6V or "shorting" NI of CM2 to -6V. These possibilities are determined by S2.

Diodes D1 and D2 protect T2 and T3 from the large transients produced when the currents in the coils of RY1 and RY2 are reduced.

Capacitors other than C1-C5 reduce pickup due to arcing at relay contacts. C1, C2 and C3 are decoupling capacitors.

(b) Mixer and Pulse Shaper (see Fig. AIII.2)

A positive pulse on the base of T1 or T2 switches the respective transistor on. If pulses are simultaneously present on the bases, then the largest pulse causes the emitters to rise to a correspondingly large value. Hence the transistor with the smallest input is cut off. Only the largest pulse is therefore passed and the mixer is non-summing.

The output of the mixer is applied to the input of CM1 which is a monostable multivibrator whose time constant is determined by R10 and C5. The output pulse width is 2 μsecs. and is A.C.-coupled via C4 to the base of T4 which provides

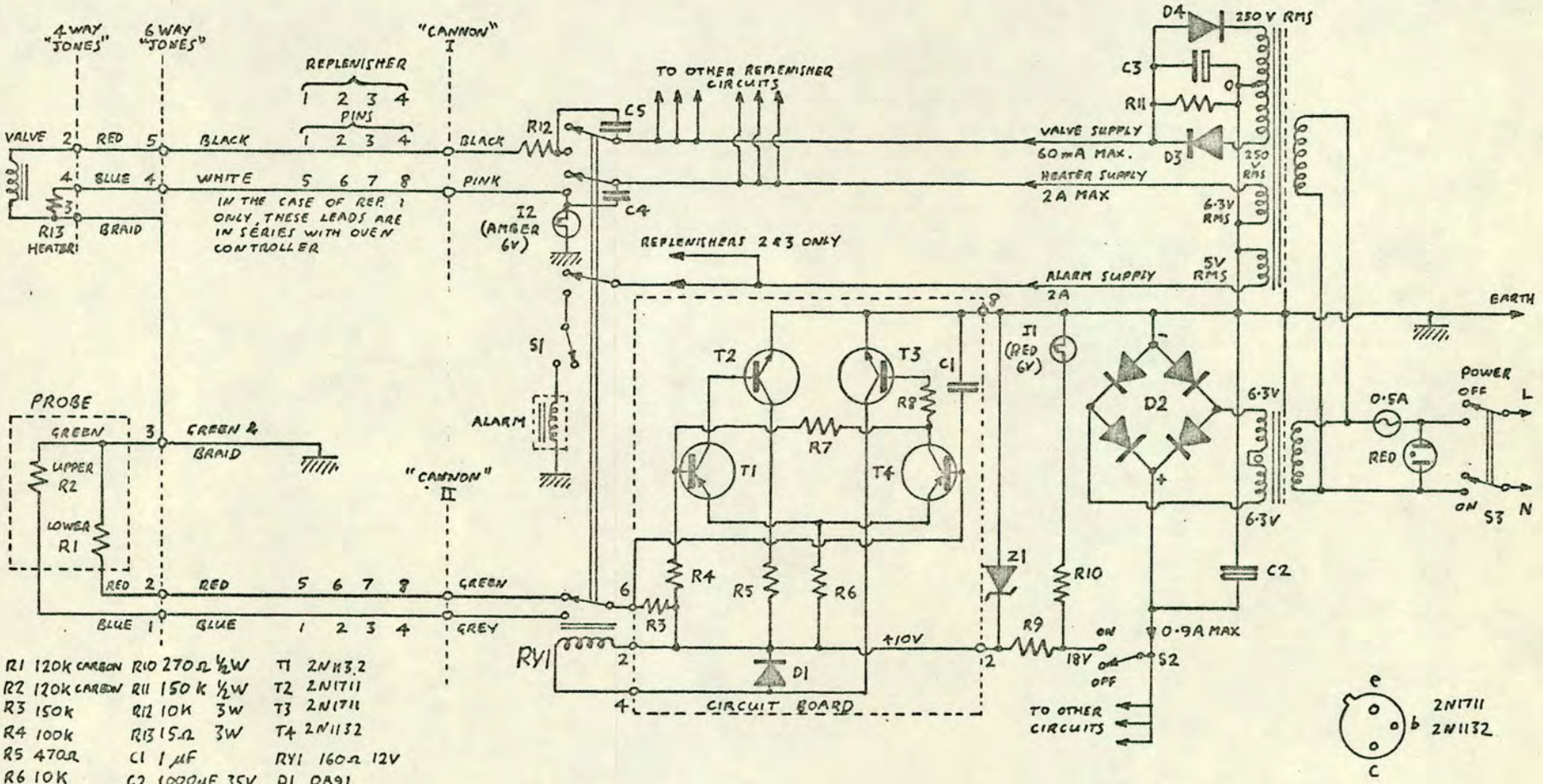

R1	120K CARBON	R10	270Ω ½W	T1	2N1132
R2	120K CARBON	R11	150 K ½W	T2	2N1711
R3	150K	R12	10K 3W	T3	2N1711
R4	100K	R13	15Ω 3W	T4	2N1132
R5	470Ω	C1	1 μF	RY1	160Ω 12V
R6	10K	C2	1000μF 35V	D1	OA91
R7	100K	C3	200μF 350V	D2	REC 43
R8	5·6K	C4	0·2μF 400V	D3,4	BY127
R9	100Ω ½W	C5	0·2μF 400V	Z1	BZY88(10V)

FIG. AIII·4
CIRCUIT FOR AUTOMATIC REPLENISHMENT OF LIQUID NITROGEN TRAPS

sufficient amplification to drive the "coincidence" input of the MCA.

Z1 and T3 provide the stabilized 5V supply to CM1. C3 is a decoupling capacitor for the -12 volt supply.

(c) Pulse Shaper and Inverter (see Fig. AIII.3)

Again an output pulse width of 800 nsecs is produced by the time-constant components, R2 and C4, of the monostable multivibrator CM1. The supply voltage is determined by zener diode Z1 and is decoupled by C1. The output D.C. level of +3V is set by R3 and R4 and is isolated from the output of CM1 by C3. C2 provides extra decoupling of the supply, which in this case had superimposed upon it, a large amount of hum.

(d) Automatic Replenisher for Liquid Nitrogen-Cooled Traps (see Fig. AIII.4)

A 25 litre dewar supplies each trap (four in all). Normally the vapour above the surface of the liquid in the dewar, is allowed to escape to the atmosphere through a solenoid-operated valve. To fill a trap, the valve on the corresponding dewar is closed causing the vapour pressure to increase until it is sufficient to force the liquid through a tube beginning near the base of the dewar and ending in the trap. A current is also passed through a resistor (R13) immersed in the liquid, providing an extra source of heat to increase the boil-off rate and hence shorten the time required for the vapour to attain sufficient pressure.

The "empty" and "full" levels of the trap are determined by the positions of resistors R_1 and R_2 respectively. At

liquid nitrogen temperatures their value is double that at 25°C. When the trap is full, control is transferred by R2 to R1. Because of the sizes, under this condition, of R1 and R2 compared to R3, the potential on the base of T4 is high (relative to earth). This tends to cut T4 off and its collector potential falls. The base potential of T1, determined by R4 and R7, therefore falls and T1 draws more current from the common emitter resistor R6, which is diverted from T4. T4 becomes completely cut off. The base potential of T3 is therefore close to zero. This transistor is also cut off, RY1 is held open and the lower probe R2, is selected. The valve and heater circuits are open to prevent any further filling. The effects of short term fluctuations in the values of R1 and R2 when they are changing is removed by C1.

As the trap empties the value of R1 falls below that of R3, the potential on the base of T4 falls, causing T4 to turn on. The potential on the base of T1 thus increases, tending to turn off T1. It emitter current is thus transferred to T4 which becomes fully conducting. T3 therefore becomes fully on, and RY1 closes transferring control to R2 which is thereby made ready to detect the "full" state of the trap. Power is also passed to the valve from the full-wave rectified supply consisting of D3, D4 and smoothing capacitor C3, the correct voltage (200V) being obtained by the drop across R12. R11 provides a discharge path for C3 when the mains supply is removed. Power is also supplied to the heater R13. The trap is thus filled until the value of R2 increases sufficiently to cause RY1 to open as described

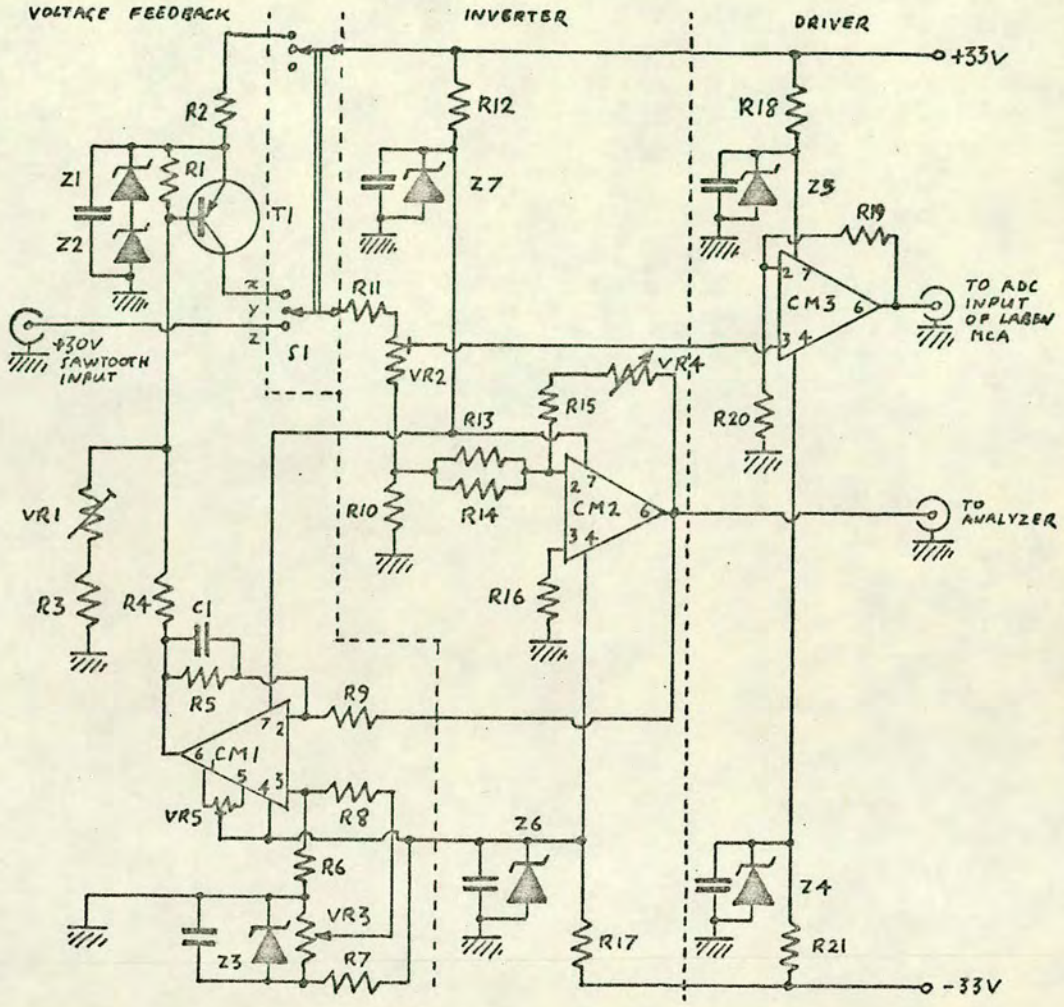

R1 680Ω	R12 2·7k	VR1 10k PRESET
R2 470Ω	R13 1k	VR2 10k PRESET
R3 39k	R14 560Ω	VR3 10k HELIPOT (ANALYSER POT.)
R4 68k	R15 1k	VR4 10k HELIPOT (SWEEP WIDTH)
R5 10M	R16 560Ω	VR5 10k PRESET (OFFSET ZERO)
R6 10M	R17 1·5k	C1 ·01μF
R7 330Ω	R18 3·3k	T1 2N1132
R8 27k	R19 100k	CM1,2,3 741-OPA
R9 27k	R20 100k	Z1,22 BZY88 (15V)
R10 1k	R21 3·3k	Z3,4,5 " (10V)
R11 22k		Z6,7 " (12V)

S1 { Z MANUAL; Y OFF; Z AUTO. SWEEP }

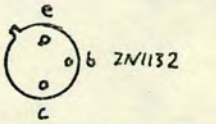

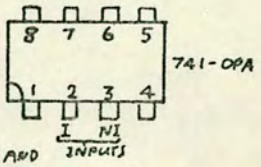

UNLESS OTHERWISE STATED ALL CAPACITORS ARE 0·1μF AND SERVE TO DECOUPLE THE VARIOUS VOLTAGE SUPPLIES.

FIG. AIII·5
ANALYZER VOLTAGE SUPPLY

above, and again select the lower probe, R1. Diode D1 protects T3 from the back EMF produced when the relay circuit is opened.

In the case of replenishers 2 and 3 whose traps, being larger, are sometimes used without the automatic filling device, an alarm can be switched into the control circuit by means of S1, and is therefore caused to sound when the traps require filling.

Power to the control circuits is provided by the full-wave rectifier D2 and smoothing capacitor C2, via S2. Its presence is indicated by I1; and R9 and Z1 determine the correct supply voltage (10V).

25 litres of liquid nitrogen is used up by traps 1,2,3 and 4, in 20 hours, 20 hours, 2 days, and 5 days respectively.

(e) Analyzer Voltage Supply (see Fig. AIII.5)

The supply can be used in either the "automatic sweep" mode; where a sawtooth voltage waveform is simultaneously applied to the analyzer and the ADC input of a Laben MCA, enabling the energy distribution of scattered electrons to be displayed by feeding pulses from the electron channel into the "sampling" input of the MCA; or in the "manual" mode where a regulated analyzer voltage in the range 0-7V can be chosen.

"Auto Sweep" Mode A positive-going, 30V amplitude sawtooth waveform from a 'scope timebase, which is correctly loaded by the series combination R11, VR2 and R10, is inverted by operational amplifier CM2 and is fed to the analyzer. The

gain of CM2 is determined by R13, R14, R15 and VR4. The setting of VR4 thus determines the energy range of the sweep.

The amplitude of the sawtooth is reduced to that corresponding to "full scale" of the MCA, by VR2. The operational amplifier CM3 provices a high impedance load for the potential divider chain and a low impedance drive to the ADC. The gain of CM3 is set at unity by R19 and R20.

Voltages of ±12 for CM2 are derived from supply voltages of ±33 by Z7, R12, Z6 and R17. Voltages of ±10 for CM3 are derived by Z5, R18, Z4 and R21.

"Manual" Mode The analyzer voltage is now derived from the +33V supply via S1, R2, Z1, Z2 and T1. CM2 again provides the necessary inversion. T1 is controlled by the output of differential amplifier CM1 via R4. A sample of the analyzer voltage is fed back to the inverting input of CM1 where it is compared with a stabilized voltage derived from R7 and Z3 and set by VR3. To prevent oscillation the gain of CM1 is limited to 370 by the ratio R5:R9 and is further reduced at high frequencies by the addition of C1. Offset is zeroed by VR5. Any difference between the analyzer voltage and that set by VR3 gives rise to a proportional, compensating output voltage which is fed to the base of T1. The working point of T1 is determined by R1, VR1 and R3. CM1 derives its supply from that of CM2.

Because, in either mode, the analyzer voltage is derived from the same divider chain, which also supplies the ADC, the analyzer can be manually "tuned in" to any desired feature on on the energy spectrum by observing the effect on the Laben display.

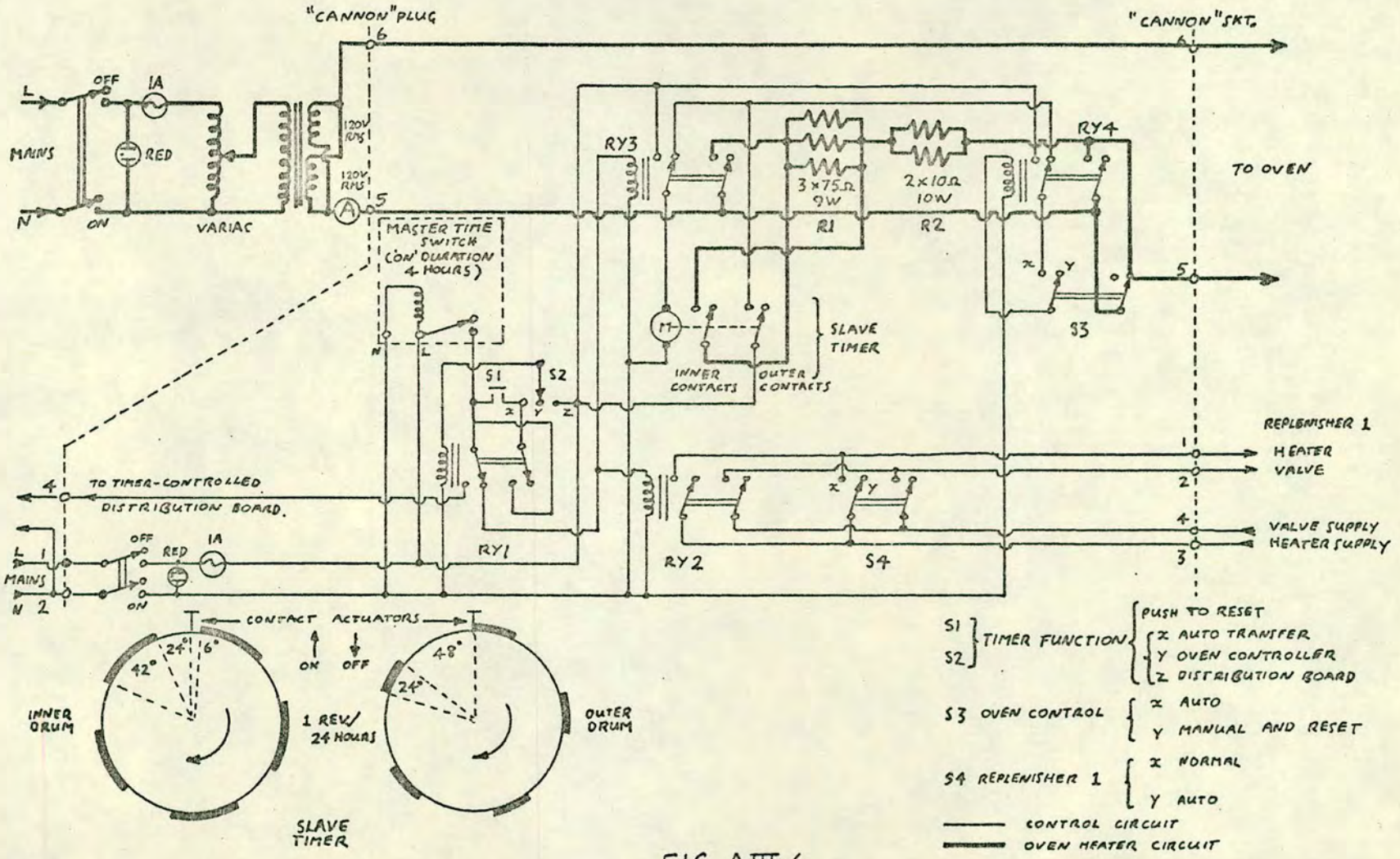

FIG. AIII·6
OVEN CONTROLLER

(f) Oven Controller (see Fig. AIII.6)

The primary function of this device (S2, posn."y", S3, posn. "x") is to commence the heating of the oven at a time determined by the setting of the "master" time switch (MTS) and increase the current after each of two further, preset intervals.

Initially, RY3 closes, the "slave" timer (ST) is thereby started and the heater supply voltage is applied to the heater via the full series resistance $R_1 + R_2$. Replenisher 1 may also be caused to commence filling at this instant, by the closing of RY2, providing the replenisher circuit has previously been switched on and S4 opened (posn. "y") to prevent premature filling.

After an interval (preset by adjustment of the ST, but in the present case 96 mins.) the inner contacts of the ST close, shorting out R1. After a further preset interval (in this case, again 96 mins.) the outer contacts also close causing RY4 to close. This shorts all the resistance in series with the heater, and permanently latches RY4 in the closed state.

The "on" duration of the MTS is set at 4 hours so that after a further 48 mins. RY3 opens and is thus reset. The ST continues to operate, control of its motor having been taken over by its own outer contacts in their closing.

After a further 48 mins. both sets of ST contacts simultaneously open. The opening of the outer contacts stops the ST motor and it is therefore reset in readiness for the next cycle of operation. RY4 can be reset by means of S3 (posn."y"). The oven takes a total of 5 hours to reach its equilibrium temperature.

It should be noted that if replenisher 1 is in the automatic mode (S4, posn "y"), then when the duration of the "on" period

of the MTS ends, RY2 will be opened , the replenisher-probe circuit will be over-ridden and the trap will be permanently prevented from filling unless S4 is closed (posn. "x").

The controller can be used in two other modes chosen by S2: It is on occasion desirable to control some external device from the MTS. This can be accomplished by putting S2 to posn. "z" when the timer contacts are now connected exclusively to an external distribution board which can be used to supply the device concerned.

The third mode (S2, posn. "x") provides transfer of control by the MTS from the distribution board to the oven circuit (RY2 and RY3) at some instant preset by the position of a second "off" cam on the MTS, preceding the other cams. Initially the MTS contacts are manually closed and control is transferred to the distribution board by depressing S1 which closes RY1. This relay latches itself in the closed state via the MTS contacts. When the MTS contacts open, RY1 opens, switching off the distribution board and transferring control by the MTS to the oven circuit in readiness for the next closing of the MTS contacts.

APPENDIX IV

TYPICAL CONTROL SETTINGS

(a) COINCIDENCE ELECTRONICS (See fig. 3·13)

2·1 μSEC. DELAY	ATTENUATOR	FAST DISCRIM.	RATEMETER	700 nSEC. DELAY	TIME PICKOFF CONTROL
Input: terminated	1/4	Output width: 2·20 (22 nsecs.)	FSD: 500 Hz.	Input: unterm.	Bias: 0·0 (min)

BUFFER	PROTECTION	SUBGROUP SELECTOR	HIGH VOLTAGE I.	HIGH VOLTAGE II	HIGH VOLTAGE CEM
Bias: 1·2V	Upper threshold: 10·0	Input: external	See chapt.	5·0 (2 KV)	9·0 (3·6 KV) — 10·0 (4·0 kV)
Trigger: internal	Lower threshold: 7·60				
Mode: leading-edge.	Mode: normal				

SHAPING AMP. I	SLOW DISCRIM. I	SHAPING AMP II	SLOW DISCRIM. II	TAC's I & II	LABEN MCA
Coarse gain: 4	Bias: 0·8V	Coarse gain: 2	Bias: 1·1 V	Range: 500 nsecs.	Display: live
Fine gain: 5·50	Delay: 10·0 (400 nsecs)	Fine gain: 6·10	Delay: 10·0 (400 nsecs.)	Gate: internal	Subgroup's: 2x200
Time const.: 0·4 μsecs., double diff.	Trigger: internal	Time const.: 0·4 μsecs., double diff.	Trigger: internal	Output width: 2 μsecs.	Input: 'low', 'direct', +ve
Inputs: terminated	Mode: crossover-pickoff	Inputs: terminated	Mode: crossover-pickoff	Output polority: +ve.	Sensitirity: 40mV/channel
					Mode: coincidence
					Dead time: fixed (47 μsec.)
					Back bias: 0·0
					Upper threshold: 10·0

(b) HELMHOLTZ COILS

PARAMETER \ COIL	1 ("EAST-WEST")	2 ("VERTICAL")	3 ("NORTH-SOUTH")
SETTING	0·15	5·14	1·81
VOLTAGE /mV	25	2860	750
CURRENT /mA	3	710	95

(c) ELECTRON GUN (BEAM ENERGY 5·0eV. POTENTIALS WRT CATHODE UNLESS OTHERWISE STATED)

CATHODE (WRT EARTH)	V_1	V_2	V_4	HORIZONTAL (X) DEFLECTION (WRT EARTH)	VERTICAL (Y) DEFLECTION (WRT EARTH)
8·84	1·65	3·35	8·76	1·04 "RIGHT"	0·64 "DOWN"
-6·70V	+38V	+230V	+22·5V	± 0·20V	± 0·05V

APPENDIX V

RELATIONSHIP BETWEEN EFFECTIVE MAGNETIC MOMENT ATOMIC-BEAM POLARIZATION, AND ASYMMETRY

(a) Effective Magnetic Moment and Polarization

Let an atom be in a magnetic field $\underline{B}$ and let the total Hamiltonian be H. Let the coordinate system be chosen such that the z axis is in the direction of $\underline{B}$. Then the force on the atom is given by the equation of motion

$$\frac{d\langle p\rangle}{dt} = \frac{1}{i\hbar}\langle[-i\hbar\underline{\nabla}, H]\rangle \equiv -\langle[\underline{\nabla},H]\rangle \qquad (A5.1)$$

where $\underline{\nabla}$ is the momentum operator of the centre of mass of the atom. If H is written as $(\nabla^2/2M + H_o)$ where H_o depends on the CM coordinates through B, the commutator in (A5.1) becomes $[\underline{\nabla}, H_o]$ and the right hand term can be further written:-

$$-\langle[\underline{\nabla},H_o]\rangle = -\langle\underline{\nabla} H_o\rangle + \langle H_o \underline{\nabla}\rangle = -\langle\underline{\nabla}W\rangle + \langle W\underline{\nabla}\rangle$$

$$= -\langle(\underline{\nabla}W)\rangle - \langle W\underline{\nabla}\rangle + \langle W\underline{\nabla}\rangle = -\langle(\underline{\nabla}W)\rangle = -\underline{\nabla}W$$

where the expectation value is taken with respect to an energy eigenstate of H_o and W is the energy eigenvalue of H_o.

For an atom with $S = \frac{1}{2}$, $L = 0$, and $J = \frac{1}{2}$, and with a nuclear spin I, W is given by the formula due to Breit & Rabi (1931):-

$$W = W_T - \frac{A}{4} - \frac{mg_I \mu_N B}{\mu_o} \pm \frac{A}{4}(2I+1)\sqrt{1 + \frac{4m}{2I+1}x + x^2}$$

where:- μ_N is the nuclear magneton $(\frac{e\mu_o\hbar}{2m_p}$, m_p being the proton mass)

$$m = m_I + m_J$$

$$x = \frac{2(g_J\mu_\beta - g_I\mu_N)B}{A(2I+1)\mu_o} .$$

W_T is the term energy.

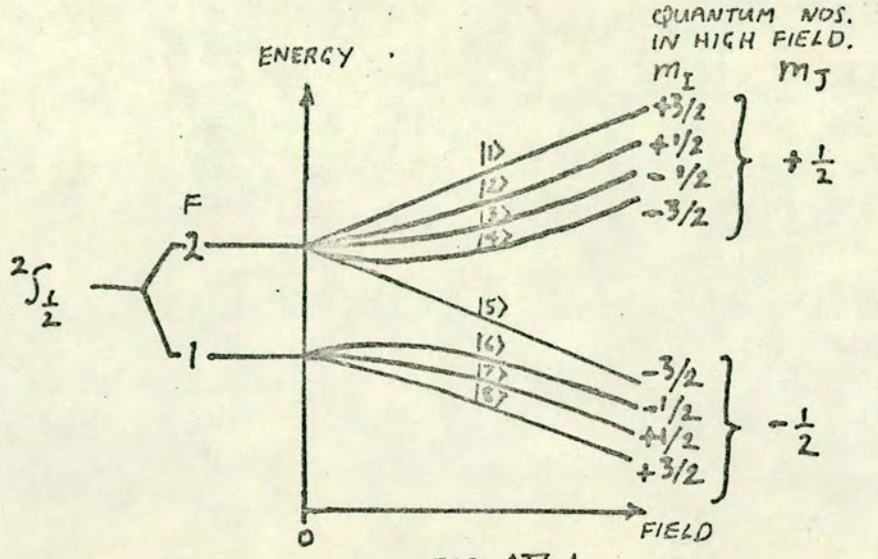

FIG. AV·1

ENERGY AS A FUNCTION OF MAGNETIC FIELD FOR THE GROUND LEVELS OF AN ALKALI WITH I = 3/2

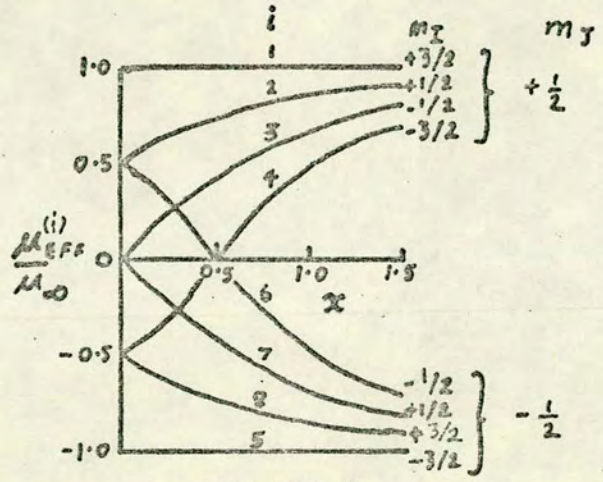

FIG. AV·2

$\mu_{EFF}^{(i)}/\mu_\infty$ AS A FUNCTION OF x FOR AN ALKALI WITH I=3/2 ($x \equiv \frac{2(g_J\mu_B - g_I\mu_N)B}{A(2I+1)\mu_\infty}$)

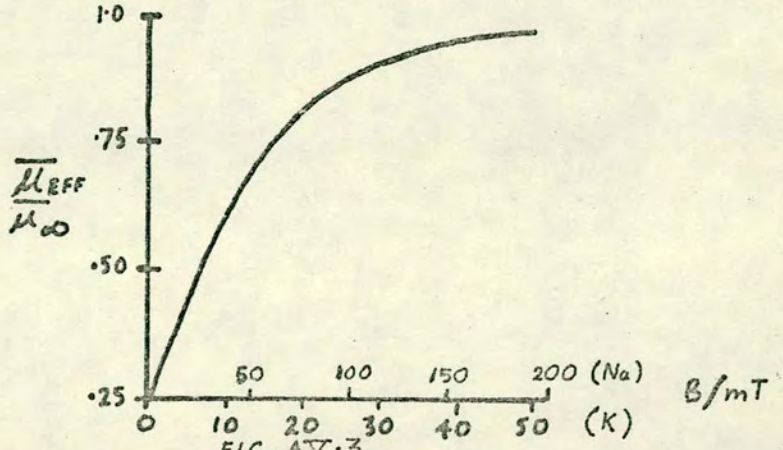

FIG. AV·3

μ_{EFF}/μ_∞ AS A FUNCTION OF MAGNETIC FIELD FOR Na AND K

μ_β is the Bohr magneton $(\frac{e \mu_o \hbar}{2m_e})$.

A is the nuclear magnetic dipole coupling constant.

W is plotted as a function of B in Fig. AV.1 (Kopfermann, 1958).

If B is spatially inhomogeneous, then all the spatial variation of W is contained in B so the equation of motion can now be written:-

$$\frac{d\langle p \rangle}{dt} = - \frac{\partial W}{\partial B} \underline{\nabla} B \quad . \qquad (A5.2)$$

The coefficient of ∇B is defined as the effective magnetic moment:-

$$\mu_{eff} \equiv - \frac{\partial W}{\partial B} \quad .$$

Use can be made of the fact that H depends on the coordinates of the centre of mass only through B. These spatially varying components of H consist of the following two terms only:-

$$\frac{g_I \mu_N \sigma_z^{(I)}}{2\mu_o} B + \frac{g_J \mu_\beta \sigma_z^{(J)}}{2\mu_o} B$$

where $\sigma_z^{(J)}$ and $\sigma_z^{(I)}$ are the z components of the Pauli spin operators associated with the electronic and nuclear spins respectively.

Thus the right-hand term of equation (A5.1) can also be written:-

$$- \langle [\underline{\nabla}, H] \rangle = - \frac{g_I \mu_N}{2\mu_o} \langle \sigma_z^{(I)} (\underline{\nabla} B) \rangle - \frac{g_J \mu_\beta}{2\mu_o} \langle \sigma_z^{(J)} (\underline{\nabla} B) \rangle$$

Because μ_N is very much less than μ_β the first term in the above expression will be neglected so that the equation of motion (A5.1) becomes:-

$$\frac{d\langle p\rangle}{dt} = -\frac{g_J\mu_\beta}{2\mu_o}\langle\sigma_z^{(J)}\rangle\,\underline{\nabla}B \quad . \qquad (A5.3)$$

Comparing the coefficients of $\underline{\nabla}B$ in equations (A5.2 and (A5.3) it can be seen that

$$\mu_{eff} \equiv -\frac{\partial W}{\partial B} = -\frac{g_J\mu_\beta}{2\mu_o}\langle\sigma_z^{(J)}\rangle \quad . \qquad (A5.4)$$

Thus the effective magnetic moment is directly proportional to the expectation value of the electronic spin (L being zero in the cases considered). μ_{eff} for $I = {}^3/2$ is shown as a function of B in Fig. AV.2) (Kopfermann, 1958) where $\mu_\infty \equiv \frac{-g_J\mu_\beta}{2\mu_o}$.

(b) Polarization and Asymmetry

Optically induced transitions between the ground state (primed quantum numbers) and the first excited state of an $I = {}^3/2$ alkali, are considered. The following assumptions will be made:-

(i) The magnetic fields used, although sufficiently strong to ensure zero overlap of the substates of the ground levels (i.e. a splitting of the order of some hundreds of MHz ($\gtrsim {}^{3A}/_2$) as compared to level widths of 10 MHz), are not sufficient to decouple the ground levels in the sense that their wavefunctions $|M_F^{(i)'}\rangle$ (see Fig. AV.1), will be superpositions of the eigenfunctions, $|M_I M_J\rangle$, of the $\{I\ J\ M_I M_J\}$ representation:-

$$|M_F^{(i)'}\rangle = \sum_{M_J'=-1/2}^{+1/2} a_{M_J'}^{(i)}(B)\,|M_F^{(i)'} - M_J', M_J'\rangle$$

where the $a_{M_J}^{(i)}(B)$ are the coupling coefficients for the intermediate-field states and are thus functions of B.

(ii) The field is, however, sufficient to decouple the excited states. This is plausible because the magnetic dipole coupling constants (A), measuring the strength of the nuclear coupling, are in general an order of magnitude smaller in the excited state than that in the ground state. The following is a list of typical data supporting this view:-

^{23}Na:-	$A(3S_{\frac{1}{2}})$	=	890 MHz	(Kusch & Taub, 1949)
	$A(3P_{3/2})$	=	19.1 "	(Perl, Rabi & Senitzky, 1955)
^{39}K :-	$A(4S_{\frac{1}{2}})$	=	232 MHz	(Kusch & Taub, 1949)
	$A(4P_{\frac{1}{2}})$	=	28.9 "	(Buck & Rabi, 1957)
	$A(4P_{3/2})$	=	6.1 "	(Ney, 1969)
^{41}K	$A(4P_{3/2})$	=	3.4 "	(Ney, 1969).

(iii) In the decoupled excited states, all the groups of magnetic substates with different values of J or M_J are excited incoherently. The strength of this assumption can be judged by calculating and comparing the splittings of these groups (assuming complete Paschen-Bach effect) and comparing these with the splittings of the substates within a group of given J and M_J (ΔW_{JM_J}).

These splittings (in MHz) are given by:-

$$\Delta W_{JM_J} = 3A/2 - \frac{g_I \mu_N B \times 10^{-6}}{\mu_o h} .$$

A is obtained from the above table and B is taken to be 34 mT which gives a value of 0.3MHz for the second term. The effect of the quadrupole interaction is only of this order also.

For a given J the separation of groups of states, each with the same M_J is $\frac{g_J \mu_\beta B}{\mu_o h \times 10^6}$ MHz which for B = 34 mT is

equal to 636 mHz for $J = {}^3/2$ and 319 mHz for $J = \frac{1}{2}$.

The extent of a group of substates with the same J and M_J is given by $3\Delta W_{JM_J}$. The values of this are shown below for the stable isotopes of Na and K.

	^{23}Na	^{39}K	^{41}K
$3\,W_{3/2\,M_J}$	84.9 MHz	26.7 MHz	14.4 MHz

The possibility of coherence effects between substates of the excited levels with the same J and M_J will not arise because of the selection rules associated with the polarization of the radiation used.

If Π radiation is used to excite a given initial state (A5.5) then the amplitude for the transition can be calculated (The assumption of incoherence justifies the neglect of radiation damping.):-

$$A_o(M_F^{(i)'} \rightarrow J\, M_I M_J) \propto \langle J\, M_I M_J |\, p_o \,|\, M_F^{(i)'} \rangle$$

where p_o is the component of the dipole operator appropriate to Π transitions.

Expanding the state $|M_F^{(i)'}\rangle$ using (A5.5):-

$$A_o \propto \sum_{M_J'} a^{(i)}_{M_J'} \langle J M_I M_J | p_o | 1/2, M_F^{(i)'} - M_J', M_J' \rangle$$

Using the Wigner-Eckart Theorem one obtains:-

$$A_o \propto \sum_{M_J'} a^{(i)}_{M_J'} (2J+1)^{-1/2} C^{JM_J'}_{1\,1/2\,0M_J'} \langle J \| p_o \| 1/2 \rangle$$

C is a Clebsch-Gordan coefficient and $\langle J||p_o||\frac{1}{2}\rangle$ is a reduced matrix element, independent of M_J or M_J'. This reduced matrix element can be transformed to the $\{L\ S\ M_L\ M_S\}$ representation (Edmonds, 1960) and one obtains:-

$$A_o \propto \sum_{M_J'} a^{(i)}_{M_J'} (-1)^{J'+5/2} \sqrt{2}\, C^{JM_J'}_{1\,1/2\,0\,M_J'} \begin{Bmatrix} L & J & 1/2 \\ 1/2 & L' & 1 \end{Bmatrix} \langle L \| p_o \| L' \rangle$$

The Racah coefficient $\begin{Bmatrix} 1 & J & \frac{1}{2} \\ \frac{1}{2} & 0 & 1 \end{Bmatrix}$ is equal to $(-1)^{J+\frac{3}{2}}/\sqrt{6}$ for both possible values of J and the reduced matrix element is the same for all possible transitions. All the constant factors will be dropped to obtain:-

$$A_o \propto \sum_{M_J'} a^{(i)}_{M_J'} C^{JM_J'}_{1\,1/2\,0\,M_J'}$$

Similarly the amplitude for the de-excitation from $|J\ M_I M_J\rangle$ to a final level of the ground state $|M_F^{(f)}{}''\rangle$ via $\sigma_\pm$ transitions is given by:-

$$A_\pm(JM_IM_J' \rightarrow M_F^{(f)}{}'') \propto \sum_{M_J''} (-1)^{J+3/2} (2J+1)^{1/2} a^{(f)}_{M_J''} C^{1/2\,M_J''}_{1\,J\,\mp 1\,M_J'}$$

$$\propto (-1)^{J+3/2} (2J+1)^{1/2} a^{(f)}_{M_J'\mp 1} C^{1/2\,M_J'\mp 1}_{1\,J\,\mp 1\,M_J'}$$

The relative intensities $I_\pm$ of the $6_\pm$ are given by:-

$$I_\pm \propto \sum_{i\,f\,J} K(J) |A_o A_\pm|^2 K(i)$$

$$\propto \sum_{j\,f\,J} K(J)K(i)(2J+1) \Big| \sum_{M_J'} a^{(i)}_{M_J'}\, a^{(f)}_{M_J'\mp 1}\, C^{JM_J'}_{1\,1/2\,0\,M_J'}\, C^{1/2\,M_J'\mp 1}_{1\,J\,\mp 1\,M_J'} \Big|^2$$

where $K(J)$ is a factor which describes the relative intensities of the components of the doublet in the excitation source and $K(i)$ describes the distribution of atoms among the initial states $|i\rangle$. Inserting the values of the Clebsch-Gordan coefficients one obtains for $I_{\pm}$

$$I_{+} = \sum_{if} \tfrac{4}{9}(K(\tfrac{3}{2})+K(\tfrac{1}{2}))K(i)|a^{(i)}_{+\frac{1}{2}}|^2|a^{(f)}_{-\frac{1}{2}}|^2 \qquad (M_F^{(f)''}=M_F^{(i)'}-1)$$

$$I_{-} = \sum_{if} \tfrac{4}{9}(K(\tfrac{3}{2})+K(\tfrac{1}{2}))K(i)|a^{(i)}_{-\frac{1}{2}}|^2|a^{(f)}_{+\frac{1}{2}}|^2 \qquad (M_F^{(f)''}=M_F^{(i)'}+1) \qquad \text{(A5.6)}$$

As concern is only with relative intensities the common constant terms will be ignored.

The hexapole prepares the distribution $K(i)$ of atoms over the initial states $|i\rangle$ in the following way:- Within the hexapole the field is sufficiently strong ($\gtrsim$ 0.1T at the pole tips) to completely decouple electronic and nuclear spins. Those atoms with $M_J = +\frac{1}{2}$ are focused on an aperture. Let N_+ atoms originally in the states $|M_J = +\frac{1}{2}\rangle$ pass through this aperture. Those atoms with $M_J = -\frac{1}{2}$ are defocused and only N_- of those originally in the states $|M_J = -\frac{1}{2}\rangle$ pass through the aperture. In the lower-field environment of the interaction region, those atoms originally in the states $|M_J = +\frac{1}{2}\rangle$ are now in the states $|i\rangle$ ($i = 1,2,3,4$) (see Fig. AV.1). As the atoms are equally distributed over these states there are $N_+/4$ atoms per state. Similarly for the states $|i\rangle$ ($i=5,6,7,8$) there are $N_-/4$ atoms per state. Therefore

$$K(i) = \begin{cases} N_+/4 & i = 1\cdots 4 \\ N_-/4 & i = 5\cdots 8 \end{cases} \qquad \text{(A5.7)}$$

Because of the symmetry of the pairs of states (see Fig. AV.2) the following relations between the expansion coefficients (a) hold:-

$$|a^{(1)}_{+1/2}|^2=|a^{(5)}_{-1/2}|^2=1\ ,\ |a^{(2)}_{+1/2}|^2=|a^{(8)}_{-1/2}|^2\ ,\ |a^{(3)}_{+1/2}|^2=|a^{(7)}_{-1/2}|^2\ ,\ |a^{(4)}_{+1/2}|^2=|a^{(6)}_{-1/2}|^2$$

$$|a^{(1)}_{-1/2}|^2=|a^{(5)}_{+1/2}|^2=0\ ,\ |a^{(2)}_{-1/2}|^2=|a^{(8)}_{+1/2}|^2\ ,\ |a^{(3)}_{-1/2}|^2=|a^{(7)}_{+1/2}|^2\ ,\ |a^{(4)}_{-1/2}|^2=|a^{(6)}_{+1/2}|^2 \qquad \text{(A5.8)}$$

These coefficients are also related by the normality of the states:-

$$|a^{(i)}_{+1/2}|^2+|a^{(i)}_{-1/2}|^2=1 \qquad \text{(A5.9)}$$

Using the fact that $\langle \sigma_z^{(i)} \rangle = |a^{(i)}_{+1/2}|^2 - |a^{(i)}_{-1/2}|^2$ and relation (A5.9) it can be shown that:-

$$\begin{aligned} |a^{(i)}_{+1/2}|^2 &= \tfrac{1}{2}(1+\langle \sigma_z^{(i)} \rangle) \\ |a^{(i)}_{-1/2}|^2 &= \tfrac{1}{2}(1-\langle \sigma_z^{(i)} \rangle) \end{aligned} \qquad \text{(A5.10)}$$

Using relations (A5.8), and (A5.10) to simplify the sums in (A5.6); and using (A5.7), it can further be shown that:-

$$I_+ + I_- = \tfrac{1}{4}(N_+ + N_-)$$

$$\begin{aligned} I_+ - I_- &= \tfrac{1}{4}(N_+ - N_-)\sum_{i=1}^{4}\langle \sigma_z^{(i)} \rangle \\ &= (N_+ - N_-)\frac{\bar{\mu}_{eff}}{\mu_\infty} \end{aligned}$$

where the last line follows from (A5.4) and where $\bar{\mu}_{eff} = \tfrac{1}{4}\sum_{i=1}^{4}\mu_{eff}^{(i)}$

Thus the asymmetry $\mathcal{A}$ is given by:-

$$\mathcal{A} \equiv \frac{I_+ - I_-}{I_+ + I_-} = \frac{\bar{\mu}_{eff}}{\mu_\infty}\frac{(N_+ - N_-)}{(N_+ + N_-)} = \frac{\bar{\mu}_{eff}}{\mu_\infty}P$$

and therefore P and $\mathcal{A}$ are related by:-

$$P = \frac{A}{\bar{\mu}_{eff}/\mu_\infty} .$$

The $\mu_{eff}^{(i)}/\mu_\infty$ can be obtained from the Breit-Rabi formula and hence $\bar{\mu}_{eff}/\mu_\infty$ can be calculated.

In the case of natural potassium which contains two stable isotopes, the appropriate $\bar{\mu}_{eff}/\mu_\infty$ is obtained by an abundance-weighted average over the values for the individual isotopes. The result of this process is shown in Fig. AV.3 (Campbell, 1971). The value of $\bar{\mu}_{eff}/\mu_\infty$ appropriate to a natural mixture of potassium in a field of 34 mT is 0.92.

APPENDIX VI

CORRECTIONS FOR ERRORS IN THE THICKNESS OF THE WAVE-PLATE

If the thickness of the wave plate is such that the phase-difference between the fast and slow directions does not equal one quarter of the wavelength of the radiation used, then a contribution from the "wrong" state of circular polarization will be obtained in the measurement of the asymmetry A .

Using the method of section 4.3, the ratio (α) of the maximum to minimum intensities transmitted as the orientation of the polaroid is changed, is found to be 1.36. Instead of producing circularly polarized light, therefore, the HNCP7 gives rise to light of elliptical polarization at potassium resonance wavelengths. It is desired to obtain correction factors as functions of α for the measured intensities $I(\sigma^{\pm})^{m}$.

Let axes be chosen such that the z-axis lies along the direction of propagation of the light, and the x and y axes lie along the major and minor axes of the resulting elliptically polarized light. Then the components of the electric vector of the radiation emerging from the plate, satisfy:-

$$a^2 = \frac{E_x^2}{1-\cos\delta} + \frac{E_y^2}{1+\cos\delta} \qquad (A6.1)$$

where a is the amplitude of the components along the fast and slow axes, of the incident electric vector and δ is the phase difference introduced between these components, by the plate. An analysis of the emerging radiation with the rotating

polaroid as described above gives the ratio of the maximum values of E_y^2 and E_x^2. These maximum values are given by putting $E_x = 0$ and $E_y = 0$ respectively in (A6.1) so one obtains, therefore,

$$\alpha \equiv \frac{E_y^2(\text{Max})}{E_x^2(\text{Max})} = \frac{1 + \cos\delta}{1 - \cos\delta} \quad .$$

This equation can be solved for δ to give:-

$$\sin\delta = \frac{2\sqrt{\alpha}}{\alpha+1} \quad . \qquad \text{(A6.2)}$$

In the measurement of atomic beam polarization, the wave plate, followed by a polaroid, is used to analyse the states of circular polarization. If new (x',y') axes are chosen to lie in the directions of the fast and slow axes of the plate, then the two orthogonal components of electric field of the wave incident on the plate are given by:-

$$E_{x'}^{(i)} = a^{\pm} \sin(\omega t \pm \pi/2)$$
$$E_{y'}^{(i)} = a^{\pm} \sin \omega t$$

where the amplitudes a^+ and a^- result from states whose electric vectors rotate anti-clockwise and clockwise respectively, when viewed in a direction opposite to that of propagation. On passing through the plate, a phase difference δ is introduced between these two components which, on emerging from the plate, become:-

$$E_{x'}^{(e)} = a^{\pm} \sin(\omega t \pm \pi/2 + \delta)$$
$$E_{y'}^{(e)} = a^{\pm} \sin \omega t \quad .$$

The components E_x, E_y in the directions initially defined

(45^{o} to the plate axes) now satisfy:-

$$a^{\pm 2} = \frac{E_x^2}{1 \pm \sin\delta} + \frac{E_y^2}{1 \mp \sin\delta} \quad . \qquad \text{(A6.3)}$$

This radiation is then analysed by a polaroid with its directional acceptance in either the x or y directions so that ideally, provided $\delta = \pi/2$, a measurement of the intensities of E_x^2 and E_y^2 yields directly a^{+2} and a^{-2} respectively. However, in the real case, as mentioned previously $\delta \neq \pi/2$ and in general the intensities measured for the two directions of the polaroid are given from equation (A6.3) as:-

Polaroid in x direction $(E_y=0)$; $E_x^2 = (1 \pm \sin\delta)a^{\pm 2}$

Polaroid in y direction $(E_x=0)$; $E_y^2 = (1 \mp \sin\delta)a^{\pm 2}$

If both states of circular polarization are present simultaneously, they both contribute to the measured intensities incoherently and one has:-

$$I(\sigma^+)^m = (1 + \sin\delta)a^{+2} + (1 - \sin\delta)a^{-2}$$
$$I(\sigma^-)^m = (1 - \sin\delta)a^{+2} + (1 + \sin\delta)a^{-2} \qquad \text{(A6.4)}$$

The true intensities needed for the calculation of polarization are:-

$$I(\sigma^+) \equiv 2a^{+2}$$
$$I(\sigma^-) \equiv 2a^{-2} \quad .$$

So, on solving the pair of equations (A6.4) for $2a^{+2}$ and $2a^{-2}$ one obtains:-

$$I(\sigma^+) = \left[(1+\sin\delta)I(\sigma^+)^m - (1-\sin\delta)I(\sigma^-)^m\right]/2\sin\delta$$
$$I(\sigma^-) = \left[(1+\sin\delta)I(\sigma^-)^m - (1-\sin\delta)I(\sigma^+)^m\right]/2\sin\delta$$

The terms involving δ can be written as functions of α using equation (A6.2) and we obtain finally:-

$$I(\sigma^+) = f^+ I(\sigma^+)^m - f^- I(\sigma^-)^m$$

$$I(\sigma^-) = f^+ I(\sigma^-)^m - f^- I(\sigma^+)^m$$

where $f^{\pm} = \frac{\alpha+1 \pm 2\sqrt{\alpha}}{4\sqrt{\alpha}}$.

If $\mathcal{A}_m$ is the measured asymmetry then the true asymmetry is thus given by:-

$$\mathcal{A} = \frac{f^+ + f^-}{f^+ - f^-} \mathcal{A}_m$$

$$= \frac{(\alpha+1)}{2\sqrt{\alpha}} \mathcal{A}_m$$

$$= 1.012 \mathcal{A}_m \quad \text{for} \quad \alpha = 1.36 .$$

If the opposite sign had been taken for $\sqrt{\alpha}$ in (A6.2) then one would have obtained:-

$$\mathcal{A} = \frac{\sqrt{\alpha}}{\alpha+1} \mathcal{A}_m$$

$$= 0.988 \mathcal{A}_m$$

but as the sense of the orientation (w.r.t. the plate axes) of the ellipse characterized by α , is unknown, so therefore is the sign of $\sqrt{\alpha}$. One is left therefore with an uncertainty in P of $\pm 1.2\%$ which, because of its relatively small size, is not included in the error bars of Fig. 4.31.

APPENDIX VII

THE METHOD OF LEAST SQUARES

The non-linear least squares method described by Ferguson (1965) and Brandt (1970) is used to fit a function to the time spectrum obtained as described in Chapter 5. A summary of the method is given below.

Let n_j be the content of MCA channel j satisfying the equation:-

$$\Phi_j \equiv n_j - \Gamma_j(x_1 \ldots x_i \ldots x_r) = 0 \quad j = 1 \ldots n$$

where r is the number of unknown parameters, n is the number of MCA channels utilized and the function Γ_j is given in the present case by:-

$$\Gamma_j = x_1 + x_2 \exp\left\{\frac{1}{4h^2x_3^2} + \frac{t_j - x_4}{x_3}\right\}\left\{1-\operatorname{erf}\left[h(t_j - x_4) + \frac{1}{2x_3}\right]\right\}$$

where $h^2 = 4\ell n2/x_5^2$, the parameters $x_1 \ldots x_5$ represent A, B, τ', T and W of Chapter 5, respectively, and t_j is the time delay represented by channel j. Let y_j be the measured content of channel j, with variance σ_j^2 (taken to be equal to y_j). Let the following column vectors be defined:-

$$\underline{x} \equiv \begin{pmatrix} x_1 \\ \vdots \\ x_r \end{pmatrix}, \quad \underline{n} \equiv \begin{pmatrix} n_1 \\ \vdots \\ n_n \end{pmatrix}, \quad \Phi \equiv \begin{pmatrix} \Phi_1 \\ \vdots \\ \Phi_n \end{pmatrix}, \quad \underline{\Gamma} \equiv \begin{pmatrix} \Gamma_1 \\ \vdots \\ \Gamma_n \end{pmatrix} .$$

Let $\underline{x}_o$ be a column vector representing a trial set of parameters. Let the following quantities be defined:-

$$\underline{\xi} \equiv \underline{x} - \underline{x}_o , \quad A \equiv \begin{pmatrix} a_{11} \cdots a_{1r} \\ \vdots \\ a_{n1} \cdots a_{nr} \end{pmatrix} , \quad a_{ji} \equiv \left(\frac{\partial \Phi_j}{\partial x_i}\right)_{\underline{x}_o} \equiv -\left(\frac{\partial \Gamma_j}{\partial x_i}\right)_{\underline{x}_o}$$

$$c_j \equiv \Phi_j(\underline{x}_o, y_j) \equiv y_j - \Gamma_j(\underline{x}_o) , \quad \varepsilon_j = \Phi_j(\underline{x}_o, y_j) - \Phi_j(\underline{x}_o, \eta_j) .$$

Let the following column vectors also be defined:-

$$\underline{c} \equiv \begin{pmatrix} c_1 \\ \vdots \\ c_n \end{pmatrix} , \qquad \underline{\varepsilon} \equiv \begin{pmatrix} \varepsilon_1 \\ \vdots \\ \varepsilon_n \end{pmatrix} .$$

Finally, let the matrix G_y and the covariance matrix C_y be defined by:-

$$C_y \equiv G_y^{-1} \equiv \begin{pmatrix} \sigma_1^2 & & 0 \\ & \sigma_2^2 & \\ 0 & & \ddots \\ & & & \sigma_n^2 \end{pmatrix}$$

A Taylor expansion of $\Phi_j(\underline{x}, \eta_j)$ about $\Phi_j(\underline{x}_o, \eta_j)$, retaining only first-order terms, can be written:-

$$0 \equiv \Phi(\underline{x}, \underline{\eta}) = A\underline{\xi} + \underline{c} - \underline{\varepsilon} \quad . \qquad \text{(A7.1)}$$

It is desired to obtain better estimates $(\underline{x}_1)$ of the parameters by the correct choice of $\underline{\varepsilon}$ (or $\underline{\xi}$ by A7.1). Using the method of maximum likelihood the least squares solution requires that :-

$$M \equiv \underline{\varepsilon}^T G_y \underline{\varepsilon} = \text{minimum.}$$

This is assured if:-

$$\frac{\partial M}{\partial x_i} = 0 \qquad i = 1 \ldots r$$

and this leads to (using A7.1):-

$$2A^T G_y (\underline{c} + A\underline{\xi}) = 0 .$$

If $r \leq n$ this can be solved to give:-

$$\tilde{\underline{\xi}} = -(A^T G_y A)^{-1} A^T G_y \underline{c}$$

with the covariance matrix given by:-

$$C_{\underline{\xi}} \equiv G_{\underline{\xi}}^{-1} = (A^T G_y A)^{-1} .$$

An improved set of parameters $(\underline{x}_1)$ are thus ob tained, given by:-

$$\underline{x}_1 = \tilde{\underline{\xi}} + \underline{x}_o$$

as x_o is fixed, the covariance matrix of $\underline{x}_1$ is given by:-

$$C_{\underline{x}_1} = C_{\underline{\xi}} .$$

The iteration process is repeated by computer until the resulting $\tilde{\underline{\xi}}$ become so small that negligible improvement is obtained by an additional step. If this occurs after s steps then the final result is:-

$$\underline{x}_s = \tilde{\underline{\xi}} + \underline{x}_{s-1}$$

$$C_{\underline{x}_s} = C_{\tilde{\underline{\xi}}} = (A^T G_y A)^{-1}$$

where A is now calculated using $\underline{x}_{s-1}$. The least squares estimate of the channel contents is given by (A7.1) as:-

$$\tilde{\underline{n}} = \underline{y} - A\tilde{\underline{\xi}} .$$

If each ε_j is assumed normally distributed, then it can be shown that the quantity $M \equiv \underline{\varepsilon}^T G_y \underline{\varepsilon}$ follows a χ^2 distribution with $q = n-r$ degrees of freedom. The values used in table 5.4 for the fractiles of the distribution are obtained from the approximate formula given by Pearson and Hartley(1962):-

$$P(\chi^2 < \tfrac{1}{2}(1.96 + \sqrt{2q-1})^2) = 97.5\% \qquad q > 100.$$

REFERENCES

Arriola, H., Teubner, P.J.O., Ugbabe, A. & Weigold, E. (1975) J. Phys. B 8, 1275-9.

Bell, R.E. (1965) α,β, and γ-Ray Spectroscopy, Vol. II, ed. K. Siegbahn (North-Holland, Amsterdam).

Bell, W.E., Bloom, A.L., and Lynch, J. (1961) Rev. Sci. Instrum. 32, 688-692.

Born, M. (1926) Zeits. f. Physik 38, 803.

Borodini, F. (1971) Nucl. Instr. & Meth. 97, 405-8.

Bosqued, J.M. & Reme, H. (1967) Nucl. Instr. & Meth. 57, 6-12.

Brandt, S. (1970) Statistical & Computational Methods in Data Analysis (North-Holland, Amsterdam).

Brash, H.M. (1969) Ph.D. Thesis, University of Edinburgh.

Brash, H.M., Campbell, D.M., Farago, P.S., Rae, A.G.A., Siegmann, H. Chr. & Wykes, J.S. (1969) Proc. Roy. Soc. Edin. 68A, 158-184.

Breit, G. & Rabi, I. (1931) Phys. Rev. A38, 2082-83.

Buck, P. & Rabi, I. (1957) Phys. Rev. A107, 1291.

Campbell, D.M. (1971) Ph.D. Thesis, University of Edinburgh.

Chase, R.L. (1968) Rev. Sci. Instrum. 39, 1318.

Clausing, P. (1931) Zeits. f. Physik 66, 471.

Cunningham, R.T. & Link, J.K. (1966) J. Opt. Soc. Am. 56, 1195-9.

Csanak, G., Taylor, H.S. & Tripathy, D.N. (1973) J. Phys. B 6, 2040-54.

Datz, S. & Taylor, E.H. (1956) J. Chem. Phys. 25, 389-394.

Dagnall, R.M. & West, T.S. (1968) Appl. Opt. 7, 1287-1294.

Dunworth, J.V. (1940) Rev. Sci. Instrum. 11, 167-172.

Edmonds, A.R. (1960) Angular Momentum in Quantum Mechanics (University Press, Princeton, New Jersey.)

REFERENCES (Contd.)

Eminyan, M., McAdam, K.B., Slevin, J. & Kleinpoppen, H. (1973) Phys. Rev. Letters 31, 576-579.

Eminyan, M., McAdam, K.B., Slevin, J. & Kleinpoppen, H. (1974) J. Phys. B 7, 1519-42.

Enemark, E.A. & Gallagher, A. (1972) Phys. Rev. A 6, 192-205.

Ferguson, A.J. (1965) Angular Correlation Measurements in γ-Ray Spectroscopy (North-Holland, Amsterdam).

Fite, W.L. & Brackman, R.T. (1958) Phys. Rev. A 112, 1141-51.

Gale, N.H. (1962) Nucl. Phys. 38, 252-8.

Gatti, E. & Svelto, V. (1966) Nucl. Instr. & Meth. 43, 248-268.

Gedcke, D.A. & McDonald, W. (1967) Nucl. Instr. & Meth. 55, 377.

Gibson, J. (1975) Private Communication.

Green, T.S. & Proca, G.A. (1970) Rev. Sci. Instrum. 41, 1409-1414.

Hafner, H. (1973) Physics Letters 43A, 275-6.

Hafner, H. & Kleinpoppen, H. (1967) Zeits. f. Physik 198, 315-320.

Harrower, G.A. (1955) Rev. Sci. Instrum. 26, 850-854.

Heddle, D.W.O. (1967) Proc. Phys. Soc. 90, 81-86.

Heron, S.W.G., McWhirter, R.W.P. & Rhoderick E.H. (1954) Nature 174, 564.

Hertel, I.V. & Stoll, W. (1974) J. Phys. B 7, 570-582, 583-592.

Holstein, T. (1947) Phys. Rev. A 72, 1212-33.

Imhof, R.E. & Read, F.H. (1970) Nucl. Instr. & Meth. 90, 109-113.

Imhof, R.E. & Read, F.H. (1971) J. Phys. B 4, 450-460.

Karule, E.M. and Peterkop, R.K. (1965) Atomic Collisions, Vol. III, ed. V. Ya. Veldre (Lat. Acad. Sciences, Riga).

Kastler, A. (1957) J. Opt. Soc. Am. 47, 460-465.

Kaul, R.D. (1966) J. Opt. Soc. Am. 56, 1262.

King, G.C. & Adams, A. (1974) J. Phys. B. 7, 1712-18.

REFERENCES (Contd.)

King, G.C., Adams, A. & Read, F.H. (1972) J. Phys. B 5, L254-7.

Kleinpoppen, H. (1969) Physics of One & Two-Electron Atoms, ed. Bopp & Kleinpoppen (North-Holland, Amsterdam).

Kleinpoppen, H. (1971) Phys. Rev. A 3, 2015-27.

Klemperer, O. (1965) Rep. Prog. Phys. 28, 77-111.

Klerk, P. de (1965) The Construction of High-Field Electromagnets (Newport Instruments Ltd.).

Kopfermann, H. (1958) Nuclear Moments (Academic Press, New York).

Kusch, P. & Taub, H. (1949) Phys. Rev. A 75, 1477.

Langmuir, D.B. (1913) Phys. Rev. 2, 450.

Langmuir, D.B. (1937) Proc. I.R.E. 25, 977.

Lapp, M. & Harris, L.P. (1966) J. Quant. Spectrosc. Radiat. Transfer 6, 169-179.

Long Jr., R.L., Raith, W. & Hughes, V.W. (1965) Phys. Rev. Lett. 15, 1-3.

McConkey, J.W., Tan, K.H., Farago, P.S. & Teubner, P.J.O. (1975) IXth Int. Conf. on Physics of Electron-Atom Collisions. Invited Paper.

McGowan, J.W. (1967) Rev. Sci. Instrum. 38, 285-7.

Macek, J. & Jaecks, D.H. (1971) Phys. Rev. A 4, 2288-2300.

Madison, D.H. & Shelton, W.N. (1973) Phys. Rev. A 7, 499-513.

Marmet, P. & Kerwin, L. (1960) Can. J. Phys. 38, 787-796.

Massey, H.S.W. & Mohr, C.B.O. (1932) Proc. Roy. Soc. 136, 289.

Mayer, H. & Rahn, A. (1968) Zeits. f. Physik 212, 408-414.

Moores, D.L. & Norcross, D.W. (1972) J. Phys. B 5, 1490.

Nesmeyanov, A.N. (1963) Vapour Pressures of the Elements (Infosearch, London).

Ney, J. (1969) Zeits. f. Physik 223, 126.

Orman, P.R. (1963) Nucl. Instr. & Meth. 21, 121-125.

REFERENCES (CONTD.)

Pearson, E.S. & Hartley, H.O. (1962) (Eds.) Biometrika Tables for Statisticians, Vol. I (Univ. Press, Cambridge).

Percival, I.C. & Seaton, M.J. (1958) Phil. Trans. Roy. Soc. A251, 113-138.

Perl, M.L., Rabi, I. & Senitzky, B. (1955) Phys. Rev. A 98, 611.

Phelps, A.V. (1958) Phys. Rev. 110, 1362-1368.

Pierce, J.R. (1939) J. Appl. Phys. 10, 715-724.

Pierce, J.R. (1954) The Theory & Design of Electron Beams. 2nd ed. (Van Nostrand, Princeton, New Jersey).

Pochat, A., Rozuel, D. & Peresse, J. (1973) J. de Physique 34, 701.

Poultney, S. (1972) Advan. Electronics. Electron Phys. 31, 39.

Rae, A.G.A. & Wykes, J.S. (1972) Private communication.

Ramsey, N.F. (1969) Molecular Beams (Clarendon Press, Oxford).

Read, F.H. (1969) J. Phys. E 2, 165-169.

Read, F.H. (1970) J. Phys. E. 3, 127-131.

Reitz, J.R. & Milford, F.J. (1962) Foundation of Electromagnetic Theory (Addison Wesley, Reading, Massachusetts).

Schmieder, R.W., Lurio, A., Happer, W. & Khadjari, A. (1970) Phys. Rev. A 2, 1216-28.

Sharber, J.R., Winningham, J.D. & Sheldon, W.R. (1968) I.E.E.E. Trans. on Nucl. Sci. NS-15, 536-540.

Simpson, J.A. (1961) Rev. Sci. Instrum. 32, 1283-93.

Simpson, J.A. & Kuyatt, C.E. (1963a) Rev. Sci. Instrum. 34, 265-268.
(1963b) J. Res. Nat. Bureau Stand. U.S.A 67C, 279-281.

Slevin, J.A., Visconti, P.J. & Rubin, K. (1972) Phys. Rev. A 5, 2065-72.

Soa, E.A. (1959) Jenaer Jahrbuch 1, 115-153.

Spangenberg, J. & Field, L.M. (1943) Elec. Comm. 21, 194-204.

Thompson, B.J. & Headrick, L.B. (1940) Proc. I.R.E. 28, 318-324.

REFERENCES (CONTD.)

Wapstra. A.H. (1965) α, β, and γ-Ray Spectroscopy, Vol. I, ed. K. Siegbahn (North-Holland, Amsterdam).

Whittaker, J.K. (1966) I.E.E.E. Trans. on Nucl. Sci. NS-13, 127-131.

Wykes, J.S. (1972a) J. Phys. B 5, 1126-37; (b) Ph.D. Thesis, University of Edinburgh.

Wykes, J.S. (1973) Private communication.

Young, A.T. (1963) Appl. Opt. 2, 51.

Zapesochnyi, I.P. & Shimon, L.L. (1965) Optika Specktrosk. 19, 480 (Soviet Optics & Spectroscopy 19, 268).

Zapesochnyi, I.P. & Sosnikov, A.K. (1965) Optika Spectrosk. 19, 864 (Soviet Optics & Spectroscopy 19, 480).

Addendum

King, G.C., Adams, A. & Cvejanovic, D. (1975) J. Phys. B. 8, 365-71.